Mobile Radio Communications

Second Edition

Second and Third Generation Cellular and WATM Systems

Edited and co-authored by

Raymond Steele and Lajos Hanzo

Contents

Preface to the Second Edition

Second generation (2G) digital cellular mobile radio systems have taken root in many countries, untethering the telephone and enabling people to conduct conversations away from the home or office and while on the move. The systems are spectrally efficient with the frequency bands assigned by the regulatory bodies being reused repeatedly over countries and even continents. At the time of writing the standardisation of three third generation (3G) systems is also well under way in Europe, the United States and in Japan. This book aims to portray the evolutionary avenue bridging the second and third generation systems.

The fixed networks have also become digital, enabling the introduction of the integrated digital service network (ISDN). No longer are communications to be restricted to voice. Instead a range of services, such as fax, video conferencing and computer data transfer is becoming increasingly available. The second generation digital cellular networks have complex radio links, connecting the mobile users to their base stations. Mobile voice and data communications are supported by elaborate network protocols that support registration and location of mobile users, handovers between base stations as the mobiles roam, call initiation and call clear-down, and so forth. In addition there are management, maintenance, and numerous other functions unseen by the user that combine to facilitate high quality mobile communications. Some of these network issues are considered in the context of the Global System of Mobile (GSM) communications in Chapter 8 and in Wireless Asynchronous Transfer Mode (WATM) systems in Chapter 11, but this book principally addresses the so-called physical layer aspects of mobile communications.

Chapter 1 is a bottom-up approach to cellular radio. Commencing with the propagation environment of a single mobile communicating with a base station, Chapter 1 progresses via multiple access methods, first generation and second generation mobile systems, to cordless telecommunications and concludes with a discussion on the teletraffic aspects of mobile radio systems. The chapter is designed to equip the reader with a range of concepts that will prepare her or him for the more focused in-depth chapters which follow.

Chapter 2 considers mobile radio propagation in a quantitative manner, establishing the background material that is the backbone of mobile radio communications. A prerequisite to digital telephony is the selection of an appropriate speech encoder, converting the analogue speech signal into a digital format. Chapter 3 provides an in-depth discourse on analysis-by-synthesis codecs.

Having encoded the speech signal, forward error correction coding is applied together with interleaving of the coded speech bits, in order to combat the channel error bursts that occur due to the fading inflicted by the mobile radio channel. Chapter 4 addresses these issues. The interleaved data are transmitted via a suitable modulator over a mobile radio channel to a distant receiver which recovers the data. There are many different methods of modulation but we opted for describing those, which are particularly appropriate for mobile communications. In Chapter 5 we consider quaternary frequency shift keying (QFSK), which was a contending modem for the pan-European cellular network. Chapter 6 deals with a more complex family of modulation schemes, which are known as generalised phase modulation arrangements. In this chapter we consider Viterbi equalisation of wideband dispersive mobile radio channels.

Frequency hopping is an important technique in mobile radio communications, whereby a user's channel hops from one frequency carrier to another in order to avoid being in a deep fade for long periods of time. Chapter 7 is devoted to slow frequency hopping cellular systems, and an estimation of their spectral efficiency is presented. This is followed by a description of the pan-European mobile radio system in Chapter 8, which is now known as the Global System of Mobile communications, or GSM. This chapter guides the reader through the complexities of this mobile radio network, providing an overall system study and amalgamating the system components introduced in the preceding chapters.

Since the standardisation of the second generation systems, such as GSM, a decade has elapsed and the wireless community has been working towards the third generation of mobile systems. There have also been important evolutionary developments on the 2G scene, such as the definition of the half-rate Japanese Personal Digital Cellular (PDC) system's speech codec and that of the GSM half-rate speech-coding standard, the introduction of a new breed of enhanced full-rate speech codecs and the spread of advanced data, fax and email services. Further important developments have taken place in the area of high-speed wireless local area networks. Motivated by these trends and a range of other new developments in the field, **this second edition incorporates three new chapters**.

Chapter 9 presents a range of multimedia system components, which have the potential to provide attractive enhanced services in the context of both the existing 2G and the forthcoming 3G systems. Specifically, various video codecs and handwriting codecs are described, in order to support wireless video telephony and electronic 'white-board' services. Chapter 9 also provides an overview of the recent activities in the field of multi-level modulation schemes, which can be advantageously invoked in so-called intelligent multi-mode transceivers that are capable of re-configuring themselves on a burst-by-burst basis, supporting more robust transmissions in hostile propagation environments while transmitting an increased number of bits per symbol in benign propagation scenarios.

Chapter 10 provides an overview of the recently proposed 3G wideband Code Division Multiple Access (W-CDMA) standards. The systems considered are the so-called 'Intelligent Mobile Telecommunications in the year 2000' (IMT-2000), the 'Universal Mobile Telecommunications System' (UMTS) scheme and the pan-American cdma2000 arrangement. Despite the call for a common global standard, there are some differences in the proposed technologies, notably the chip rates and inter-cell operation. These differences are partly due to the 2G infrastructure already in use all over the world, specifically the GSM and the IS-95 systems; an issue elaborated in Chapter 10.

Our final chapter is rather different from the others in that it is concerned with network issues related to wireless asynchronous transfer mode (WATM) networks. With the aid of a WATM simulator numerous scenarios for the transport of multimedia traffic over cellular networks are addressed. The results verify the effectiveness of the WATM concept, successfully mixing real-time, non-real-time, constant bit rate, and variable bit rate services. A number of network control enhancements have been suggested. The simulations confirm that the medium access control protocols, data link control protocols, and network management schemes must be dynamic and intelligent, and should take into account the instantaneous traffic loading on each BS and in the surrounding network. Intelligent handover and call admission schemes can provide vast improvements in the Quality of Service (QoS). The rapid re-assignment of capacity over a wide area would be beneficial. It must be emphasised that, given current bandwidth availabilities, satisfying the QoS expected in the fixed ATM network is economically impractical in wireless networks. Therefore, acceptable mobile service grades should be defined, or the available radio spectrum increased.

To our original text dealing with many of the fundamentals of the physical aspects of mobile communications, we have added new chapters dealing with the exciting subjects of multimedia mobile communications, the proposed 3G CDMA systems, and WATM. It is our hope that you will find this second edition comprehensive, technically challenging, valuable and above all, enjoyable.

Raymond Steele
Lajos Hanzo

Acknowledgements

The book has been written by the staff in the Electronics and Computer Science Department at the University of Southampton and at Multiple Access Communications Ltd. The names of the authors of each chapter are presented at the beginning of their chapters. All of the contributors are indebted to our many colleagues who have enhanced our understanding of the subject. These colleagues and valued friends, too numerous all to be mentioned, have influenced our views concerning various aspects of wireless multimedia communications and we thank them for the enlightment gained from our collaborations on various projects, papers and books. We are grateful to J. Brecht, Jon Blogh, Marco Breiling, M. del Buono, Clare Brooks, Peter Cherriman, Stanley Chia, Byoung Jo Choi, Joseph Cheung, Peter Fortune, Lim Dongmin, D. Didascalou, S. Ernst, Eddie Green, David Greenwood, Hee Thong How, Thomas Keller, W.H. Lam, C.C. Lee, M.A. Nofal, Xiao Lin, Chee Siong Lee, Tong-Hooi Liew, Matthias Muenster, V. Roger-Marchart, Redwan Salami, David Stewart, Juergen Streit, Jeff Torrance, Spiros Vlahoyiannatos, William Webb, John Williams, Jason Woodard, Choong Hin Wong, Henry Wong, James Wong, Lie-Liang Yang, Bee-Leong Yeap, Mong-Suan Yee, Kai Yen, Andy Yuen and many others with whom we enjoyed an association.

We also acknowledge our valuable associations with Roke Manor Research, BT Laboratories, the Department of Trade and Industry and the Radiocommunications Agency. Our sincere thanks are also due to the EPSRC, UK; the Commission of the European Communities, Brussels; and Motorola ECID, Swindon, UK for sponsoring some of our recent research.

Those authors who did not typeset their final manuscripts in Latex thank Jenny Clark, Debbie Sheridan and Denise Harvey for the work they did on their behalf in preparing the camera-ready copy. We are grateful to Phil Evans for the production of many of the drawings, and we feel particularly indebted to Peter Cherriman and Rita Hanzo for their skilful assistance with the final typesetting in Latex. Similarly, our sincere thanks are due to Juliet Booker, Mark Hammond and a number of other staff from John Wiley & Sons Ltd for their kind assistance throughout the preparation of this second edition.

Raymond Steele
Lajos Hanzo

Contributors

Editors:

R. Steele, BSc, PhD, DSc, FEng, FIEE, FIEEE,
Professor of Telecommunications, University of Southampton and
Chairman of Multiple Access Communications Ltd, UK

L. Hanzo, Dipl-Ing., PhD, MIEE, SMIEEE,
Professor of Telecommunications, University of Southampton and
Consultant to Multiple Access Communications Ltd, UK

Co-authors

Chapter 1: R. Steele
Chapter 2: D. Greenwood, L. Hanzo
Chapter 3: R.A. Salami, L. Hanzo, F.C.A. Brooks, R. Steele
Chapter 4: K.H.H. Wong, L. Hanzo
Chapter 5: I.J. Wassell, R. Steele
Chapter 6: I.J. Wassell, R. Steele
Chapter 7: Y.F. Ko, D.G. Appleby
Chapter 8: L. Hanzo, J. Stefanov
Chapter 9: L. Hanzo
Chapter 10: K. Yen, L. Hanzo
Chapter 11: P. Pattullo, R. Steele

Chapter 9

Wireless QAM-based Multi-media Systems: Components and Architecture

L. Hanzo[1]

9.1 Motivation and Background

Previous chapters of this book attempted to portray the state-of-the-art of various system components, such as source and channel codecs, modems, multiple access schemes, etc. used in mobile communications, leading to a detailed discussion on the Pan-European GSM system in Chapter 8, which is the most widespread operational cellular system world-wide at the time of writing. The GSM system's example was invoked, in order to amalgamate the various system components in a system design study. This chapter has a similar goal in the context of modern wireless multi-media systems and endeavours to speculate on some of the evolutionary features of TDMA-based systems, while providing a system design study. We will amalgamate a range of system components into multi-media systems [1], portraying the interconnection of system components and characterising the expected system performance. Apart from the employment of low-rate speech and video codecs, multi-level modems [2] can also substantially

[1]University of Southampton and Multiple Access Communications Ltd

contribute towards reducing the required user bandwidth and can accommodate either an increased number of users, or provide potentially higher user bit-rates, if their increased channel SNR and co-channel interference requirements can be satisfied. Hence, Quadrature Amplitude Modulation (QAM) schemes are introduced in this chapter and their ability to support multi-mode operation is demonstrated. Specifically, when the instantaneous channel quality or SNR is increased, an increased number of bits per symbol can be transmitted, supporting an increased bit-rate. When the channel quality degrades, a more error-resilient, but less bandwidth-efficient modem mode can be invoked. At the time of writing the feasibility of such systems is being researched, for example as a potential evolutionary path for the well-established and widespread GSM system or for other future arrangements.

While the second-generation digital mobile radio systems of Table 1.1 are now widespread across the globe, researchers endeavour world wide to define the **third-generation** personal communications network (PCN), which is referred to as a personal communications system (PCS) in North America. The European Community's Research in Advanced Communications Equipment (RACE) programme [3, 4] and the follow-up research framework referred to as Advanced Communications Technologies and Services (ACTS) programme [5] spear-headed these initiatives in Europe. Similar campaigns were also conducted in Japan and the USA. In the European RACE programme there were two dedicated projects, endeavouring to resolve the on-going debate as regards to the most appropriate multiple access scheme, studying Time Division Multiple Access (TDMA) and Code Division Multiple Access (CDMA). The basic advantages and disadvantages of these multiple access schemes were highlighted in Chapter 1 and the most prominent TDMA system, namely the GSM system, was the topic of Chapter 8. At the time of writing in the third-generation era, however, CDMA seems to be emerging as the favourite in Europe [17], Japan and the USA, although the proposed CDMA systems are different from eachother. The design aspects of CDMA systems and the emerging third-generation European, Japanese and American system proposals will be the topic of Chapter 10, while the second-generation Pan-American so-called IS-95 CDMA system [16] was highlighted in Chapter 1.

A common requirement of all modern wireless systems is the ability to support services on a more flexible basis, than the somewhat rigid second-generation standards, promising to allocate bit-rates upto 2 Mbps on a demand basis. Therefore third-generation systems are expected to be more amenable to wireless multi-media transmission, than second generation systems. A wide variety of further associated aspects of modern wireless systems were treated in references [3]- [13].

The range of existing and future systems can be characterised with the aid of Figure 9.1 in terms of their expected **grade of mobility and bit-rate**, which are the two most fundamental parameters in terms of determining the systems' potential in terms of wireless multi-media applications. Specifically, the fixed networks are evolving from the basic 2.048 Mbit/s Integrated Services Digital Network (ISDN) towards higher-rate broad-band ISDN or B-ISDN. In comparison to these fixed networks, a higher grade of mobility, which we refer to here as **portability**, is a feature of cordless telephones (CTs), such as the Digital European Cordless Telephone (DECT), the British CT2 and the Japanese Personal Handyphone (PHP) systems, although their transmission rate is more limited than that of the fixed ISDN network. Recall that these systems were characterised in Table 1.1. The DECT system is the most flexible CT amongst them, allowing the multiplexing of 23 single-user channels in one of the duplex links between the portable station (PS) and base station (BS), which provides rates up to 23×32 kbps = 736 kbps for advanced services - although this bit-rate potential is eroded to around 500 kbps due to the various control channel overheads encountered. As suggested by Figure 9.1, wireless local area networks (WLAN) can support higher bit-rates of up to 155 Mbits/s in order to extend existing Asynchronous Transfer Mode (ATM) links to portable terminals, but they usually do not support full mobility functions, such as location update or hand-over from one base station to another. Another ambitious European initiative is targeted at high-rate, high-mobility system studies hallmarked by the so-called Mobile Broadband System (MBS), which is also featured in Figure 9.1. By contrast, as seen in the Figure, contemporary second-generation Public Land Mobile Radio (PLMR) systems, such as the Pan-European GSM, the American IS-54 and the Japanese Digital Cellular (JDC) systems cannot support high bit-rate services, since they typically have to communicate over lower quality, dispersive mobile channels, but they exhibit the highest grade of mobility - in the case of GSM including also high-speed international roaming capabilities. Again, the basic features of second-generation systems were summarised in Table 1.1 of Chapter 1.

Again, in this chapter we turned our attention to specific algorithmic and system architectural aspects of complete voice/video multi-media transceivers, which may be employed as evolutionary successors of existing second-generation systems, such as GSM or IS-54. We also evaluated their expected performance. Hence the system bandwidth was assumed to be 30 kHz, as in the American IS-54 standard [14], which allowed us to assess the potential of the proposed scheme in the context of a well-known existing system. As a further system design study, we also contrived a slightly more complex intelligent multi-mode transceiver, which was studied in the context of the 200 kHz bandwidth Pan-European GSM system.

This chapter is organised as follows. Section 9.2 gives a brief overview of recent developments in speech coding and, with reference to Chapter 3, it describes the 4.8 kbit/s so-called transformed binary pulse excited (TBPE) speech codec used in our system study. This is followed by the portrayal of a bit sensitivity analysis technique invoked in order to assist in mapping the

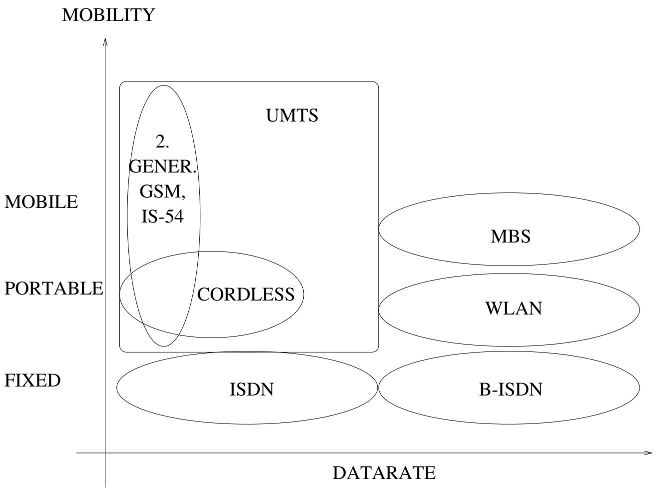

Figure 9.1: Stylised mobility versus bit-rate plane classification of existing and future wireless systems.

speech bits to different bit-protection classes, employing source-sensitivity matched error protection. A brief discussion is provided on the design of video codecs, in particular on that of the proposed fixed-rate video codec and the ITU H.263 standard video scheme in Section 9.3, while Section 9.5 is focused on the choice of modulation, in particular on 16-level quadrature amplitude modulation (16-QAM). Since the so-called full-response, linearly amplified modulation techniques have not been treated in previous chapters of this book, more attention is devoted to this topic than to other, previously considered system components. Section 9.6 highlights how packet reservation multiple access (PRMA) improves the efficiency of the TDMA radio link by surrendering passive time slots for active users contending for an available slot. Finally, two novel voice-video systems are proposed and investigated in Section 9.7 in the context of the 30 kHz bandwidth IS-54 system and the 200 kHz bandwidth GSM system, in order to be able to relate their performance to that of these well-known systems, before concluding in Section 9.8.

9.2 Speech Coding Aspects

9.2.1 Recent Speech Coding Advances

Let us commence our discourse on speech coding aspects with a brief overview of the recent speech compression literature [20]- [48], noting that Chapter 3 provided an in-depth treatment of speech coding. Following the International Telecommunications Union's (ITU) 64 kbit/s Pulse Code

Modulation (PCM) and 32 kbps Adaptive PCM (ADPCM) G.721 standards, in 1986 the 13 kbit/s Regular Pulse Excitation (RPE) [28,29] codec was selected for the Pan-European mobile system known as GSM, and more recently Vector Sum Excited Linear Prediction (VSELP) [30,31] codecs operating at 8 and 6.7 kbit/s were favoured in the American IS-54 and the JDC wireless networks. These developments were followed by the 4.8 kbit/s American Department of Defence (DoD) codec [32]. The state-of-art was documented in a range of excellent monographs by O'Shaughnessy [33], Furui [34], Anderson and Mohan [35], Kondoz [36], Kleijn and Paliwal [37] and in a tutorial review by Gersho [38]. More recently the 5.6 kbit/s half-rate GSM quadruple-mode Vector Sum Excited Linear Predictive (VSELP) speech codec standard developed by Gerson et al [39] was approved, while in Japan the 3.45 kbit/s half-rate JDC speech codec invented by Ohya, Suda and Miki [40] using the so-called Pitch Synchronous Innovation (PSI) CELP principle was standardised. Other currently investigated schemes are the Prototype Waveform Interpolation (PWI) proposed by Kleijn [41], Multi-Band Excitation (MBE) suggested by Griffin and Lim [42] and Interpolated Zinc Function Prototype Excitation (IZFPE) codecs advocated by Hiotakakos and Xydeas [43]. In the low-delay, but more error sensitive backward adaptive class the 16 kbps ITU G.728 codec [44] developed by Chen *et.al.* from the AT&T speech team hallmarks a significant step. This was followed by the equally significant development of the more robust, forward-adaptive 10 ms delay G.728 ACELP arrangement proposed by the Cherbrook team [46,47], AT&T and NTT [48]. Lastly, the standardisation of the 2.4 kbps DoD codec led to intensive research in this very low-rate range and the Mixed Excitation Linear Predicitve (MELP) codec by Texas Instrument was identified [49] in 1996 as the best overall candidate scheme.

Following the above speech coding review let us now briefly concentrate on the specific 4.8 kbps codec employed in our 30-kHz bandwidth multimedia system.

9.2.2 The 4.8 kbit/s Speech Codec [22, 51, 55]

Again, speech codecs were discussed in depth in Chapter 3, where we have shown that in code excited linear predictive (CELP) codecs a Gaussian process with slowly varying power spectrum is used to represent the residual signal after short-term and long-term prediction, and the speech waveform is generated by filtering Gaussian distributed stochastic excitation vectors through the time-varying linear pitch and LPC synthesis filters [50]. Here we follow the approach of Section 3.4, since at bit-rates around 4.8 kbps CELP codecs and their derivatives are the most successful schemes and restrict our discussion on speech codecs to a terse summary, in order to allow readers to consult this chapter in isolation from the rest of the book.

More specifically, in the CELP codec of Figure 3.34 in Section 3.4 the Gaussian distributed excitation vectors of dimension N are either stored in a codebook or generated in real-time, in order to avoid excessive storage requirements and the optimum excitation sequence is determined by the exhaustive search of the excitation codebook. The codebook entries $c_k(n)$ of Figure 3.34, $k = 1 \ldots L$, $n = 0 \ldots N-1$, after scaling by a gain factor G_k, are filtered through the synthesis filter, in order to produce the weighted synthetic speech $\tilde{s}_w(n)$, which is compared to the weighted original speech $s_w(n)$ for finding the specific codebook entry, which results in the best possible N-sample synthetic speech segment.

However, for a typical excitation frame length of $N = 40$ and codebook size $L = 1024$, the complexity of the original CELP codec proposed by Atal and Schroeder [52, 53] becomes excessively high for real-time implementation. Hence a plethora of computationally efficient solutions have been suggested in the literature [30,31,51,54] in order to ease the computational load encountered, while still maintaining perceptually high speech quality. As mentioned above, the VSELP principle [30, 31] was favoured in the American IS-54 [14], the JDC [15] and in the Pan-European half-rate GSM standards [39], while the Algebraic CELP (ACELP) [54] excitation was incorporated in the ITU G.729 [46] and G.723 recommendations. When the bit-rate is reduced below about 4.8 kbps, other approaches, such as that employed in the Japanese 3.45 kbit/s half-rate JDC speech codec invented by Ohya, Suda and Miki [40] using the so-called Pitch Synchronous Innovation (PSI) CELP can be employed. Multi-Band Excitation (MBE) suggested by Griffin and Lim [42], the Interpolated Zinc Function Prototype Excitation (IZFPE) codecs proposed by Hiotakakos and Xydeas [43] and the DoD MELP codec [49] are also efficient at rates below 4.8 kbps.

In our experiments here we opted for the 4.8 kbps transformed binary pulse excited (TBPE) speech codec of Section 3.5.1 proposed by Salami [22, 51, 55], but our system-design hints are applicable to any other 4.8 kbps codec, such as the DoD codec [32] or the ACELP scheme of Section 3.4.2.4 and reference [19]. A leading-edge half-rate system can also be contrived on the basis of the previously mentioned US DoD 2.4 kbps MELP codec, which can double the number of users supported in the 30-kHz bandwidth of the proposed system. The attraction of TBPE codecs when compared to CELP codecs accrues from the fact that the excitation optimisation can be achieved in a direct computation step [51], as it was shown in Section 3.5.1.

The TBPE algorithm of Section 3.5.1 is summarised here briefly for convenience, where the Gaussian excitation vector is assumed to take the form of:

$$\mathbf{c} = \mathbf{A}\mathbf{b}, \tag{9.1}$$

and the binary vector $\mathbf{b}$ has M elements of ± 1, while the $M \times M$ matrix $\mathbf{A}$ represents an orthogonal transformation. Due to the orthogonality of $\mathbf{A}$ the binary excitation pulses of $\mathbf{b}$ are transformed into independent, unit variance Gaussian components of $\mathbf{c}$. The set of 2^M binary excitation vectors gives rise to 2^M Gaussian vectors of the original CELP codec.

Parameter	Number of Bits
10 LSFs	36
LTPD	$2 \cdot 7 + 2 \cdot 5$
LTPG	$4 \cdot 3$
GP	$4 \cdot 2$
EG	$4 \cdot 4$
Excitation	$4 \cdot 12$
Total	144/30 ms

Table 9.1: Bit-allocation scheme of the 4.8 Kbit/s TBPE codec.

The block diagram of the TBPE codec was shown in Figure 3.41 of Chapter 3. As seen in the Figure, the weighted synthetic speech is generated for all $2^M = 1024$ codebook vectors and subtracted from the weighted input speech in order to find the one resulting in the best synthesised speech quality. The synthetic speech is generated at the output of the weighted synthesis filter, which is excited by the vectors given by the superposition of the adaptive codebook vector scaled by the long term predictor gain (LTPG) - which is synonymously also referred to as the adaptive codebook gain - and that of the orthogonally transformed binary vectors output by the binary pulse generator scaled by the stochastic excitation gain.

The bit allocation of our TBPE codec is summarised in Table 9.1. We note that a similar 4.8 kbps Algebraic Code Excited Linear Predicitve (ACELP) codec exhibiting the same bit-allocation scheme - apart from the different encoding of the excitation vectors - can be designed using the excitation model of Section 3.4.2.4. This ACELP excitation model was used in our system proposed in reference [19]. Returning to the bit-allocation table, the spectral envelope is represented by ten line spectrum frequencies (LSFs), which are scalar quantised using 36 bits, as it was detailed in Chapter 3. The 30 ms long speech frames hosting 240 samples are divided into four 7.5 ms subsegments having 60 samples. The subsegment excitation vectors $\mathbf{b}$ have 12 transformed duo-binary samples with a pulse-spacing of $D = 5$. The long term predictor (LTP) delays (LTPD) are quantised with seven bits in odd and five bits in even indexed subsegments, while the LTP gain (LTPG) is quantised with three bits. The excitation gain (EG) factor is encoded with four bits, while the grid position (GP) of candidate excitation sequences by two bits. A total of 28 or 26 bits per subsegment is used for quantisation, which yields $36 + 2 \cdot 28 + 2 \cdot 26 = 144$ bits/30 ms, i.e. a bit-rate of 4.8 kbit/s. In the next subsection we will give a rudimentary introduction to objective speech quality measures, which will be used in our bit-sensitivity evaluation carried out in order to design an appropriate embedded error correction scheme. Let us now provide a brief introduction to speech quality measures, which can be used in our bit sensitivity investigations.

9.2.3 Speech Quality Measures

In general the speech quality of communications systems is difficult to assess and quantify. However, in our system performance evaluations an easily evaluated objective speech quality measure is needed. The most reliable speech quality evaluation methods are based on subjective quality assessments, such as the so-called mean opinion score (MOS), which uses a five-point scale between one and five. MOS-tests use evaluation of speech by untrained listeners, but their results depend on the test conditions. Specifically, the selection and ordering of the test material, the language, and listener expectations all influence their outcome. A variety of other subjective measures is discussed in references [56]- [58], but subjective measures are tedious to derive and difficult to quantify during system development.

Objective speech quality measures do not provide results that could be easily converted into MOS values, but they facilitate quick comparative measurements during research and development. Most objective speech quality measures quantify the distortion between the speech communications system's input and output either in the time or frequency domain. The conventional SNR can be defined as

$$\mathrm{SNR} = \frac{\sigma_{in}^2}{\sigma_e^2} = \frac{\sum_n s_{in}^2(n)}{\sum_n [s_{out}(n) - s_{in}(n)]^2}, \tag{9.2}$$

where $s_{in}(n)$ and $s_{out}(n)$ are the sequences of input and output speech samples, while σ_{in}^2 and σ_e^2 are the variances of the input speech and that of the error signal, respectively. A major drawback of the conventional SNR is its inability to give equal weighting to high- and low-energy speech segments, because its computation will be dominated by the higher-energy voiced speech segments. Therefore the reconstruction fidelity of voiced speech is given higher priority than that of low-energy unvoiced sounds, when computing the arithmetic mean of the SNR. Hence a system optimised for maximum SNR usually is suboptimum in terms of subjective speech quality.

Some of the problems of SNR computation can be overcome by using the segmental SNR (SEGSNR)

$$\mathrm{SEGSNR}^{dB} = \frac{1}{M} \sum_{m=1}^{M} 10 \log_{10} \frac{\sum_{n=1}^{N} s_{in}^2(n)}{\sum_{n=1}^{N} [s_{out}(n) - s_{in}(n)]^2}, \tag{9.3}$$

where N is the number of speech samples within a segment of typically 15-25 ms, while M is the number of 15-25 ms segments, over which $\mathrm{SEGSNR}^{\mathrm{dB}}$ is evaluated. The advantage of using $\mathrm{SEGSNR}^{\mathrm{dB}}$ over conventional SNR is that it averages the $\mathrm{SNR}^{\mathrm{dB}}$ values related to 15-20 ms speech segments, giving a better weighting to low-energy unvoiced segments by effectively computing the geometric mean of the SNR values due to averaging in the logarithmic domain instead of the arithmetic mean. Hence the SEGSNR values correlate better with subjective speech quality measures, such as the MOS.

For linear predictive hybrid speech codecs, such as the 13 kbps RPE GSM codec, spectral domain measures typically have better correlation with perceptual assessments than time domain measures. The so-called cepstral distance measure physically represents the logarithmic spectral envelope distortion and is computed as [56, 57] :

$$\mathrm{CD} = \sqrt{\left[C_0^{in} - C_0^{out}\right]^2 + 2\sum_{j=1}^{3p}\left[C_j^{in} - C_j^{out}\right]^2}, \tag{9.4}$$

where C_j^{in} and C_j^{out}, $j = 0 \ldots 3p$ are the cepstral coefficients of the input and output speech, respectively, and p is the order of the short-term predictor filter which is typically 8-10. These cepstral coefficients can be readily computed from the coefficients of the short-term predictor using the results of reference [57]. Using these measures, let us now briefly consider the error sensitivity of the TBPE encoded bits, which will allow us to assign the bits to appropriate bit protection classes.

9.2.4 Bit Sensitivity Analysis

In our bit sensitivity investigations [55] we systematically corrupted each bit of a 144 bit TBPE frame and evaluated the SEG-SNR and CD degradation. Our results are depicted for the first 63 bits of a TBPE frame in terms of SEGSNR (dB) in Figure 9.2, and in terms of CD (dB) in Figure 9.3. For the sake of completeness we note that we previously reported our findings on a somewhat more sophisticated sensitivity evaluation technique in reference [19], where the effects of error propagation across speech frame boundaries due to filter memories was also taken into account by integrating or summing these degradations over all consecutive frames, where the error propagation inflicted measurable SEGSNR and CD reductions. However, for simplicity, in this treatise we refrain from using this technique and demonstrate the principles of source sensitivity-matched error protection using a less complex procedure.

Specifically, we recall from Table 9.1 that the first 36 bits represent the 10 LSFs describing the speech spectral envelope. Concentrating on the LSF bits initially, the SEG-SNR degradations of Figure 9.2 indicate the most severe waveform distortions for the first 10 bits describing the first 2-3 LSFs. The CD degradation in Figure 9.3, however, was quite severe for all LSFs, particularly for the most significant bits (MSBs) of the individual parameters. This was confirmed by our informal subjective tests. Whenever possible, at least the MSBs of the LSF bits should be protected against corruption.

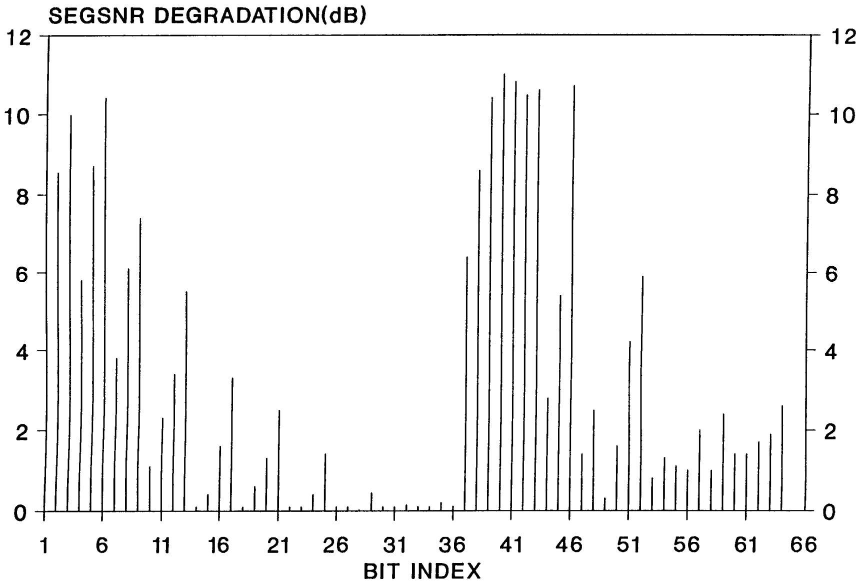

Figure 9.2: Bit sensitivities for the 4.8 Kbit/s codec expressed in terms of SEGSNR (dB).

Considering the remaining 27 bits seen in Figures 9.2 and 9.3, the parameters concerned are the LTPD, LTPG, GP, EG and Excitation pulse parameters for the first subsegment. We highlight our findings for the case of the first 27-bit subsegment only, as the other subsegments have identical behaviours. Bits 37-43 represent the LTP delays and bits 44-47 the LTP gains. Their errors are more significant in terms of SEG-SNR than in CD, as demonstrated by Figures 9.2 and 9.3. This is because the LTPD and LTPG parameters describe the spectral fine structure and do not seriously influence the spectral envelope distortion evaluated in terms CD, although they seriously degrade the recovered waveform, as indicated by the associated SEGSNR degradation. As the TBPE codec is a stochastic codec with random excitation patterns, bits 48-63 assigned to the excitations and their gains are not particularly vulnerable to transmission errors. This is because the redundancy in the signal is removed by the long-term and short-term predictors. Furthermore, the TBPE codec exhibits exceptional inherent excitation robustness, as the influence of a channel error is restricted to one component of the vector **b** and its effect in the excitation is spread and diminishes after the orthogonal transformation $\mathbf{c} = \mathbf{Ab}$. In conventional CELP codecs this is not the case, as a codebook address error causes the decoder to select a different excitation pattern from its codebook causing considerably more speech degradation than encountered by the TBPE codec.

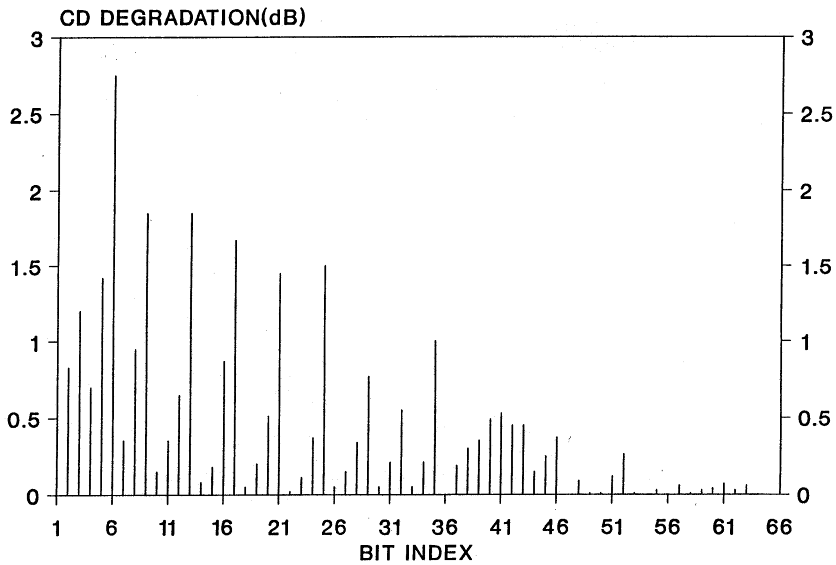

Figure 9.3: Bit sensitivities for the 4.8 Kbit/s codec expressed in terms of CD (dB).

In general, most robust performance is achieved if the bit protection is carefully matched to the bit sensitivities, but the SEG-SNR and CD sensitivity measures portrayed in Figures 9.2 and 9.3 often contradict. Therefore we combine the two measures to give a sensitivity figure S, representing the average sensitivity of a particular bit. The bits must be first ordered both according to their SEG-SNR and CD degradations portrayed in Figures 9.2 and 9.3, respectively, in order to derive their 'grade of prominence', where 1 represents the highest and 63 the lowest sensitivity. Observe that the highest CD degradation is caused by bit 6, which is the MSB of the second LSF in the speech frame, while the highest SEG-SNR degradation is due to bit 40 in the group of bits 37-43, representing the LTP delay. Furthermore, bit 6 is the seventh in terms of its SEG-SNR degradation, hence its sensitivity figure is $S = 1 + 7 = 8$, as seen in the first row of Table 9.2. On the other hand, the corruption of bit 40, the most sensitive in terms of SEG-SNR, results in a relatively low CD degradation, as it does not degrade the spectral envelope representation characterised by the CD, but spoils the pitch periodicity and hence the spectral fine-structure. This bit is the 19 th in terms of its SEG-SNR degradation, giving a sensitivity figure contribution of 19 plus 1 due to CD degradation, i.e. the combined sensitivity figure is $S = 20$, as shown by row 6 of Table 9.2. The combined sensitivity figures for all the LSFs and the first 27-bit subsegment are similarly summarised in ascending order in column 3 of Table 9.2, where column 2 represents the

Bit no. in frame	Bit index in frame	Sensitivity figure	Bit no. in frame	Bit index in frame	Sensitivity figure
1	6	8	36	57	76
2	9	14	37	10	79
3	5	16	38	28	80
4	3	16	39	19	80
5	41	19	40	61	80
6	40	20	41	59	82
7	13	21	42	62	84
8	2	23	43	15	85
9	43	24	44	60	88
10	8	25	45	34	89
11	46	25	46	50	91
12	42	26	47	31	92
13	17	27	48	55	95
14	39	31	49	27	95
15	4	31	50	23	97
16	21	32	51	14	97
17	12	37	52	47	98
18	38	38	53	58	102
19	25	43	54	54	103
20	16	44	55	53	105
21	52	45	56	56	105
22	7	45	57	18	105
23	1	45	58	33	108
24	37	48	59	49	109
25	45	49	60	26	109
26	11	55	61	30	110
27	20	58	62	22	119
28	51	60	63	36	125
29	29	60			
30	35	60			
31	44	63			
32	32	68			
33	48	69			
34	24	71			
35	63	76			

Table 9.2: Bit-sensitivity figures for the 4.8 Kbit/s TBPE codec

bit-index in the first 63-bit segment of the 144-bit TBPE frame.

On the basis of the above bit-sensitivity analysis [55] the speech bits were assigned in three sensitivity classes for embedded source-matched forward error correction to be detailed in Subsection 9.7.2.1. In closing we note that a more detailed discussion on various speech compression and transmission techniques will be provided in a forthcoming monograph [20]. Having described the proposed 4.8 kbit/s TBPE speech codec we now focus our attention on the design of the fixed, but arbitrarily programable videophone codec proposed for our multi-media communicator.

9.3 Video Coding Issues [112]

9.3.1 Recent Video Coding Advances

The theory and practice of image compression has been consolidated in a number of monographs by Netravali and Haskell [115], Jain [103], Jayant and Noll [80] and Hanzo *et. al.* [112]. Hence in this chapter we refrain from detailing the basics of video compression and concentrate mainly on the associated system aspects. A plethora of various video codecs have been proposed in the excellent special issues edited by Tzou, Mussmann and Aigawa [59], by Hubing [60], Gharavi et al [114] and Girod et al [61] for a range of bit-rates and applications, but the individual contributions by a number of renowned authors are too numerous to review.

Khansari, Jalali, Dubois and Mermelstein [62, 113] as well as Mann Pelz [63] reported promising results on adopting the International Telecommunications Union's (ITU) standardised H261 variable-rate codec [112] for wireless applications, which was originally designed for benign, low error-rate Gaussian channels. Since this codec employs so-called variable-length coding techniques, a single bit error can result in the erroneous decoding of an entire run-length coded string of bits, potentially leading to catastrophic video degradations. By invoking powerful signal processing and error-control techniques the authors succeeded in remedying the inherent source coding problems inflicted by stretching the codec's application domain to hostile wireless environments. Further important contributions in the field were due, for example, to Chen *et. al.* [64], Illgner and Lappe [65], Zhang [66], Ibaraki, Fujimoto and Nakano [67], Watanabe et al [68] etc. and the MPEG4 consortium's endeavours [71], as well as due to the efforts of the mobile audio-video terminal (MAVT) consortium. The applicability of the ITU standard H.263 codec [70, 72] to mobile videophony was investigated for example by Färber, Steinbach and Girod [69] as well as Cherriman and Hanzo [106]- [112]. A common feature of the above codecs is that unless an efficient bit-rate control mechanism, such as the adaptive packetisation algorithm of reference [110, 112] is used, the scheme has a time-variant bit-rate, which cannot be readily accommodated by contemporary second-generation wireless systems.

As a different design alternative, Streit and Hanzo offered [102] a comparative study of a range of fixed but arbitrarily programmable-rate 176×144 pixel head-and-shoulders Quarter Common Intermediate Format (QCIF) video codecs specially designed for fixed-rate videotelephony over existing and future mobile radio speech systems on the basis of a recent research programme [75,92,99–101,112]. These codecs employ novel motion-compensation and -tracking techniques as well as video 'activity' identification and tracking, which will be highlighted during our further discourse. Various motion compensated error residual coding techniques were compared, which dispensed with the self-descriptive, zig-zag scanning and run-length coding principle of the H.261 and H.263 codecs [112] for the sake of maintaining a time-invariant bit-rate and improved robustness against channel errors, while tolerating some compression ratio reduction. Within the implementational complexity and bit-rate limits always an optimum constant bit allocation was sought in order to be able to adapt the codec to the requirements imposed by existing second-generation wireless speech systems. Having reviewed some of the recent advances in video compression, let us now briefly highlight the rudimentary principles of video coding and commence our elaborations by considering the removal of temporal redundancy using motion compensation, before highlighting the concepts used by the above-mentioned fixed-rate video codecs.

9.3.2 Motion Compensation

The ultimate goal of low-rate image coding is to remove redundancy, predictability or self-similarity in both spatial and temporal domains, which correspond to the so-called intra-frame and inter-frame redundancy, manifesting themselves within a given video frame and with respect to consecutive frames, respectively. These redundancy reduction measures allow us to reduce the required transmission bit rate. The temporal correlation between successive image frames is typically removed using so-called block-based motion compensation, where each segment or block of the video frame to be encoded is assumed to be a motion-translated version of the corresponding block in the previously encoded video frame. How this can be achieved is the subject of this subsection.

The vector describing the above-mentioned motion translation is referred to as the motion vector (MV), which is typically found with the aid of correlation techniques, as it will be described during our forthcoming discourse. Specifically, as portrayed in Figure 9.4, a motion translation region or search scope is stipulated within the previous frame. To be more explicit, instead of using the previous original frame, the so-called 'locally decoded' frame is used in the motion compensation, where the phrase 'locally decoded' implies decoding it at the encoder, i.e. where it was encoded. This 'local decoding' yields an exact replica of the video frame at the distant decoder's output. This so-called local decoding operation is necessary,

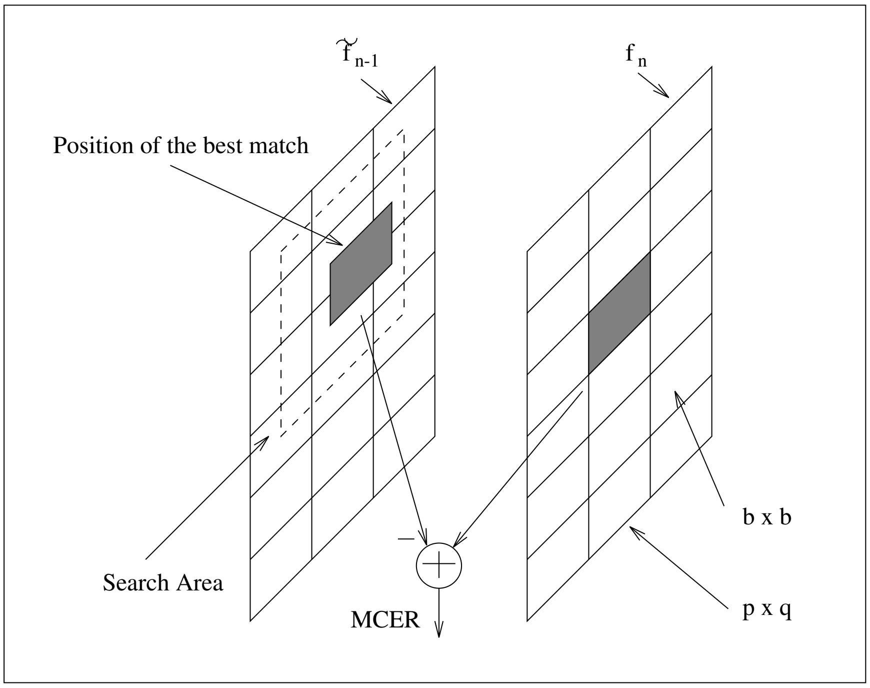

Figure 9.4: Simplified schematic of motion compensation ©J. Streit [98], 1996.

since the previous original frame is not available at the distant decoder and hence without the local decoding operation the distant decoder would have to use the reconstructed version of the previous frame in its attempt to reconstruct the current frame. The absence of the original video frame would lead to a mismatch between the operation of the encoder and decoder, a phenomenon, which will become more clear during our further elaborations.

In order to accomplish motion compensation, the current block to be encoded is slid over the previously stipulated search region of the locally decoded previous frame and the location of the highest correlation is deemed to be the destination of the motion translation. As suggested by Figure 9.4, motion compensation (MC) is then carried out by subtracting the appropriately motion translated previous 'locally decoded' block from the current block to be encoded, in order to generate the so-called motion compensated error residual (MCER). Clearly, the image is decomposed in motion translation described by means of the MVs and in the MCER. Both the MVs and the MCER have to be encoded and transmitted to the decoder for image reconstruction.

Again, the motion compensation removes the temporal inter-frame redundancy and hence the variance of the MCER becomes typically lower than that of the original image, unless there is a substantial amount of new information introduced in the current frame, which cannot be predicted on the basis of the previous frame. Hence MC typically improves the codec's bit-rate economy, although in high quality video coding, where there is a limited interframe correlation due to newly introduced picture objects, the situation is often reversed. This is mainly due to the fact that albeit the MC-engendered MCER-reduction is rather modest, a substantial fraction of the bit-rate budget must be dedicated to the encoding of the MVs. Efficient codecs can circumvent this problem by carrying out an intra/inter-coded decision on a block-by-block basis, which is signalled to the decoder using a one-bit flag. This measure prevents the codec from 'wasting' bits on encoding the inefficient motion vectors in the case of blocks, where the inter-frame correlation is low. Having considered the basic principles of motion compensation, let us now consider how the MCER can be encoded for transmission to the decoder.

The MCER frame can be represented using a range of techniques [102, 112], including subband coding [85,86] (SBC), wavelet coding [87], Discrete Cosine Transformation [78,79,99,103] (DCT), vector quantisation (VQ) [90, 91] or Quad-tree [88,89,95,100] (QT) coding. In this chapter we will restrict our treatment of video compression issues to a rudimentary overview, the interested reader is referred to the literature cited above, in order to probe further, although some aspects of DCT-based MCER-coding schemes will be discussed during our forthcoming elaborations.

When a low codec complexity and low bit-rate are required, the motion compensation technique described above can be replaced by a simple technique, often referred to as frame-differencing. In frame-differencing the whole of the previous locally decoded image frame is subtracted from the frame to be encoded without the need for the above correlation-based motion prediction, which may become very computationally intensive for high-resolution, high-quality video portraying high-dynamic scenes. The schematic of such a simple video codec based on simple frame-differencing is shown in Figure 9.5, which will be described in the next paragraph. Although the variance or energy of the MCER remains somewhat higher for frame-differencing than in case of full motion compensation, there is no pattern-matching search, which reduces the complexity and no MVs have to be encoded, which may reduce the overall bit-rate.

Returning to Figure 9.5, observe that after frame-differencing the encoded MCER is conveyed to the transceiver and also locally decoded. As mentioned earlier, this is necessary to be able to generate the locally reconstructed video signal, which is invoked by the encoder in subsequent MC steps. Again, the encoder uses the locally reconstructed, rather than the original input video frames in the MC process, since the original uncoded frames are unavailable at the decoder. Hence invoking the original previous video frame at the encoder, while the reconstructed one at the decoder, would result in 'mis-alignment' between the encoder and decoder

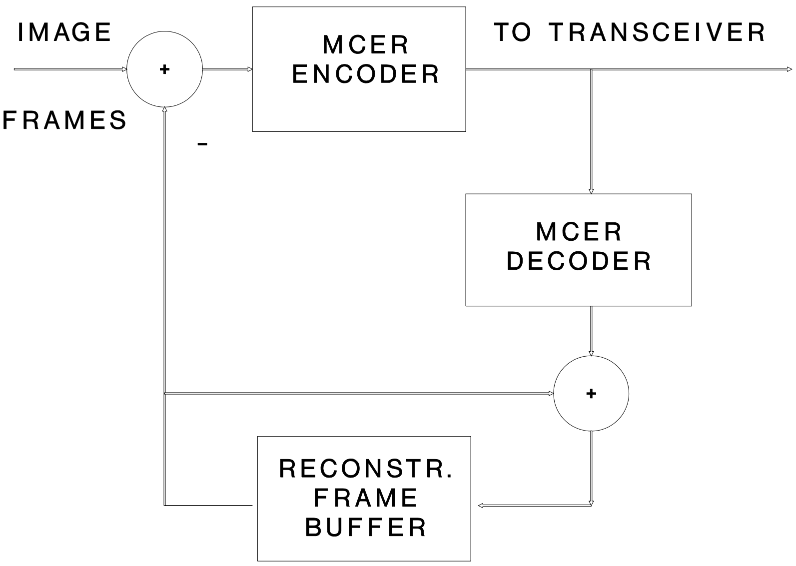

Figure 9.5: Simple video codec schematic.

due to using different frames at both ends for motion compensation. This so-called local reconstruction operation is carried out by the adder in the Figure, superimposing the decoded MCER on the previous locally decoded video frame. The philosophy of the codec's operation is similar, if full MC is used. As alluded to before, efficient codecs, such as for example the ITU H.263 scheme [112], often combine the so-called inter-frame and intra-frame coding techniques on a block-by-block basis, where MC is employed only if it was deemed advantageous in MCER reduction terms.

In case of highly correlated consecutive video-frames the MCER typically exhibits 'line-drawing' characteristics, where large sections of the frame difference signal are 'flat', characterised by low pixel magnitude values, while the motion contours, where the frame differencing has failed to predict the current pixels on the basis of the previous locally decoded frame, are represented by larger values. Consequently, efficient MCER residual coding algorithms must be able to represent such textured MCER patterns adequately. Again, some examples of encoding the MCER efficiently by subband coding [85, 86] (SBC), wavelet coding [87], Discrete Cosine Transformation [78,79,99,103] (DCT), vector quantisation (VQ) [90,91] or Quad-tree [88,89,95,100] (QT) coding can be found in the literature [112]. At this point we concentrate our attention on the rudimentary portrayal of a fixed-rate DCT-based videophone codec, suitable for the proposed multimedia system.

9.3.3 A Fixed-rate Videophone Codec [22, 99][2]

In this subsection we set out to briefly describe the philosophy of fixed-rate video source coding, which was portrayed in depth in references [99–102, 112] by Streit and Hanzo. The particular codec advocated here was detailed in reference [99]. The video codec's outline is depicted in Figure 9.6, which will be detailed below. The coding algorithm was designed to produce a fixed, but programmable bit-rate, which was adjusted to 852 bits/90 ms$\approx$9.47 kbps in order to match the bit-packing requirements of the proposed 30 kHz bandwidth system. The codec's operation is initialised in the intra-frame coded mode, but once it switched to the inter-frame coded mode, any further mode switches are optional and only required if a drastic video scene change occurs.

9.3.3.1 The Intra-Frame Mode

As seen at the bottom of Figure 9.6, in the intra-frame mode the encoder transmits the coarsely quantised block averages for the current frame, which provides the low-resolution initial frame required for the operation of the inter-frame codec at the commencement of video communications. This results in a very coarse intra-frame coded initial frame, which is used by the inter-frame coded mode of operation in order to improve the video quality in successive coding steps. This initial 'warm-up' phase of the codec typically is imperceptible to the untrained viewer, since it typically takes less than 1-2 s and it is a consequence of the fixed bit-rate constraint imposed by contemporary second-generation mobile radio systems.

Furthermore, the intra-frame mode is also invoked during later coding stages in a number of blocks in order to mitigate the effect of transmission errors and hence prevent encoder/decoder misalignment, as it will be detailed during our later elaborations. In this context this operation is often referred to as partial forced updating (PFU), since the specific blocks concerned are partially updated by superimposing an attenuated version of the intra-frame coded block averages. For 176×144 pixel CCITT standard Quarter Common Intermediate Format (QCIF) images we limited the number of video encoding bits per frame to 852. In order to transmit all block averages with a 4-bit resolution, while not exceeding the 852 bits per video frame budget, the forced-update block size was fixed to 11×11 pixels, since there are 852/4=213 blocks that can be encoded on this basis, yielding a block size of $176\times144/213 \approx 119$ or 11×11 pixels.

9.3.3.2 Cost/Gain Controlled Motion Compensation

In motion-compensation often 8×8 blocks are used, since the associated MC complexity of the correlation operation would be quadrupled due to

[2] This subsection is supported by a down-loadable video compression demonstration package under the WWW address http://www-mobile.ecs.soton.ac.uk

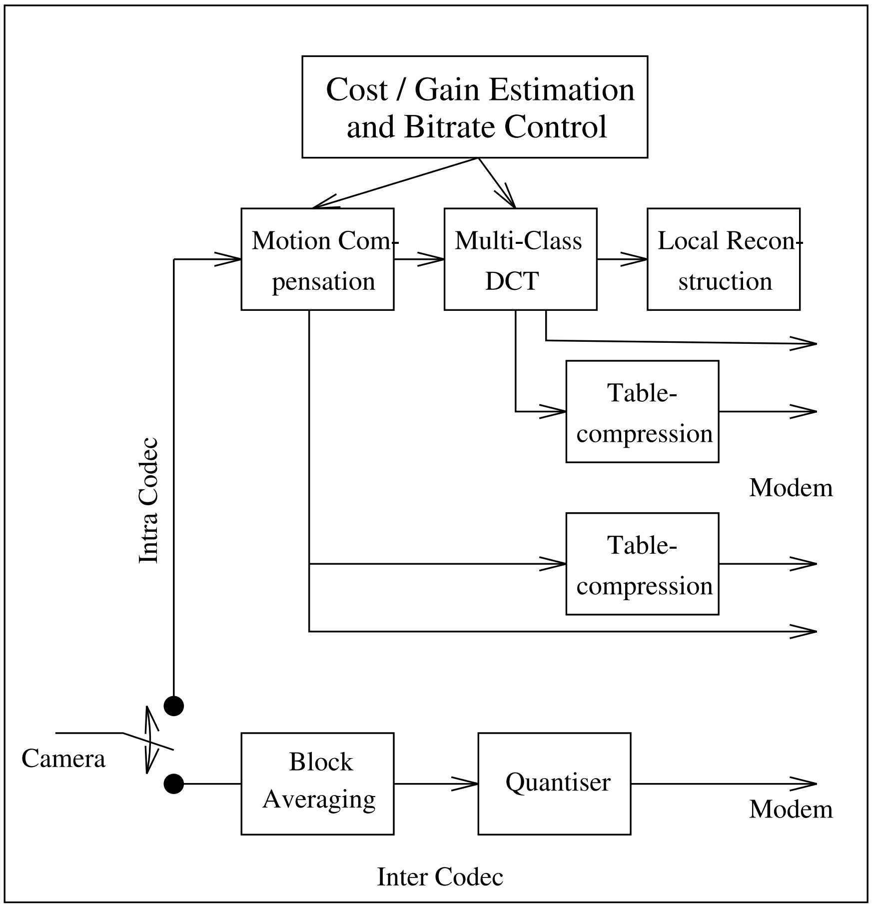

Figure 9.6: Fixed-rate DCT-based codec schematic ©Kluwer, Hanzo, Streit et al, 1995 [22].

doubling the block size, although the number of MVs could be reduced to a quarter - at the cost of some MCER reduction penalty. At the commencement of the encoding procedure the motion compensation (MC) scheme determines a MV for each of the 8×8 blocks using full-search [103, 112]. The MC search window is fixed to 4 × 4 pixels around the centre of each block and hence a total of 4 bits are required for the encoding of 16 possible positions for each MV. Although this search window is relatively small, it was found adequate in limited-motion head-and-shoulders videotelephony. Before the actual motion compensation takes place, the codec tentatively determines the potential benefit of the motion compensation in terms of motion compensated error energy reduction. Then the codec selects those blocks as 'motion-active' ones, whose MCER reduction gain exceeds a cer-

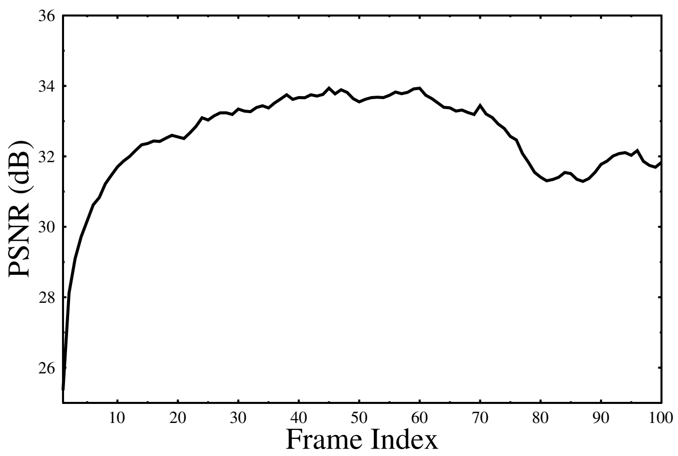

Figure 9.7: PSNR versus frame index performance of the 9.47 kbps video codec for the 'Miss America' sequence, ©Kluwer, Hanzo, Streit et al, 1995 [22].

tain threshold. This method of classifying the blocks as 'motion-active' and 'motion-passive' results in an 'active/passive table', which consists of a one bit activity flag for each block, marking it as passive or active. In case of 8×8 blocks and 176×144 pel QCIF images this table consists of 396 entries, which can be compressed using a technique reminiscent of a two stage so-called quad-tree based compression [99, 112], the details of which are beyond the scope of this chapter As a result, a typical 396-bit active/passive table containing 30 active flags can be compressed to less than 150 bits.

This implies that constrained by the extremely low bit-rate budget of 852 bits/frame, in this codec only a total of about 30 8×8 blocks can be marked as motion-active, corresponding to about 10% of the total video frame area. For the remaining motion-passive blocks simple frame-differencing is invoked, since employing full motion compensation is not justified in terms of the achievable MCER reduction, especially in the light of the required MC search complexity and the increased number of MV encoding bits.

If, however, the number of bits allocated to the compressed activity tables and active motion vectors exceeds half of the total number of available bits/frame, i.e. 852/2=426, a number of blocks satisfying the motion-active criterion will be relegated to the motion-passive class. This process takes account of the subjective importance of various blocks and does not ignore motion-active blocks in the central eye and lip regions of the image, while relegating those, which are closer to the fringes of the image. Pursuing a similar approach, gain control is also applied to the Discrete Cosine Transform (DCT) based compression [103] of the MCER. Let us however initially consider briefly the philosophy of DCT-based compression in the next section.

9.3.3.3 Transform Coding

9.3.3.3.1 One-dimensional Transform Coding As it is well-known from Fourier theory, signals are often synthesised by so-called orthogonal basis functions, a term, which will be augmented during our further discourse. Specifically, when using Fourier transforms, an analogue time-domain signal, which can be the luminance variation along a scan-line of a video frame, can be decomposed into its constituent frequencies.

For signals, such as the above-mentioned video signal representing the luminance variation along a scan-line of a video frame, orthogonal series expansions can provide a set of coefficients, which equivalently describe the signal concerned. We will make it plausible that these equivalent coefficients may become more amenable to quantisation, than the original time-domain signal.

For example, for a one-dimensional time-domain sample sequence $\{x(n), 0 \le n \le N-1\}$ a so-called unitary transform is given in a vectorial form by $\underline{X} = \underline{\underline{A}}\underline{x}$, which can also be expressed in a less compact scalar form as [103]:

$$X(k) = \sum_{n=0}^{N-1} a(k,n) \cdot x(n), \quad 0 \le k \le N-1 \tag{9.5}$$

where the transform is referred to as unitary, if $\underline{\underline{A}}^{-1} = \underline{\underline{A}}^{*T}$ holds. The associated inverse operation requires us to invert the matrix $\underline{\underline{A}}$ and due to the above-mentioned unitary property we have $\underline{x} = \underline{\underline{A^{-1}X}} = \underline{\underline{A}}^{*T}\underline{X}$, yielding [103]:

$$x(n) = \sum_{k=0}^{N-1} X(k) a^*(k,n), \quad 0 \le k \le N-1 \tag{9.6}$$

which gives a **series expansion** of the time-domain sample sequence $x(n)$ in the form of the **transform coefficients** $X(k)$. The columns of $\underline{\underline{A}}^{*T}$, i.e. the vectors $\underline{a_k^*} \triangleq \{a^*(k,n), 0 \le n \le N-1\}$ are the so-called basis vectors of $\underline{\underline{A}}$ or the **basis vectors of the decomposition**. According to the above principles the time-domain signal $x(n)$ can be equivalently described in the form of the **decomposition** in Equation 9.6, where the **basis functions** $a^*(k,n)$ are weighted by the transform coefficients $X(k)$

and then superimposed on each other, which corresponds to their summation at each pixel position of the transformed block. The transform-domain weighting coefficients $X(k)$ can be determined from Equation 9.5.

The transform-domain coefficients $X(k); k = 0 \cdots N-1$ often give a more 'compact' representation of the time-domain samples $x(n)$, implying that if the original time-domain samples $x(n)$ are correlated, then in the transform-domain most of the signal's energy is concentrated in a few transform-domain coefficients. To elaborate a little further - according to the Wiener-Khintshin theorem - the autocorrelation function (ACF) and the power spectral density (PSD) are Fourier transform pairs. Due to the Fourier-transformed relationship of the ACF and PSD it is readily seen that a slowly decaying autocorrelation function, which indicates a predictable signal $x(n)$ in the time-domain is associated with a PSD exhibiting a rapidly decaying low-pass nature. Therefore, in the case of correlated time-domain $x(n)$ sequences the transform-domain coefficients $X(k)$ tend to be statistically small for high frequencies, i.e. for high transform coefficient indices and exhibit large magnitudes for low-frequency transform-domain coefficients, i.e. for low transform-domain indices. This concept will be exposed in a little more depth below, but for a deeper exposure to these issues the reader is referred to Jain's excellent book [103].

9.3.3.3.2 Two-dimensional Transform Coding The above one-dimensional signal decomposition can also be extended to two-dimensional (2D) signals, such as 2D image signals of a video frame, as follows [103]:

$$X(k,l) = \sum_{m=0}^{N-1}\sum_{n=0}^{N-1} x(m,n) \cdot a_{k,l}(m,n) \quad 0 \le k,l \le N-1 \tag{9.7}$$

$$x(m,n) = \sum_{k=0}^{N-1}\sum_{l=0}^{N-1} X(k,l) \cdot a^*_{k,l}(m,n) \quad 0 \le m_1 n \le N-1 \tag{9.8}$$

where $\{a^*_{k,l}(m,n)\}$ is a set of discrete two-dimensional basis functions, $X(k,l)$ are the 2D transform-domain coefficients and $\underline{\underline{X}} = \{X(k,l)\}$ constitutes the transformed image.

As in the context of the one-dimensional transform, the two-dimensional (2D) time-domain signal $x(m,n)$ of a video block to be encoded can be equivalently described in the form of the decomposition in Equation 9.8, where the 2D basis functions $a^*_{k,l}(m,n)$ are weighted by the coefficients $X(k,l)$ and then superimposed on each other, which again, corresponds to their summation at each pixel position in the video frame. The transform-domain weighting coefficients $X(k,l)$ can be determined from Equation 9.7. Once a spatially correlated image block $x(m,n)$ of for example $N \times N$=8×8 pixels is orthogonally transformed using the Discrete Cosine Transform

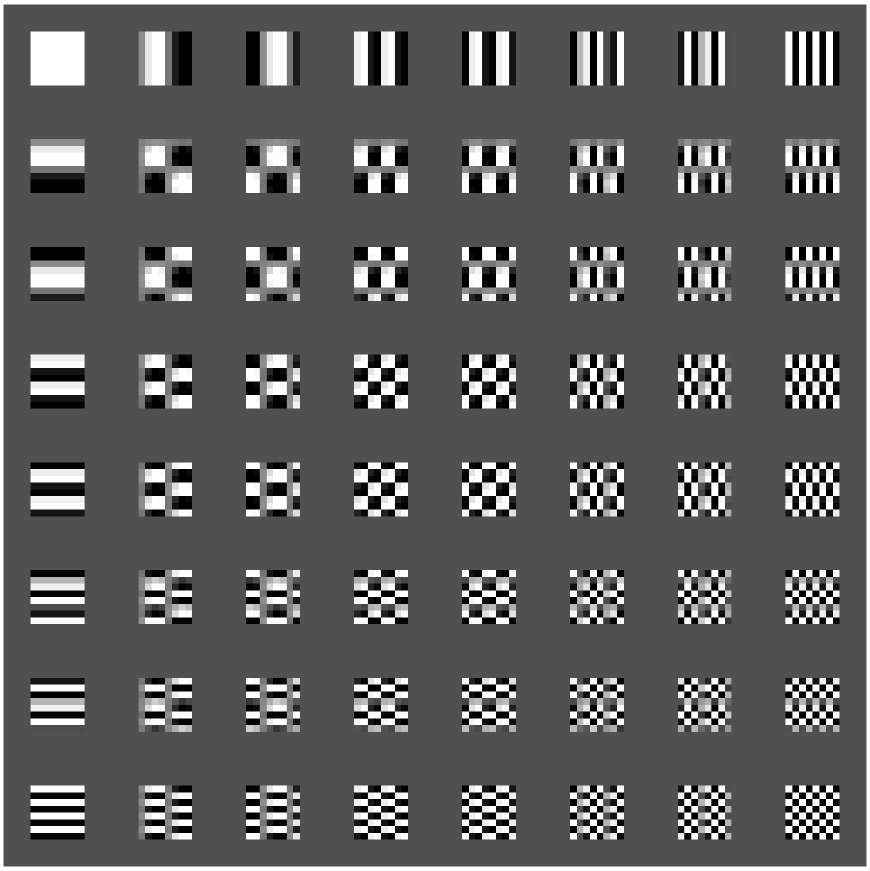

Figure 9.8: 8×8 DCT basis images ©A. Sharaf [104].

(DCT) matrix $\underline{\underline{A}}$ defined as [103]:

$$A_{mn} = \frac{2c(m)c(n)}{N} \sum_{i=0}^{N} \sum_{j=0}^{N} b(i,j) \cos\frac{(2i+1)m\pi}{2N} \cos\frac{(2j+1)n\pi}{2N}$$
$$c(m) = \begin{cases} \frac{1}{\sqrt{2}} & \text{if}(m=0) \\ 1 & \text{otherwise} \end{cases} \tag{9.9}$$

the transform-domain image described by the DCT coefficients can be quantised for transmission to the decoder. **The rationale behind invoking the DCT is that the frequency-domain coefficients $X(k,l)$ can typically be quantised using a lower number of bits, than the original image pixel values $x(m,n)$,** which will be further augmented during our forthcoming discourse.

For illustration's sake the associated two-dimensional 8×8 DCT **basis-**

images are portrayed in Figure 9.8, where for example the top left-hand corner represents the zero horizontal and vertical spatial frequency, since there is no intensity or luminance change in any direction across this basis image. Following similar arguments, the bottom right corner corresponds to the highest vertical and horizontal frequency, which can be represented using 8×8 basis images, since the luminance changes from black to white between adjacent pixels in both the vertical and horizontal directions. Similarly, the basis image in the top right-hand corner corresponds to the highest horizontal frequency, but zero vertical frequency component and by contrast, the bottom left basis image represents the highest vertical frequency, but zero horizontal frequency. **In simple terms the decomposition of Equations 9.7, 9.8 can be viewed as finding the required weighting coefficients $X(k,n)$, in order to superimpose the weighted versions of all the 64 different 'patterns' in Figure 9.8 for the sake of re-constituting the original 8×8 video block.** In other words, each original 8×8 video block is represented as the sum of the 64 appropriately weighted 8×8 basis images.

It is plausible that for blocks, over which the video luminance or gray shade does not change dramatically, i.e. at a low 'spatial frequency', most of the video frame's conveyed energy is associated with these low spatial frequencies. Hence the associated low-frequency transform-domain coefficients $X(k,n)$ are high and the high-frequency coefficients $X(k,n)$ are of low magnitude. By contrast, if there is a lot of fine-detail in a video frame, such as in a finely striped pattern or in a checker-board pattern, most of the video frame's conveyed energy is associated with high spatial frequencies. Most practical images contain more low spatial frequency energy, than high-frequency energy. This is also true for those motion-compensated video blocks, where the motion compensation was efficient and hence resulted in a 'flat' block, associated with a low spatial-frequency. For these blocks therefore most of the high-frequency DCT coefficients can be set to zero at the cost of neglecting only a small fraction of the video block's energy, residing in the high spatial-frequency DCT coefficients. In simple terms this corresponds to gentle low-pass filtering, which in perceptual terms results in a slight blurring of the high spatial-frequency image fine details.

In other words, upon exploiting that the human eye is rather insensitive to high spatial frequencies, in particular, when these appear in moving pictures, the spatial frequency-domain block is amenable to data compression. Again, this can be achieved by more accurately quantising and transmitting the high-energy, low-frequency coefficients, while typically coarsely representing or masking out the low-energy, high-frequency coefficients. We note, however that in motion-compensated codecs there may be blocks along the edges of moving objects, where the MCER does not retain the above-mentioned spatial correlation and hence the DCT does not result in significant energy compaction. Again, for a deeper exposure to the DCT the reader is referred to for example reference [103].

3	2	1	0	0	0	0	0	2	1	0	0	0	0	0	0
2	1	0	0	0	0	0	0	3	2	0	0	0	0	0	0
1	0	0	0	0	0	0	0	1	1	0	0	0	0	0	0
0	0	0	0	0	0	0	0	0	0	0	0	0	0	0	0
0	0	0	0	0	0	0	0	0	0	0	0	0	0	0	0
0	0	0	0	0	0	0	0	0	0	0	0	0	0	0	0
0	0	0	0	0	0	0	0	0	0	0	0	0	0	0	0
0	0	0	0	0	0	0	0	0	0	0	0	0	0	0	0
2	3	1	0	0	0	0	0	2	2	1	0	0	0	0	0
1	2	1	0	0	0	0	0	2	2	0	0	0	0	0	0
0	0	0	0	0	0	0	0	1	0	0	0	0	0	0	0
0	0	0	0	0	0	0	0	0	0	0	0	0	0	0	0
0	0	0	0	0	0	0	0	0	0	0	0	0	0	0	0
0	0	0	0	0	0	0	0	0	0	0	0	0	0	0	0
0	0	0	0	0	0	0	0	0	0	0	0	0	0	0	0
0	0	0	0	0	0	0	0	0	0	0	0	0	0	0	0

Table 9.3: Bit allocation tables for the four DCT quantisers, where the top left-hand corner indicates the number of bits allocated to the DC-component of the DCT ©IEEE, Hanzo, Streit, 1995 [99].

9.3.3.4 Gain Controlled Quadruple-Class DCT

Having reviewed the basics of DCT, let us now return to the DCT-based video codec schematic of Figure 9.6 and consider the specific codec design. Focusing our attention on the gain-controlled DCT-based MCER compression, every 8×8 block is tentatively DCT transformed, quantised and transformed back to the temporal domain, in order to assess the potential benefit of marking the block as DCT-active, when judged in terms of MCER reduction. In order to take account of the above-mentioned time-variant, non-stationary nature of the MCER and its time-variant frequency-domain distribution, four different sets of DCT quantisers were designed. The quantisation distortion associated with each quantiser is computed by quantising the MCER tentatively, in order to be able to choose the best quantiser. This measure improves the video quality at the cost of increased complexity. As it was shown in reference [99], a total of ten bits are allocated for each of the four quantisers, which are characterised by the bit allocation scheme of Table 9.3. The four DCT quantisers correspond to different DCT coefficient energy distributions across the spatial frequency domain, where the top left-hand corner indicates the number of bits allocated to the DC-component of the DCT.

Each quantiser is a trained Max-Lloyd quantiser [103], catering for a specific frequency-domain energy distribution class. However, a joint feature of all of them is that the high-frequency components were masked out. All DCT blocks, whose coding gain exceeds a certain threshold are marked as DCT-active, resulting in a similar 'active/passive table' as for the motion vectors. For the DCT-activity table we also applied the same run length compression technique [99, 112], as above in the context of the motion activity table. Again, if the number of bits required for the encoding of the DCT-active blocks exceeds half of the maximum allowable number of bits, i.e. 852/2=426, the blocks around the fringes of the image are considered DCT-passive, rather than those in the central eye and lip sections. If, however, the active DCT coefficients and activity-tables do not fill the 852-bit fixed-length transmission burst, the number of active DCT blocks is increased and all activity tables are recomputed.

The codec's bit-allocation scheme is summarised in Table 9.4. The so-called frame-alignment word (FAW) or unique word is used to allow the codec to re-synchronise at the beginning of each 852-bit frame in the case of transmission errors. Furthermore, 22 blocks out of the 25 384 pixels/(8 $\cdot$ 8)=396-block QCIF frame are partially forced up-dated using the block means, partially overlaid on the contents of the local reconstructed frame buffer in order to enhance the codec's robustness. The corresponding bit-rate contribution seen in the Table due to PFU is 22$\times$4=96 bits. A total of 30 blocks are marked as DCT- and motion-active, yielding a total of 852 bits per frame, or a video rate of 852 bits/90 ms$\approx$9.47 kbps, as seen in Table 9.4.

FAW	PFU	MV	DCT	Total
22	22$\times$4	< 376	< 376	852

Table 9.4: Video codec bit allocation scheme [98] Streit, 1996.

The encoded FAW, PFU, MV and DCT parameters are then transmitted to the decoder and also locally decoded in order to be used in future motion predictions. The video codec's Peak Signal to Noise Ratio (PSNR) versus frame index performance is shown in Figure 9.7, where an average PSNR of about 33.3 dB was achieved for the widely used QCIF-resolution Miss America (MA) sequence.

The associated subjective video quality is adequate for the transmission of low-activity head-and-shoulders videophone sequences, but for high-activity sequences typically higher transmission rates are required. Consequently, the higher video-rate necessitates the allocation of more than one speech slot per transmission frame for video communications, which may compromise the voice capacity of the multi-media system. In this respect a higher flexibility can be guaranteed by the 200 kHz bandwidth system to be described in Section 9.7.3, which is capable of supporting more timeslots and users than the 30 kHz system of Section 9.7.2.

For a more detailed discourse on the proposed video codec the interested reader is referred to [99, 112]. Further fixed-rate wireless videophone systems were proposed in references [100, 101, 112], which are based on

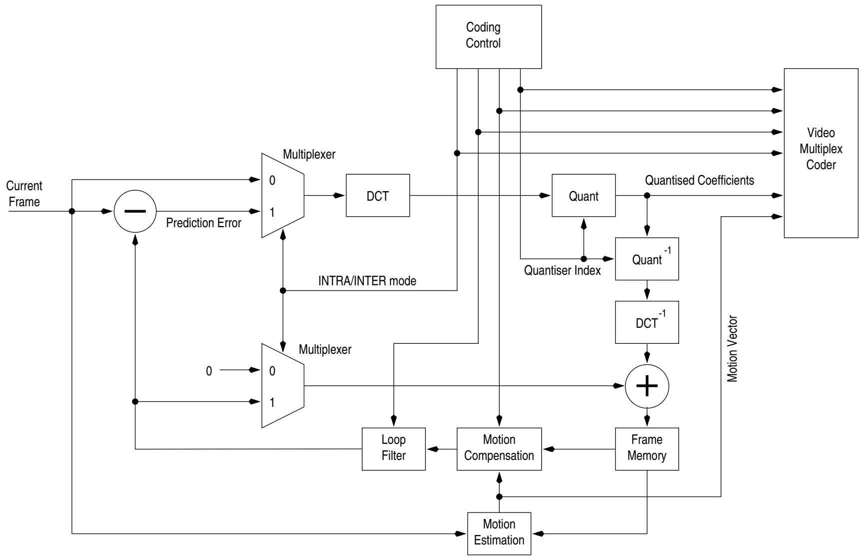

Figure 9.9: Simplified H.261/H.263 schematic©Cherriman [105] 1995.

fixed-rate QCIF codecs operating in the range of 8-13 kbps at 10 frames/s. As expected, the performance of these video codecs improves, as the affordable bit-rate increases and adequate subjective videophone quality can be maintained for moderate-activity QCIF images at bit-rates in excess of 8-15 kbps, when using a scanning rate around 10 frames/s. As mentioned before, in references [106]- [112] Cherriman and Hanzo proposed various system design alternatives based on the H.263 standard video codec, which will be briefly highlighted below.

9.3.4 The H.263 Standard Video Codec

As a potential programmable-rate design alternative to the previously proposed fixed-rate video codec, here we briefly introduce the H.261 and H.263 ITU standard codecs [105, 112], which will be employed in our 200 kHz bandwidth candidate system described in Section 9.7.3. Although the H.263 codec is flexible in terms of supporting five different video resolutions, including the 288×352 pixel ITU Common Intermediate Format (CIF), the Quarter CIF (QCIF), Sub-QCIF (SQCIF), as well as the higher resolution 4×CIF and 16×CIF video formats, for low-rate wireless videophony we are restricted to QCIF or SQCIF images. The full description of the H.263 codec can be found in reference [72], while various features of the proposed video system were discussed in [106]- [112], hence here only a brief exposure is offered.

The H.261 and H.263 codecs share the simplified schematic of Figure 9.9 and they operate under the instructions of the coding control block, selecting the required inter/intra frame mode, the quantisation and bit-allocation scheme etc. Similarly to our previously described fixed-rate codec, DCT [103, 115] is invoked also in the H.261/H.263 codecs of Figure 9.9, in order to compress either the blocks of the current original frame in the intra-frame coded mode or the motion compensated prediction error blocks in the inter-frame coded mode. This is controlled by the Multiplexer in the Figure. Whether the intra- or inter-frame coded mode is enabled by the Coding Control block, depends on a number of factors, such as the required bit-rate, robustness against channel errors, etc. As mentioned before, there may be input sequences, for which intra-frame coding is just as efficient as inter-frame coding, since due to the lack of correlation in the motion compensated error residual the DCT does not always lead to energy compaction.

A large selection of quantisers are stored and invoked in the H.261/H.263 codecs, depending on the required bit-rate and video quality, where again, the index of the quantiser to be used is selected by the Coding Control block of Figure 9.9. The quantised DCT coefficients are then transmitted to the decoder via the Video Multiplex Coder and also locally inverse-quantised by the QUANT^{-1} block, before inverse-DCT (DCT^{-1}) is employed, in order to generate the locally decoded replica of the signal that was subjected to DCT. Specifically, to reconstruct either the motion compensated prediction error or the original intra-coded current frame, in the latter case the '0' signal shown in the schematic of Figure 9.9 is gated through by the Multiplexer in order to reconstruct and store the locally decoded frame in the Frame Memory. In contrast, if inter-frame coding is used, the locally decoded motion prediction error is gated through by the Multiplexer and added to the previous locally decoded frame.

Observe in the Figure that in the inter-frame coded mode both the current video frame and the previous locally decoded frame that was stored in the Frame Memory are input to the Motion Estimation block, which then generates the Motion Vectors. The MVs are transmitted to the decoder and are also employed by the Motion Compensation block in order to properly position the best matching replica of the current block to be encoded, which was identified in the previously reconstructed block. Motion compensation is then carried out by subtracting the motion translated best matching block of the previous decoded frame from the current original block. Finally, all encoded information is multiplexed for transmission by the Video Multiplex Coder.

The H.263 [72, 73, 112] ITU standard codec scheme is in many respects similar to its predecessor, the H.261 codec [74, 112], but it incorporates a number of recent advances in the field, such as for example using half-pixel resolution in the motion compensation, which improves the MC process and hence reduces the variance of the MCER. Invoking the half-pixel resolution requires an interpolation process, which generates an additional pixel amongst all the existing pixels and hence supports a potentially improved MC process at the cost of an increased complexity. Furthermore, the H.263 scheme allows configuring the codec for a lower datarate or better error resilience and supports four so-called 'negotiable coding options', which are detailed in the Recommendation. These negotiable options can be 'negotiated' by the encoder and decoder about to commence communications, in order to use the 'lowest common denominator' of their optional features in their communications.

The bitstream generated by the H.261 and H.263 codecs is structured in a number of hierarchical layers, including the so-called picture layer, group of blocks layer, macroblock layer and block layer [72, 73], each of which represents a gradually reduced-size video-frame segment, commencing with specifying the coded information of the whole video frame - down to the 8×8 block layer. In order to allow a high grade of flexibility and to adapt to various images, each of these layers has a 'self-descriptive' structure, specifying the various coding parameters of the given layer. The coded information of the upper three layers commences with a unique word, allowing the codec to re-synchronise after loss of synchronisation following transmission errors. The 'self-descriptive' received bitstream typically informs the decoder as to the inter- or intra-coded nature of a frame, the video resolution used, whether to expect any more information of a certain type, the index of the currently used quantiser, the location of encoded blocks containing large transform coefficients, etc.

The H.263 scheme achieves a high compression ratio for transmissions over channels exhibiting a low bit error rate, but since the bit stream is 'self-descriptive', any transmission error can corrupt the segments describing the coding parameters used, resulting in catastrophic error events associated with using mismatching decoders. Hence the H.263 codec is rather vulnerable to channel errors. In references [106]- [112] Cherriman and Hanzo reported on the design of a low-rate video transceiver, where the H.263 codec was constrained to operate at a near-constant bit-rate using an appropriate bit-rate control and packetisation algorithm, which adjusted the quantiser such that it would output the required number of bits per frame. Furthermore, using a low-rate feedback channel, the contents of the local and remote decoder was 'frozen', when transmission errors occurred, which prevented the propagation of errors across blocks and allowed the codec to operate over hostile wireless channels. A more detailed exposure of video compression and transmission aspects is provided in the monograph [112].

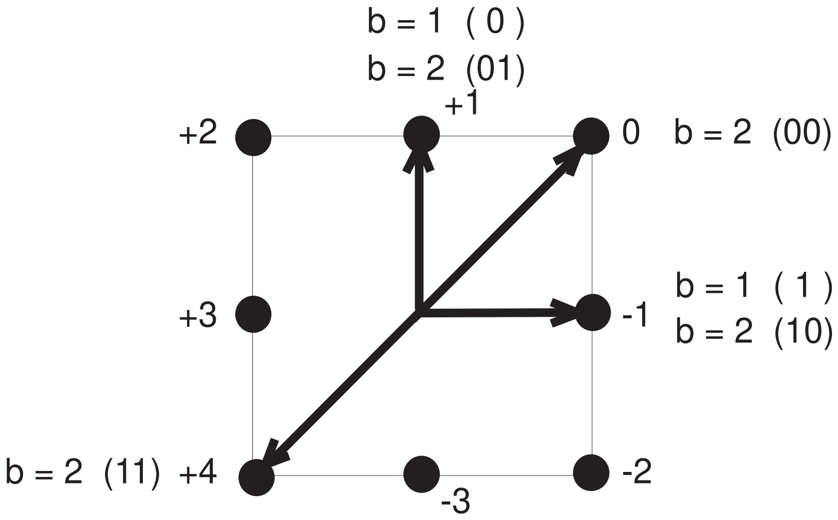

Figure 9.10: Coding ring ©ETT, Hanzo and Yuen [195].

9.4 Graphical Source Compression

9.4.1 Introduction to Graphical Communications

Telewriting is a multi-media telecommunication service enabling the bandwidth-efficient transmission of handwritten text and line graphics through fixed and wireless communication networks [196]- [201]. Differential chain coding (DCC) has been successfully used for graphical communications over E-mail networks or teletext systems [198], where bit-rate economy is achieved by exploiting the correlation between successive vectors. reference [202] addressed also some of the associated communications aspects. A plethora of further excellent treatises were contributed to the literature of chain coding by R. Prasad and his colleagues from Delft University [198]- [205].

9.4.2 Fixed-Length Differential Chain Coding

In chain coding (CC) a square-shaped coding ring is slid along the graphical trace from the current pixel, which is the origin of the legitimate motion vectors, in steps represented by the vectors portrayed in Figure 9.10. The bold dots in the Figure represent the next legitimate pixels during the graphical trace's evolution. In principle the graphical trace can evolve to any of the surrounding eight pixels and hence a three-bit codeword is required for lossless coding. Differential chain coding [199]- [201] (DCC) exploits that the most likely direction of stylus movement is a straight extension, with a diminishing chance of 180^o turns. This suggests that the

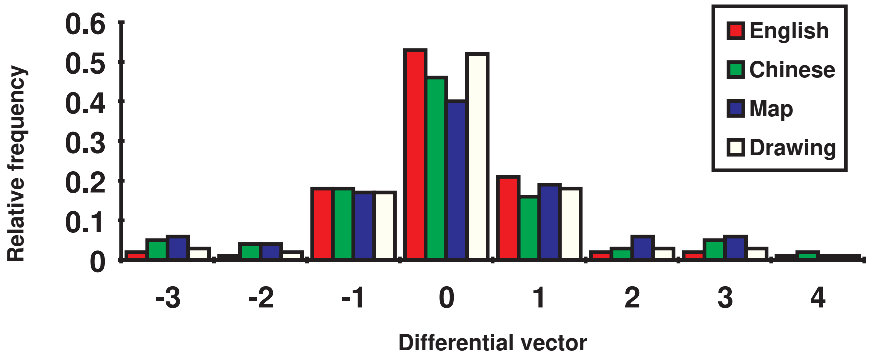

Figure 9.11: Relative frequency of differential vectors for a range of dynamo-graphical source signals ©ETT, Hanzo and Yuen [195].

coding efficiency can be improved using the principle of entropy coding by allocating shorter codewords to more likely transitions and longer ones to less likely transitions. This argument is supported by the histogram of the differential vectors of a range of graphical source signals, including English and Chinese handwriting, a Map and a technical Drawing, portrayed in Figure 9.11, where the vectors 0, +1 and -1 are seen to have the highest relative frequency.

In this section we embark on exploring the potential of a novel graphical coding scheme dispensing with the variable length coding principle of conventional DCC codecs, which we refer to therefore as fixed length differential chain coding (FL-DCC). FL-DCC was contrived in order to comply with the time-variant resolution- and/or bit-rate constraints of intelligent adaptive multi-mode terminals, which can be re-configured under network control, in order to satisfy the momentarily prevailing tele-traffic, robustness, quality, etc. system requirements. In order to maintain lossless graphics quality under lightly loaded traffic conditions, the FL-DCC codec can operate at a rate of $b = 3$ bits/vector, although it has a higher bit-rate than DCC. However, since in voice and video coding typically perceptually unimpaired lossy quantisation is used, we embark on exploring the potential of the re-configurable FL-DCC codec under $b < 3$ low-rate, lossy conditions.

Based on our findings in Figure 9.11 concerning the relative frequencies of the various differential vectors, we decided to evaluate the performance of the FL-DCC codec using the $b = 1$ and $b = 2$ bit/vector lossy schemes. As demonstrated by Figure 9.10, in the b = 2-bit mode the transitions to pixels -2, -3, $+2$, $+3$ are illegitimate, while vectors 0, $+1$, -1 and $+4$ are legitimate. In order to minimise the effects of transmission errors the Gray codes seen in Figure 9.10 were assigned. It will be demonstrated

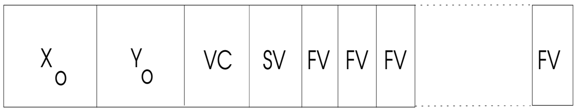

Figure 9.12: Coding syntax ©ETT, Hanzo and Yuen [195].

that, due to the low probability of occurance of the illegitimate vectors, the associated subjective coding impairment is minor. Under degrading channel conditions or higher tele-traffic load the FL-DCC coding rate has to be reduced to $b = 1$, in order to be able to invoke a less bandwidth efficient, but more robust modulation scheme or to generate less packets contending for transmission. In this case only vectors +1 and -1 of Figure 9.10 are legitimate. The subjective effects of the associated zig-zag trace will be removed by the decoder, which can detect these characteristic patterns and replace them by a fitted straight line.

In general terms the size of the coding ring is given by $2n\tau$, where $n = 1, 2, 3 \ldots$ is referred to as the order of the ring and τ is a scaling parameter, characteristic of the pixel separation distance. Hence the ring shown in Figure 9.10 is a first order one. The number of nodes in the ring is $M = 8n$.

The data syntax of the FL-DCC scheme is displayed in Figure 9.12. The beginning of a trace can be marked by a typically 8 bit long pen-down (PD) code, while the end of trace by a pen-up (PU) code. In order to ensure that these codes are not emulated by the remaining data, if this were incurred, bit stuffing must be invoked. We found however that in complexity and robustness terms using a 'vector counter' (VC) for signalling the trace-length to the decoder constituted a more attractive alternative for our system. The starting coordinates X_0, Y_0 of a trace are directly encoded using for example 10 and 9 bits in the case of a video graphics array (VGA) resolution of 640×480 pixels.

The first vector displacement along the trace is encoded by the best fitting vector defined by the coding ring as the starting vector (SV). The coding ring is then translated along this starting vector to determine the next vector. A differential approach is used for the encoding of all the following vectors along the trace, in that the differences in direction between the present vector and its predecessor are calculated and these vector differences are mapped into a set of 2^b fixed length b-bit codewords, which we refer to as 'fixed vectors' (FV). We will show that the coding rate of the proposed FL-DCC scheme is lower for $b = 2$ and $b = 1$ than that of DCC.

When a curve is encoded by FL-DCC, it is sliced by the coding ring into small segments. Consider a sampled curve segment s. Let v be the vector link produced by the coding ring. The coding rate of a chain code

	$b = 1$ bit/vector	$b = 2$ bit/vector	DCC bit/vector
English script	0.8535	1.7271	2.0216
Chinese script	0.8532	1.7554	2.0403
Map	0.8536	1.7365	2.0396
Drawing	0.8541	1.7911	1.9437
Theoretical	0.9	1.80	2.03

Table 9.5: Coding rate comparison.

is defined [198], [200] in bits per unit length of the curve segment as

$$r = \frac{E[b(s,v)]}{E[l_n(s)]} \tag{9.10}$$

where $b(s,v)$ is the number of bits used to encode a vector link v, $l_n(s)$ is the length of the curve segment s, while $E(x)$ represents the expected value of a random variable x. It has been shown [201] that for the set of all curves, the product of a segment length $l_n(s)$ and the probability $p(\alpha)$ that this segment occurs with a direction α must be constant. Thus the expected curve segment length for a ring of order n is given by [199]:

$$E[l_n(s)] = \int_0^{\pi/4} \frac{8 \cdot n \cdot \tau}{\cos\alpha} \cdot p(\alpha) d\alpha = \frac{\pi \cdot n \cdot \tau}{2 \cdot \sqrt{2}}. \tag{9.11}$$

Therefore, the theoretical coding rate of FL-DCC becomes:

$$r = \frac{E[b(s,v)]}{\pi \cdot n \cdot \tau / (2 \cdot \sqrt{2})}. \tag{9.12}$$

The theoretical and experimental coding rates of the $b = 1$ and $b = 2$ FL-DCC schemes are shown in Table 9.5. In the next Section the associated transmission issues are considered.

9.4.3 FL-DCC Graphical Codec Performance

The performance of the proposed FL-DCC graphical codecs was evaluated for a range of graphical source signals, including an English script, a Chinese script, a drawing and a map using a coding ring of $M = 8$. Table 9.5 shows the associated coding rates produced by FL-DCC for $b = 1$ and $b = 2$ as well as by DCC along with the corresponding theoretical coding rates. Both FL-DCC schemes achieve a lower coding rate than DCC. The corresponding subjective quality is portrayed in Figure 9.13 for two of the input signals previously used in Table 9.5. Observe that for $b = 2$ no subjective degradation can be seen and the degradation associated with $b = 1$ is also fairly low. This is due to the fact that the typical fuzzy granular error pat-

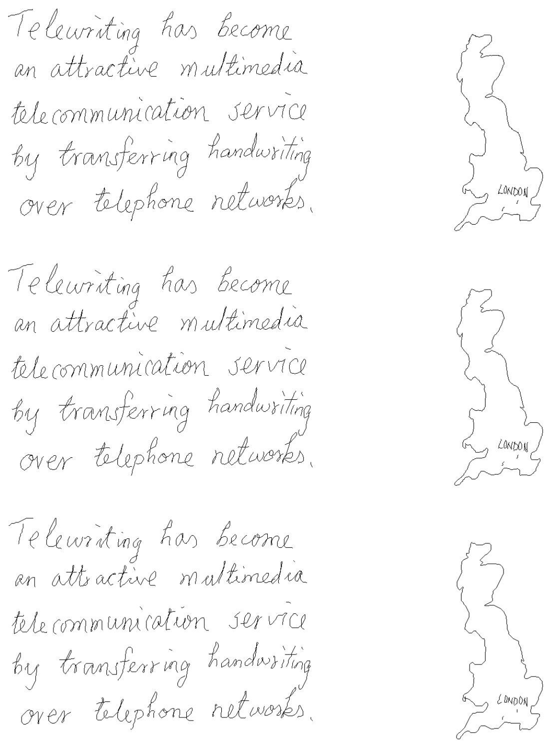

Figure 9.13: Decoded information for FL-DCC with $b = 1$ (bottom), $b = 2$ (centre) and DCC (top).

terns inflicted by the $b = 1$ FL-DCC scheme, when a straight line section is approximated by a zig-zag pattern, can be detected and smoothed by the decoder. The overall graphical system performance will be highlighted in the forthcoming system performance section.

Following the above speech, video and graphical source coding issues, we now address the transmission aspects of the proposed multi-media systems. Let us initially consider the factors affecting the choice of modulation.

9.5 Modulation Issues

9.5.1 Choice of Modulation

The appropriate choice of the modem scheme is based on the interplay of equipment complexity, power consumption, spectral efficiency, robustness against channel errors, co-channel and adjacent channel interference as well as the propagation phenomena, which depends on the cell size. Equally important are the associated issues of linear or non-linear amplification and filtering, the applicability of non-coherent, differential detection, soft-decision detection, equalisation and other associated issues [2], most of which will be addressed in a certain depth during our further discourse. The above, often conflicting factors led to a proposal by the European Research in Advanced Communications Equipment (RACE) project, which is referred to as the Advanced Time Division Multiple Access (ATDMA) initiative [116, 117]. This proposal did not become a third-generation standard. Nonetheless, the main features of the ATDMA system framework are interesting, since this proposal reflects the philosophy and spirit of discussions leading to the European UMTS standard proposals to be highlighted in Chapter 10. Furthermore, some of the ATDMA features may influence the evolution of existing second-generation systems, such as GSM. Hence the main ATDMA features are summarised in Table 9.6 [116, 117], which will be described during our forthcoming discourse. Suffice to say at this stage that these features were defined on the basis of providing higher bitrates and bandwidth-efficiency for benign indoor picocells, while ensuring backwards compatibility with existing second-generation systems, such as GSM, for example.

Specifically, the Pan-European GSM system described in Chapter 8 or the Digital European Cordless Telecommunications (DECT) scheme highlighted in Chapter 1 employ constant envelope partial response Gaussian Minimum Shift Keying (GMSK), which was the topic of Chapter 6. The main advantage of GMSK is that since it is a so-called constant envelope modulation scheme, it ignores any fading-induced or amplifier-specific amplitude fluctuations present in the received signal and hence facilitates the utilisation of power-efficient non-linear class-C amplification. In benign pico- and micro-cellular propagation conditions, however, low transmitted power and low signal dispersion are the typical characteristics. Hence the employment of more bandwidth efficient multilevel modulation schemes becomes realistic [2]. In fact the American IS-54 [14] and JDC [15] second-generation digital systems have already opted for 2 bits/symbol modulation. in the case of the so-called multi-level full-response modulation schemes the influence of each modulation symbol is restricted to its own signalling interval, as opposed to the partial response GMSK modems of Chapter 6. Since these multi-level modems have not been treated in preceeding chapters of this book, this section attempts to provide a rudimentary overview of some of the associated multi-level modulation issues in a slightly more detailed style. For a more detailed account on full-response multi-level modulation schemes the reader is referred to [2].

Returning to Table 9.6, the ATDMA European proposal identified the following cellular structures, as the most typical propagation environments: 'long' or large macro cells, 'short' or small macro cells, micro cells and pico

Cell type	Long-macro	Short-macro	Micro	Pico
Modulation	GMSK	4/16-QAM		
Baud-rate (kBd)	360	225	900	
Carrier spacing (kHz)	276.92		$1107.69 = 4 \times 276.92$	
Bit-Rate (kbps)	360	450/900	1800/3600	
Bwidth eff. (bps/Hz)	1.3	1.625/3.25		

Table 9.6: ATDMA cell types and modulation schemes.

cells. As the propagation environment becomes more friendly, higher channel SNRs may be maintained and hence more bandwidth-efficient modem schemes can be employed, moving from the 1 bit/symbol partial-response GMSK scheme to 2 bits/symbol or even to 4 bits/symbol full-response signalling. In ATDMA parlance the latter two schemes are referred to as 1 and 2 bits/symbol Offset Quadrature Amplitude Modulation (OQAM), where the so-called inphase (I) and quadrature phase (Q) components are offset by half of the signalling interval, which will limit the encountered signal envelope swing, since only one of the I and Q components can change at any instant. Hence OQAM is less sensitive to power amplifier non-linearities [2] than conventional QAM, since the latter allows a simultaneous change of both the I and Q components. In conventional terminology, however, 1 and 2 bits/symbol OQAM corresponds to 4-level or 16-level QAM, which is our preferred terminology. Here we will restrict our treatment to a rudimentary overview of QAM techniques; for a more detailed treatise on the subject the interested reader is referred to reference [2].

Observe furthermore in Table 9.6 that the carrier spacing and signalling rate are also different for the various cell sizes, which is a consequence of the lower signal dispersion or excess delay spread of picocells due to their low transmitted power and propagation distances. This is justified for example by the fact that the large-cell GSM system at a signalling rate of 271 kbps using a bit-interval of 3.69 μs experiences dispersive long-delay multipath components and hence requires a channel equaliser, while DECT at 1152 kbps, where the bit-interval duration is reduced by a factor of four, does not. The 'long-macro' GMSK ATDMA signalling rate is then 360 kBaud, which results in a bandwidth efficiency of 360 kBaud/276.92 kHz=1.3 bps/Hz. This is very similar to the 271 kbps/200 kHz$\approx$1.35 bps/Hz GSM bandwidth efficiency. As seen in Table 1.1 of Chapter 1, in the American IS-54 system a signalling rate of 24.3 kBaud or a bit-rate of 48.6 kbps was accommodated in a 30 kHz bandwidth, yielding a bandwidth efficiency of 1.62 bps/Hz. This was achieved using a Nyquist filter (see Section 9.5.2) with a so-called roll-off factor of $\alpha = 0.35$ and then allowing adjacent channels to slightly overlap, while tolerating the associated adjacent channel interference. Specifically, this corresponds to allowing an overlap of the adjacent channel spectra for attenuations higher than 24 dB with respect to the signal level measured at the carrier frequency. A similar philosophy was pursued in the ATDMA proposal, where using 2bits/symbol 4-QAM signalling in a bandwidth of 276.92 kHz, and assuming a Nyquist excess filtering bandwidth (see Section 9.5.2) of 35% the achievable bit-rate became 450 kbps. The corresponding bandwidth efficiency is again 1.62 bps/Hz. Lastly, for 4bits/symbol signalling under identical filtering requirements an efficiency of 3.2 bps/Hz is maintained in the more benign indoor propagation scenarios of Table 9.6, provided that the required channel SNR and Signal-to-Interference Ratio (SIR) can be maintained.

Although many of the ATDMA parameters of Table 9.6 are non-integer values, all physical layer clocks and carrier bit-rates can be derived from a single reference oscillator frequency of 14.4 MHz, which is an important practical consideration. We note furthermore that slots in picocells can be concatenated to give so-called 'double slots' with increased bit-rates, since the associated dispersion is low due to the low pathlength differences. Here we curtail our discussion on the ATDMA proposal, a more detailed discourse on the various ATDMA transport modes can be found in references [116, 117].

Here we simply introduce the ATDMA framework as an example of the recently often quoted so-called 'software radio' concept, where the transceiver is designed to reconfigure itself in a number of different modes, adapting to various propagation environments, teletraffic requirements, etc., facilitated by the flexible base-band 'algorithmic tool-box', as detailed in [8]. Since the family of constant envelope partial response GMSK modems was fully characterised in Chapter 6, here we refrain from detailing partial-response modems. Let us now turn our attention to the class of multi-level full-response modems, which can exploit the higher Shannonian channel capacity of high-SNR channels by transmitting several bits per information symbols and hence ensure high bandwidth efficiency. These modems are also often referred to as Quadrature Amplitude Modulation (QAM) schemes [2].

9.5.2 Quadrature Amplitude Modulation [2]

9.5.2.1 Background

Until quite recently QAM developments were focused at the benign AWGN telephone line and point-to-point radio applications [123], which led to the definition of the CCITT telephone circuit modem standards V.29-V.33 based on various QAM constellations ranging from uncoded 16-QAM to trellis coded (TC) 128-QAM [2]. In recent years QAM research for hostile fading mobile channels has been motivated by the ever-increasing bandwidth efficiency demand for mobile telephony [124]- [133], although QAM schemes require power-inefficient class A or AB linear amplification [134]- [137]. However, the power consumption of the low-efficiency class-A amplifier [136], [137] is less critical than that of the digital speech, image and channel codecs. Out-of-band emissions due to class AB amplifier non-linearities generating adjacent channel interferences can be reduced by some 15 dB using the adaptive predistorter proposed by Stapleton *et.al.* [171, 172]. The spectral efficiency of QAM in various macro- and micro-cellular frequency re-use structures was studied in comparison to a range of other modems in Chapter 17 of reference [2], while burst-by-burst adaptive modem arrangements were proposed for example in references [144]- [169]. Let us now highlight the basic concepts of quadrature amplitude modulation.

9.5.2.2 Modem Schematic

Multi-level full-response modulation schemes have been considered in depth in reference [2]. In this chapter only a terse introduction is offered, concentrating on the fundamental modem schematic of Figure 9.14.

If an analogue source signal must be transmitted, the signal is first low-pass filtered and analogue-to-digital converted (ADC) using a sampling frequency at least twice the signal's bandwidth - hence satisfying the Nyquist criterion. The generated digital bitstream is then mapped to complex modulation symbols by the MAP block, as seen in Figure 9.15 in case of mapping 4 bits/symbol to a 16-QAM constellation.

9.5.2.2.1 Gray Mapping and Phasor Constellation The process of mapping the information bits onto the bitstreams modulating the I and Q carriers plays a fundamental role in determining the properties of the modem, which will be elaborated on at a later stage in Section 9.5.2.3. Suffice to say here that the mapping can be represented by the so-called constellation diagram of Figure 9.15. A range of different constellation diagrams or so-called phasor diagrams was introduced in Figure 1.38 of Chapter 1, where a phasor constellation was defined as the resulting two-dimensional plot when the amplitudes of the I and Q levels of each of the points which could be transmitted (the constellation points) are drawn in a rectangular coordinate system. For a simple binary amplitude modulation scheme, the constellation diagram would be two points both on the positive x axis. For a binary PSK (BPSK) scheme the constellation diagram would consist again of two points on the x axis, but both equidistant from the origin, one to the left and one to the right. The 'negative amplitude' of the point to the left of the origin represents a phase shift of 180 degrees in the transmitted signal. If we allow phase shifts of angles other than 0 and 180 degrees, then the constellation points move off the x axis. They can be considered to possess an amplitude and phase, the amplitude representing the magnitude of the transmitted carrier, and the phase representing the phase shift of the carrier relative to the local oscillator in the transmitter. The constellation points may also be considered to have cartesian, or complex co-ordinates, which are normally referred to as inphase (I) and quadrature

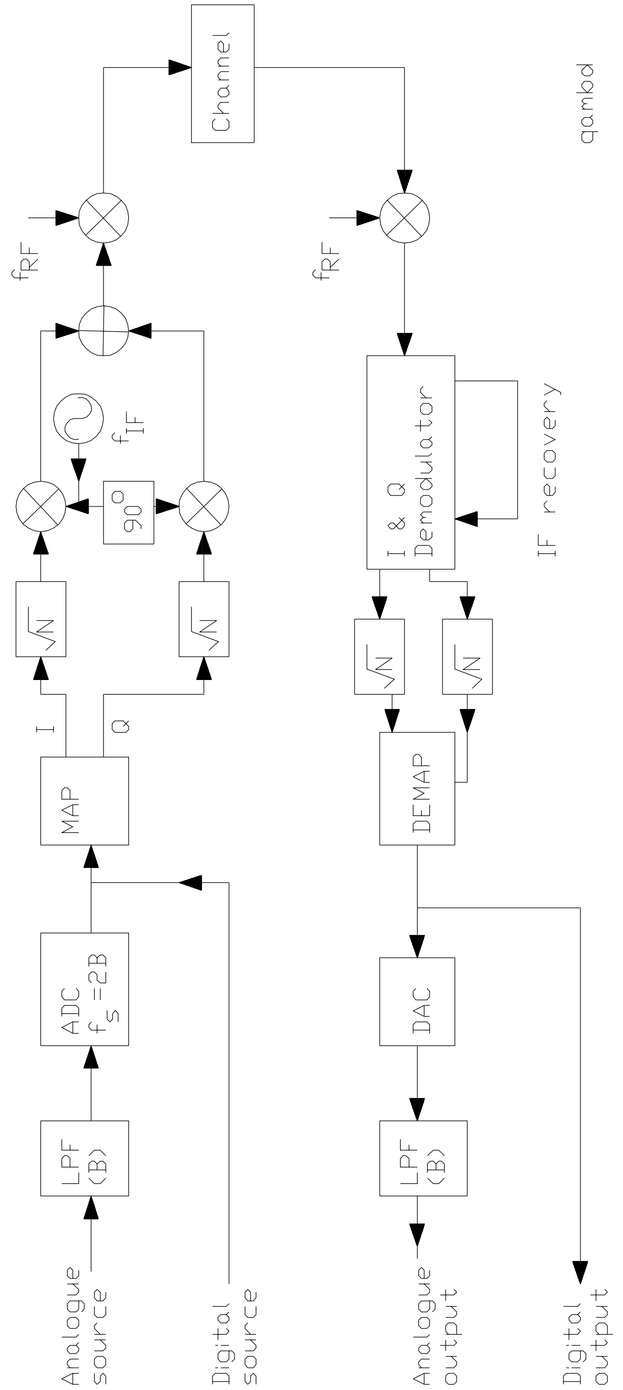

Figure 9.14: Simplified QAM modem schematic ©Webb, Hanzo 1994 [2].

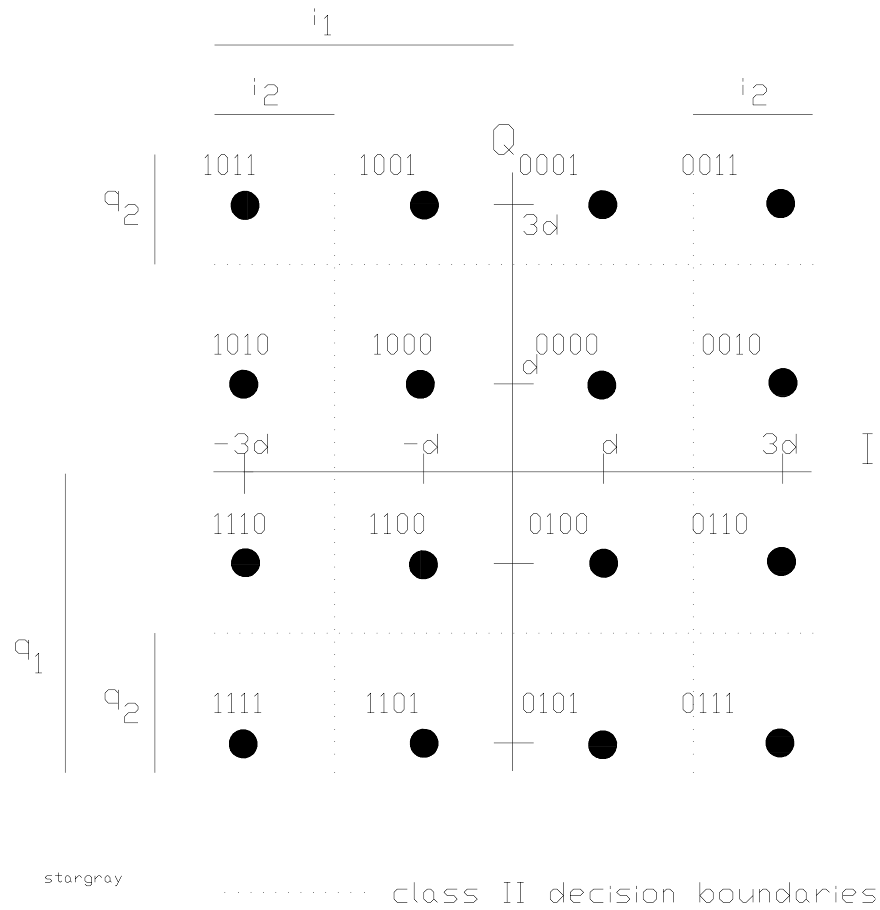

Figure 9.15: 16-QAM square constellation ©Webb, Hanzo 1994 [2].

(Q) components corresponding to the x and y axes, respectively.

In the square-shaped 16-QAM constellation of Figure 9.15 each phasor is represented by a four-bit symbol, constituted by the in-phase bits i_1, i_2 and quadrature bits q_1, q_2, which are interleaved to yield the sequence i_1, q_1, i_2, q_2. The quaternary quadrature components I and Q are Gray encoded by assigning the bits *01, 00, 10* and *11* to the levels *3d, d, -d* and *-3d*, respectively. This constellation is widely used because it has equidistant constellation points arranged in a way that the average energy of the phasors is maximised. Using the geometry of Figure 9.15 the average energy is computed as

$$E_0 = (2d^2 + 2 \times 10d^2 + 18d^2)/4 = 10 \times d^2. \quad (9.13)$$

For any other phasor arrangement the average energy will be less and therefore, assuming a constant noise energy, the signal to noise ratio required to achieve the same bit error rate (BER) will be higher, a topic to be studied comparatively in the context of two different 16-QAM constellations at a later stage in Section 9.5.2.3.

Notice from the mapping in Figure 9.15 that the Hamming distance amongst the constellation points, which are 'closest neighbours' with a Euclidean distance of $2d$ is always one. The Hamming distance between any two points is the difference in the mapping bits for those points, so points labelled 0101 and 0111 would have a Hamming distance of 1, and points labelled 0101 and 0011 would have a Hamming distance of 2. This is a fundamental feature of the Gray coding process and ensures that whenever a transmitted phasor is corrupted by noise sufficiently that it is incorrectly identified as a neighbouring constellation point, the demodulator will choose a phasor with a single bit error. This minimises the error probability.

It is plausible that the typical quaternary I or Q component sequence generated by the MAP block of Figure 9.14 would require an infinite transmission bandwidth due to the abrupt changes at the signalling interval boundaries. Hence these signals must be bandlimited before transmission in order to contain the spectrum within a limited band and so minimise interference with other users or systems sharing the spectrum. This filtering is indicated in Figure 9.14 by the square-root Nyquist-filter blocks denoted by $\sqrt{N}$, where the rationale behind the notation will become clear in the next section.

9.5.2.2.2 Nyquist Filtering A full theoretical treatment of Nyquist filtering was provided in reference [2], hence here we restrict our discussions to a rudimentary introduction. An ideal linear-phase low-pass filter (LPF) with a cut-off frequency of $f_N = f_s/2$, where $f_s = 1/T$ is the signalling frequency, T is the signalling interval duration and $f_N = 1/(2T)$ is the so-called Nyquist frequency, would be able to pass most of the energy of the quadrature components I and Q within a compact frequency band. Due to the linear phase response of the filter all frequency components would exhibit the same group-delay. Because such a filter has a $(\sin x)/x$ function shaped impulse response with equidistant zero-crossings at the sampling instants $n \cdot T$, this ideal low-pass filter does not result in inter-symbol-interference (ISI) between consecutive signalling symbols. After its inventor Nyquist [118] this ideal low-pass transfer function and its derivatives about to be introduced in the next paragraph are referred to as the Nyquist characteristic. However, such an ideal low-pass filter is unrealisable, as all practical low-pass (LP) filters exhibit amplitude and phase distortions, particularly towards the transition between the pass- and stop-band. Conventional Butterworth, Chebichev or inverse-Chebichev LP filters have impulse responses with non-zero values at the equi-spaced sampling instants $n \cdot T$ and hence introduce ISI. They therefore degrade the bit error rate (BER) performance.

Nyquist's fundamental theoretical work [118] suggested that special pulse shaping filters must be deployed, ensuring that the total transmission path, including the transmitter, receiver and the channel, has an impulse response with a unity value at the current signalling instant and zero-crossings at all other consecutive sampling instants $n \cdot T$. He showed that any odd-symmetric frequency-domain extension characteristic fitted to the ideal LPF amplitude spectrum yields such an impulse response, and is therefore free from ISI. Two examples of the corresponding filter characteristics are shown in Figure 9.16, which will be described during our forthcoming deliberations.

A practical odd-symmetric extension characteristic is the so-called raised-cosine (RC) characteristic fitted to the above-mentioned ideal low-pass filter characteristic [2]. The parameter controlling the bandwidth of the Nyquist filter is the so-called roll-off factor α, which is unity, if the ideal LPF bandwidth is doubled by the extension characteristic. If $\alpha = 0.5$ a total bandwidth of $1.5 \times f_N = 1.5/(2T)$ results, and so on. The lower the value of the roll-off factor, the more compact the spectrum becomes, but the higher the complexity of the required filter and other receiver circuitry, such as clock and carrier recovery [2]. The stylised frequency response of these filters is shown in Figure 9.16 for $\alpha = 0.9$ and $\alpha = 0.1$. It follows from Fourier theory that the wider the transmission band, the more sharply decaying the impulse response. A sharply decaying impulse response has a favourable effect concerning the mitigation of the potential ISI in the case of imperfect clock recovery, when there is a time-domain jitter superimposed on the optimum sampling instant. Hence in terms of system performance an $\alpha = 1$ filtering scheme is more favourable than a more sharply filtered but more bandwidth-efficient scheme.

In case of additive white Gaussian noise (AWGN) with a uniform power spectral density (PSD) the noise power admitted to the receiver is proportional to its bandwidth. Therefore it is also necessary to limit the received signal bandwidth at the receiver to a value close to the transmitter's bandwidth. Optimum detection theory [119] shows that the SNR is maximised, if so-called matched filtering is used, where the Nyquist characteristic of Figure 9.16 is divided between two identical filters, a transmitter- and a receiver-filter, each characterised by the square root of the Nyquist shape, as suggested by the filters $\sqrt{N}$ in Figure 9.14.

In conclusion of our discourse on filtering issues we note that Feher [121] proposed non-linear filtering (NLF) as a low-complexity alternative to Nyquist-filtering, which operates by simply fitting a time-domain quarter period of a sine wave between two symbols for both of the quadrature carriers. This technique can be simply implemented by using a look-up table and there is no contribution from previous symbols at any sample point, which is advantageous when complex high-level QAM constellations are transmitted. The disadvantage of this form of filtering is that it is less

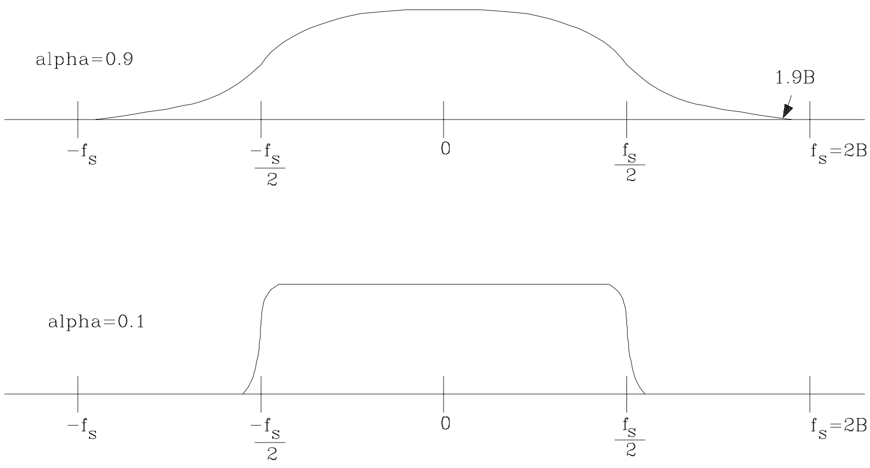

Figure 9.16: Stylised frequency response of two Nyquist filters with $\alpha = 0.9$ and 0.1 ©Webb, Hanzo 1994 [2].

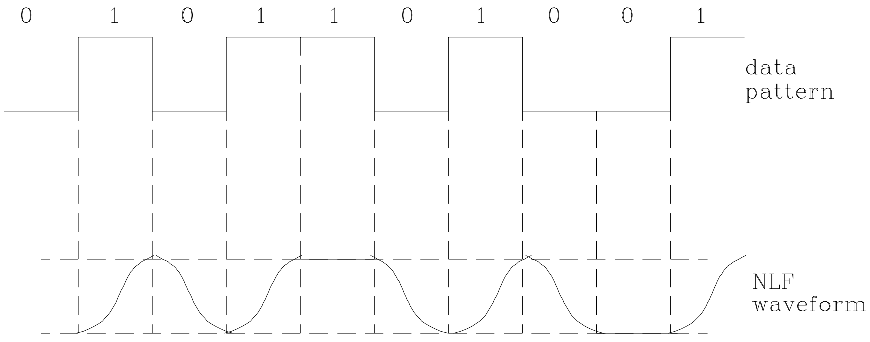

Figure 9.17: Stylised NLF waveforms ©Webb, Hanzo 1994 [2].

spectrally efficient than optimal partial-response filtering schemes. Nevertheless, its implementational advantages often render this loss of efficiency acceptable. The power spectrum of a NLF signal is given by [121]:

$$S(f) = T\left(\frac{\sin 2\pi fT}{2\pi fT}\frac{1}{1-4(fT)^2}\right)^2 \tag{9.14}$$

and the corresponding original and NLF waveforms are given in Figure 9.17 for the I or Q quadrature component.

9.5.2.2.3 Modulation and Demodulation Once the analogue I and Q signals have been generated and filtered, they are modulated by an I-Q modulator as shown in Figure 9.14. This modulator essentially consists of

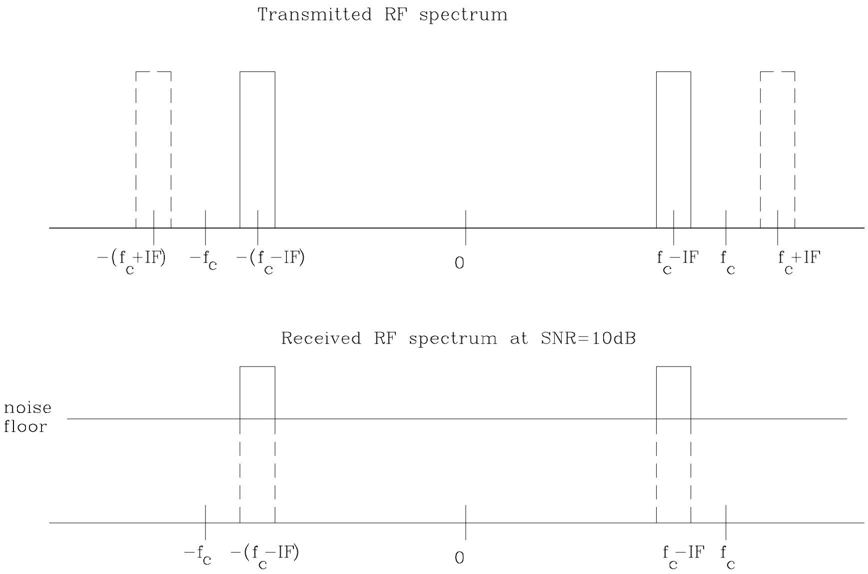

Figure 9.18: Stylised transmitted and received spectra ©Webb, Hanzo 1994 [2].

two mixers, one for the I channel and another for the Q channel. The I channel is mixed with an intermediate frequency (IF) signal that is in phase with respect to the carrier, and the Q channel is mixed with an IF that is 90 degrees out of phase. This process allows both signals to be transmitted over a single channel within the same bandwidth using quadrature carriers. In a similar fashion, the signal is demodulated at the receiver. Provided that the signal degradation is kept to a minimum, the orthogonality of the I and Q channels will be retained and their information sequences can be independently demodulated.

Following I-Q modulation, the signal is modulated by a radio frequency (RF) mixer, increasing its frequency to that used for transmission. Since the IF signal occurred at both positive and negative frequencies, it will occur at both the sum and difference frequencies when mixed up to the RF. Since there is no reason to transmit two identical sidebands, one is usually filtered out, as seen plotted in dashed lines in Figure 9.18. We also note that in theory one could dispense with the IF stage, mixing the base-band component directly to the transmission frequency, if it were possible to design the required extremely narrow-band so-called notch-filters at the RF for removing the unwanted modulation products and out-of-band spectral spillage. Since this results in filter-design problems, in practical systems the signal is converted up to the RF usually in two or more mixing stages.

The transmission channel is often the most critical factor influencing the performance of any communications system. Here we consider only the addition of noise based on the signal to noise ratio (SNR). The noise is often the major contributing factor to signal degradation and its effect exhibits itself in terms of a noise floor, as portrayed in the received RF spectrum of Figure 9.18.

The RF demodulator mixes the received signal down to the IF for the I-Q demodulator. In order to accurately mix the signal back to the appropriate intermediate frequency, the RF mixer operates at the difference between the IF and RF frequencies. Since the I-Q demodulator includes IF recovery circuits, the accuracy of the RF oscillator frequency is not critical. However, it should be stable, exhibiting a low phase noise, since any noise present in the down-conversion process will be passed on to the detected I and Q baseband signals, thereby adding to the possibility of bit errors. The recovered IF spectrum is similar to the transmitted one but with the additive noise floor seen in the RF spectrum of Figure 9.18.

Returning to Figure 9.14, I-Q demodulation takes place in the reverse order to the modulation process. The signal is split into two paths, with each path being mixed down with IFs that are 90 degrees apart. Since the exact frequency of the original reference must be known to determine the absolute phase, IF carrier recovery circuits are used to reconstruct the precise reference frequency at the receiver. The recovered I component should be almost identical to that transmitted, with the only differences being caused by noise.

9.5.2.2.4 Data Recovery Once the analogue I and Q components have been recovered, they must be digitised. This is carried out by the bit detector. The bit detector determines the most likely bit transmitted by sampling the I and Q signals at the correct sampling instants and comparing them to the legitimate I and Q values of $-3d, -d, d, 3d$ in the case of a square 16-QAM constellation. From each I and Q decision two bits are derived, leading to a 4-bit 16-QAM symbol. The four recovered bits are then passed on to the DAC. Although the process might sound simple, it is complicated by the fact that the 'right time' to sample is a function of the clock frequency at the transmitter. The data clock must be regenerated upon recovery of the carrier. Any error in clock recovery will increase the BER. Again, these issues are treated in more depth in reference [2].

If there is no channel noise or the SNR is high, the reconstructed digital signal is identical to the original input signal. Provided the DAC operates at the same frequency and with the same number of bits as the input ADC, then the analogue output signal after low-pass filtering with a cut-off frequency of B, is also identical to the output signal of the LPF at the input of the transmitter. Hence it is a close replica of the input signal. Following the above basic modem schematic description let us now consider two often used 16-QAM constellations.

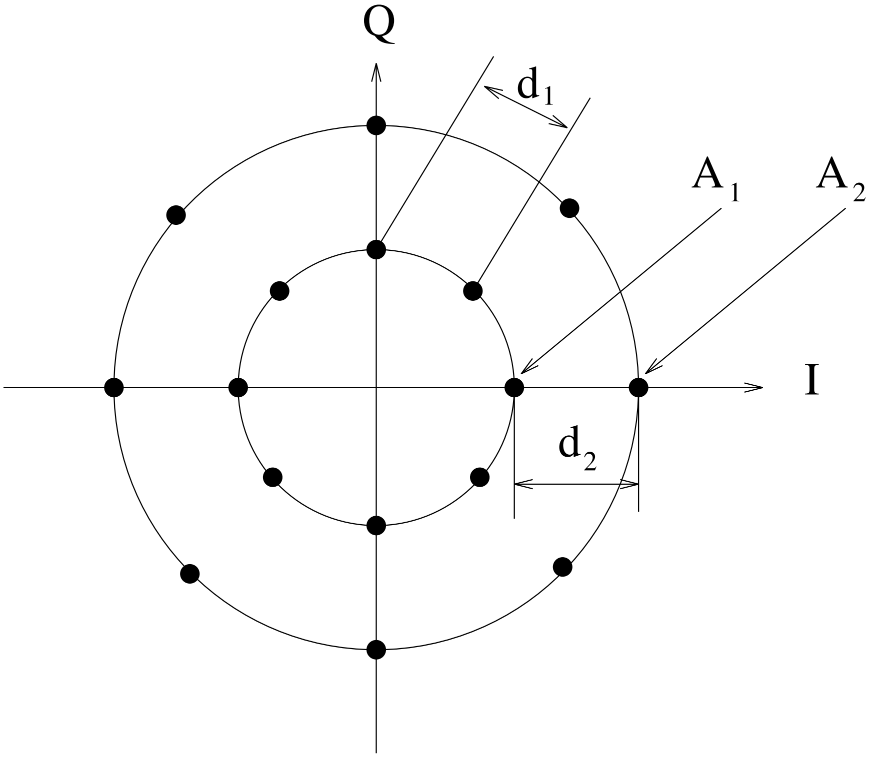

Figure 9.19: Star 16-QAM constellation.

9.5.2.3 QAM Constellations

A variety of different constellations have been proposed for QAM transmissions over Gaussian channels. However, in practice often the constellations shown in Figures 9.15 and 9.19 are preferred. The essential problem is to maintain a high minimum distance, d_{min}, between constellation points whilst keeping the average power required for the constellation to a minimum. Calculation of d_{min} and the average power is a straightforward geometric procedure, and has been performed for a range of constellations by Proakis [138]. The results show that the square constellation of Figure 9.15 is optimal for Gaussian channels. We will show that the star constellation of Figure 9.19 requires a higher energy to achieve the same minimum distance d_{min} amongst constellation points than the square constellation of Figure 9.15 and hence the latter is often preferred for Gaussian channels. However, there may be implementational reasons for favouring circular constellations over the square ones.

When designing a constellation, consideration must be given to:

1. The minimum Euclidean distance amongst phasors, which is characteristic of the noise immunity of the scheme.

2. The minimum phase rotation amongst constellation points, determining the phase jitter immunity and hence the scheme's resilience against clock recovery imperfections and channel phase rotations.

3. The ratio of the peak-to-average phasor power, which is a measure of robustness against non-linear distortions introduced by the power amplifier.

It is quite instructive to estimate the optimum ring ratio RR for the star constellation of Figure 9.19 in AWGN under the constraint of a constant average phasor energy E_0. Accordingly, a high ring ratio value implies that the Euclidian distance amongst phasors on the inner ring is reduced, while the distance amongst phasors on different rings is increased. In contrast, upon reducing the ring ratio the cross-ring distance is reduced and the distances on the inner ring become larger.

Intuitively, one expects that there will be an optimum ring ratio, where the overall bit error rate (BER) constituted by detection errors on the same ring plus errors between rings is minimised. Suffice to say here that the minimum Euclidean distance amongst phasors is maximised if $d_1 = d_2 = A_2 - A_1$ in the star constellation of Figure 9.19. Using the geometry of Figure 9.19 we can write that:

$$\begin{aligned} \cos 67.5^o &= \frac{d_1}{2} \cdot \frac{1}{A_1} \\ d_1 &= 2 \cdot A_1 \cdot \cos 67.5^o \end{aligned}$$

and hence

$$A_2 - A_1 = d_1 = d_2 = 2 \cdot A_1 \cdot \cos 67.5^o.$$

Upon dividing both sides by A_1 and introducing the ring ratio RR we arrive at:

$$\begin{aligned} RR - 1 &= 2 \cdot \cos 67.5^o \\ RR &\approx 1.77. \end{aligned}$$

Simulation results using a variety of ring ratios in the interval of $1.5 < RR < 3.5$ both over Rayleigh and AWGN channels showed [2, 139] that the BER does not strongly depend on the ring ratio, exhibiting a flat BER minimum for RR values in the above range.

Under the constraint of having identical distances amongst constellation points, when $d_1 = d_2 = d$, the average energy E_0 of the star constellation can be computed as follows:

$$E_0 = \frac{8 \cdot A_1^2 + 8 \cdot A_2^2}{16} = \frac{1}{2}(A_1^2 + A_2^2)$$

where

$$A_1 = \frac{d}{2 \cdot \cos 67.5^o} \approx \frac{d}{0.765} \approx 1.31d$$

and
$$A_2 \approx 1.77 \cdot A_1 \approx 2.3d$$
yielding
$$E_0 \approx 0.5 \cdot (5.3 + 1.72)d^2 \approx 3.5d^2.$$
The minimum distance of the constellation for an average energy of E_0 becomes:
$$d_{min} \approx \sqrt{E_0/3.5} \approx 0.53 \cdot \sqrt{E_0},$$
while the peak-to-average phasor energy ratio is:
$$r \approx \frac{(2.3d)^2}{3.5d^2} \approx 1.5.$$
The minimum phase rotation θ_{min}, the minimum Euclidean distance d_{min} and the peak-to-average energy ratio r are summarised in Table 9.7 for both of the above constellations.

Let us now derive the above characteristic parameters for the square constellation. Observe from Figure 9.19 that $\theta_{min} < 45^o$, while the distance between phasors is $2 \cdot d$. Hence the average phasor energy becomes:
$$\begin{aligned} E_0 &= \frac{1}{16}\left[4 \cdot (d^2 + d^2) + 8(9d^2 + d^2) + 4 \cdot (9d^2 + 9d^2)\right] \\ &= \frac{1}{16}(8d^2 + 80 \cdot d^2 + 72d^2) \\ &= 10d^2. \end{aligned}$$
Hence, assuming the same average phasor energy E_0 as for the star constellation we now have a minimum distance of
$$d_{min} = 2d = 2 \cdot \sqrt{E_0/10} = \sqrt{E_0/2.5} \approx 0.63 \cdot \sqrt{E_0}.$$
Lastly, the peak-to-average energy ratio r is given by:
$$r = \frac{18d^2}{10d^2} = 1.8.$$
The square constellation's characteristics are also summarised in Table 9.7. Observe that the star constellation has a higher jitter immunity and a slightly lower peak-to-average energy ratio than the square scheme. However, the square phasor constellation has an almost 20 % higher minimum distance at the same average phasor energy and hence it is very attractive for AWGN channels, where noise is the dominant channel impairment. Let us now consider the bit error rate (BER) versus channel Signal-to-Noise Ratio (SNR) performance of the maximum-minimum distance square-constellation 16-QAM over AWGN channels.

Type	θ_{min}	d_{min}	r
Star	45^o	$0.53\sqrt{E_0}$	1.5
Square	$< 45^o$	$0.63 \cdot \sqrt{E_0}$	1.8

Table 9.7: Comparison of the star and square constellations.

9.5.2.4 16-QAM BER versus SNR Performance over AWGN Channels

9.5.2.4.1 Decision Theory Before analysing the effects of errors let us briefly review the roots of decision theory in the spirit of Bayes' theorem formulated as follows:

$$P(X/Y) \cdot P(Y) = P(Y/X) \cdot P(X) = P(X, Y), \qquad (9.15)$$

where the random variables X and Y have probabilities of $P(X)$ and $P(Y)$, their joint probability is $P(X, Y)$ and their conditional probabilities are given by $P(X/Y)$ and $P(Y/X)$.

In decision theory the above theorem is invoked in order to infer from the noisy analogue received sample y, what the most likely transmitted symbol was, assuming that the so-called *a priori* probability $P(x)$ of the transmitted symbols $x_n, n = 1 \ldots M$ is known. Given that the received sample y is encountered at the receiver, the conditional probability $P(x_n/y)$ quantifies the chance that x_n has been transmitted:

$$P(x_n/y) = \frac{P(y/x_n) \cdot P(x_n)}{P(y)}, \qquad n = 1 \ldots N \qquad (9.16)$$

where $P(y/x_n)$ is the conditional probability of the continuous-valued noise-contaminated sample y, given that $x_n, n = 1 \ldots N$ was transmitted. The probability of encountering a specific y value will be the sum of all possible combinations of receiving y, given that $x_n, n = 1 \ldots N$ was transmitted, which can be written as:

$$P(y) = \sum_{n=1}^{N} P(y/x_n) \cdot P(x_n) = \sum_{n=1}^{N} P(y, x_n). \qquad (9.17)$$

Let us now consider the case of binary phase shift keying (BPSK), where there are two legitimate transmitted values, x_1 and x_2 which are contaminated by noise, as portrayed in Figure 9.20. The conditional probability of receiving any particular noise-contaminated analogue sample y, given that x_1 or x_2 was transmitted is quantified by the Gaussian probability density

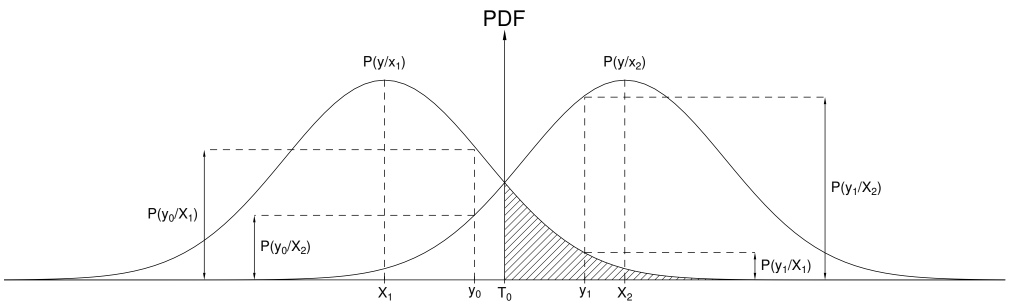

Figure 9.20: Transmitted samples and noisy received samples for BPSK.

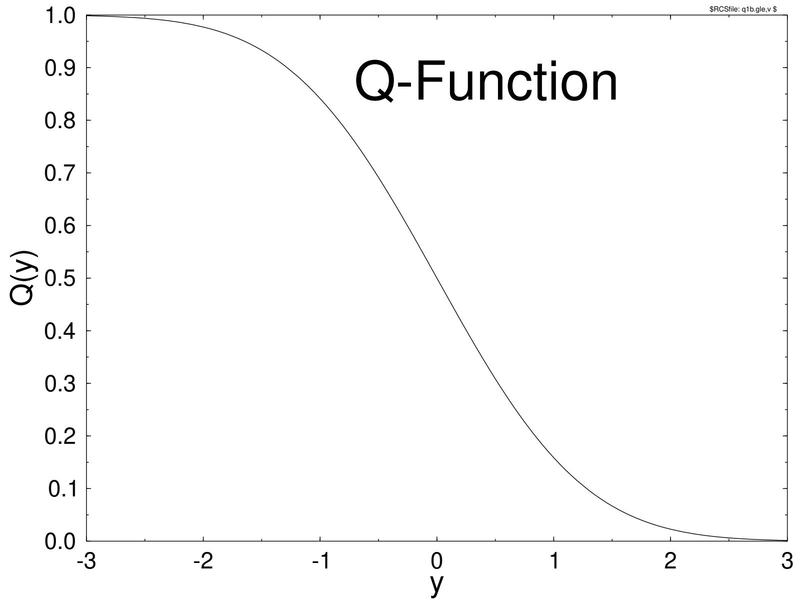

Figure 9.21: Gaussian Q-function

functions (PDFs) seen in Figure 9.20, which are described by:

$$P(y/x) = \frac{1}{\sigma\sqrt{2\pi}} e \frac{-(y-x)^2}{2\sigma^2}, \qquad (9.18)$$

where $x = x_1$ or x_2 is the mean and σ^2 is the variance.

Observe from the Figure that the shaded area represents the probability of receiving values larger than the threshold T_0, when x_1 was transmitted and this is equal to the probability of receiving a value below T_0, when x_2 was transmitted. As displayed in the Figure, when receiving a specific $y = y_0$ sample, there is an ambiguity, as to which symbol was transmitted. The corresponding conditional probabilities are given by $P(y_0/x_1)$ and $P(y_0/x_2)$ and their values are also marked on Figure 9.20. Given the knowledge that x_1 was transmitted, we are more likely to receive y_0 than with the premise that x_2 was transmitted. Hence, upon observing $y = y_0$ statistically speaking it is advisable to decide that x_1 was transmitted. Following similar logic, when receiving y_1 as seen in Figure 9.20, it is logical to conclude that x_2 was transmitted.

Indeed, according to optimum decision theory [188], the optimum decision threshold above which x_2 is inferred is given by:

$$T_0 = \frac{x_1 + x_2}{2} \tag{9.19}$$

and below this threshold x_1 is assumed to have been transmitted. If $x_1 = -x_2$ then $T_0 = 0$ is the optimum decision threshold minimising the bit error probability.

In order to compute the error probability in the case of transmitting x_1, the PFD $P(y/x_1)$ of Equation 9.18 has to be integrated from x_1 to ∞, which gives the shaded area under the curve in Figure 9.20. In other words, the probability of a zero-mean noise sample exceeding the magnitude of x_1 is sought, which is often referred to as the *noise protection distance*, given by the so-called Gaussian Q-function:

$$Q(x_1) = \frac{1}{\sigma\sqrt{2\pi}} \int_{x_1}^{\infty} e^{\frac{-y^2}{2\sigma^2}} dy, \tag{9.20}$$

where σ^2 is the noise variance. Notice that since $Q(x_1)$ is the probability of exceeding the value x_1, it is actually the complementary cumulative density function (CDF) of the Gaussian distribution.

Assuming that $x_1 = -x_2$, the probability that the noise can carry x_1 across $T_0 = 0$ is equal to that of x_2 being corrupted in the negative direction. Hence, assuming that $P(x_1) = P(x_2) = 0.5$, the overall error probability is given by:

$$\begin{aligned} P_e &= P(x_1) \cdot Q(x_1) + P(x_2) \cdot Q(x_2) \\ &= \frac{1}{2}Q(x_1) + \frac{1}{2}Q(x_1) = Q(x_1). \end{aligned} \tag{9.21}$$

The values of the Gaussian Q-function plotted in Figure 9.21 are tabulated in many textbooks [188], along with values of the Gaussian PDF in the case of zero-mean, unit-variance processes. For abscissa values of $y > 4$ the following approximation can be used:

$$Q(y) \approx \frac{1}{y\sqrt{2\pi}} e^{\frac{-y^2}{2}} \quad \text{for} \quad y > 4. \tag{9.22}$$

Having provided a rudimentary introduction to decision theory, let us now focus our attention on the demodulation of 16-QAM signals in AWGN.

9.5.2.4.2 QAM Modulation and Transmission In general the modulated signal can be represented by

$$s(t) = a(t)\cos[2\pi f_c t \ + \ \Theta(t)] = Re[a(t)e^{j[w_c t + \Theta(t)]}], \tag{9.23}$$

where the carrier $\cos(w_c t)$ is said to be amplitude modulated if its amplitude $a(t)$ is adjusted in accordance with the modulating signal, and is said to be phase modulated if $\Theta(t)$ is varied in accordance with the modulating signal. In QAM the amplitude of the baseband modulating signal is determined by $a(t)$ and the phase by $\Theta(t)$. The inphase component I is then given by

$$I \ = \ a(t)\cos\Theta(t) \tag{9.24}$$

and the quadrature component Q by

$$Q \ = \ a(t)\sin\Theta(t). \tag{9.25}$$

This signal is then corrupted by the channel. Here we will only consider AWGN. The received signal is then given by

$$r(t) \ = \ a(t)\cos[2\pi f_c t \ + \ \Theta(t)] \ + \ n(t) \tag{9.26}$$

where $n(t)$ represents the AWGN, which has both an inphase and quadrature component. It is this received signal which we will attempt to demodulate.

9.5.2.4.3 16-QAM Demodulation in AWGN The demodulation of the received QAM signal is achieved by performing quadrature amplitude demodulations using the decision boundaries constituted by the coordinate axes and the dotted lines portrayed in Figure 9.15 for the I and Q components, as shown below for the bits i_1 and q_1:

$$\begin{array}{llll} \text{if} & \text{I,Q} \geq 0 & \text{then} & i_1, q_1 = 0 \\ \text{if} & \text{I,Q} < 0 & \text{then} & i_1, q_1 = 1 \end{array} \tag{9.27}$$

The decision boundaries for the 3rd and 4th bits i_2 and q_2, respectively, are again shown in Figure 9.15, and thus:

$$\begin{array}{lcccccl} \text{if} & & & \text{I,Q} & \geq & 2d & \text{then} & i_2, q_2 = 1 \\ \text{if} & --2d & \leq & \text{I,Q} & < & 2d & \text{then} & i_2, q_2 = 0 \\ \text{if} & --2d & > & \text{I,Q} & & & \text{then} & i_2, q_2 = 1. \end{array} \tag{9.28}$$

We will show that in the process of demodulation the positions of the bits in the QAM symbols associated with each point in the QAM constellation have an effect on the probability of them being in error. In the case of the two most significant bits (MSBs) of the four bit symbol i_1, q_1, i_2, q_2, i.e. i_1 and q_1, the distance from a demodulation decision boundary of each received phasor in the absence of noise is $3d$ for 50 % of the time, and d for 50 % of the time; if each phasor occurs with equal probability. The average protection distance for these bits is therefore $2d$ although the bit error probability for a protection distance of $2d$ would be dramatically different from that calculated. Indeed, the average protection distance is never encountered, we only use this term to aid our investigations. The two least significant bits (LSB), i.e. i_2 and q_2 are always at a distance of d from the decision boundary and consequently the average protection distance is d. We may consider our QAM system as a class one (C1) and as a class two (C2) subchannel, where bits transmitted via the C1 subchannel are received with a lower probability of error than those transmitted via the C2 subchannel.

Observe in the phasor diagram of Figure 9.15 that upon demodulation in the C2 subchannel, a bit error will occur if the noise exceeds d in one direction or $3d$ in the opposite direction, where the latter probability is insignificant. Hence the C2 bit error probability becomes

$$P_{2G} = Q\left\{\frac{d}{\sqrt{N_0/2}}\right\} = \frac{1}{\sqrt{2\pi}} \int_{\frac{d}{\sqrt{N_0/2}}}^{\infty} \exp(-x^2/2)dx \tag{9.29}$$

where $N_0/2$ is the double-sided spectral density of the AWGN, $\sqrt{N_0/2}$ is the corresponding noise voltage, and the $Q\{\}$ function was given in Equation 9.20 and Figure 9.21. As the average symbol energy of the 16-level QAM constellation computed for the phasors in Figure 9.15 is

$$E_0 = 10d^2, \tag{9.30}$$

then we have that

$$P_{2G} = Q\left\{\sqrt{\frac{E_0}{5N_0}}\right\}. \tag{9.31}$$

For the C1 subchannel data the bits i_1 and q_1 are at a protection distance of d from the decision boundaries for half the time, and their protection distance is $3d$ for the remaining half of the time. Therefore the probability of a bit error is

$$P_{1G} = \frac{1}{2}Q\left\{\frac{d}{\sqrt{N_0/2}}\right\} + \frac{1}{2}Q\left\{\frac{3d}{\sqrt{N_0/2}}\right\} = \frac{1}{2}\left[Q\left\{\sqrt{\frac{E_0}{5N_0}}\right\} + Q\left\{3\sqrt{\frac{E_0}{5N_0}}\right\}\right]. \tag{9.32}$$

The C1 and C2 error probabilities P_{1G} and P_{2G} as a function of E_b/N_0 are given by *Equation 9.31* and *9.32* and displayed in Figure 9.22 as a function of the channel SNR in contrast to a range of other modulation schemes. Note that for 1 bit/symbol uncoded transmissions the E_b/N_0 and SNR values are identical, but for example for 2 bit/symbol transmissions for a given signal and noise energy, i.e. channel SNR, the E_b/N_0 value must be reduced by a factor of two or 3.01 dB. Viewing this observation from a different angle, 2 bit/symbol transmissions require a 3 dB higher signal energy or SNR for maintaining a constant E_b/N_0 value. Similarly, for 4 bit/symbol transmissions a factor four E_b/N_0 reduction is necessary for a fixed SNR value, which corresponds to a 6.02 dB higher channel SNR. Returning to the Figure, the BER versus channel SNR performance of binary phase shift keying (BPSK), quaternary phase shift keying (QPSK), 16-QAM and 64-QAM BER are portrayed. For 16-QAM the two protection classes differ by a factor of two in terms of their BER. Similarly to our above deliberations, in reference [2] we also showed that 64-QAM exhibits three subchannels, whose BERs are also shown in the Figure. Observe in the Figure that given a certain channel SNR, i.e. a constant signal power, in harmony with our expectations, 2 bit/symbol transmissions require about 3 dB higher channel SNR for a given BER than binary signalling. A further 6 dB is necessitated by 16-QAM and an additional 6 dB by 64-QAM transmissions. The average probability P_{AV} of bit error for the 16-level QAM system is then computed as:

$$P_{AV} = (P_{1G} + P_{2G})/2. \tag{9.33}$$

Our simulation results gave virtually identical curves to those in Figure 9.22, exhibiting a BER advantage in using the C1 subchannel over using the C2. The computation of the error rate over Rayleigh fading channels is more involved. For the square 16-QAM constellation Cavers [178] provided symbol error rate formulae, while for the star constellation analytical error rate formulae were disseminated by Adachi [189]. With the above considerations in mind let us now concentrate our attention on multilevel communications over Rayleigh fading channels, which were described in Chapter 2.

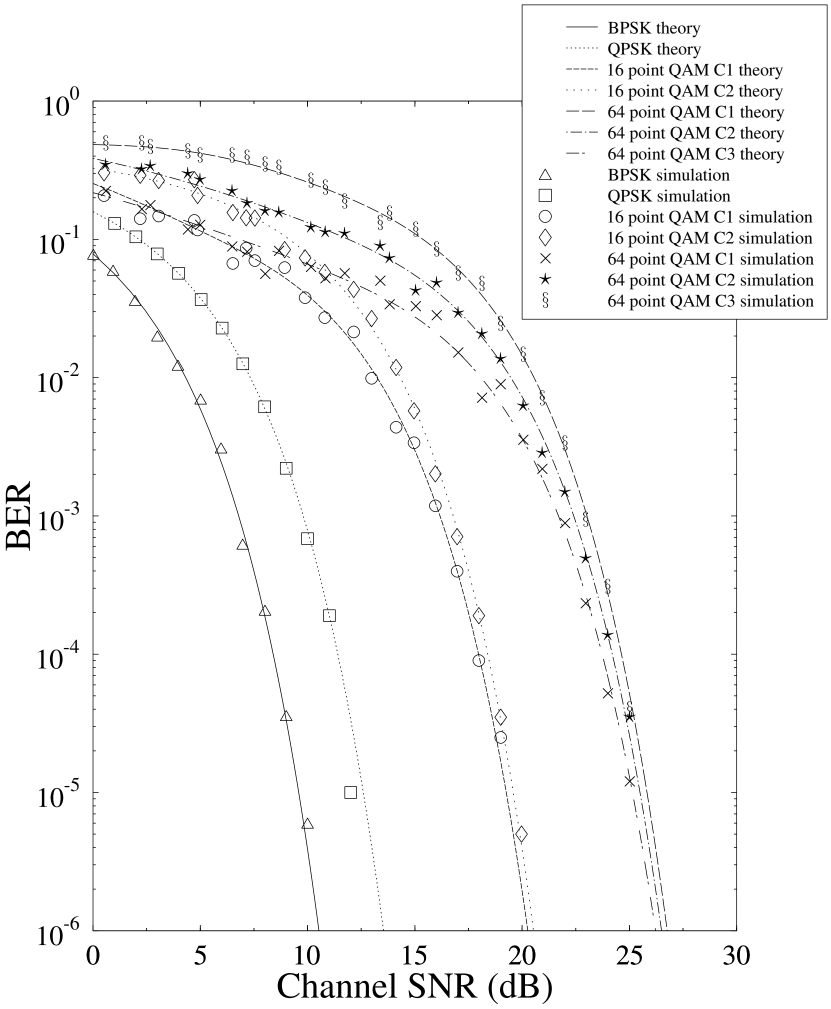

Figure 9.22: BPSK, QPSK, 16-QAM and 64-QAM BER versus channel SNR performance over AWGN channels ©Torrance, 1996 [179].

9.5.2.5 Reference Assisted Coherent QAM for Fading Channels

Over fading channels a number of additional measures have to be taken in order be able to invoke bandwidth-efficient multi-level QAM schemes. The major difficulty is that over fading channels the transmitted phasors' magnitude is attenuated and their phase is rotated by the channel, as it was shown in Figure 1.1. Two powerful methods have been proposed in order to ensure adequate QAM operation in fading environments. Both these techniques deliver channel measurement information in terms of attenuation and phase shift due to fading. The first is transparent tone in band (TTIB) assisted modulation proposed by McGeehan, Bateman *et.al* [180]- [187], where a pilot carrier is inserted typically in the centre of the modulated spectrum. At the receiver the signal is extracted and used to estimate the channel-induced attenuation and phase rotation, as it was detailed also in [2]. A disadvantage of TTIB schemes is their relatively high complexity and expanded spectral occupancy, since the pilot tone is inserted in one or several spectral gaps created by segmenting the signal spectrum and shifting the contiguous spectrum segments apart.

An alternative lower complexity technique is pilot symbol assisted modulation (PSAM) [178], where known channel sounding phasors are periodically inserted into the transmitted time-domain signal sequence. Similarly to the frequency domain pilot tone, these known symbols deliver channel measurement information. Let us here concentrate our attention on the latter, implementationally less complex technique.

9.5.2.5.1 PSAM System Description Following Caver's approach [178], the block diagram of a general PSAM scheme is depicted in Figure 9.23, where the pilot symbols p are cyclically inserted into the data sequence prior to pulse shaping, as demonstrated by Figure 9.24.

A frame of data is constituted by M symbols, and the first symbol in every frame is assumed to be the pilot symbol $b(0)$, followed by $(M-1)$ useful data symbols $b(1), b(2) \ldots b(M-1)$.

Detection can be carried out by matched filtering, and the output of the matched filter is split into data and pilot paths, as seen in Figure 9.23. The set of pilot symbols can be extracted by decimating the matched filter's sampled output sequence using a decimation factor of M. The extracted sequence of pilot symbols must then be interpolated in order to derive a channel estimate $v(k)$ for every useful received information symbol $r(k)$. Decision is carried out against a decision level reference grid, scaled and rotated according to the instantaneous channel estimate $v(k)$.

Observe in Figure 9.23 that the received data symbols must be delayed according to the interpolation and prediction delay incurred. This delay becomes longer, if interpolation is carried out using a longer history of the received signal to yield better channel estimates. Consequently, there is a trade-off between processing delay and accuracy, an issue documented by

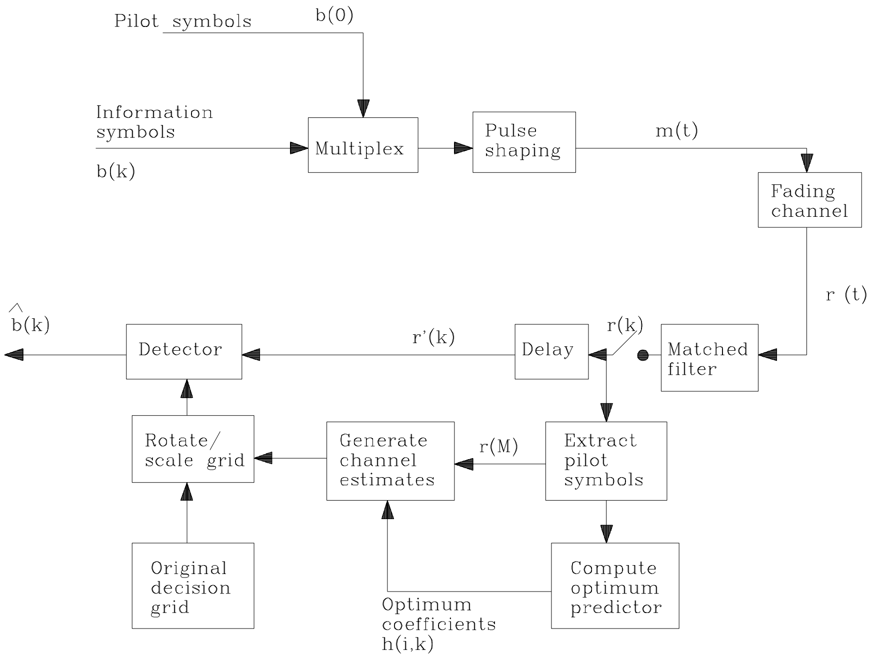

Figure 9.23: PSAM schematic © [178] ©IEEE, 1991, Cavers.

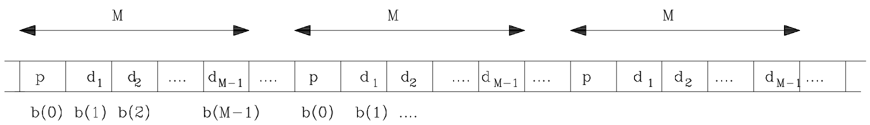

Figure 9.24: Insertion of pilot symbols in PSAM ©Webb and Hanzo 1994. [2]

Torrance and Hanzo [143] for a wide range of parameters. The interpolation coefficients can be kept constant over a whole pilot-period of length M, but better channel estimates can be obtained, if the interpolator's coefficients are optimally updated for every received symbol.

The complex envelope of the modulated signal can be formulated as:

$$m(t) = \sum_{k=-\infty}^{\infty} b(k)p(t - kT), \tag{9.34}$$

where $b(k) = -3, -1, 1$ or 3 represents the quaternary I or Q components of the 16-QAM symbols to be transmitted, T is the symbol duration and $p(t)$ is a band-limited unit-energy signalling pulse, for which we have:

$$\int_{-\infty}^{\infty} |p(t)|^2 dt = 1. \tag{9.35}$$

The value of the pilot symbols $b(kM)$ can be arbitrary, although sending a sequence of known pseudo-random symbols instead of using always the same phasor avoids the transmission of a periodic tone, which would increase the detrimental adjacent channel interference [140].

The narrowband Rayleigh channel is assumed to be 'flat'-fading, which implies that all frequency components of the transmitted signal suffer the same attenuation and phase shift. This condition is met, if the transmitted signal's bandwidth is much lower than the channel's coherence bandwidth. The received signal is then given by:

$$r(t) = c(t) \cdot m(t) + n(t), \tag{9.36}$$

where $n(t)$ is the AWGN and $c(t)$ is the channel's complex gain. Assuming a Rayleigh-fading envelope $\alpha(t)$, a uniformly distributed phase $\phi(t)$ and a residual frequency offset of f_0, we have:

$$c(t) = \alpha(t)e^{j\phi(t)} \cdot e^{j\omega_0 t}. \tag{9.37}$$

The matched filter's output symbols at the sampling instants kT are then given as:

$$r(k) = b(k) \cdot c(k) + n(k). \tag{9.38}$$

Without imposing limitations on the analysis, Cavers [178] assumed that in every channel sounding block $b(0)$ was the pilot symbol and considered the detection of the useful information symbols in the range $\lfloor -M/2 \rfloor \leq k \leq \lfloor (M-1)/2 \rfloor$, where $\lfloor \bullet \rfloor$ is the integer of $\bullet$. Optimum detection is achieved if the corresponding channel gain $c(k)$ is estimated for every received symbol $r(k)$ in the above range. The channel gain estimate $v(k)$ can be derived as a weighted sum of the surrounding K received pilot symbols $r(iM)$, $\lfloor -K/2 \rfloor \leq i \leq \lfloor \mathrm{K}/2 \rfloor$, as shown below:

$$v(k) = \sum_{i=\lfloor -K/2 \rfloor}^{\lfloor K/2 \rfloor} h(i,k) \cdot r(iM), \tag{9.39}$$

and the weighting coefficients $h(i,k)$ explicitly depend on the symbol position k within the frame of M symbols.

The estimation error $e(k)$ associated with the gain estimate $v(k)$ is computed as:

$$e(k) = c(k) - v(k). \tag{9.40}$$

Let us now consider the computation of the optimum channel gains.

9.5.2.5.2 Channel Gain Estimation in PSAM While previously proposed PSAM schemes used either a low-pass interpolation filter [140] or an approximately Gaussian filter [141], Cavers employed an optimum Wiener filter [142] to minimise the channel estimation error variance

$\sigma^2{}_e(k) = E\{e^2(k)\}$, where $E\{\ \}$ represents the expectation. This well-known estimation error variance minimisation problem can be formulated as follows:

$$\begin{aligned}\sigma_e^2(k) &= E\{e^2(k)\} = E\{[c(k) - v(k)]^2\} \\ &= E\left\{\left[c(k) - \sum_{i=\lfloor -K/2\rfloor}^{\lfloor K/2\rfloor} h(i,k)\cdot r(iM)\right]^2\right\}.\end{aligned} \tag{9.41}$$

In order to find the optimum interpolator coefficients $h(i,k)$, minimising the estimation error variance $\sigma^2{}_e(k)$ we consider estimating the k th sample and set:

$$\frac{\partial\sigma_e^2(k)}{\partial h(i,k)} = 0 \quad \text{for} \quad \lfloor -K/2\rfloor \le i \le \lfloor K/2\rfloor. \tag{9.42}$$

Then using Equation 9.41 we have:

$$\frac{\partial\sigma^2{}_e(k)}{\partial h(i,k)} = E\left\{2\left[c(k) - \sum_{i=\lfloor -K/2\rfloor}^{\lfloor K/2\rfloor} h(i,k)\cdot r(iM)\right]\cdot r(jM)\right\} = 0. \tag{9.43}$$

After multiplying both square bracketed terms with $r(jM)$, and computing the expected value of both terms separately, we arrive at

$$E\{c(k)\cdot r(jM)\} = E\left\{\sum_{i=\lfloor -K/2\rfloor}^{\lfloor K/2\rfloor} h(i,k)\cdot r(iM)\cdot r(jM)\right\}. \tag{9.44}$$

Observe that

$$\Phi(j) = E\{c(k)\cdot r(jM)\} \tag{9.45}$$

is the cross-correlation of the received pilot symbols and complex channel gain values, while

$$R(i,j) = E\{r(iM)\cdot r(jM)\} \tag{9.46}$$

represents the pilot symbol autocorrelations; hence Equation 9.44 yields:

$$\sum_{i=\lfloor -K/2\rfloor}^{\lfloor K/2\rfloor} h(i,k)\cdot R(i,j) = \Phi(j), \quad j = \left\lfloor -\frac{k}{2}\right\rfloor \ldots \left\lfloor \frac{k}{2}\right\rfloor. \tag{9.47}$$

If the fading statistics can be considered stationary, the autocorrelations $R(i,j)$ will only depend on the difference $|i-j|$, giving $R(i,j) = R(|i-j|)$. Therefore Equation 9.47 can be written as:

$$\sum_{i=\lfloor -K/2\rfloor}^{\lfloor K/2\rfloor} h(i,k)\cdot R(|i-j|) = \Phi(j), \quad j = \lfloor -K/2\rfloor \ldots \lfloor K/2\rfloor, \tag{9.48}$$

which is a form of the well-known Wiener-Hopf equations [142], often used in estimation and prediction theory, as we have shown with reference to optimum linear prediction of speech signals in Chapter 3.

This set of K equations contains K unknown prediction coefficients $h(i,k)$, $i = \lfloor -K/2 \rfloor \ldots \lfloor K/2 \rfloor$, which must be determined in order to arrive at a minimum error variance estimate of $c(k)$ by $v(k)$. First the correlation terms $\Phi(j)$ and $R(|i-j|)$ must be computed and to do this the expectation value computations in Equations 9.45 and 9.46 need to be restricted to a finite duration window. This approach is referred to as the *autocorrelation method*, which was detailed in the context of speech coding in Chapter 3. The pilot autocorrelation, $R(i,j)$, may then be calculated from the fading estimates at the pilot positions within this window. Calculation of the received pilots' and the complex channel gains' cross correlation is less straightforward, because in order to calculate the cross-correlation the complex channel gains have to be known at the position of the data symbols as well as the pilot symbols. However, the channel gains are only known at the pilot positions, while for the data symbol positions they must be derived by interpolation. Hence in reference [143] Torrance and Hanzo proposed fitting a polynomial to the known samples of $R(|i-j|)$ and then estimated the values of $\Phi(j)$ for the unknown positions in order to provide a wide range of PSAM modem BER versus channel SNR performance figures for 1, 2 and 4 bits/symbol signalling.

The set of Equations 9.48 can also be expressed in a convenient matrix form as:

$$\begin{bmatrix} R(0) & R(1) & R(2) & \ldots & R(K) \\ R(1) & R(0) & R(1) & \ldots & R(K-1) \\ R(2) & R(1) & R(0) & \ldots & R(K-2) \\ \vdots & \vdots & \vdots & \ldots & \vdots \\ R(K) & R(K-1) & R(K-2) & \ldots & R(0) \end{bmatrix} \tag{9.49}$$
$$\cdot \begin{bmatrix} h\left(\lfloor -\frac{K}{2} \rfloor, k\right) \\ h\left(\lfloor -\frac{K}{2}+1 \rfloor, k\right) \\ h\left(\lfloor -\frac{K}{2}+2 \rfloor, k\right) \\ \vdots \\ h\left(\lfloor \frac{K}{2} \rfloor, k\right) \end{bmatrix} = \begin{bmatrix} \Phi\left(\lfloor -\frac{K}{2} \rfloor\right) \\ \Phi\left(\lfloor -\frac{K}{2}+1 \rfloor\right) \\ \Phi\left(\lfloor -\frac{K}{2}+2 \rfloor\right) \\ \vdots \\ \Phi\left(\lfloor \frac{K}{2} \rfloor\right) \end{bmatrix},$$

which can be solved for the optimum predictor coefficients $h(i,k)$ by matrix inversion using Gauss-Jordan elimination or the recursive Levinson-Durbin algorithm of Chapter 3. Once the optimum predictor coefficients $h(i,k)$ are known, the minimum error variance channel estimate $v(k)$ can be derived from the received pilot symbols using Equation 9.39, as also demonstrated by Figure 9.23.

9.5.2.5.3 PSAM Performance [143] Torrance *et.al.* in reference [143] also compared the performance of the above Cavers-interpolator with that of the conventional linear, low-pass and a higher-order polynomial interpolator using 1, 2 and 4 bit/symbol modems and concluded that in the fast-fading IS-54 environment investigated the highest-complexity minimum mean-squared error Cavers-interpolator did not significantly outperform the above low-complexity linear, low-pass or polynomial interpolators in terms of reduced residual BER. In these experiments the propagation frequency was increased from the 900 MHz IS-54 frequency to the 1.8 GHz propagation frequency of the next generation of systems, the vehicular speed was fixed at 50 km/h or approximately 30 mph, and the signalling rate was set to 20 kBd, which corresponded to a modulation excess bandwidth of 50 %, when using the the standard IS-54 bandwidth of 30 kHz. The corresponding Doppler frequency f_d was

$$f_d = (v \cdot f_p)/c = (13.88\text{m/s} \cdot 1.8 \cdot 10^9\text{Hz})/(3 \cdot 10^8\text{m/s}) \approx 83.3\text{Hz},$$

where v is the vehicular speed and f_p is the propagation frequency. The corresponding normalised Doppler frequency is

$$f_d \cdot T = 83.3\text{Hz} \cdot 1/(20 \cdot 10^3\text{Baud}) \approx 0.0042.$$

Due to its approximately 13-times higher signalling rate of 271 kbps the GSM-like DCS1800 system under identical propagation conditions results in a relative Doppler frequency of 0.0003, which is associated with a less dramatically fading signal envelope and hence better fade tracking properties. The 1 bit/symbol, 2 bit/symbol and 4 bit/symbol modulation schemes were combined with all four interpolators and their bit error rate (BER) performance was evaluated at channel SNRs of 20, 30 and 40 dB, which yielded $3 \cdot 4 \cdot 3 = 36$ sets of results. In each set of results pilot Buffer lengths of 3, 5, 7, 9, 11 PSAM frames and pilot separation or Gap values of 10, 20, 40, 60, 80, 100, 116 were employed, leading to a plethora of performance curves, which allowed us to generate a corresponding set of 3-dimensional (3D) graphs of BER versus Buffer and Gap. These results are presented in Figure 9.25 as a set of 3-dimensional (3D) graphs of BER versus Buffer and Gap for pilot-assisted square-constellation 16-QAM. The corresponding graphs for BPSK and QPSK were presented by Torrance in reference [179], while a variety of further results can be found in [143]. As an alternative to the above coherent PSAM scheme let us now consider the advantages and disadvantages of non-coherent differential detection using the star constellation of Figure 9.19.

9.5.2.6 Differentially Detected QAM [2]

We have shown above that the so-called 'maximum minimum distance' square-shaped QAM constellation [122] is optimal for transmissions over

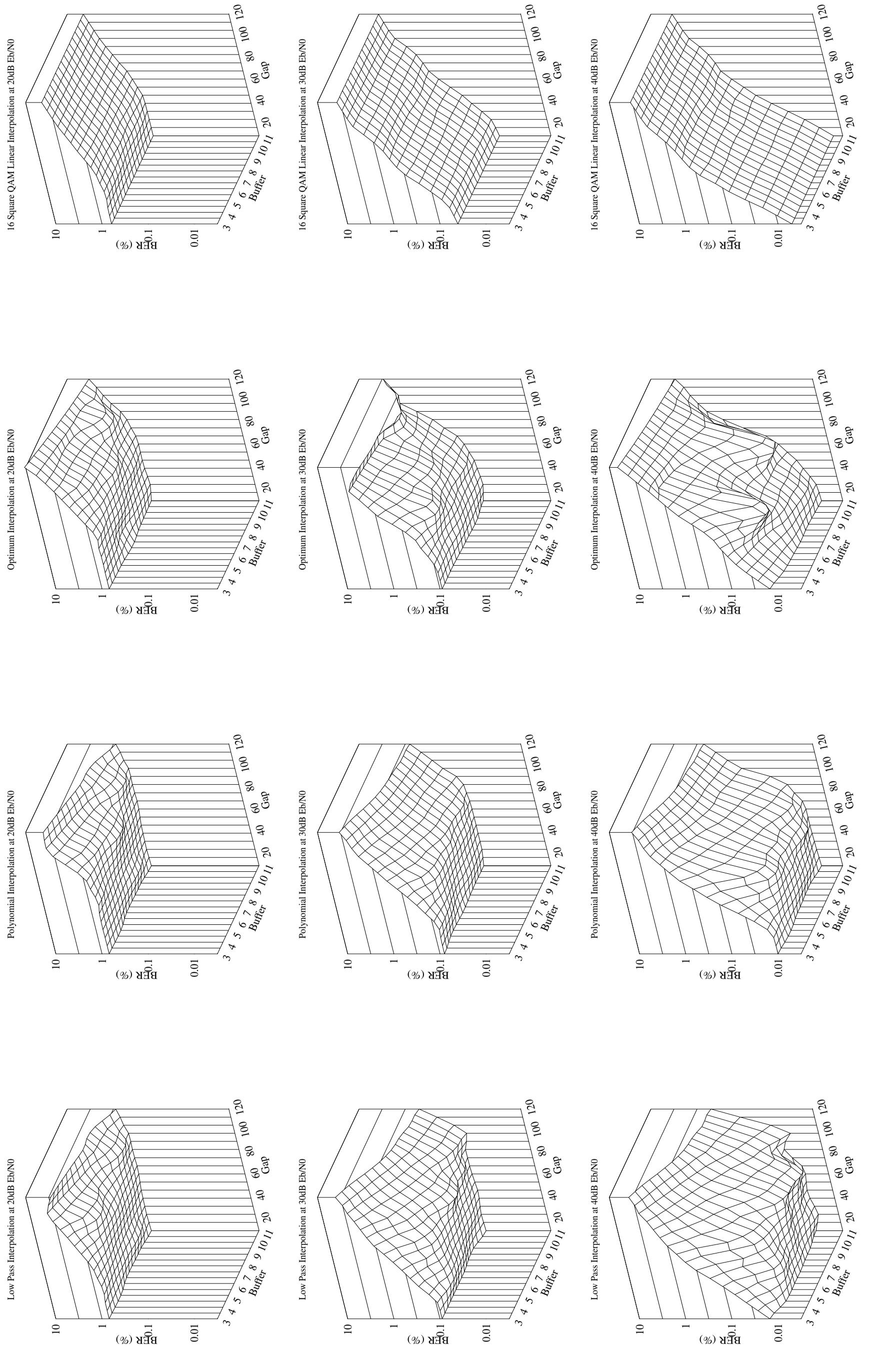

Figure 9.25: BER versus ‘Buffer’ length and pilot ‘Gap’ performance of pilot-assisted 16-QAM over Rayleigh channels at 20 kBd, 50 km/h, 1.8 GHz ©IEE 1995 Torrance, Hanzo [143].

Additive White Gaussian (AWGN) channels, since it has the highest average distance amongst its constellation points, yielding the highest noise protection distances for a given average power. We have also introduced the star QAM constellation in Figure 9.19 and compared some of its properties with those of the square constellation of Figure 9.15 in Table 9.7. In this subsection we will introduce a differentially encoded version of the star constellation shown in Figure 9.19, which can be often advantageously employed over fading channels.

When using the previously discussed square-shaped 16-QAM constellation, it is essential to be able to separate the information modulated onto the in-phase (I) and quadrature-phase (Q) carriers with the aid of coherent demodulation, invoking the Transparent-tone-in-band (TTIB) principle invented by McGeehan and Bateman [181], [187], [190] or employing the above PSAM schemes [178]. In order to achieve this, a perfectly phase-coherent replica of the transmitter's I and Q carrier has to be recovered by the carrier recovery circuitry. In contrast, in the so-called differentially encoded schemes it is not necessary to derive this phase-coherent reference carrier, an issue which will be elaborated on below.

The pivotal point of differentially encoded non-coherent QAM demodulation is that of finding a rotationally symmetric QAM constellation, where all constellation points are rotated by the same amount. Such a rotationally symmetric, differentially encoded 'star-constellation' was proposed by Webb *et.al.* in reference [133], which is similar to the star scheme shown in Figure 9.19 in terms of the location of its phasors, but differentially encoded, as it will be described below. We have seen in Table 9.7 that a disadvantage of the proposed star 16-QAM (16-StQAM) constellation is its lower average energy.

Our differential encoder obeys the following rules. The first bit $b1$ of a four-bit symbol is differentially encoded onto the phasor magnitude, yielding a ring-swap for an input logical one and maintaining the current magnitude, i.e., ring for $b1 = 0$. Bits $(b2, b3, b4)$ are then differentially Gray-coded onto the phasors of the particular ring pin-pointed by $b1$. Accordingly, $(b2, b3, b4) = (0, 0, 0)$ implies no phase change, $(0, 0, 1)$ a change of 45^o, $(0, 1, 1)$ a change of 90^o, etc.

The corresponding non-coherent differential 16-StQAM demodulation is equally straightforward, having decision boundaries at a concentric ring of radius $B = (A_1 + A_2)/2$ and at phase rotations of $(22.5^o + n.45^o)$ $n = 0 \ldots 7$. Assuming received phasors of P_t and P_{t+1} at consecutive sampling instants of t and $t + 1$, respectively, bit $b1$ is inferred by evaluating the condition:

$$\left| \frac{P_{t+1}}{P_t} \right| \geq (A_1 + A_2)/2. \tag{9.50}$$

If this condition is met, $b1 = 1$ is assigned, otherwise $b1 = 0$ is demodulated.

Bits $(b2, b3, b4)$ are then recovered by computing the phase difference

$$\Delta\Theta = (\Theta_{t+1} - \Theta_t) \pmod{2\pi} \tag{9.51}$$

and comparing it against the decision boundaries $(22.5^o + n.45^o)$ $n = 0 \ldots 7$. Having decided which rotation interval the received phase difference $\Delta\Theta$ belongs to, Gray-decoding delivers the bits $(b2, b3, b4)$.

From our previous discourse it is plausible that the less dramatic the fading envelope and phase trajectory fluctuation between adjacent signalling instants, the better this differential scheme works. This implies that lower vehicular speeds are preferred by this arrangement, if the signalling rate is fixed. Therefore the modem's performance improves for low pedestrian speeds, when compared to typical vehicular scenarios. Alternatively, for a fixed vehicular speed higher signalling rates are favourable, since the relative amplitude and phase changes introduced by the fading channel between adjacent information symbols are less drastic.

Similar differentially encoded and non-coherently detected constellations can be used in conjunction with any number bits/symbol. In reference [143] Torrance *et.al.* presented the BER of pilot-symbol assisted 1, 2 and 4 bits/symbol BPSK, QPSK and 16-QAM for channel SNRs of 20, 30 and 40 dB in contrast to their lower-complexity differentially detected counterparts. These comparative results are reproduced in Figure 9.26 [143] as a set of BER versus number of bits per symbol curves for both the pilot-assisted and differential schemes using channel SNRs of 20, 30 and 40 dB. Explicitly, the bold symbols in the Figure represent the PSAM schemes, while the hollow symbols correspond to the differentially detected schemes. Observe in the Figure that as the modulation constellation becomes less complex, ie the number of bits per symbol is reduced, the benefits of coherent modulation are reduced, although this is also a function of the channel SNR. In contrast, for higher order constellations, such as QPSK and 16Q-AM, PSAM does reduce the residual BER of the slightly less complex, differentially detected schemes while having a somewhat higher delay.

For a full treatise on various aspects of QAM the interested reader is referred to [2], where the modem performance was documented for various constellations and channel conditions. As a brief performance comparison, we remind the reader that in Figure 9.26 we portrayed the coherent and non-coherent modem's residual BER performances for 1, 2 and 4 bits/symbol signalling under identical conditions. Observe in the Figure that the differentially detected scheme has typically a factor two higher BER due to the fact that in the case of an erronnous decision errors occur in both the current and the forthcoming signalling interval, where the current phasor is used as a reference in deriving the next one. Some further BER degradation is expected due to the reduced distance of the constellation points in the star constellation, although this does not appear to be a significant factor over fading channels. In conclusion, star- and

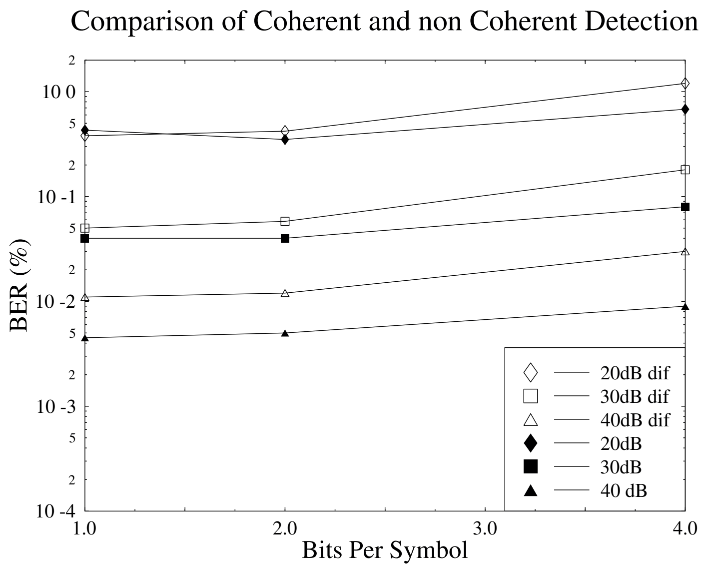

Figure 9.26: Residual BER for 1,2 and 4 bits per symbol PSAM modulation compared with equivalent differential schemes ©IEE [143] Torrance and Hanzo, 1995.

square-constellation QAM have a high bandwidth efficiency in exchange for a typically higher channel SNR and SIR requirement. The BER versus channel SNR performance of coherently detected pilot-assisted QAM is slightly higher than that of the lower complexity star-QAM, providing the system designer with a choice of implementational options. In the next section we consider burst-by-burst adaptive QAM schemes.

9.5.2.7 Burst-by-burst Adaptive Modems

Burst-by-burst adaptive multi-level modulation was first suggested by Steele and Webb in references [2, 144, 145] for slowly-fading wireless pedestrian channels, inspiring intensive further research in recent years [147]-[162], in particular by Kamio, Sampei, Sasaoka, Morinaga, Morimoto, Harada, Okada, Komaki and Otsuki at Osaka University and the Ministry of Post in Japan [146]- [149], as well as by Goldsmith *et.al.* [150]- [156] at Stanford University in the USA or by Pearce, Burr and Tozer [157] in the UK. The proposed schemes provide a means of realising some of the time-variant channel capacity potential of the fading wireless channel [165], invoking a more robust Transmission Scheme (TS) on a burst-by-burst basis, when the channel is of low quality and vice-versa, while maintaining

Switching levels(dB)	l_1	l_2	l_3	l_4
Mean-Speech (1%)	3.31	6.48	11.61	17.64
Mean-BER Data (0.01%)	7.98	10.42	16.76	26.33

Table 9.8: Switching levels for speech and computer data systems through a Rayleigh channel, shown in instantaneous channel SNR (dB) to achieve Mean BERs of 1×10^{-2} and 1×10^{-4}, respectively.

a certain target bit error rate (BER) performance. The most appropriate TS is dependent upon the time-variant instantaneous Signal-to-Noise Ratio (SNR) and Signal-to-Interference Ratio (SIR). The TS can be chosen according to the following regime [158]:

$$\text{TS} = \begin{cases} \text{No Transmission (Notx)} & \text{if} \quad l_1 > s^2/N \\ \text{BPSK} & \text{if} \quad l_1 \leq s^2/N < l_2 \\ \text{QPSK} & \text{if} \quad l_2 \leq s^2/N < l_3 \\ \text{Square 16 Point QAM} & \text{if} \quad l_3 \leq s^2/N < l_4 \\ \text{Square 64 Point QAM} & \text{if} \quad s^2/N \geq l_4, \end{cases} \tag{9.52}$$

where s is the instantaneous signal level, N is the average noise power, and l_1, l_2, l_3 and l_4, are the BER-dependent optimised switching levels. Time Division Duplex (TDD) was proposed, in order to exploit the reciprocity of the channel under high SIR conditions, which allowed us to estimate the prevalent SNR on a burst-by-burst basis [159]. The reciprocity of the up- and down-link channel conditions in the TDD frame is best approximated, if the corresponding TDD slots are adjacent. This requirement, however, imposes various practical constraints on the transceiver design, which are beyond the scope of this book.

In reference [158] the analytical upper-bound performance of such a scheme was characterised over slow Rayleigh-fading channels, while in [161] an unequal protection phasor constellation for signalling the current TS was proposed. The problem of appropriate power assignment was discussed for example in [148, 150].

In reference [158] a combined BER- and Bits per Symbol (BPS) based optimisation cost-function was defined and minimised, in order to find the required TS switching levels for maintaining average target BERs of 1×10^{-2} and 1×10^{-4}, irrespective of the instantaneous channel SNR. These BER values can then be further mitigated by forward error correction coding and in the case of the lower BER scheme can be rendered virtually error-free. The former scheme was referred to as the speech TS, and the latter as the adaptive data TS. The optimised TS switching levels l_1, l_2, l_3 and l_4 are summarised in Table 9.8 [158]. The average BPS performance B of this adaptive modem was derived for a Rayleigh fading

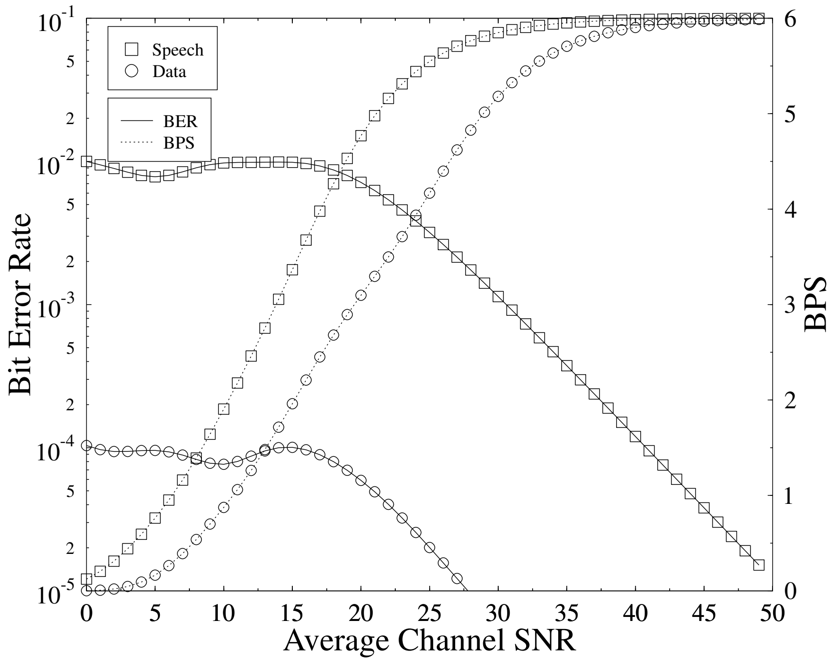

Figure 9.27: Upper bound BER and BPS performance of adaptive QAM in Rayleigh channel optimised separately for 'Speech' and 'Data' transfer ©IEE Torrance and Hanzo, 1996 [158].

channel in reference [158], which can be written as:

$$\begin{aligned} B \;=\;& 1 \cdot \int_{l_1}^{l_2} F(s,S)\,ds + 2 \cdot \int_{l_2}^{l_3} F(s,S)\,ds \\ &+ 4 \cdot \int_{l_3}^{l_4} F(s,S)\,ds + 6 \cdot \int_{l_4}^{\infty} F(s,S)\,ds, \end{aligned} \tag{9.53}$$

where $F(s,S)$ is the PDF of the Rayleigh channel, which was given in Chapter 2, S is the average power and the integrals characterise the received signal level domains, where the 0, 1, 2, 4 and 6 bits/symb TSs of Equation 9.52 are used. Since the transmissions can be disabled for the duration of deep channel fades, the transmitted information has to be buffered, which results in latency. In references [162, 163] the latency performance of these schemes was quantified and frequency hopping as well as statistical multiplexing were proposed to mitigate its latency and buffer requirements.

Considering Figure 9.27, the desired BER is achieved between 0 and 50 dB for both the speech and computer data schemes, when using the switching thresholds of Table 9.8, which were optimised for maintaining

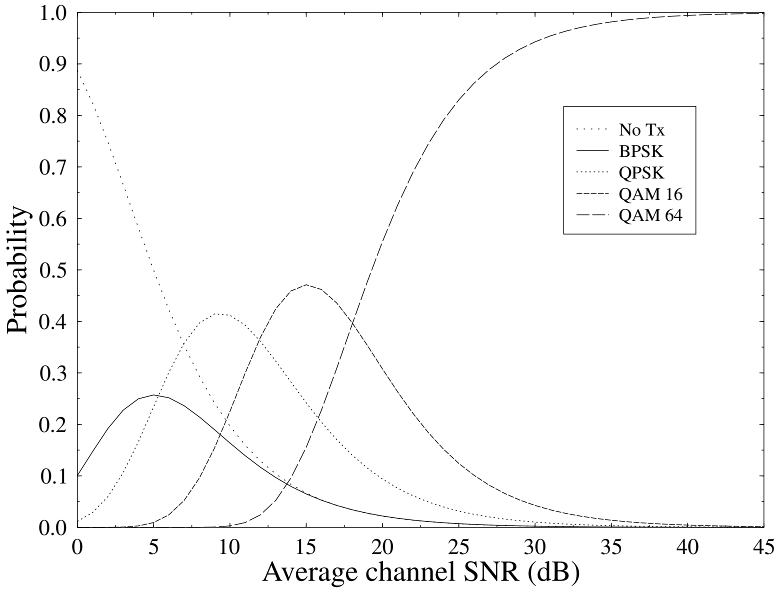

Figure 9.28: Probability of the individual AQAM modem modes optimised for speech transmission at an average BER of 1% plotted against average channel SNR for a Rayleigh channel ©Torrance, Hanzo, 1996 [176].

mean BERs of 1×10^{-2} and 1×10^{-4}, respectively. The targeted BPS performance is achieved at about 18 dB and 19 dB average channel SNRs for the speech and computer data schemes, respectively. Observe in the Figure that both the speech and data BER profiles outperform the BER requirements for average channel SNRs higher than these values, since the modem cannot switch to higher order modes than 64-QAM. The system was capable of maintaining the target BER performances at extremely low average SNR values. This robust performance was achieved at the cost of reducing the BPS throughput below that of BPSK, which was possible due to disabling transmissions for low instantaneous SNR values.

In Figure 9.28 the probability density function (PDF) of the various AQAM modem modes versus the average channel SNR performance was documented. Note in Figure 9.28 that given a certain average channel SNR, there is a finite probability that the AQAM modem assumes potentially any of its legitimate modes of operation. However, for example at an average SNR of 15 dB the most frequently invoked mode is 16-QAM, while in excess of this SNR 64-QAM is employed predominantly. Nonetheless, even the No TX mode has a finite probability of occurrence above 15 dB, which is a consequence of channel estimation errors.

A variety of decision feed-back equalised wideband burst-by-burst adaptive modem schemes were studied in references [166]- [169]. Specifically, the maximum achievable throughput or BPS performance of decision feedback equalised AQAM was compared to the Shannonian channel capacity limit, in order to gauge the potential gains due to adaptivity, while the block turbo coded performance of AQAM was the topic of [167–169], exhibiting channel SNR gains up to 20 dB in comparison to conventional non-adaptive systems. Although AQAM research is in its infancy, the initial results are encouraging and hence they are likely to stimulate further research.

9.5.2.8 Summary of Multi-level Modulation

In closing we note that in cellular frequency-reuse structures, where the co-channel interference is a dominant impairment, the bandwidth-efficiency of these schemes is often eroded due to the increased frequency reuse factor required by the higher interference sensitivity of these schemes. In Chapter 17 of reference [2] we have shown that the true spectral efficiency - which is also often referred to as area spectral efficiency - of a modulation scheme, taking into account the effect of the required frequency reuse factor is dependent on the bit error ratio (BER) targeted. The required BER in turn is dependent on the robustness of the source codecs used. However, for example in the indoor picocells of the ATDMA system of Table 9.6 the partitioning walls and floors mitigate the co-channel interference and this facilitates the employment of 16-QAM.

In this rudimentary introduction to QAM techniques we assumed perfect clock recovery and dispensed with considering a range of important aspects of the transceiver design, such as clock and carrier recovery, wideband aspects and channel equalisation, the effects of co- and adjacent-channel interference, trellis coding, etc. which are treated in depth in the corresponding chapters of reference [2]. The analytical error rate performance of square and star QAM was characterised in references [178] and [189] by Cavers and Adachi, respectively. We note that the advantages and disadvantages of the above modem schemes will be elaborated on again in Section 9.7 in the context of two different systems based on non-coherently detected star 16-QAM and coherently detected square 16-QAM. Let us now briefly consider the principles of Packet Reservation Multiple Access (PRMA) in the next section.

9.6 Packet Reservation Multiple Access

PRMA is a relative of slotted ALOHA contrived for conveying speech signals on a flexible demand basis via time division multiple access (TDMA) systems. PRMA was documented in a series of excellent treatises by Nanda, Goodman *et.al.* [191], while a PRMA-assisted adaptive differential pulse code modulation (ADPCM) transceiver was proposed in reference [26]. The voice activity detector (VAD) [26] queues the active speech spurts to contend for an up-link TDMA time-slot for transmission to the BS. Alternatively, a VAD similar to that of the GSM system described in Chapter 8 can be employed. Inactive users' TDMA time slots are offered by the BS to other users, who become active and are allowed to contend for the unused time slots with a less than unity permission probability. This measure prevents previously colliding users from consistently colliding in their further attempts to attain a time-slot reservation. For a seven-slot PRMA system the optimum permission probability allowing to support the highest number of users was found to be 0.6, as shown in Table 9.9.

If several users contend for an available slot, neither of them will be granted it, while if only one user requires the time slot, he can reserve it for future communications. When many users are contending for a reservation, the collision probability is increased and hence a speech packet might have to contend for a number of consecutive slots, until its maximum contention delay of typically 32 ms expires. In this case the speech packet must be dropped, but the packet dropping probability must be kept below 1%, a value inflicting minimal degradation in perceivable speech quality in contemporary speech codecs. As an example, the 8 kbps G.729 CCITT/ITU ACELP candidate codec's target was to inflict less than 0.5 Mean Opinion Score (MOS) degradation in the case of a speech frame error rate of 3% [46].

The performance of communications systems is often evaluated in terms of the teletraffic carried, while maintaining a set of communications quality measures. In conventional TDMA mobile systems the grade of service (GOS) degrades due to speech impairments caused by call blocking, hand-over failures and speech frame interference engendered by noise, as well as co- and adjacent-channel interference. In PRMA-assisted systems calls are not blocked due to the lack of an idle time-slot, but the packet dropping probability is increased gracefully. Hand-overs will be performed in the form of contention for an idle time slot provided by the specific BS offering the highest signal quality amongst the potential hand-over target BSs.

The specific physical up-link to the BS offering the best signal quality during decoding the packet header is not likely to substantially degrade during the life-time of an active speech spurt having a typical mean duration of 1 s or some thirty consecutive 30 ms speech frames. If, however, the link degrades before the next active spurt is due for transmission, the subsequent contention phase is likely to establish a link with another BS. Hence this process will have a favourable effect on the channel's quality, effectively simulating a diversity system having independent fading channels and limiting the time spent by the MS in deep fades, thereby avoiding channels with high noise or interference.

This advantageous property can be exploited to train a self-adjusting adaptive system using the channel segregation scheme proposed for PRMA systems in reference [170]. Accordingly, each BS evaluates and ranks the quality of its idle physical channels constituted by the unused time slots on a frame-by-frame basis and identifies a certain number of slots, N, with the highest quality, i.e. lowest noise and interference. These high-quality, low-interference channels are segregated for contention, while the lower quality idle slots contaminated by noise and interference are temporarily disabled. Hence upon a new access request the BS is likely to receive a signal having low interference, which maximizes the chances of successful packet decoding, unless a collision caused by a simultaneous MS attempt to attain a reservation has occurred. When a successful, uncontended reservation takes place, the BS promotes the highest quality disabled time slot to the set of N segregated channels, unless its quality is unacceptably low. It appears plausible that if N is high, the packet dropping probability becomes low, but the physical channels constituted by the time slots might become heavily interfered with, while if N is low, we have a packet dropping-dominated scenario, which equally limits the GOS.

Clearly, the main cause of GOS degradation in PRMA systems is limited to speech packet corruption due to noise or interference and packet dropping [192]. They both result in different subjective speech or GOS degradation, which we will attempt to quantitatively compare in terms of the objective segmental signal to noise ratio (SEGSNR) degradation. Quantifying these GOS degradations in relative terms in contrast to each other will allow us to appropriately split the acceptable overall degradation between packet dropping and packet corruption. With the system elements described in previous Sections of this chapter, in the next section we focus our attention on the amalgamated PCS transceiver proposed.

9.7 Multi-mode Multi-media Transceivers

9.7.1 Flexible Transceiver Architecture

It transpired from our previous discussions that a high-performance transceiver is expected to be reconfigurable in a number of different operational modes for reasons to be augmented below. The schematic of such a flexible, toolbox-based multi-media system is portrayed in Figure 9.29. The key optimisation criterion of such a multi-media PS is that of finding the best compromise amongst a number of contradicting design factors, such as power consumption, robustness against transmission errors, spectral efficiency, audio/video quality and so forth. As argued before, the time-variant optimisation criteria of a flexible multi-media system can only be met by an adaptive scheme, comprising the firmware of a suite of system components and invoking that combination of speech codecs, video codecs, embedded channel codecs, voice activity detector (VAD) and modems, which fulfils the prevalent one [2]. A few examples are maximising the teletraffic carried or the robustness against channel errors, while in other cases minimisation

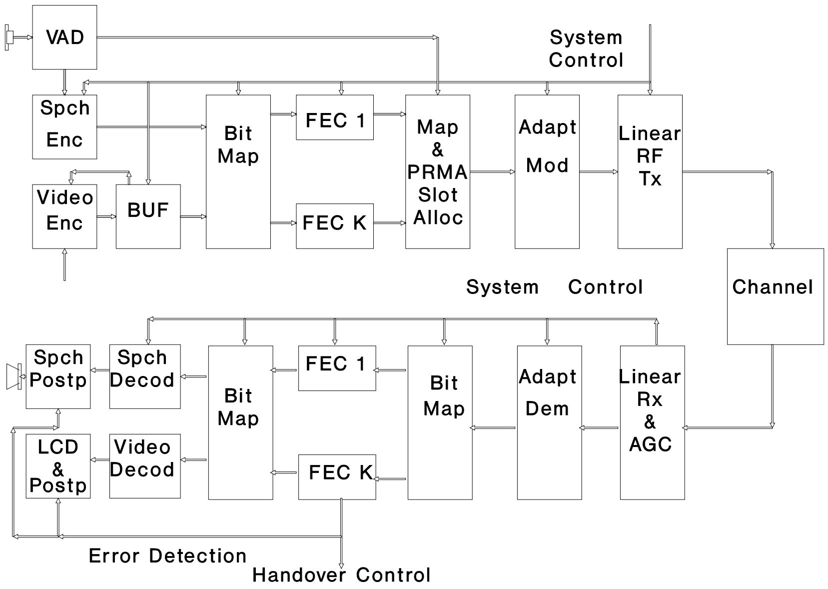

Figure 9.29: Flexible Multi-media Communicator Schematic, ©IEEE, Hanzo, 1998, [1].

of the bandwidth occupancy, the call blocking probability or the power consumption is of prime concern.

Focusing our attention on the speech and video links displayed in Figure 9.29, the voice activity detector (VAD) is employed to control the packet reservation multiple access (PRMA) slot allocator [2], multiplexing speech and video. Control traffic and system information is carried by packet headers added to the composite signal by the 'Bit Mapper' before K-class source sensitivity-matched forward error correction coding (FEC) takes place. Observe that the 'Video Encoder' supplies its bits to an adaptive buffer (BUF) having a feed-back loop. If the PRMA video packet delay becomes too high or the buffer fullness exceeds a certain threshold, the video encoder is instructed to reduce its bit-rate, implying a concomitant dropping of the image quality.

The Bit Mapper assigns the most significant source coded bits (MSB) to the input of the strongest FEC codec, FEC K, while the least significant bits (LSB) are protected by the weakest one, FEC 1. K-class FEC coding is used after mapping the speech and video bits to their appropriate bit protection classes, which ensures source sensitivity-matched transmission. 'Adaptive Modulation' originally proposed by Steele and Webb [194], which was discussed in Section 9.5.2.7 is employed [2], [146]- [175] with the number of modulation levels, the FEC coding power and the speech/video source coding algorithm adjusted by the 'System Control' according to the dominant propagation conditions, bandwidth and power efficiency requirements, channel blocking probability or PRMA packet dropping probability. If the communications quality or the prevalent system optimisation criterion cannot be improved by adaptive transceiver re-configuration, the serving BS will hand the PS over to another BS providing a better grade of service.

One of the most important and reliable parameters used to control these algorithms is the 'Error Detection' flag of the FEC decoder of the most significant bit (MSB) class of speech and video bits, namely FEC K. This flag can also be invoked to control the speech and video 'Postprocessing' algorithms. The adaptive modulator transmits the user bursts from the PS to the BS using the specific PRMA slot allocated by the BS for the PS's speech, data or video information via the linear radio frequency (RF) transmitter (Tx). Although the linear RF transmitter has a low power efficiency, its power consumption is less critical due to the low transmitted power requirement of the multi-media PCN than that of the digital signal processing (DSP) hardware.

The receiver structure essentially follows that of the transmitter. After linear class-A amplification and automatic gain control (AGC) the 'System Control' information characterising the type of modulation and the number of modulation levels must be extracted from the received signal, before demodulation can take place. This information also controls the various internal bit mapping algorithms and invokes the appropriate speech and video decoding as well as FEC decoding procedures. After 'Adaptive Demodulation' at the BS the source bits are mapped back to their original bit protection classes and FEC decoded. As mentioned, the error detection flag of the strongest FEC decoder, FEC K, is used to control hand-overs or speech and video post-processing. The FEC decoded speech and video bits are finally source decoded and the recovered speech arrives at the earpiece, while the video information is displayed on a flat liquid crystal display (LCD).

The system control algorithms of the re-configurable mobile multi-media communicator will dynamically evolve over the years. PSs of widely varying complexity will coexist, with newer ones providing backward compatibility with existing ones, while offering more intelligent new services and more convenient features. Following the above rudimentary system-level overview of multi-mode transceivers, in the next two subsections we incorporate the previously highlighted system components in two different transceivers, in order to provide guidelines for designers of novel transceivers and to characterise the expected performance of such systems. Two well-understood system design contexts were selected for hosting the system components and for evaluating their performance, namely that of a 30 kHz bandwidth and a 200 kHz bandwidth system, which are the bandwidths of the Pan-American IS-54 system and the Global System of Mobile communications, known as GSM. We note, however that the systems studied are different from the standard schemes mentioned, only their bandwidths are identical. Nonetheless, systems similar to those studied in this chapter may become evolutionary successors of the IS-54 and GSM schemes, respectively. Let us initially consider the proposed 30 kHz bandwidth system in the next subsection, commencing with a brief description of the channel coding schemes used to protect the source-coded speech and video bits.

9.7.2 A 30 kHz Bandwidth Multi-media System

9.7.2.1 Channel-coding and Bit-mapping

Both convolutional and block error correction codes were portrayed in depth in Chapter 4, hence here we retsrict our discussions to the practical aspects of the FEC scheme proposed for our multi-media system shown in Figure 9.29.

Encoding a speech packet using an integer number of FEC-coded blocks allows us to carry out direct comparisons between different sources of speech impairments on the basis of dropped PRMA packets due to network overload or corrupted speech packets due to channel impairments. Furthermore, in our proposed packet radio transceivers we opted for binary Bose-Chaudhuri-Hocquenghem (BCH) block codes (see Section 4.4.3), since we found that the subjective speech quality of BCH-coded speech was often preferable to convolutionally coded speech due to longer unimpaired speech segments, even if the objective Segmental Signal to Noise Ratio (SEGSNR) and Bit Error Rate (BER) performances of the convolutional and block codes were similar. This was because the speech quality is typically more strongly dependent on the frame error rate (FER) than on decoded BER. Furthermore, powerful block codes also have a reliable error detection capability, which can be advantageously exploited in order to invoke speech post-enhancement in the case of error events [193].

A set of appropriate FEC codes for the 4.8 kbps TBPE speech codec is constituted by the BCH5=BCH(63,36,5), BCH2=BCH(63,51,2) and BCH1=BCH(63,57,1) codes, correcting 5, 2 and 1 bits per 63-bit frame, respectively. Accordingly, the most sensitive class 1 (C1) 36 speech bits of Table 9.2 are protected by the powerful BCH(63,36,5) code, while the less vulnerable 51 class 2 (C2) and 57 class 3 (C3) bits are encoded by the BCH(63,51,2) and BCH(63,57,1) codes, respectively. The total number of protected bits is 144. The packet header, which is conveying control information, is also BCH(63,36,5) coded, hence $4 \cdot 63 = 252$ bits per 30 ms are transmitted. This corresponds to transmitting 252/4=63 four-bit 16-QAM symbols and, upon adding three so-called ramp-symbols, yields a signalling rate of 66 symbols/30 ms = 2.2 kBd. The total bit-rate became 8.4 kbit/s. Recall from Chapter 8 that the ramping symbols are included, in order to assist the transceiver to power up and down smoothly, as it was highlighted in the context of the power ramping mask of the GSM system in Figure 8.29, which was necessary for mitigating the spurious adjacent channel emissions.

The above FEC scheme has the advantage of curtailing error propagation across speech frame boundaries and over-bridging deep channel fades for typical urban vehicular speeds. For example, for a vehicular speed of 30 mph or 13.3 m/s the travelling distance is 39.9 cm/30 ms speech frame. For a propagation frequency of 1.8 GHz the wavelength is about 15 cm, and therefore interleaving over a time-domain interval corresponding to a travelled distance of about 40 cm ensures adequate error randomisation for the FEC scheme to work efficiently. However, for pedestrian speeds there is a danger of idling in deep fades, in which case the employment of a switch-diversity scheme or frequency hopping, as in Chapters 7 and 8 is essential.

The 852-bit video frame is encoded using 12 BCH(127,71,9) code-words, yielding a total of 1524 FEC-coded bits per video frame. A pair of these BCH codewords form a video packet of 254 bits or 64 four-bit 16-QAM symbols, which is expanded by two ramp symbols in order to generate a 66-symbol packet. For delivering the 1524-bit BCH-coded video frame, 1524/254=6 such 66-symbol packets are necessary, but during the 90 ms video frame repetition time there are only three 30 ms speech frames, implying that two reserved time-slots per 30 ms PRMA frame are required for video users. This is equivalent to a video signalling rate of $2 \times 2.2 = 4.4$ kBd. The video transceiver also obeys the structure of Figure 9.29.

The receiver seen in Figure 9.29 carries out the inverse functions of the transmitter. The error detection capability of the strongest BCH(63,36,5) decoder is exploited to initiate hand-overs and to invoke speech post-processing [193], if the FEC decoder's error correction capability happens to be overloaded due to interference or contention-induced PRMA packet collision. The system elements of Figure 9.29 were simulated and the key transceiver parameters of both the non-coherently detected 30-kHz bandwidth system and those of the coherently detected 200-kHz bandwidth schemes are summarised in Table 9.12, while the associated system performance will be characterised in the following two subsections.

The transmitted Baud-rate of our non-coherent transceiver was fixed to 20 kBd, in order for the PRMA signal to fit in a 30 kHz channel slot, as in the IS-54 system, when using a modem excess bandwidth of 50 % [2]. Hence our transceiver can accommodate TRUNC(20 kBd/2.2 kBd) = 9 time slots, where TRUNC represents truncation to the nearest integer. The slot duration was 30 ms/9 $\approx$ 3.33 ms and one of the PRMA users was transmitting speech signals recorded during a telephone conversation, while all the other users generated negative exponentially distributed speech spurts and speech gaps with mean durations of 1 and 1.35 s. The PRMA parameters used are summarised in Table 9.9, where it was made explicit again that two

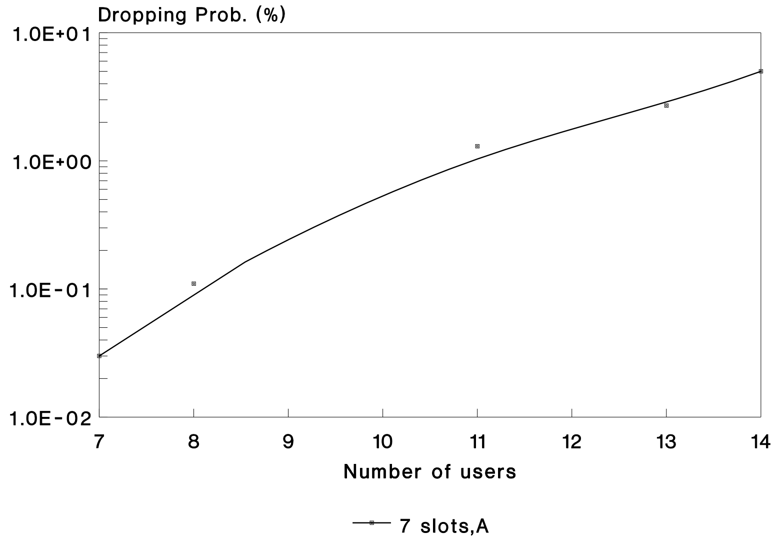

Figure 9.30: Packet dropping versus number of speech users performance ©Kluwer, 1995 Hanzo et al, [22].

PRMA parameter	30 kHz bandwidth system	200 kHz bandwidth system
Channel rate (kBd)	20	100
Speech rate (kBd)	2.2	3.1
Video rate (kBd)	4.4	16
Frame duration (ms)	30	30
Total no. of slots	9	32
No. of PRMA speech slots	7	32/42/47
No. of TDMA video slots	2	No. of users×6
Slot duration (ms)	3.33	0.9375
Packet header length (bits)	63	63
Maximum speech delay (ms)	32	30
Speech perm. prob.	0.6	0.2
Video perm. prob.	1	1

Table 9.9: Summary of PRMA/TDMA parameters.

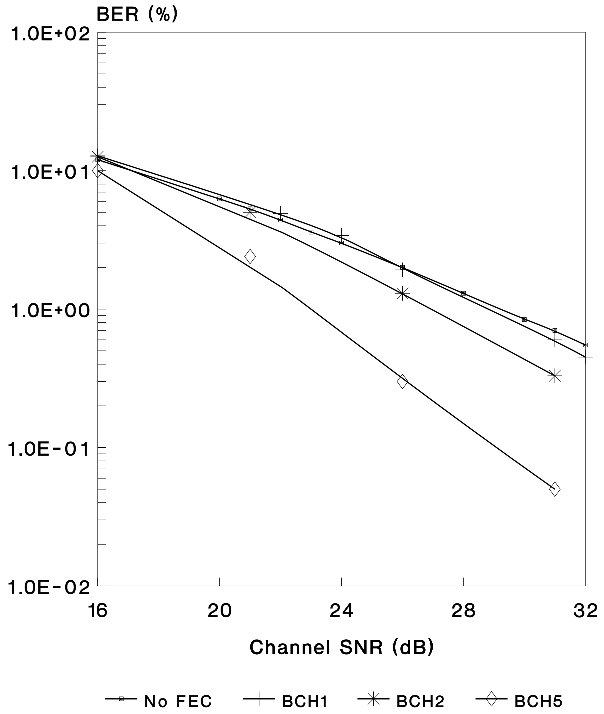

Figure 9.31: Non-coherent 16-QAM BER versus channel SNR performance over Rayleigh-fading channels for a vehicular speed of 30 mph, propagation frequency of 1.8 GHz and signalling rate of 20 kBD without diversity using BCH1, BCH2 and BCH5 coding©Kluwer, 1995 Hanzo *et al* [22].

time slots are reserved for a videophone user all the time and 7 slots are dynamically assigned to PRMA for the speech users. Let us now consider the robustness of the non-coherently detected 30-kHz bandwidth candidate system against channel effects.

9.7.2.2 Performance of a 30-kHz Bandwidth Multi-media System

In order to be able to contrast the performance of our multi-media system with that of an existing second-generation benchmarker, the system performance was evaluated for a narrowband Rayleigh-fading channel exhibiting a propagation frequency of 1.8 GHz, vehicular speed of 30 mph and signalling rate of 20 kBd, which is characteristic of an up-converted IS-54 system. The corresponding modem performance of the star and square QAM schemes was comparatively studied by Torrance and Hanzo in ref-

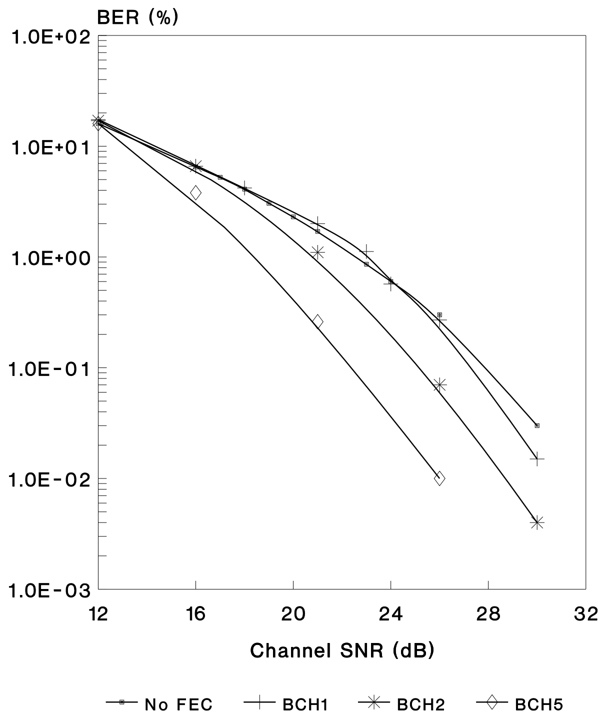

Figure 9.32: Non-coherent 16-QAM BER versus channel SNR performance over Rayleigh-fading channels for a vehicular speed of 30 mph, propagation frequency of 1.8 GHz and signalling rate of 20 kBD with diversity using BCH1, BCH2 and BCH5 coding ©Kluwer, 1995 Hanzo *et al* [22].

erence [143] and was summarised in Figure 9.26. Note that instead of the 24.3 kBaud signalling rate of the IS-54 scheme the more conservative 20 kBaud was used here, but a further potentially 20 % higher number of users can be supported, when increasing the Bd-rate to 24.3 kBd. The packet dropping probability versus number of PRMA speech users curve of the proposed system is portrayed in Figure 9.30. Observe that about 10-11 users can be supported by our 7-slot PRMA scheme with $P_{drop} < 1\%$, a value inflicting almost negligible speech degradation, while also supporting a videophone user.

The BER versus channel SNR performance of our 16-QAM transceiver with and without second-order selection diversity and BCH1, BCH2 and BCH5 FEC coding is depicted in Figures 9.7.2.1 and 9.7.2.1. When no diversity is invoked, at a channel SNR of about 28 dB the most important C1 bits protected by the BCH5 codec have a BER of about 0.1%, while the less

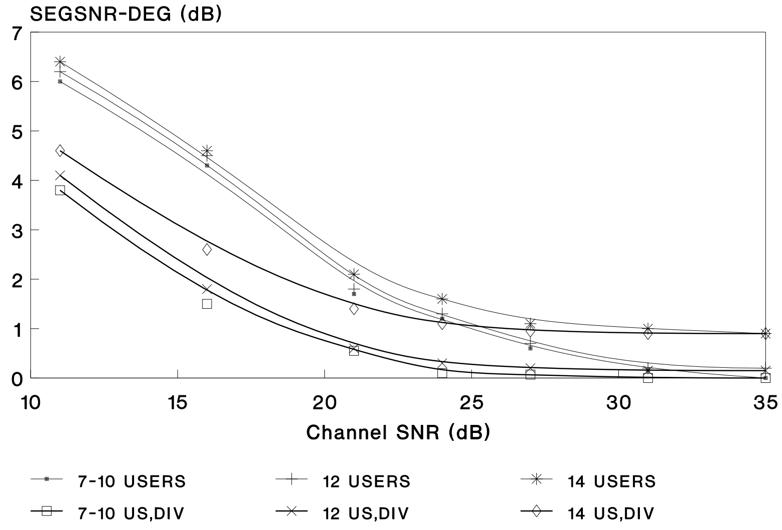

Figure 9.33: SEGSNR-DEG versus channel SNR performance of the proposed non-coherent 16-StQAM transceiver over Rayleigh-fading channels for a vehicular speed of 30 mph, propagation frequency of 1.8 GHz and signalling rate of 20 kBD with and without diversity parameterised with the number of PRMA users supported ©Kluwer, 1995 Hanzo et al, [22].

sensitive C2 and C3 bits attain BERs of about 0.5 and 1 %, respectively. These values are sufficiently low for nearly unimpaired speech transmission. When second-order diversity is used, these target BERs are achieved around 24 dB channel SNR. Although the lowest integrity C3 BCH1 codec does not provide a reduced BER for the least significant bits, since it is often overloaded, it ensures periods of unimpaired transmission for the most robust speech bits, which has a favourable subjective effect on the perceived speech quality. The 16-QAM modem is sensitive to co-channel interference, requiring SIR values similar to the minimum channel SNR necessitated [2]. Therefore it is beneficial to use the channel segregation algorithm proposed in references [170, 192] for mitigating the co-channel interference by classifying the slots on the basis of how interfered they are. Severely interfered slots can be temporarily disabled, at the cost of reducing the number of actively utilised slots, while high-quality, low-interference slots can guarantee the SIR required for unimpaired communications. No time-slot classification is necessary, if the system is used in an indoor environment, where the partitioning walls and floors naturally contribute towards the interference

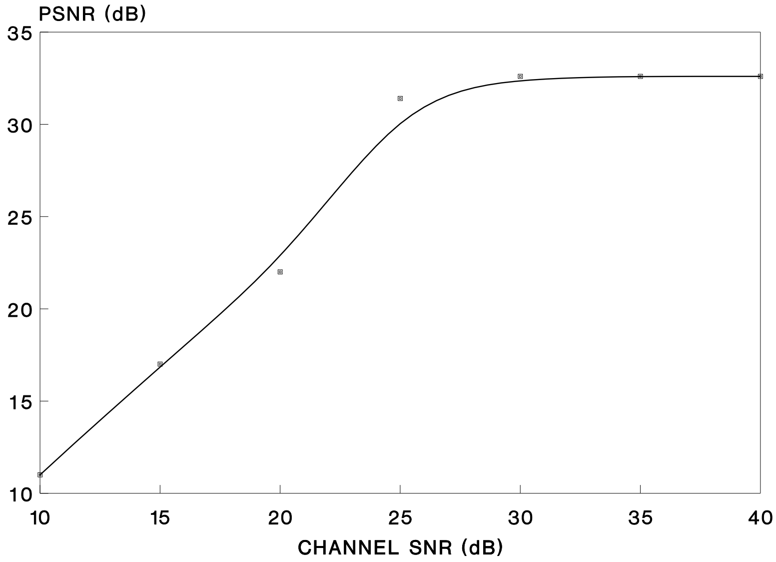

Figure 9.34: PSNR versus channel SNR performance of the proposed diversity-assisted non-coherent 16-QAM videophone scheme over Rayleigh-fading channels for a vehicular speed of 30 mph, propagation frequency of 1.8 GHz and signalling rate of 20 kBD ©Kluwer, 1995 Hanzo et al, [22].

mitigation.

The overall objective SEGSNR degradation (SEGSNR-DEG) versus channel SNR performance of our diversity-assisted PCS transceiver is displayed in Figure 9.33 parameterised with the number of PRMA users supported. While for 7-10 users no speech degradation can be observed, if the channel SNR is in excess of about 24 dB, for 12 users the SEGSNR-DEG due to PRMA packet dropping becomes noticeable, although not subjectively objectionable. in the case of 14 users, however, there is a consistent SEGSNR-DEG of about 1 dB due to the 4-5 % packet dropping probability seen in Figure 9.30. Without diversity about 5 dB higher channel SNR is necessitated in order to achieve a similar performance to that of the diversity-assisted scheme.

The PSNR versus channel SNR performance of the diversity-assisted video transceiver is portrayed in Figure 9.34, where in harmony with the voice transceiver a channel SNR of about 22-25 dB is required for near-unimpaired video quality. Without diversity the video scheme lacks robustness, since the corrupted run-length coded activity tables affect the whole of each video frame. We note that the video codec's robustness can be significantly improved upon dispensing with the quad-tree based motion- and DCT-activity table compression, as it was demonstrated in reference [99], at the cost of about 30% higher bit-rate requirement.

Let us now focus our attention on the 200-kHz bandwidth coherently detected multi-media system in the next subsection.

9.7.3 A 200 kHz Bandwidth Multi-mode, Multi-media System

In contrast to the previous subsection, where we used a non-coherent star 16-QAM multi-media scheme evaluated in the framework of a 30-kHz bandwidth system, here we portray the performance of a coherent multi-mode arrangement in the context of a GSM-like system following the approaches proposed by Hanzo and Woodard [19] as well as Cherriman *et.al.* [106]-[112]. While our discourse on the 30-kHz bandwidth system was somewhat more detailed, now we restrict our treatment to a brief summary of the rationale behind this system. These investigations will allow us to gauge the expected system performance in comparison to that of a well-known and widespread benchmarker, namely the GSM system. The basic differences between the two systems are as follows:

- The bandwidth was increased from 30 kHz to 200 kHz.
- Instead of the previous 4.8 kbps TBPE speech codec here a dual-rate 4.7/6.5 kbps Algebraic Code Excited Linear Predictive (ACELP) codec was employed [19], which was detailed in Section 3.4.2.4.
- The fixed-rate proprietary DCT video codec of Section 9.3.3 was exchanged against the programmable-rate ITU standard H.263 video codec of Section 9.3.4.
- The non-coherent star 16-QAM scheme of Section 9.5.2.6 was replaced by a coherent 4/16/64-QAM pilot-assisted scheme of Section 9.5.2.5, although for voice transmissions only the latter two modes were employed. The more vulnerable video codec necessitated the employment of the lower-rate, lower-quality but more robust 4-QAM mode.
- The system was arranged to convey the lower-quality 4.7 kbps ACELP-coded speech using the more robust 16-QAM mode, while the 6.5 kbps-coded higher-quality speech was transmitted at the same user Baud-rate within the same bandwidth, but requiring higher channel SNRs for 64-QAM transmissions.
- Similarly, the H.263 video codec was programmed to generate 1176, 2352 or 3560 bits per QCIF video frame for 4, 16 and 64-QAM transmission, respectively, which resulted in the same signalling rate, irrespective of the modem mode of operation used.
- A novel graphical source codec was introduced, in order to facilitate graphical correspondence with the aid of multiplexing speech, video and graphical signals using PRMA.

Codec Mode	4.7 kbps	6.5 kbps
LSF Parameters	34 bits/30 ms	34 bits/30 ms
Excitation and LTP	$4 \cdot 27$=108 bits/30 ms	$6 \cdot 27$=162 bits/30 ms
Total	142 bits/30 ms	196 bits/30 ms

Table 9.10: 4.7/6.5 kbps dual-rate ACELP codec bit-allocation.

The components of this scheme were described during our earlier discussions. Specifically, the principles of ACELP coding were addressed in Section 3.4.2.4, while the dual-rate codec's bit-allocation scheme and our bit sensitivity investigations were described in [19, 20]. Suffice to say here that the ACELP codec uses 34 Line Spectral Frequency (LSF) bits for spectral quantisation in both of its modes and a total of 27 bits per subsegment for the LTP and excitation parameters. In its 4.7 kbps mode there are four 7.5 ms excitation optimisation subsegments per 30 ms, while in the 6.5 kbps mode there are six 5 ms subsegments. Hence the total number of bits per 30 ms frame is either $34+4\times27=142$ or $34+6\times27=196$, yielding the required rates, as it is also shown in Table 9.10. Let us now consider some of the system-level details of this intelligent dual-mode scheme.

9.7.3.1 Low-quality Speech Mode

In this subsection we highlight our code design approach using the 4.7 kbit/s codec and note that similar principles were followed in case of the 6.5 kbit/s codec. The sensitivity of the 4.7 kbps ACELP source bits was evaluated similarly to the bit-sensitivities of the TBPE codec. Our detailed bit-sensitivity analysis was portrayed in [19, 20], which used the weighted SEGSNR and CD based approach introduced earlier in the context of the TBPE codec, but it also took account of the different error propagation properties of the various bits over consecutive speech frames.

Intuitively, one would expect that the more closely the FEC protection power is matched to the source sensitivity, the higher the system's robustness. In order to limit the system's complexity and the variety of candidate schemes, in the case of the 4.7 kbit/s ACELP codec we experimented with a single-class or full-class BCH codec, a twin-class and a quad-class scheme, while maintaining the same channel coding rate. We found that similar results were obtained for the twin- and quadruple-class scheme, hence we opted for the lower-complexity twin-class protection [19].

Our propagation conditions were characterised by a pedestrian speed of v =3 mph, propagation frequency of f_p =1.8 GHz, pilot symbol spacing of P=10 and a signalling rate of 100 kBd, which fitted in a bandwidth of 200 kHz, when using a unity Nyquist roll-off factor. The corresponding

Doppler frequency f_d was:

$$f_d = (v \cdot f_p)/c = (1.388\text{m/s} \cdot 1.8 \cdot 10^9\text{Hz})/(3 \cdot 10^8\text{Hz}) \approx 8.33\text{Hz},$$

while the corresponding normalised Doppler frequency was:

$$f_d \cdot T = 8.33\text{Hz} \cdot 1/(10^5\text{Baud}) \approx 0.0000833,$$

which is a slower fading rate than that of the previous non-coherent system due to the ten-fold reduced speed of 3 mph and the five-fold increased signalling rate.

Note however that the above conservative choice of roll-off factor and the associated bandwidth efficiency can be improved substantially, when opting for a roll-off factor of 0.5, as in the case of the previously described star 16-QAM system, or even for 0.35, as proposed for the ATDMA system, at the cost of a slight complexity increase and clock jitter sensitivity. We found that for a channel SNR of about 20 dB the pilot-assisted 16-QAM modem provided two independent QAM subchannels exhibiting different bit error rates (BERs), which was demonstrated earlier in Figure 9.22 over AWGN channels. The BER is about a factor of three times lower for the higher integrity path referred to as the Class 1 (C1) subchannel than for the C2 subchannel over Rayleigh-fading channels [2,19]. We capitalised on this feature to provide unequal source sensitivity-matched error protection combined with different BCH codecs for our ACELP codecs.

If the ratio of the BERs of these QAM subchannels does not match the sensitivity constraints of the ACELP codec, it can be 'fine-tuned' with the aid of different BCH codecs, while maintaining the same number of BCH-coded bits in both subchannels. However, the increased number of redundancy bits of stronger BCH codecs requires that a higher number of sensitive bits are directed to the lower integrity C2 subchannel, whose channel coding power must be concurrently reduced in order to accommodate more source bits. This non-linear optimisation problem can only be solved experimentally, assuming a certain sub-division of the source bits, which would match a given pair of BCH codecs.

When designing the twin-class protection scheme and opting for the approximately half-rate BCH(127,71,9) codec in both subchannels, the ACELP source bits have to be split into two classes, each hosting 71 bits. From our bit sensitivity analysis [19,20] we observed that the more sensitive bits require almost an order of magnitude lower BER than the more robust bits, in order to inflict a similar SEGSNR penalty. Hence both classes must be protected by different codes, and after some experimentation we found that the BCH(127,57,11) and BCH(127,85,6) codes employed in the C1 and C2 16-QAM subchannels provide the required integrity. Each 142-bit ACELP frame is encoded by two BCH codewords, yielding $2 \cdot 127 = 254$ encoded bits and curtailing error propagation at the transmission packet boundaries. The FEC-coded speech bit-rate became $\approx$8.5 kbps, implying an overall coding rate of 4.7 kbps/8.8 kbps $\approx$ 0.553.

The PRMA control header was allocated a BCH(63,24,7) code and hence the total PRMA framelength became 317 bits, representing 30 ms speech and yielding a total bit-rate of $\approx$ 10.57 kbps. The 317 bits constitute 80 16-QAM symbols, and 9 pilot symbols as well as 2+2=4 ramp symbols must be added, resulting in a PRMA transmission packet-length of 93 symbols per 30 ms speech frame. Hence the signalling rate becomes 3.1 kBd. Using a PRMA bandwidth of 200 kHz, similarly to the Pan-European GSM system, and a filtering excess bandwidth of 100 % allowed us to accommodate 100 kBd/3.1 kBd $\approx$ 32 PRMA slots. When using an excess bandwidth of 50%, as in our star 16-QAM system, the signalling rate would be 133 kBd, accommodating 42 PRMA time slots. Similarly, when opting for the ATDMA excess bandwidth of 35%, the signalling rate could be increased to 148 kBd, supporting 47 PRMA slots, which in turn would further increase the PRMA gain expressed in terms of the number of users supported.

9.7.3.2 High-quality Speech Mode

Following the approach proposed in the previous subsection we designed a triple-class source-matched protection scheme for the 6.5 kbps ACELP codec. The reason for using three protection classes this time is that the 6.5 kbps ACELP codec's higher bit-rate must be accommodated by a 64-level QAM constellation, which inherently provides three different integrity subchannels, which again, was shown earlier in Figure 9.22 over AWGN channels. When using second-order switched-diversity and pilot-symbol assisted coherent square-constellation 64-QAM [2] amongst our previously stipulated propagation conditions with a pilot-spacing of P=5 and channel SNR of about 25 dB, the C1, C2 and C3 subchannels have BERs of about 10^{-3}, 10^{-2} and $2 \cdot 10^{-2}$, respectively [2].

The source sensitivity-matched codes for the C1, C2 and C3 subchannels are BCH(126,49,13), BCH(126,63,10) and BCH(126,84,6), while the packet header was allocated again a BCH(63,24,7) code. The total number of BCH-coded bits becomes $3 \cdot 126 + 63$=441/30 ms, yielding a bit rate of 14.7 kbps. The resulting 74 64-QAM symbols are amalgamated with 15 pilot and 4 ramp symbols, giving 93 symbols/30 ms, which is equivalent to a signalling rate of 3.1 kBd, as in the case of the low-quality mode of operation. Again, 32 PRMA slots can be created, as for the low-quality system, accommodating more than 50 speech users in a bandwidth of 200 kHz and yielding an equivalent speech user bandwidth of about 200 kHz/50 users = 4 kHz, while maintaining a packet dropping probability of about 1 %.

9.7.3.3 Multi-mode Video Transmission [110, 112] [3]

Similarly to the above dual-mode philosophy, we also contrived a multi-mode videophone scheme, where the H.263 video codec was used and a number of speech slots were dedicated to videophony. In this system again, we considered transmitting QCIF images, where the video codec was programmed to generate 3560, 2352 or 1176 bits per frame, which were then transmitted using 64-, 16- or 4-QAM, respectively, at a constant signalling rate, requiring the same bandwidth.

Earlier in this chapter in Figure 9.22 we have shown that in square-constellation QAM schemes the bits can be assigned to a number of different integrity classes. The number of integrity classes depends on the number of modulation levels, and in 4-QAM there is only one integrity class, in 16-QAM there are 2, while in 64-QAM there are 3 classes, often also referred to as sub-channels. By using different strength FEC codes on each QAM sub-channel it is possible to equalise the probability of errors on the QAM sub-channels for video transmission. This means that all sub-channels' FEC codes should break down at approximately the same channel SNR. This is desirable, if all bits to be transmitted are equally important. Since the H.263 datastreams are variable length coded, one error can cause a loss of synchronisation and corrupt the rest of the frame. Therefore in this case most bits are equally important, and hence 'equalisation' of the QAM sub-channels' BER is desirable. The FEC codes used in our system in order to achieve a similar BER in all QAM sub-channels are summarised in Table 9.11.

Eight of each of the codewords are required for the encoding of the generated 3560, 2352 and 1176 bits/frame in all three modes of operation. In order to generate video packets compatible with the speech packets, again, the same BCH(63,24,7) packet header was selected. In the 4-QAM mode the 255+63=318 bits constitute 159 2-bit symbols, and after adding 17 pilot symbols as well as 2+2=4 so-called ramp symbols, during which the power amplifier is smoothly ramped up and down, in order to mitigate out-of-band spectral spillage, the resulting framelength becomes 180 symbols. Hence for delivering the 180-symbol video packets we require double-length speech slots, since the speech slots were 93 symbol long. Consequently, for the transmission of an FEC-coded video frame eight such 180-symbol packets per 90 ms are necessary, which can be accommodated by reserving three double-length speech slots per 30 ms PRMA frame, capable of delivering up to nine such video packets per 90 ms frame repetition interval. The corresponding video signalling rate including the packet header becomes 8×180 symb/90 ms = 16 kBaud. It is worth noting that it is possible to packetise the FEC-coded 1176 video bits as 4-bit 16-QAM symbols, rather than 2-bit 4-QAM symbols, which halves the length of the transmission burst

[3]This subsection is supported by a range of video demonstrations using various channel conditions under the WWW address http://www-mobile.ecs.soton.ac.uk

Modulation scheme	FEC codes used
4 QAM	BCH(255,147,14)
16 QAM	Class 1: BCH(255,179,10) Class 2: BCH(255,115,21)
64 QAM	Class 1: BCH(255,199,7) Class 2: BCH(255,155,13) Class 3: BCH(255,91,25)

Table 9.11: FEC codes used for the 4, 16 and 64 QAM transmission modes in conjunction with H.263 video coding ©Cherriman, Hanzo [110], 1995.

expressed in terms of modulation symbols. Consequently, this stream then can be arranged to occupy single, rather than double slots. Therefore the signalling rate can be reduced to 8 kBd at the cost of requiring higher channel SNR and SIR values than the more robust, but higher-rate 16 kBd 4-QAM system. Alternatively, the number of video bits can be doubled, which improves the associated video quality. Clearly, these different system configuration modes highlight the underlying trade-offs that designers of such flexible systems are faced with [112].

When comparing the 16-QAM modes of operation of the coherent and non-coherent video transceivers, in the non-coherent star 16-QAM system an 9.47 kbps video codec was used, while in the coherent 16-QAM scheme a bit-rate of 2352 bits/(90 ms) ≈26.13 kbps was maintained. Furthermore, the coherent scheme uses a stronger FEC scheme and some channel capacity is also dedicated to pilot symbols. Similar arguments are also valid for the 64-QAM mode, which can improve the associated video quality, delivering 3560 bits/frame, at the cost of higher required channel SNRs. Again, six time slots must be dedicated to support an H.263-based videophone call, which substantially reduces the system's speech capacity.

9.7.3.4 Packet reservation multiple access assisted multi-level graphical communications [195]

9.7.3.4.1 Graphical Transmission Issues In order to complement the proposed multi-rate FL-DCC graphical source codec discussed in Section 9.4, we used the previously introduced re-configurable multi-mode QAM modem. The most robust, but least bandwidth efficient 4-level Quadrature Amplitude Modulation (4-QAM) [2] mode can be used in outdoor scenarios in conjunction with the $b = 1$ mode of the FL-DCC codec. The less robust but more bandwidth efficient 16-QAM mode may be invoked in friendly indoor cells in order to accommodate the $b = 2$ mode of operation of the FL-DCC codec. When the channel conditions are extremely favourable, the modem can also be configured as a 64-QAM scheme,

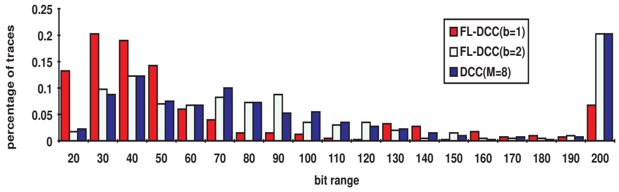

Figure 9.35: Histogram of the average trace length ©ETT, Hanzo and Yuen [195].

in which case it can deliver $b = 3$ bits per FL-DCC vector, allowing lossless coding.

As in our previous multi-mode schemes, we exploited that the BER of the lower quality class 2 (C2) 16-QAM subchannel was found to be a factor 2-3 times higher, than that of the higher integrity class 1 (C1) subchannel. Hence the more vulnerable FL-DCC coded bits were transmitted via the C1 subchannel, while the more robust bits over the C2 16-QAM subchannel. For error correction coding we used binary BCH codes, which were the topic of Chapter 4. Their specific coding parameters will be specified during our forthcoming discourse.

9.7.3.4.1.1 Graphical Packetisation Aspects In order to determine the desirable length of the transmission packets, in Figure 9.35 we evaluated the histogram of the average trace length, which exhibited a very long low-probability tail. This probability tail was represented by the bars at an encoded trace-length of 200 bits in the Figure. Observe furthermore that, as expected, the highest concentration of short traces was recorded for $b = 1$, which was followed by $b = 2$ and the DCC mode of operation. However, most traces generated less than a few hundred bits, even when $b = 2$ was used. In order to be able to use a fixed packet length, while maintaining robustness against channel errors and curtailing transmission error propagation across packets and/or traces, we decided to tailor the number of bits per trace to the packet length of 222 bits. If a longer trace was encountered, it was forcibly truncated to this length and the next packet started with a new 'artificial' pen-down code. If, however, a shorter trace was encountered, a second trace was also fitted into the current packet and eventually truncated to the required length for transmission. Unfortunately, the additional forcibly included VC code and the X_0, Y_0 coordinates portrayed in Figure 9.12 increased the number of bits generated but mitigated the error propagation effects. The proportion of the bit-rate increase evaluated in terms of percent for various packet lenghts in the case of the FL-DCC $b = 1$ scheme is portrayed in Figure 9.36.

Recall that the C1 16-QAM subchannel had a factor 2-3 times better BER than the C2 subchannel. This ratio would remain approximately

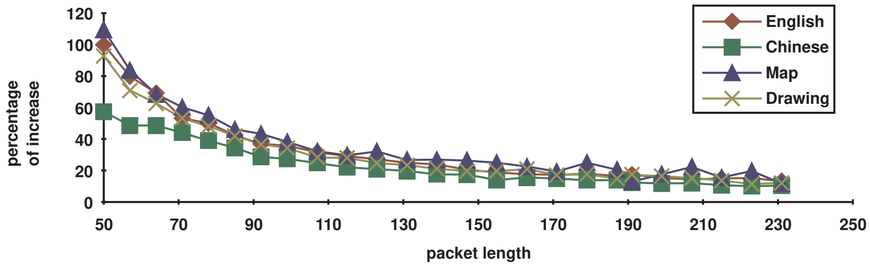

Figure 9.36: Proportion of bit-rate increase due to fixed-length trace termination versus packet length for the FL-DCC $b = 1$ scheme ©ETT, Hanzo and Yuen [195].

the same if we were to use the same FEC code in both subchannels, but the C2 BER would remain excessively high for the transmission of the starting vectors (SV) and fixed-length vectors (FV) of Figure 9.12. The BCH(255,131,18) and BCH(255,91,25) codes were found to ensure the required balance between the more and less robust FL-DCC bits, when employed in the C1 and C2 16-QAM subchannels, respectively. In other words, employing the more powerful BCH(255,91,25) codec in the higher-BER C2 16-QAM subchannel reduced the integrity difference between the subchannels and ensured the required source-sensitivity matched unequal error protection. The $2\times255=510$ BCH-coded bits constitute 128 4-bit 16-QAM symbols. After adding 14 pilot symbols according to a pilot spacing of 10 and concatenating 4 ramp symbols for smooth power amplifier ramping in order to minimise the out-of-band emissions, the resulting 146-symbol packets are queued for transmission to the BS. The same packet format can be used for the voice/video packets. Both the voice and the video codecs generate in their 8 kbps mode of operation 160 bits/20 ms frame and hence the 222-bit packet can accommodate a 62-bit signalling and control header in each 146-symbol packet. The corresponding single-user voice/video signalling rate becomes 146 symbols/20 ms = 7.3 kBd. Due to their significantly lower rates and higher delay tolerance, graphical users assemble their 146-symbol transmission packets over a longer period, before their transmission. The issue of maximum achievable graphical data rate will be addressed in the Results Section.

In the event of channel quality degradation the more robust 4-QAM mode can be invoked under BS control. However, since the 4-QAM packets can only convey half the number of bits, when compared to 16-QAM, the re-configurable graphical source codec has to halve its bit-rate, as we have seen in the case of our voice and video codecs earlier in this chapter. Explicitly, under unfavourable channel conditions the FL-DCC graphical source encoder can reduce the number of bits from $b = 2$ to 1 under the control of the BS, while providing adequate graphics quality. Again, these issues will be discussed in more depth during our further discussions. In order to maintain the same 222-bit long framing structure, as in the case of the 16-QAM mode of operation, we used two codewords of the shortened BCH(255,111,21) code in conjunction with the 4-QAM modem scheme, since the 4-QAM modem does not have different integrity sub-channels.

9.7.3.4.2 Graphics, Voice and Video Multiplexing using PRMA

Packet reservation multiple access (PRMA) was introduced earlier in this chapter as a convenient technique of surrendering passive speech or video slots, in favour of users, who are becoming active. Here PRMA is also invoked in order to multiplex the graphics source information with the voice and video packets for transmission to the base station. We have argued before that the packet dropping probability due to packet collision must remain below $P_{drop} = 1$ % [206], in order to minimise the speech degradation. Fortunately this initial speech spurt clipping is hardly perceivable, if the 1 % dropping probability requirement is not violated.

In contrast to speech, graphical data packets cannot be dropped, but tolerate longer delays and can be allocated to slots, which are not reserved by speech users in the present frame. In our exepriments the user transmitted graphical traces generated by a writing tablet. A less than unity permission probability either allowed or disabled permission to contend during any particular slot for a reservation within the current PRMA frame. Wong and Goodman noted [207] that it is advantageous to control data packet contentions on the basis of the fullness of the contention buffer. Specifically, contentions are disabled, until a certain number of packets awaits transmission, which reduces the probability of potential packet collisions due to the frequent transmission of short graphical data bursts. While speech communications stability can be defined as a dropping probability $P_{drop} < 1\%$, data transmission stability is specified in terms of maximum graphical data delay or buffer requirement. The PRMA packet multiplexer is depicted in Figure 9.37, and as an example, we indicated in the Figure a set of permission probabilities P, which could be employed by the various speech, data and video users in order to satisfy their corresponding delay and packet dropping constraints, while maximising the multiplexer's throughput capacity. The specific permission probability values indicated in the Figure were only used for the sake of illustration, they have to be optimised for the specific prevalent service quality requirements.

9.7.3.5 Performance of the 200 kHz Bandwidth Multi-mode, Multi-media System

9.7.3.5.1 Speech Performance The PRMA parameters used in our 100 kBaud, 200-kHz bandwidth multi-media system are summarised in Table 9.9 in contrast to those of the previously described 30-kHz bandwidth scheme. Observe in the Table that the most significantly different system

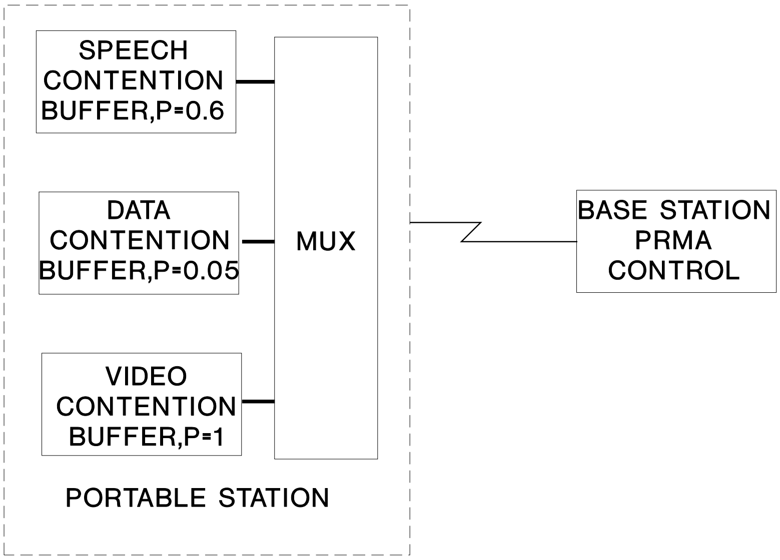

Figure 9.37: PRMA packet multiplexer ©ETT, Hanzo and Yuen [195].

parameters are the signalling rate and hence the number of PRMA slots and the number of users supported. Furthermore, the GSM-like scheme uses stronger error correction coding, which increased the non-coherent systems's speech Baud-rate from 2.2 to 3.1 kBaud. Furthermore, the optimum permission probability is reduced from 0.6 to 0.2 at a concomitant increase of the number of slots form 7 to 31, since best PRMA performance is achieved, if the number of users contending at any instant is kept approximately proportional to the total number of slots available.

The number of speech users supported by the 32-slot PRMA system becomes explicit from Figure 9.38, where the packet dropping probability versus number of users is displayed. Observe that more than 55 users can be served with a dropping probability below 1 %. The number of PRMA users per slot becomes about 1.72, which is higher than the 1.43 PRMA user/slot parameter of the 30-kHz bandwidth, 20 kBaud non-coherent multi-media scheme. This is a consequence of the higher statistical multiplexing gain associated with a higher number of slots and users. In order to restrict the subjective effects of PRMA-imposed packet dropping, according to Figure 9.38 the number of users must be below 60. As a comparative basis it is worth noting that the 8 kbps CCITT/ITU ACELP speech codec's target was to inflict less than 0.5 Mean Opinion Score (MOS) degradation in case of a speech frame error rate of 3% [46]. Again, in case of roll-off factors of

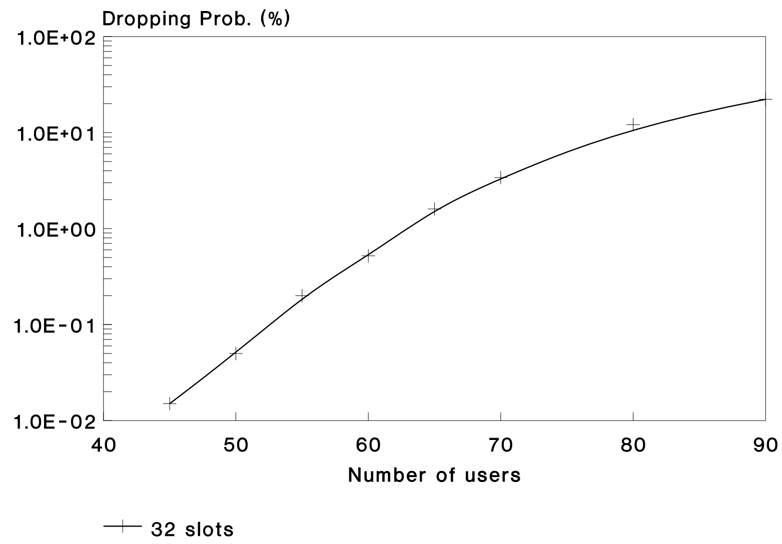

Figure 9.38: Packet dropping probability versus number of users for 32-slot PRMA ©IEEE, Hanzo, Woodard 1995, [19].

0.5 and 0.35 the 200 kHz system can accommodate 42 and 47 PRMA slots, supporting up to 70 and 80 users, respectively, when assuming 1.72 PRMA users per slot.

The SEGSNR versus channel SNR performance of the re-configurable 100 kBd transceiver using 32-slot PRMA is shown in Figure 9.39 for different number of conversations. Observe in the Figure that in contrast to the 30 kHz bandwidth system here we used SEGSNR, rather than SEGSNR degradation, as a system performance measure, since we wanted to portray the quality difference between the higher and lower quality modes of operations. We emphasise furthermore again that the number of users (us.) here is related to the 100 kBd, 100% excess bandwidth, 32-slot scenario. For the 42 and 47-slot scenarios similar tendencies can be observed. When the channel SNR was in excess of about 25 dB, the 6.5 kbps/64-QAM system outperformed the 4.7/16-QAM scheme in terms of both objective and subjective speech quality. Furthermore, at around 25 dB channel SNR, where the 16-QAM and 64-QAM SEGSNR curves cross each other in Figure 9.39 it is preferable to use the inherently lower quality but unimpaired mode of operation. When supporting more than 32 users, as in our PRMA-assisted system, speech quality degradation is experienced due to packet corruption caused by channel impairments and packet dropping caused by PRMA

Parameter	30 kHz System	200 kHz System
		Low/High Quality Mode
Speech Codec	4.8 kbps TBPE	4.7/6.5 kbps ACELP
Speech FEC	Triple-class BCH	Twin-/Triple-class Binary BCH
FEC-coded Speech Rate	8.6 kbps	8.5/12.6 kbps
Video Codec	Fixed-rate DCT	Packetised H.263
No. of Video bits/fr	852	1176, 2352 or 3560
Video Rate (kbps)	9.47	13.1, 26.1 or 39.6
Video FEC	BCH(127,71,9)	see Table 9.11
Modulation for Speech	Star 16-QAM	Square 16-QAM/64-QAM
Modulation for Video	Star 16-QAM	Square 4-/16-/64-QAM
Demodulation	Non-coh.	Coherent, Diversity, PSAM
Equaliser	No	No
Speech Signalling Rate (kBd)	2.2	3.1
Video Signalling Rate (kBd)	4.4	8/16
VAD	GSM-like (Chap 3)	GSM-like
Multiple Access	7-slot PRMA + 2-slot TDMA	(32/42/47-slot PRMA)- No. of Video Slots (n$\times$6 or 3)
Speech Frame Length (ms)	30	30
Slot Length (ms)	3.33	0.94/0.71/0.64
Channel rate (kBd)	20	100-148
System Bandwidth (kHz)	30	200
No. of PRMA Speech Users	> 10	$>$ 50-80
No. of PRMA Users/slot	1.43	> 1.72
Equiv. Speech User Bandwidth	3	2.5-4
Min. Channel SNR/SIR (dB)	24	15/25

Table 9.12: Transceiver parameters.

packet collisions. These impairments yield different subjective perceptual degradations, which we will attempt to compare in terms of the objective SEGSNR degradation. Quantifying these speech imperfections in relative terms in contrast to each other will allow system designers to adequately split the tolerable overall speech degradation between packet dropping and packet corruption. Observe in Figure 9.39 that the rate of change of the SEGSNR curves is more dramatic due to packet corruption caused by low-SNR channel conditions than due to increasing the number of users. As long as the number of users does not significantly exceed 50, the subjective effects of PRMA packet dropping show an even more benign speech quality penalty than that suggested by the objective SEGSNR degradation, because frames are typically dropped at the beginning of a speech spurt due to a failed contention, rather than during active speech spurts.

In conclusion, our re-configurable transceiver has a single-user rate of 3.1 kBd, and can accommodate 32 PRMA slots at a PRMA rate of 100 kBd in a bandwidth of 200 kHz. The number of users supported is in excess of 50 and the minimum channel SNR for the lower speech quality mode is about 15 dB, while for the higher quality mode it is about 25 dB. The number of time slots can be further increased to 42, when opting for a modulation access bandwidth of 50%, accommodating a signalling rate of 133 kBd within the 200 kHz system bandwidth. This will inflict a slight bit error rate penalty, but will pay dividends in terms of increasing the number of PRMA users by about 20. The parameters of the proposed transceiver

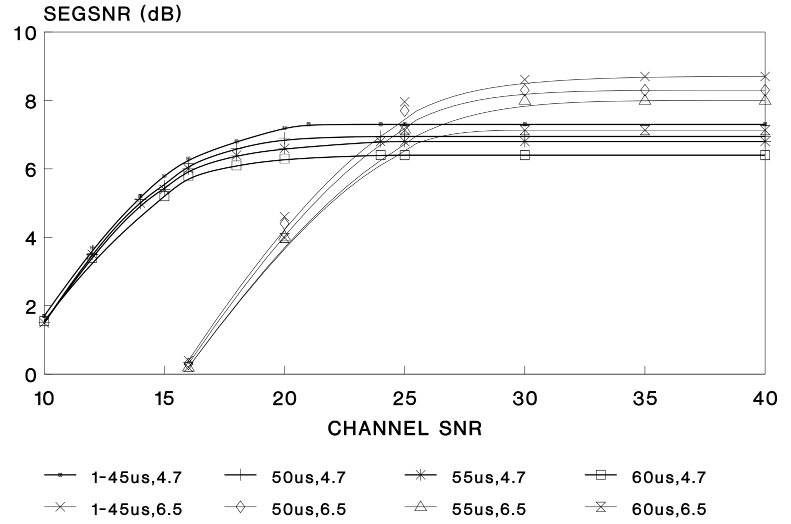

Figure 9.39: SEGSNR versus channel SNR performance of the re-configurable 100 kBd transceiver using 32-slot PRMA for different number of conversations ©IEEE, Hanzo, Woodard 1995, [19].

are summarised in Table 9.12. In order to minimise packet corruption due to interference, the employment of a time-slot quality ranking algorithm is essential for invoking the appropriate mode of operation. When serving 50 users, the effective user bandwidth becomes 200 kHz/50 = 4 kHz, which guarantees the convenience of wireless digital speech communication in a bandwidth similar to conventional analogue telephone channels. The 4 kHz user bandwidth can be further reduced to 200 kHz/70 users $\approx$ 2.9 or even to 200 kHz/80 users = 2.5, when using a modulation roll-off factor of 0.5 or 0.35, respectively, hence accommodating more PRMA slots and therefore supporting more PRMA users.

9.7.3.5.2 Video Performance The corresponding H.263-based video system performance was also evaluated under the same propagation conditions, but in addition to the previous 4.7 kbps 16-QAM and 6.5 kbps 64-QAM modes the more robust 4-QAM mode was introduced, in order to provide higher robustness for the more error-sensitive video bits. In the various operating modes investigated the PSNR versus channel SNR curves of Figures 9.40 and 9.41 were obtained for AWGN and Rayleigh channels, respectively. Since both the H.261 and H.263 source codecs have

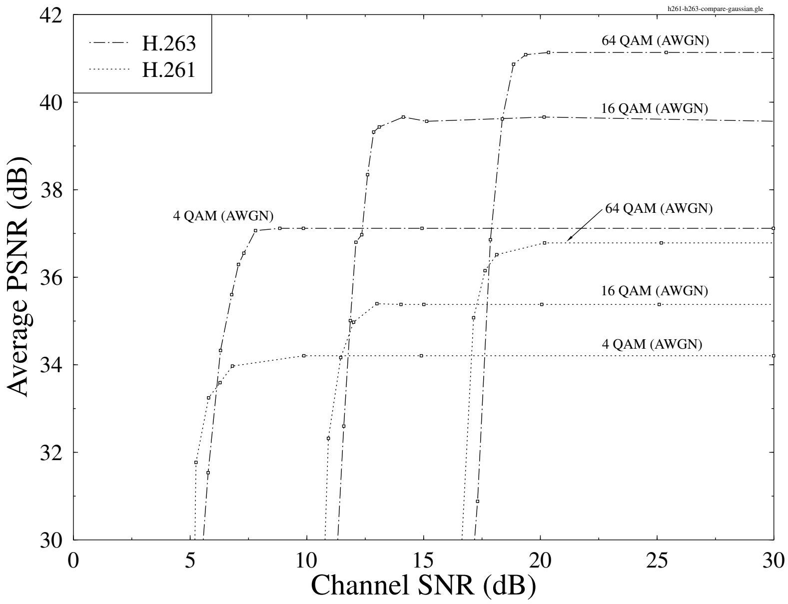

Figure 9.40: Performance comparison of the proposed adaptive H261 and H263 transceivers over AWGN channels ©Cherriman, Hanzo [110], 1995.

had similar robustness against channel errors, and their transceivers were identical, the associated 'corner SNR' values, where unimpaired communications broke down, were virtually identical for both systems over both AWGN and Rayleigh channels. However, as expected, the H.263 codec exhibited always higher video quality at the same bit-rate or system bandwidth. We note in closing that the described H.263-based video scheme reduces the speech capacity of the GSM-like system by six speech users, every time a new video user is admitted to the system. Let us now conclude our findings throughout this chapter.

9.7.3.5.3 Graphical System Performance The overall graphical system robustness is characterised below in terms Figures 9.42-9.45. The graphical representation quality was evaluated in terms of both the mean squared error (mse) and the Peak Signal to Noise Ratio (PSNR). In analogy to the previous PSNR in video telephone quality evaluation, the graphical PSNR was defined as the squared ratio of the maximum possible spatial deviation from the uncoded graphical trace across the graphical screen, related to the quantisation-induced deviation from the original graphical trace, which is the equivalent of the quantisation distortion.

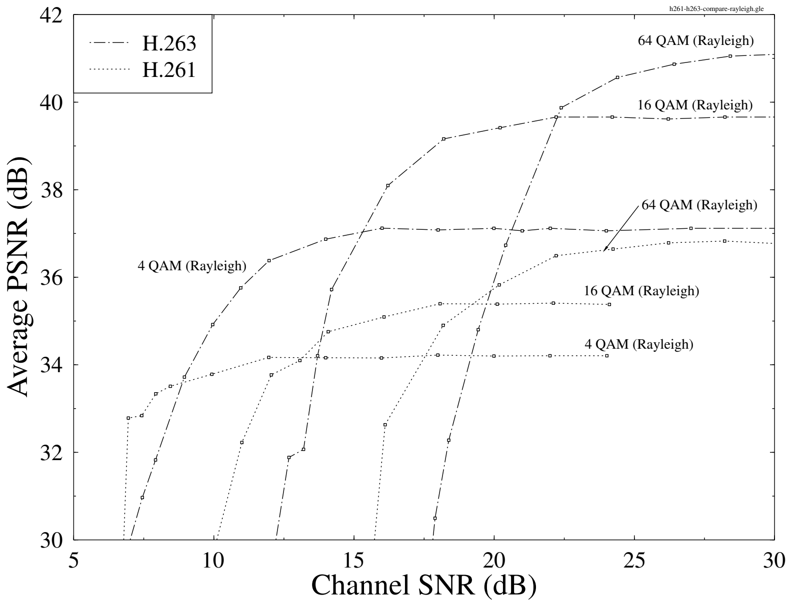

Figure 9.41: Performance comparison of the proposed adaptive H261 and H263 transceivers over Rayleigh channels ©Cherriman, Hanzo [110], 1995.

When using a resolution of 640×480 pixels, the maximum spatial deviation energy is 640^2+480^2=640 000, corresponding to a maximum diagonal spatial deviation of 800 pixels. The lossy coding energy was measured as the mean squared value of the pixel-to-pixel spatial distance between the original graphical input and the FL-DCC graphical output. For perfect channel conditions the $b = 1$ and $b = 2$ FL-DCC codec had PSNR values of 49.47 and 59.47 dB, respectively. As we showed in Figure 9.13, the subjective effects of a 10 dB PSNR degradation due to using $b = 1$ instead of $b = 2$ are not severe in terms of readability.

The system's robustness was characterised in Figures 9.42-9.45 upon transmitting the handwriting sequence of Figure 9.13 a high number of times, in order to ensure the statistical soundness of the graphical quality investigations. The best-case propagation scenario was encountering the stationary Additive White Gaussian Noise (AWGN) channel. The more bandwidth-efficient but less robust 16QAM mode of operation is characterised by Figure 9.42. Observe that transmissions over Rayleigh channels with diversity (RD) and with no diversity (RND) are portrayed using both one (TX1) and three (TX3) transmission attempts, in order to improve the system's robustness. Two-branch selection diversity using two independent

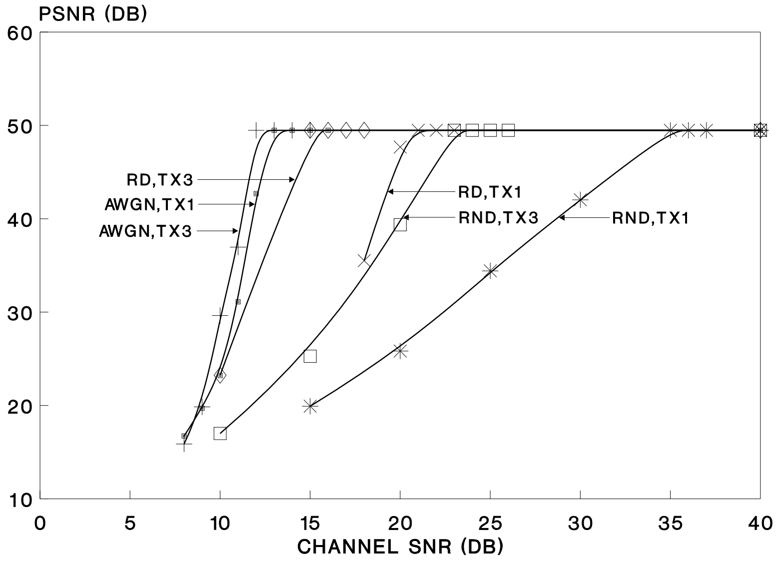

Figure 9.42: Graphical PSNR versus channel SNR performance of the b = 1-bit FL-DCC/16-QAM mode of operation over various channels ©ETT, Hanzo and Yuen [195].

Rayleigh channels was studied in conjunction with various selection criteria and we found that using the channel with the minimum phase shift between pilots slightly outperformed the maximum energy criterion. Similarly, over AWGN channels one or three transmission attempts were invoked.

As seen in Figures 9.42 and 9.43 in the case of the 16-QAM mode, over AWGN channels the required channel SNR for unimpaired graphical communications is around 11 dB with ARQ and 12 dB without ARQ. This marginal improvement is attributable to the fact that the AWGN channel exhibits always a fairly constant bit error rate (BER) and hence during re-transmission attempts the chances of successful transmissions are only marginally improved. In contrast, over Rayleigh channels the received signal has a high probability of emerging from a deep fade by the time the packet is re-transmitted. This is the reason for the significantly improved robustness of the ARQ-assisted Rayleigh scenarios of Figures 9.42 and 9.43. Specifically, with diversity the ARQ attempts reduced the required channel SNR by about 5 dB to around 15 dB, while without diversity an even higher 10-12 dB ARQ gain is experienced. When using the b = 2-bit FL-DCC scheme, Figure 9.43 shows that the error-free PSNR was increased to nearly 60 dB, while the system's robustness against channel errors and the

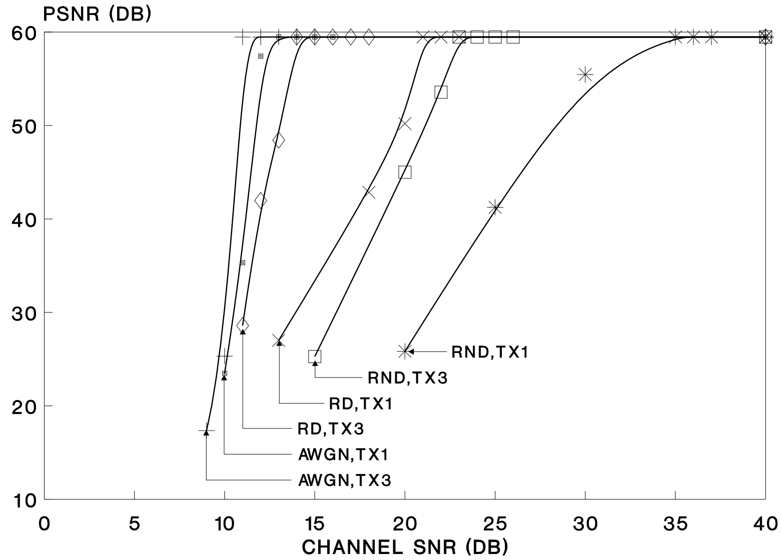

Figure 9.43: Graphical PSNR versus channel SNR performance of the b = 2-bit FL-DCC/16-QAM mode of operation over various channels ©ETT, Hanzo and Yuen [195].

associated 'corner SNR' values remained unchanged.

Figure 9.44 demonstrates that when the more robust 4-QAM mode was invoked, over AWGN channels SNR values of 5 and 8 dB were necessitated by the ARQ-aided TX3 scheme and the non-ARQ assisted TX1 systems, respectively. The diversity-assisted RD, TX3 and RD, TX1 systems required a minimum SNR of about 10 and 17 dB for unimpaired graphical communications, which had to be increased to 20 and 27 dB without diversity. Clearly, both the ARQ- and diversity-assistance played a crucial role in terms of improving the system's robustness. The same tendencies can be noted in Figure 9.45 as regards the $b = 2$-bit FL-DCC scheme. When using the lossless $b = 3$-bit FL-DCC or the conventional DCC scheme, the graphical PSNR becomes infinite, hence the corresponding PSNR versus channel SNR curves cannot be plotted. However, the transceiver's performance predetermines the minimum channel SNR values required for unimpaired graphical quality, which are about the same as for the above schemes. We note furthermore that since each packet commences with a pen-down code, the system can switch between the 4- and 16-QAM modes arbitrarily frequently without any objectionable perceptual quality degradation or graphical switching transients.

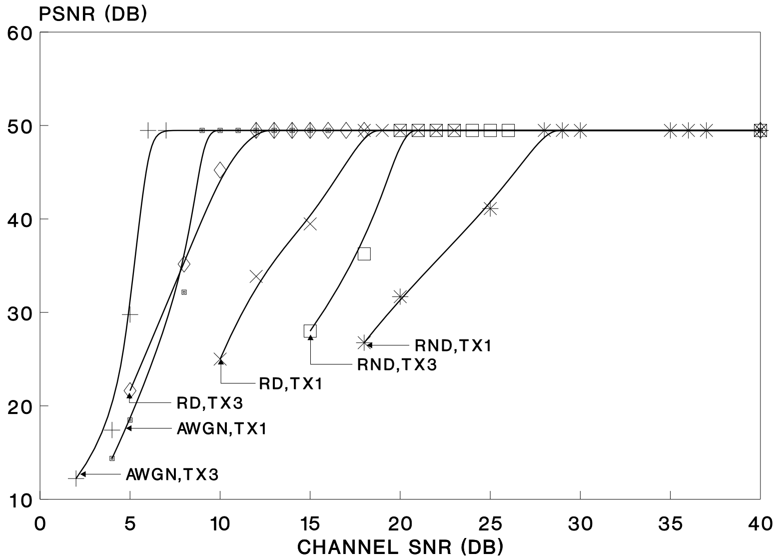

Figure 9.44: Graphical PSNR versus channel SNR performance of the $b = 1$-bit FL-DCC/4-QAM mode of operation over various channels ©ETT, Hanzo and Yuen [195].

The subjective effects of channel errors are demonstrated by Figure 9.46 in the case of the diversity- and ARQ-assisted Rayleigh 16-QAM, FL-DCC $b = 1$ scenario, where the graphical PSNR was gradually reduced from the error-free 49.47 dB at the top left hand corner to 42.57, 37.42, 32.01, 27.58 and 21.74 dB at the bottom right hand corner, respectively. Here we quoted the PSNR values, rather than the channel SNR values, since the associated graphical quality can be ensured by various system configuration modes under different channel conditions. The corresponding channel SNRs for the various system configuration modes can be inferred from the intercept points of the horizontal line corresponding to a particular PSNR value in Figures 9.42-9.45. Note that when the channel BER becomes high and hence the PSNR is degraded by more than about 5 dB, the graphical artifacts become rather objectionable. In this case it is better to disable the decoder's output by exploiting the error detection capability of the BCH decoder.

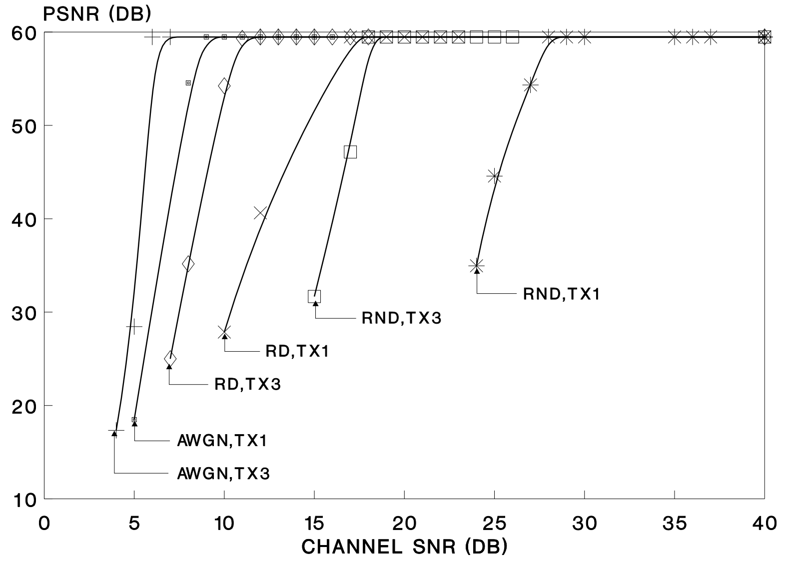

Figure 9.45: Graphical PSNR versus channel SNR performance of the $b = 2$-bit FL-DCC/4-QAM mode of operation over various channels ©ETT, Hanzo and Yuen [195].

9.8 Summary and Conclusions

In contrast to previous chapters of this book, which mainly dealt with a range of system components, ranging from speech codecs to channel codecs and modems, this chapter attempted to address system design and performance issues in the context of a 30-kHz bandwidth and a 200-kHz bandwidth system, which are the bandwidths of two well-known systems, namely the Pan-American IS-54 and the Pan-European GSM system. Following a brief overview of speech and video coding advances as well as bit sensitivity issues, a slightly deeper discussion was offered on bandwidth-efficient full-response multi-level modem schemes, since these modems were not detailed in previous chapters.

Then the potential of a bandwidth-efficient 2.2 kBd PRMA-assisted TBPE, DCT, BCH, 16-QAM scheme has been investigated under the assumption of benign channel conditions. Within the 30-kHz bandwidth about 10 voice users plus a video telephone user can be supported, if channel SNR and SIR values in excess of about 24 dB can be maintained. The main transceiver features are summarised in contrast to those of the 200-kHz bandwidth dual-mode speech system in Table 9.12.

The system performance of the 30-kHz bandwidth non-coherent

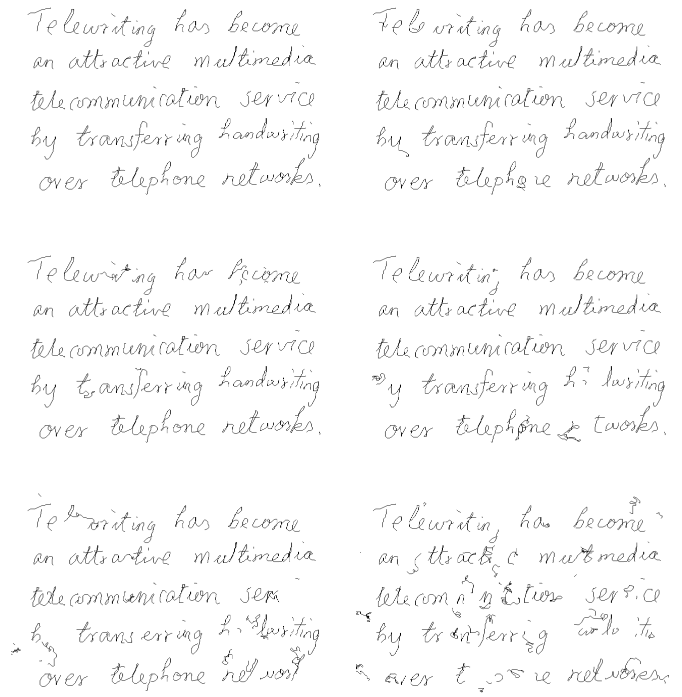

Figure 9.46: Subjective effects of transmission errors for the $b = 1$ 16-QAM, RD, TX3 scheme for PSNR values of (left to right, top to bottom) 49.47, 42.57, 37.42, 32.01, 27.58 and 21.74 dB, respectively. ©ETT, Hanzo and Yuen [195].

transceiver was further improved at the cost of slightly higher implementational complexity, when using a more sophisticated multi-mode, pilot symbol assisted, block-coded coherent square-constellation modem. The potential of this system was evaluated and the main system features were summarised also in Table 9.12 in contrast to those of the non-coherent star 16-QAM 30-kHz bandwidth system. As seen in the Table, the coherent scheme employed stronger overall error correction coding and a more robust modem, requiring lower SNR and SIR values over the more slowly-fading ($f_d \cdot T \approx 0.0000833$) DCS1800-like pedestrian channel than the lower-complexity non-coherent scheme over the slower-fading ($f_d \cdot T \approx 0.0042$) IS-54-like channel.

Furthermore, the increased system bandwidth of 200 kHz supports more time slots than the 30-kHz bandwidth system, which improves the statistical multiplexing gain of the PRMA scheme from 1.43 to 1.72 and hence increases also the number of users per PRMA slot. Lastly, due to its multi-mode nature, this scheme can also adapt to time-variant propagation environments. This multi-mode transceiver was then also exploited to transmit three different quality video signals at bit-rates of 13.1, 26.1

or 39.6 kbps in one of the 4-, 16- or 64-QAM modes, depending on the prevalent channel conditions. Overall, as expected, in performance terms we favour PSAM-assisted schemes, if their slightly higher complexity is acceptable, since it was more robust against transmission impairments and had a lower effective user bandwidth requirement than the non-coherent scheme.

An adaptive FL-DCC graphical coding scheme was also proposed for graphical communications, which has a lower coding rate and similar graphical quality to DCC in the case of $b = 1$ and 2. The codec can be adaptively re-configured to operate at $b = 1$, $b = 2$ or even at $b = 3$ in order to comply with the prevailing network loading and/or propagation conditions, as well as graphical resolution requirements. The proposed FL-DCC codec was employed in an intelligent, re-configurable wireless adaptive multimedia communicator, which was able to support a mixture of speech, video and graphical users. The minimum required channel SNR in the ARQ-assisted 16-QAM mode was 11 dB and 15 dB over AWGN and diversity-aided Rayleigh channels, respectively. The system's robustness against channel errors was improved at a concomitantly reduced graphical resolution, when 4-QAM was invoked.

In order to probe further into the field of wireless multimedia communications, the interested reader is referred to reference [2] for a range of novel transceiver components, including channel equalisers, clock and carrier recovery circuitries, orthogonal frequency division multiplex schemes and adaptive transceivers, while various multimedia systems were proposed and analysed in references [19–22, 25, 26, 55, 75, 86, 92, 99–101, 112].

9.9 Acknowledgement

Over the years I have had the privilege of collaborating with many former and current colleagues in the Department of Electronics and Computer Science at the University of Southampton, UK, while working on various research projects. These colleagues and valued friends, too numerous to mention, have influenced my views concerning various aspects of wireless multimedia communications and I am grateful for the enlightment gained form our collaborations on various projects, papers and books. I am particularly indebted to Raymond Steele, Professor of Communications and the Editor of this book, whose long-term vision motivated many of the investigations reported. I am also grateful to J. Brecht, Jon Blogh, Marco Breiling, M. del Buono, Clare Brooks, Peter Cherriman, Byoung Jo Choi, Joseph Cheung, Peter Fortune, Peter Cherriman, Joseph Cheung, Lim Dongmin, D. Didascalou, S. Ernst, David Greenwood, Hee Thong How, Thomas Keller, Xiao Lin, Chee Siong Lee, Tong-Hooi Liew, Matthias Muenster, V. Roger-Marchart, Redwan Salami, Juergen Streit, Jeff Torrance, Spiros Vlahoyiannatos, William Webb, John Williams, Jason Woodard, Choong Hin Wong, Henry Wong, Lie-Liang Yang, Bee-Liong Yeap, Mong-Suan Yee, Kai Yen, Andy Yuen and many others, with whom I have enjoyed an association. My sincere thanks are also due to the EPSRC, UK, the Commission of the European Communities, Brussels, Belgium and Motorola ECID, Swindon, UK for sponsoring some of my recent research.

$*$ $*$

The topic of this chapter was a range of powerful multimedia systems based on bandwidth-efficient multi-level modulation, which can accommodate more users in a given bandwidth, than their second generation counterparts, such as the systems in Table 1.1 and hence these solutions may offer an evolutionary path for the existing systems. The system design principles introduced can also be invoked in the context of the forthcoming third-generation systems. In the next chapter we will concentrate on the third-generation proposals currently under consideration in Europe, the US and Japan.

Bibliography

[1] **L. Hanzo**, "Bandwidth-efficient Wireless Multimedia Communications", *Proc. of the IEEE*, July 1998, Vol. 86, No. 7, pp 1342-1382

[2] **W.T. Webb** and **L. Hanzo**, "Modern quadrature amplitude modulation: Principles and applications for fixed and wireless channels", *IEEE Press-John Wiley co-publication,* ISBN 0-7273-1701-6, p 557, 1994

[3] **J. D. Gibbson**, "The mobile communications handbook", *IEEE Press-CRC Press,* 1996

[4] **IEEE Personal Communications**, "Special Issue: The European Path Toward UMTS", *The magazine of nomadic communications and computing*, Feb. 1995, Vol. 2, No. 1

[5] *Advanced Communications Technologies and Services (ACTS), Workplan, European Commission, DGXIII-B-RA946043-WP, Aug. 1994*

[6] **IEEE Personal Communications** "Feature Topic: Wireless Personal Communications" *The magazine of nomadic communications and computing,* Apr. 1995, Vol. 2, No. 2

[7] **IEEE Communications Magazine**, "Feature Topic: Universal Telecommunications at the Beginning of the 21st Century", Nov. 1995, Vol. 33, No. 11

[8] **IEEE Communications Magazine**, "Feature Topic: "Software Radios", Vol. 33 No. 5, May 1995

[9] **IEEE Communications Magazine**, "Feature Topic: Wireless Personal Communications", Jan. 1995, Vol. 33, No. 1.

[10] **IEEE Communications Magazine**, "Feature Topic: European Research in Mobile Communications", Vol. 34, No. 2, pp 60-106, Feb. 1996

[11] **D.C. Cox**, "Wireless personal communications: A perspective", *in J.D. Gibbson (Ed.): The mobile communications handbook, IEEE Press-CRC Press*, pp 209-241, 1996

[12] **A.D. Kucar**, "Mobile radio: An overview", *in J.D. Gibbson (Ed.): The mobile communications handbook, IEEE Press-CRC Press,* pp 242-262, 1996

[13] **V.O.K. Li, X. Qiu**, "Personal Communications Systems". *Proc. of the IEEE,* Vol. 83, No. 9, pp 1210- 1243, Sept. 1995

[14] *Dual-mode subscriber equipment- Network equipment compatibility specification, Interim Standard IS-54, Telecomm. Industry Association (TIA), Washington, DC, 1989, TIA*

[15] *Public Digital Cellular (PDC) Standard, RCR STD-27, Research and Development Centre for Radio Systems, Japan, PDC*

[16] *Mobile station - Base station compatibility standard for dual-mode wideband spread spectrum cellular system, EIA/TIA Interim Standard IS-95, Telcomm. Industry Association (TIA), Washington, DC, 1993, TIA*

[17] **P.W. Baier, P. Jung** and **A. Klein**, "Taking the challenge of multiple access for third-generation cellular mobile radio systems - A European View", *IEEE Comms. Mag.*, Vol. 34, No. 2, pp 82-89, Feb. 1996

[18] **R. Prasad**, "CDMA for wireless personal communications", *Artech House,* 1996

[19] **L. Hanzo** and **J.P. Woodard**, "An intelligent multimode voice communications system for indoors communications", *IEEE Tr. on Veh. Technology,* Vol. 44, No. 4, pp 735-749, ISSN 0018-9545, Nov. 1995

[20] **L. Hanzo, J.P. Woodard**, "Modern Voice Communications", in preparation

[21] **L. Hanzo, R. Salami, R. Steele** and **P.M. Fortune**, "Transmission of Digitally Encoded Speech at 1.2 KBd for PCN", *IEE Proc-I,* Vol. 139, No 4, pp 427-447, Aug. 1992

[22] **L. Hanzo** ***et.al.*** "A low-rate multi-level voice/video transceiver for personal communications", *Wireless Personal Communications, Kluwer Academic Publishers,* Issue 2:3, pp 213-230, Nov. 1995

[23] **J Woodard** and **L. Hanzo**, "A re-configurable speech transceiver", *Proc. of 2nd International Workshop on Mobile Multimedia Communications, MoMuc-2, Bristol, UK.* 11-13 Apr, 1995

[24] **J. Williams, L. Hanzo** and **R. Steele**, "Performance comparison of wireless speech communications schemes", *Proc. of 2nd International Workshop on Mobile Multimedia Communications, MoMuc-2, Bristol, UK.* 11-13 Apr, 1995

[25] **J. Williams, L.Hanzo, R.Steele** and **J.C.S Cheung**, "A comparative study of microcellular speech transmission schemes", *IEEE Tr. on Veh. Technology,* Vol. 43, No. 4 pp 909-925, Nov. 1994

[26] **L.Hanzo,** ***et al.*** "A packet reservation multiple access assisted cordless telecommunications scheme", *IEEE Tr on VT.,* vol. 43, No. 2, pp 234-245, May 1994

[27] **J.C.S. Cheung, L. Hanzo, W.T. Webb** and **R. Steele**, "Effects of Packet Reservation Multiple Access on Objective Speech Quality", *Electr. Letters,* 21, Vol. 29, No. 2, pp 152-153, Jan. 1993

[28] **P. Kroon** and **E.F. Deprettere**, "Regular Pulse Excitation - A Novel Approach to Effective Multipulse Coding of Speech", *IEEE Trans. on Acoustics, Speech and Signal Processing,* pp. 1054–1063, 1986

[29] **P. Vary, K. Hellwig, R. Hofmann, R. Sluyter, C. Galland** and **M. Rosso**, "Speech Codec for the European Mobile Radio System", *Proc. ICASSP*, pp. 227–230, April 1988

[30] **I.A. Gerson** and **M.A. Jasuik**, "Vector Sum Excited Linear Prediction (VSELP) Speech Coding at 8 kbps," *IEEE Journal on Selected Areas in Communications*, pp. 461–464, 1990

[31] **I.A. Gerson** and **M.A. Jasiuk**, "Vector Sum Excited Linear Prediction (VSELP)," in *Advances in Speech Coding* (Bishnu S. Atal, Vladimir Cuperman and Allen Gersho, ed., pp. 69–80, Kluwer Academic Publishers, 1991

[32] **J. Campbell, V. Welch** and **T. Tremain**, "An Expandable Error-protected 4800 bps CELP Coder (U.S. Federal Standard 4800 bps Voice Coder)," *Proc. ICASSP*, pp. 735–738, 1989

[33] **D. O'Shaughnessy**, *Speech Communication, Human and Machine*, Addison-Wesley Publishing Company, 1987

[34] **S. Furui**, *Digital Speech Processing, Synthesis and Recognition*, Marcel Dekker Inc., 1989

[35] **J.B. Anderson** and **S. Mohan**, *Source and Channel Coding - An Algorithmic Approach*, Kluwer Academic Publishers , 1991

[36] **A.M. Kondoz**, *Digital Speech: Coding for Low Bit-Rate Communications Systems* , John Wiley, 1994

[37] **W.B. Kleijn** and **K.K. Paliwal**, *Speech Coding and Synthesis*, Elsevier Science, 1995

[38] **Allen Gersho**, "Advances in Speech and Audio Compression", *Proceedings of the IEEE*, pp. 900–918, June 1994

[39] **I.A. Gerson, M.A. Jasiuk, J-M. Muller, J.M. Nowack** and **E.H. Winter**, "Speech and Channel Coding for the half-rate GSM Channel". *Proceedings ITG-Fachbericht 130, VDE-Verlag, Berlin*, pp. 225–233, Nov 1994

[40] **T. Ohya, H. Suda** and **T. Miki**, "5.6 kbits/s PSI-CELP of the half-rate PDC speech coding standard ", *Proceeding of the IEEE Conference on Vehicular Technology*, pp. 1680–1684, June 1994

[41] **W. B. Kleijn**, "Encoding Speech Using Prototype Waveforms", *IEEE Trans. on Acoustics, Speech and Signal Processing*, pp. 386–399, Oct 1993

[42] **D. W. Griffin** and **J. S. Lim**, "Multiband Excitation Vocoder", *IEEE Trans. on Acoustics, Speech and Signal Processing*, pp. 1223–1235, Aug 1988

[43] **D.J. Hiotakakos** and **S. Xydeas**, "Low Bit-Rate Coding Using an Interpolated Zinc Excitation Model", *Proceeding of the IEEE Singapore International Conference on Communications Systems* , pp. 865–869, Nov 1994

[44] **J.-H.Chen, R.V. Cox, Y.-C. Lin, N. Jayant** and **M.J. Melchner**, "A Low-Delay CELP Coder for the CCITT 16 kb/s Speech Coding Standard", *IEEE Journal on Selected Areas in Communications*, pp. 830–849, June 1991

[45] **Coding of Speech at 16 kbit/s Using Low-Delay Code Excited Linear Prediction**, *CCITT Recommendation G.728*, 1992

[46] **R.A.Salami, C.Laflamme, J.-P. Adoul** and **D. Massaloux**, "A Toll Quality 8 Kb/s Speech Codec for the Personal Communications System (PCS)", *IEEE Transactions on Vehicular Technology*, pp. 808–816, August 1994

[47] **Coding of Speech at 8 kbit/s Using Conjugate-Structue Algebraic Code-Excited Linear Prediction (CS-ACELP)**, *ITU Draft Recommendation G.729*, February 1996

[48] **A. Kataoka, J-P. Adoul, P. Combescure** and **P. Kroon**, "ITU-T 8-kbits/s Standard Speech Codec for Personal Communication Services", *Proceedings of International Conference on Universal Personal Communications, Tokyo, Japan*, pp. 818–822, Nov 1995

[49] **A. McCree *et.al.***, "A 2.4 kbit/s MELP candidate for the new US federal standard", *Proc. of ICASSP'96, Atalanta, Georgia, US*, pp 200-203, 1996.

[50] **M.R. Schroeder** and **B.S. Atal**, "Code-Excited Linear Prediction (CELP): High Quality Speech at Very Low Bit-Rates", *Proc. of ICASSP'85*, pp. 937-941, 1985.

[51] **R.A. Salami**,"Binary pulse excitation: a novel approach to low complexity CELP coding" in *Advances in speech coding,* Kluwer Academic Publishers, pp. 145-156, 1991

[52] **B.S. Atal** and **M.R. Schroeder.** "Stochastic coding of speech signals at very low bit-rates". *IEEE Int. Conf. Commun.,* May 1984.

[53] **M.R. Schroeder** and **B.S. Atal.** "Code-Excited Linear Prediction (CELP): High quality speech at very low bit-rates". *Proc. ICASSP'85, Tampa, Florida, USA* pp. 937–940, 26-29 March, 1985.

[54] **J-P. Adoul *et.al.***, "Fast CELP coding based on algebraic codes", *Proc. ICASSP'87,* pp. 1957-1960, 1987

[55] **L. Hanzo, R. Salami, R. Steele** and **P.M. Fortune**, "Transmission of Digitally Encoded Speech at 1.2 KBd for PCN", *IEE Proc.-I, vol. 139, no. 4*, pp. 437-447, Aug. 1992

[56] **N. Kitawaki, M. Honda** and **K. Itoh**, "Speech-Quality Assessment Methods for Speech-coding Systems", *IEEE Communications Magazine*, vol. 22, no. 10, pp. 26-33, Oct. 1984

[57] **A.H. Gray** and **J.D. Markel**, "Distance Measures for Speech Processing", *IEEE Tr. on Acoutics, Speech and Signal Processing*, vol. ASSP-24, no. 5, pp. 380-391, Oct. 1976

[58] **N. Kitawaki, H. Nagabuchi** and **K. Itoh**, "Objective Quality Evaluation for Low-Bit-Rate Speech Coding Systems", *IEEE Tr. JSAC*, vol. 6, no. 2, pp. 242-249, Febr. 1988

[59] Guest Editors:, **K.H. Tzou, H.G. Mussmann** and **K. Aizawa**, "Special issue on very low bit-rate video coding", *IEEE Transactions on Circuits and Systems for Video Technology*, 4(3):213–357, June 1994

[60] Guest Editor: **N. Hubing**, "Speech and image coding", *Special Issue of the IEEE Journal on JSAC*, 10(5):793–976, June 1992

[61] Guest Editors: **B. Girod *et.al.***, "Special issue on image sequence compression", *IEEE Transactions on Image Compression*, 3(5):465–716, September 1994

[62] **M. Khansari, A. Jalali, E. Dubois** and **P. Mermelstein**, "Robust low bit-rate video transmission over wireless access systems", In *Proc. of International Comms. Conf. (ICC)*, pages 571–575, 1994

[63] **R. Mann Pelz**, "An unequal error protected px8 kbit/s video transmission for DECT", In *Vehicular Technology Conference*, pages 1020–1024. IEEE, 1994

[64] **T.C. Chen**, "A real-time software based end-to-end wireless visual communications simulation platform", In *Proc. of SPIE Conf. on Visual Communications and Image Processing*, pages 1068–1074, 1995

[65] **K. Illgner** and **D. Lappe**, "Mobile multimedia communications in a universal telecommunications network", In *Proc. of SPIE Conf. on Visual Communications and Image Processing*, pages 1034–1043, 1995

[66] **Y.Q. Zhang**, "Very low bit-rate video coding standards", In *Proc. of SPIE Conf. on Visual Communications and Image Processing*, pages 1016–1023, 1995

[67] **H. Ibaraki *et.al.***, "Mobile video communication techniques and services", In *Proc. of SPIE Conf. on Visual Communications and Image Processing*, pages 1024–1033, 1995

[68] **K. Watanabe *et.al.***, "A study on transmission of low bit-rate coded video over radio links", In *Proc. of SPIE Conf. on Visual Communications and Image Processing*, pages 1025–1029, 1995

[69] **N. Färber, E. Steinbach** and **B. Girod**, "Robust H.263 video transmission over wireless channels," *in Proc. of International Picture Coding Symposium (PCS)*, (Melborne, Australia), pp. 575–578, March 1996.

[70] **M. W. Whybray** and **W. Ellis**, "H.263 - video coding recommendation for PSTN videophone and multimedia," *in IEE Colloquium (Digest)*, pp. 6/1–6/9, IEE, England, Jun 1995.

[71] **P. Sheldon, J. Cosmas** and **A. Permain**, "Dynamically adaptive control system for MPEG-4", In *Proceedings of the 2nd International Workshop on Mobile Multimedia Communications*, 1995

[72] **ITU-T**, *Draft Recommendation H.263: Video coding for low bit-rate communication*,

[73] **Telenor Research and Development**, P.O.Box 83, N-2007 Kjeller, Norway, *H.263 Software Codec*

[74] **ITU-T**, *Recommendation H.261: Video codec for audiovisual services at px64 Kbit/s*, March 1993

[75] **J.Streit** and **L.Hanzo.** "A fractal video communicator", In *IEEE Conference on Vehicular Technology*, pages 1030–1034, Stockholm, Sweden, June 1994

[76] **N. Jayant**, "Signal compression: Technology targets and research directions", in *Speech and Image Coding, Special Issue of the IEEE JSAC*, June 1992, Vol. 10, No. 5, pp 793-976, pp 796-818

[77] **Guest Editor: N. Hubing**, "Speech and Image Coding", *Special Issue of the IEEE JSAC*, Vol. 10, No. 5, pp 793-976, June 1992

[78] **ISO/IEC 11172 MPEG 1 International Standard**, "Coding of moving pictures and associated audio for digital storage media up to about 1.5 Mbit/s", Parts 1-3

[79] **ISO/IEC CD 13818 MPEG 2 International Standard**, "Information Technology, Generic coding of moving video and associated audio information", Parts 1-3.

[80] **N.S. Jayant** and **P. Noll**, "Digital coding of waveforms", Prentice-Hall, 1984

[81] *Proceedings of the 2nd International Workshop on Mobile Multimedia Communications, MoMuC-2, Apr. 11-13, Bristol, UK, 1995*

[82] **S. Sheng, A. Chandrakashan** and **R.W. Brodersen**, "A Portable Multimedia Terminal", *IEEE Comms. Mag.*, Vol. 30. No. 12, pp 64-75, Dec 1992

[83] "Special Issue on Very Low Bit-Rate Video Coding", *IEEE Transactions on Circuits and Systems for Video Technology*, Vol 4, No. 3, pp 213-357, June 1994

[84] "Special Issue on Image Sequence Compression", *IEEE Tr. on Image processing*, Sept. 1994, Vol. 3, No. 5, Guest Editors: B. Girod et al

[85] **J.W. Woods (Ed.)**. *Subband image coding*, Kluwer Academic Publishers, 1991

[86] **R. Stedman, H. Gharavi, L. Hanzo** and **R. Steele** "Transmission of Subband-Coded Images via Mobile Channels", *IEEE Tr. on Circuits and Systems for Video Technology*, Vol.3, No. 1, pp 15-27, Feb 1993

[87] **J. Katto, J. Ohki, S. Nogaki** and **M. Ohta**, "A wavelet codec with overlapped motion compensation for very low bit-rate environment", *IEEE Tr. on Video Technology*, Vol. 4, No. 3, pp 328-338, June 1994

[88] **P. Strobach**, "Tree-Structured Scene Adaptive Coder", *IEEE Trans. Commun.*, vol COM-38, pp 477-486, 1990

[89] **J. Vaisey** and **A. Gersho**, "Image compression with variable block size segmentation", *IEEE Tr. on Signal Processing*, Vol. 40, No. 8, pp 2040-2060, Aug 1992

[90] **A. Gersho** and **R.M. Gray**, *Vector Quantization and Signal Compression*, Kluwer Academic Publishers, 1992

[91] **B. Ramamurthi** and **A. Gersho**, "Classified Vector Quantization of Images", *IEEE Tr. on Com.*, Vol 31, No 11, pp 1105-1115, Nov. 1986

[92] **L. Hanzo *et.al.***, "A Portable Multimedia Communicator Scheme", in *R.I. Damper, W. Hall and J.W. Richards (Ed.) Multimedia Technologies and Future Applications*, pp 31-54, Pentech Press, London, 1993

[93] **S.Liu** and **F.M. Wang**, "Hybrid video coding for low bit-rate applications", *Proc. of IEEE ICASSP*, 19-22, pages 481–484, April 1994

[94] **J.F. Arnold X. Zhang** and **M.C. Cavenor**, "Adaptive quadtree coding of motion -compensated image sequences for use on the broadband ISDN", *IEEE Transactions on Circuits and Systems for Video Technology*, Vol 3,No 3, pp 222–229, June 1993

[95] **E. Shustermann** and **M. Feder**, "Image Compression via Improved Quadtree Decomposition Algorithms", *IEEE Transactions on Image Processing*, Vol 3, No 2, pp 207-215, March 1994

[96] *Proceedings of the International Workshop on Coding Techniques for Very Low Bit-rate Video, Hi-Vision Hall, Shinagawa, Tokyo, 8-10 Nov. 1995*

[97] **P. Sheldon, J. Cosmas** and **A. Permain**. "Dynamically adaptive control system for MPEG-4", *Proceedings of the 2nd International Workshop on Mobile Multimedia Communications, Apr. 11-13, Bristol, UK*

[98] **J. Streit**, "Digital Image Compression". *Phd. Thesis*, Dept. of Electr., Univ. of Southampton, 1996

[99] **L. Hanzo** and **J. Streit**, "Adaptive low-rate wireless videophone systems", *IEEE Tr. on Video Technology*, Vol. 5, No. 4, 305-319, ISSN 1051-8215, Aug 1994

[100] **J. Streit** and **L. Hanzo**. "Quadtree-based parametric wireless videophone systems", *IEEE Tr. on Circuit and Systems for Video Technology*, pp 225-237, Apr 1996

[101] **J. Streit** and **L. Hanzo**, "Vector-quantised low-rate cordless videophone systems", Submitted to IEEE Transactions Vehicular Technology

[102] **J. Streit** and **L. Hanzo**, "Comparative study of programmable-rate videophone codecs for existing and future multimode wireless systems", Vol.8, Issue No 6, 1997, pp 551-572

[103] **A.K. Jain**, *Fundamentals of Digital Image Processing*, Prentice-Hall, 1989

[104] **A. Sharaf**: Video coding at very low bit-rates using spatial transformations, *PhD Thesis*, Dept. of Electr. and Electr. Eng., King's College, London, 1997

[105] **P. Cherriman**, "Packet video communications", *Phd Thesis*, Dept. of Electr., Univ. of Southampton, UK, 1999

[106] **P. Cherriman** and **L. Hanzo**, "ARQ-assisted H.261 and H.263-based programable video transceivers", *1995 Research Journal of the Dept. of Electr., Univ. of Southampton, UK*, 1996

[107] **P. Cherriman** and **L. Hanzo**, H261 and H263-based Programable Video Transceivers, *Proc. of ICCS'96/ISPACS'96 Singapore*, 25-29. Nov. 1996, pp 1369-1373

[108] **P. Cherriman** and **L. Hanzo**, Robust H.263 Video Transmission Over Mobile Channels in Interference Limited Environments, *Proc. of First Wireless Image/Video Communications Workshop*, 4-5 Sept, 1996, Loughborough, UK, pp 1-7

[109] **P. Cherriman** and **L. Hanzo**, Power-controlled H.263-based wireless videophone performance in iterference-limited scenarios, *Proc. of Personal, Indoor and Mobile Radio Communications*, PIMRC'96, Taipei, Taiwan, 15-18 Oct., 1996, pp 158-162

[110] **P. Cherriman** and **L. Hanzo**, Programable H.263-based wireless video transceivers for interference-limited environments, *IEEE Tr. on CSVT*, June 1997, Vol. 8, No.3, pp 275-286

[111] **P. Cherriman, T. Keller** and **L. Hanzo**, Orthogonal Frequency Division Multiplex transmission of H.263 encoded video over highly frequency-selective wireless networks http://www-mobile.ecs.soton.ac.uk/peter/robust-h263/robust.html, to appear in IEEE Tr. on CSVT, 1999

[112] **L. Hanzo, P. Cherriman** and **J. Streit**,Modern Video Communications: Principles and applications for fixed and wireless channels, IEEE Press, in preparation [4]

[113] **M. Khansari, A. Jalali, E. Dubois** and **P. Mermelstein**, "Low bitrate video transmission over fading channels fo wireless microcellular systems", *IEEE TR. on CSVT*, Vol. 6, No. 1, pp 1-11, Feb 1996

[114] **H. Gharavi, H. Yasuda** and **T. Meng**, "Special issue on wireless visual communications", *IEEE Tr. on CSVT*, Vol. 6, No. 2, Apr. 1996

[115] **A.N. Netravali** and **B.G. Haskell**, *Digital pictures: representation and compression*, Plenum Press, 1988

[116] **A. Urie, M. Streeton** and **C. Mourot**, "An advanced TDMA mobile access system for UMTS", *IEEE Comms. Mag.*, pp 38-47, Feb 1995

[117] **European RACE D731 Public Deliverable**, "Mobile communication networks, general aspects and evolution", Sept. 1995

[118] **H. Nyquist**, "Certain factors affecting telegraph speed", *Bell System Tech Jrnl*, p 617, Apr. 1928

[119] **H.R. Raemer**, "Statistical communication theory and applications", Prentice Hall, Inc., Englewood Cliffs, New Jersey, 1969

[120] **N.G.Kingsbury**, "Transmit and receive filters for QPSK signals to optimise the performance on linear and hard limited channels", *IEE Proc. Pt.F*, Vol.133, No.4, pp345-355, July 1996

[121] **K.Feher**, *Digital communications - satellite/earth station engineering*, Prentice Hall 1983

[122] **C.N. Campopiano** and **B.G. Glazer**, "A Coherent Digital Amplitude and Phase Modulation Scheme", *IRE Trans. Commun. Systems*, Vol CS-10, pp 90- 95, 1962

[123] **G.D. Forney *et.al.***, "Efficient Modulation for Band-Limited Channels", *IEEE Journal on Selected Areas in Communications*, Vol SAC-2, No 5, pp 632-647, Sept 1984

[124] **K. Feher**, "Modems for Emerging Digital Cellular Mobile Systems", *IEEE Tr. on VT*, Vol 40, No 2, pp 355-365, May 1991

[125] **M. Iida** and **K. Sakniwa**, "Frequency Selective Compensation Technology of Digital 16-QAM for Microcellular Mobile Radio Communication Systems", *Proc. of VTC'92, Denver, Colorado*, pp 662-665

[4] For detailed contents please refer to http://www-mobile.ecs.soton.ac.uk

[126] **R.J. Castle** and **J.P. McGeehan**, "A Multilevel Differential Modem for Narrowband Fading Channels", *Proc. of VTC'92, Denver, Colorado*, pp 104-109

[127] **D.J. Purle, A.R. Nix, M.A. Beach** and **J.P. McGeehan**, "A Preliminary Performance Evaluation of a Linear Frequency Hopped Modem", *Proc. of VTC'92, Denver, Colorado*, pp 120-124

[128] **Y. Kamio** and **S. Sampei**, "Performance of Reduced Complexity DFE Using Bidirectional Equalizing in Land Mobile Communications", *Proc. of VTC'92, Denver, Colorado*, pp 372-376

[129] **T. Nagayasu, S. Sampei** and **Y. Kamio**, "Performance of 16-QAM with Decision Feedback Equalizer Using Interpolation for Land Mobile Communications", *Proc. of VTC'92, Denver, Colorado*, pp 384-387

[130] **E. Malkamaki**, "Binary and Multilevel Offset QAM, Spectrum Efficient Modulation Schemes for Personal Communications", *Proc. of VTC'92, Denver, Colorado*, pp 325-378

[131] **Z. Wan** and **K. Feher**, "Improved Efficiency CDMA by Constant Envelope SQAM", *Proc. of VTC'92, Denver, Colorado*, pp 51-55

[132] **H. Sasaoka**, "Block Coded 16-QAM/TDMA Cellular Radio System Using Cyclical Slow Frequency Hopping", *Proc. of VTC'92, Denver, Colorado*, pp 405-408

[133] **W.T. Webb, L. Hanzo** and **R. Steele**, "Bandwidth-Efficient QAM Schemes for Rayleigh-Fading Channels", *IEE Proceedings*, Vol 138, No 3, pp 169- 175, June 1991

[134] **A.S. Wright** and **W.G. Durtler**, "Experimental Performance of an Adaptive Digital Linearized Power Amplifier", *IEEE Tr. on VT*, Vol 41, No 4, pp 395- 400, Nov. 1992

[135] **M. Faulkner** and **T. Mattson**, "Spectral Sensitivity of Power Amplifiers to Quadrature Modulator Misalignment", *IEEE Tr. on VT*, Vol 41, No 4, pp 516-525, Nov. 1992

[136] **P.B. Kennington *et.al.***, "Broadband Linear Amplifier Design for a PCN Base-Station", *Proc. of 41st IEEE VTC*, pp 155-160, May 1991

[137] **R.J. Wilkinson *et.al.***, "Linear Transmitter Design for MSAT Terminals", *2nd Int. Mobile Satellite Conference*, June 1990

[138] **J.G.Proakis**, *Digital Communications*, McGraw Hill 1983

[139] **Y. C. Chow, A. R. Nix** and **J. P. McGeehan**, "Analysis of 16-APSK modulation in AWGN and Rayleigh fading channel", *Electronic Letters*, Vol 28, pp 1608-1610, Nov 1992

[140] **M.L. Moher** and **J.H. Lodge**, "TCMP – A Modulation and Coding Strategy for Rician Fading Channels", *IEEE J. Select. Areas Commun.*, Vol. 7, pp. 1347-1355, Dec. 1989

[141] **S. Sampei** and **T. Sunaga**, "Rayleigh Fading Compensation Method for 16-QAM in Digital Land Mobile Radio Channels", *Proc. IEEE Veh. Technol. Conf.*, San Francisco, CA, pp. 640-646, May 1989

[142] **S. Haykin**, *Adaptive Filter Theory*, Prentice Hall, 1991

[143] **J. Torrance** and **L. Hanzo**, "A comparative study of pilot symbol assisted modem schemes", *Proc. of IEE RRAS'95 Conference*, 26-28 Sept., 1995, Bath, UK, Conf. Public. No. 415, pp 36- 41

[144] **R. Steele** and **W.T. Webb**, "Variable rate QAM for data transmission over Rayleigh fading channels," in *Wireless '91, Calgary, Alberta*, pp. 1–14, IEEE, 1991.

[145] **W. Webb** and **R. Steele**, "Variable rate QAM for mobile radio", *IEEE Transactions on Communications*, 1995, Vol. 43, No. 7, pp 2223-2230

[146] **Y. Kamio, S. Sampei, H. Sasaoka** and **N. Morinaga**, "Performance of modulation-level-control adaptive-modulation under limited transmission delay time for land mobile communications," in 45^{th} *Vehicular Technology Conference*, pp. 221–225, IEEE, 1995.

[147] **S. Sampei, S. Komaki** and **N. Morinaga**, Adaptive Modulation/TDMA Scheme for Large Capacity Personal Multi-Media Communication Systems, *IEICE Transactions on Communications*, 1994, Vol. 77. No. 9, pp 1096-1103

[148] **M. Morimoto, H. Harada, M. Okada** and **S. Komaki**, A study on power assignment of hierarchical modulation schemes for digital broadcasting, *IEICE Transactions on Communications*, 1994, Vol. 77, No. 12, pp 1495-1500

[149] **S. Otsuki, S. Sampei** and **N. Morinaga**, "Square-QAM adaptive modulationTDMA/TDD systems using modulation level estimation with Walsh function.*Electronics Letters*, November 1995. pp 169-171.

[150] **S.G. Chua** and **A. Goldsmith**, "Variable-rate variable-power mqam for fading channels," in 46^{th} *Vehicular Technology Conference*, pp. 815–819, IEEE, 1996.

[151] **A. Goldsmith** and **S. Chua**, "Variable-rate variable-power MQAM for fading channels," *to appear in IEEE Tr. on Veh. Techn.*, 1997. http://www.systems.caltech.edu.

[152] **A. Goldsmith**, "The capacity of downlink fading channels with variable rate and power," *IEEE Tr. on Veh. Techn.*, vol. 46, pp. 569–580, Aug. 1997.

[153] **A. Goldsmith** and **P. Varaiya**, "Capacity of fading channels with channel side information," *to appear in IEEE Tr. in Inf. Theory*, 1998. http://www.systems.caltech.edu.

[154] **M.-S. Alouini** and **A. Goldsmith**, "Capacity of fading channels under different adaptive transmission and diversity techniques," *submitted to IEEE Tr. on Veh. Techn.*, 1998. http://www.systems.caltech.edu.

[155] **M.-S. Alouini** and **A. Goldsmith**, "Area spectral efficiency of cellular mobile radio systems," *submitted to IEEE Tr. on Veh. Techn.*, 1998. http://www.systems.caltech.edu.

[156] **A. Goldsmith** and **S. Chua**, "Adaptive coded modulation," *submitted to IEEE Tr. on Communications*, 1998. http://www.systems.caltech.edu.

[157] **D. A. Pearce, A. G. Burr** and **T. C. Tozer**, "Comparison of countermeasures against slow Rayleigh fading for TDMA systems," in *Colloquium on Advanced TDMA Techniques and Applications*, pp. 9/1–9/6, IEEE, 1996.

[158] **J. M. Torrance** and **L. Hanzo**, "Upper bound performance of adaptive modulation in a slow Rayleigh fading channel." *Electronics Letters*, April 1996. pp 169-171.

[159] **J. M. Torrance** and **L. Hanzo**, "Adaptive modulation in a slow Rayleigh fading channel," in *Proceedings of the 7^{th} Personal, Indoor and Mobile Radio Communications (PIMRC) Conference*, pp. 497–501, IEEE, 1996.

[160] **J. M. Torrance** and **L. Hanzo**, "Optimisation of switching levels for adaptive modulation in a slow Rayleigh fading channel." *Electronics Letters*, June 1996. pp 1167 - 1169.

[161] **J.M. Torrance** and **L. Hanzo**, Demodulation level selection in adaptive modulation, *Electr. Letters*, Vol. 32, No. 19, 12th of Sept., 1996, pp 1751-1752

[162] **J. Torrance** and **L. Hanzo**, Latency considerations for adaptive modulation in slow Rayleigh fading, *Proc. of IEEE VTC'97*, Phoenix, USA, 1997, pp 1204-1209

[163] **J. Torrance** and **L. Hanzo**, Statistical Multiplexing for Mitigating Latency in Adaptive Modems, *PIMRC'97*, 1-4. Sept. 1997, Helsinki, Finland, pp 938-942

[164] **M-S Alouini** and **A. Goldsmith**, Area spectral efficiency of cellular mobile radio systems, *Proc. of IEEE VTC'97*, Phoenix, USA, pp 652-656

[165] **M-S Alouini** and **A. Goldsmith**, Capacity of Nakagami Multipath Fading Channels, *Proc. of IEEE VTC'97*, Phoenix, USA, pp 652-656

[166] **C.H. Wong** and **L. Hanzo**, Upper-bound Performance of a Wideband Burst-by-burst Adaptive Modem, *Proc. of VTC'99, 1999, Houston, USA*

[167] **T.H. Liew, C.H. Wong** and **L. Hanzo**, Block turbo coded burst-by-burst adaptive modems; *Proceeding of Microcoll'99*, Budapest, Hungary, 21-24 March, 1999

[168] **C.H. Wong, T.H. Liew** and **L. Hanzo**, Blind modem mode detection aided block turbo coded burst-by-burst wideband adaptive modulation; *Proceedings of ACTS'99*, Sorrento, Italy, June, 1999

[169] **C.H. Wong, T.H. Liew** and **L. Hanzo**, Blind-detection Assisted, Block Turbo Coded, Decision-feedback Equalised Burst-by-Burst Adaptive Modulation; *submitted to IEEE Tr. on Comms.*, 1998

[170] **M. Frullone, G. Riva, P. Grazioso** and **C. Carciofy**, "Investigation on Dynamic Channel Allocation Strategies Suitable for PRMA Schemes", *1993 IEEE Int. Symp. on Circuits and Systems, Chicago*, pp 2216-2219, May 1993

[171] **S.P. Stapleton** and **F.C. Costescu**, "An Adaptive Predistorter for a Power Amplifier Based on Adjacent Channel Emissions", *IEEE Tr. on VT*, Vol 41, No 1, pp 49-57, Febr. 1992

[172] **S.P. Stapleton, G.S. Kandola** and **J.K. Cavers**, "Simulation and Analysis of an Adaptive Predistorter Utilizing a Complex Spectral Convolution", *IEEE Tr. on VT*, Vol 41, No 4, pp 387-394, Nov. 1992

[173] **Norihiko Morinaga**, "Advanced wireless communication technologies for achieving high-speed mobile radios", *IEICE Transactions on Communications*, vol. 78, no. 8, pp. 1089–1094, 1995

[174] **J.M. Torrance** and **L. Hanzo**, "Upper bound performance of adaptive modulation in a slow Rayleigh-fading channel", *Electr. Letters*, Vol. 32, No. 8, pp 718-719, 11th Apr. 1996

[175] **J.M. Torrance** and **L. Hanzo**, "Optimisation of Switching Levels for Adaptive Modulation in Slow Rayleigh Fading", *Electr. Letters*, Vol. 32, 20th June, 1996, No. 13, pp 1167-1169

[176] **J.M. Torrance** and **L. Hanzo**, "Performance upper bound of adaptive QAM in slow Rayleigh-fading environments", *Proc. of ICCS'96/ISPAC'96 Singapore*, Nov. 1996, pp 1653-1657

[177] **J. Torrance** and **L. Hanzo**, "Adaptive modulation in a slow Rayleigh fading channel", Proc. of Personal, Indoor and Mobile Radio Communications, *PIMRC'96*, Taipei, Taiwan, 15-18 Oct., 1996, pp 1049-1053

[178] **J.K. Cavers**, "An Analysis of Pilot Symbol Assisted Modulation for Rayleigh Fading Channels", *IEEE Tr. on VT*, Vol 40, No 4, pp 686-693, Nov 1991

[179] **J.M. Torrance**, " Adaptive Full Response Digital Modulation for Wireless Communication Environments", *Phd Thesis*, Dept. of Electr., Univ. of Southampton, UK, 1997

[180] **J.P.McGeehan** and **A. Bateman**, "Phase-locked transparent tone in band (TTIB): A new spectrum configuration particularly suited to the transmission of data over SSB mobile radio networks", *IEEE Trans Comm, Vol.COM-32*, pp81-87, 1984

[181] **A.Bateman** and **J.P.McGeehan**, "Feedforward transparent tone in band for rapid fading protection in multipath fading", *IEE Int. Conf. Comms.* Vol.68, pp9-13, 1986

[182] **A.Bateman** and **J.P.McGeehan**, "The use of transparent tone in band for coherent data schemes", *IEEE Int. Conf. Comms., Boston, Mass.*, 1983

[183] **A.Bateman, G.Lightfoot, A.Lymer** and **J.P.McGeehan**, "Speech and data transmissions over a 942MHz TAB and TTIB single sideband mobile radio system", *IEEE Trans Veh. Tech., Vol.VT-34* pp13-21, 1985

[184] **A.Bateman** and **J.P.McGeehan**, "Data transmissions over UHF fading mobile radio channels", *Proc IEE Pt.F, Vol.131*, 1984, pp364-374

[185] **J.P.McGeehan** and **A.Bateman**, "A simple simultaneous carrier and bit synchronisation system for narrowband data transmissions", *Proc. IEE, Pt.F, Vol.132*, pp69-72, 1985

[186] **J.P.McGeehan** and **A.Bateman**, "Theoretical and experimental investigation of feedforward signal regeneration", *IEEE Trans. Veh. Tech., Vol.VT-32*, pp106-120, 1983

[187] **A.Bateman**, "Feedforward transparent tone in band: Its implementation and applications", *IEEE Trans. Veh. Tech.* Vol.39, No.3, pp235-243, Aug 1990

[188] **B.Sklar**, "Digital communications", *Prentice Hall*, 1988

[189] **F. Adachi**, "Error rate analysis of differentially encoded and detected 16APSK under Rician fading", *IEEE Tr. on Veh. Techn.*, Vol. 45, No. 1, pp 1-12, Feb 1996

[190] **J.K.Cavers**, "The performance of phase locked transparent tone in band with symmetric phase detection", *IEEE Trans. on Comms.*, Vol.39, No.9, pp1389-1399, Sept 1991

[191] **S. Nanda, D.J. Goodman** and **U. Timor**, "Performance of PRMA: A Packet Voice Protocol for Cellular Systems", *IEEE Tr. on VT*, Vol 40, No 3, , pp 584-598, Aug 1991

[192] **M. Frullone, G. Falciasecca, P. Grazioso, G. Riva, A. M.** and **Serra**, "On the performance of packet reservation multiple access with fixed and dynamic channel allocation", *IEEE Tr. on Veh. Techn.*, Vol. 42. No. 1, pp 78-86, Feb 1996

[193] **Goodman, D.J., Lockhart, G.B., Wasem, O.J.,** and **Wong, W.C.**, "Waveform substitution techniques for recovering missing speech segments in packet voice communications", *IEEE Tr. on ASSP*, vol. 34, pp 1440-1448, Dec. 1986

[194] **R.Steele** and **W. T. Webb**, "Variable rate QAM for data transmissions over mobile radio channels", *Keynote paper, Wireless 91, Calgary Alberta*, July 1991

[195] **L. Hanzo** and **H. Yuen**: "Robust programmable-rate wireless graphical correspondence", *European Tr. on Communications*, No. 3, Vol. 8, May-June, 1997, pp 271-283

[196] **J.C. Arnbak, J.H. Bons** and **J.W. Vieveen**: "Graphical correspondence in electronic-mail networks using personal computers," *IEEE Journal on Selected Areas in Communications*, Feb. 1989, SAC-7, pp.257-267

[197] **M. Klerk, R. Prasad, J.H. Bons** and **N.B.J. Weyland**: "Introducing high-resolution line graphics in UK teletext using differential chain coding," *IEE Proceedings*, Part I, vol. 137, pp. 325-334, Dec. 1990.

[198] **D.L. Neuhoff** and **K.G. Castor**: "A rate and distortion analysis of chain codes for line drawings, " *IEEE Tran. Information Theory*, vol. IT-31, pp. 53-68, Jan. 1985.

[199] **K. Liu** and **R. Prasad**: "Performance analysis of differential chain coding," *European Transaction on Telecommunications and Related Technology*, vol. 3, pp. 323-330, Jul-Aug. 1992

[200] **A. B. Johannessen, R. Prasad, N.B.J. Weyland** and **J.H. Bons**: "Coding efficiency of multiring differential chain coding," *IEE Proceedings*, Part I, vol. 139, pp. 224-232, April 1992.

[201] **R. Prasad, J.W. Vivien, J.H. Bons** and **J.C. Arnbak**: "Relative vector probabilities in differential chain coded line drawings", *Proc. of IEEE Pacific Rim Conference on Comms., Computers and Signal Processing*, pp 138-142, Victoria, Canada, June 1989

[202] **L. Yang, H.I. Cakil** and **R. Prasad**: "On-line handwritting processing in indoor and outdoor radio environment for multimedia", *Proc. of IEEE VTC'94*, Stockholm, Sweden, 1015-1019

[203] **R. Prasad, P.A.D. Spaargaren and J.H. Bons**: "Teletext reception in a mobile channel for a broadcast tele-information system", *IEEE Tr. on VT.*, Vol. 42, No. 4, Nov. 1993, pp 535-545

[204] **L-P.W. Niemel** and **R. Prasad**: "A novel description of handwritten characters for use with generalised Fourier descriptors", *ETT* Vol. 3, No. 5, Sept-Oct. 1992, pp 455-464

[205] **L-P.W. Niemel** and **R. Prasad**: "An improved character description method based on generalized Fourier descriptors", *ETT* Vol. 5, No. 3, May-June 1994, pp 371-376

[206] **D.J. Goodman** and **X.S. Wei**: Efficiency of packet reservation multiple access, *IEEE Transactions on vehicular technology*, Vol. 40, No. 1, Febr. 1991, pp. 170-176.

[207] **W. Wong** and **D. Goodman**: A packet reservation access protocol for integrated speech and data transmission, *Proc. of the IEE*, Part-I, Dec. 1992, Vol 139, No 6, pp 607-613.

Glossary

ACELP	Algebraic Code Excited Linear Prediction
ACTS	Advanced Communications Technologies and Services
ADC	Analogue Digital Converter
ADPCM	Adaptive Differential Pulse Code Modulation
ATDMA	Advanced Time Division Multiple Access
ATM	Asynchronous Transfer Mode
AWGN	Additive White Gaussian Noise
B-frames	Bi-directional-frames
B-ISDN	Broadband-ISDN
BCH	Bose-Chaudhuri-Hocquenghem, A class of forward error correcting codes (FEC)
BER	Bit Error Rate, the number of the bits received incorrectly
BPSK	Binary Phase Shift Keying
BS	Base Station
CD	Cepstral Distance
CD-DEG	Cepstral Distance Degradation
CDMA	Code Division Multiple Access
CELP	Code Excited Linear Prediction
CT2	British Cordless Telephone System
DAC	Digital Analogue Converter
DCT	The Discrete Cosine Transform, transforms data into the frequency domain. Commonly used for video compression by removing high frequency components in the video frames

DECT	Digital European Cordless Telephone
DFD	Displaced Frame Difference
DoD	US Department of Defence
EG	Excitation Gain
FAW	Frame Alignment Word
FEC	Forward Error Correction
FPLMTS	Future Public Land Mobile Telecommunications System
G.728	ITU 16 kbps speech coding standard
G.729	ITU 8 kpbs speech coding standard
GMSK	Gaussian Minimum Shift Keying
GOS	Grade of Service
GP	Grid Position
GSM	A Pan-European digital mobile radio standard, operating at 900 MHz.
H.261	A video coding standard [74], published by the ITU in 1990
H.263	A video coding standard [72], due to be published by the ITU in 1996
I-component	Inphase-component
IF	Intermediate Frequency
ISDN	Integrated Services Digital Network, digital replacement of the analogue telephone network
ISI	Inter Symbol Interference
ITU	International Telecommunications Union, formerly the CCITT, standardisation group
IZFPE	Interpolated Zinc Function Pulse Excitation
LP filtering	Low-Pass filtering
LPF	Low-Pass Filter
LSB	Least Significant Bit
LSF	Line Spectra Frequency
LTP	Long Term Prediction
LTPD	Long Term Prediction Delay
LTPG	Long Term Prediction Gain
MAVT	Mobile Audio Video Terminal
MBE	Multi Band Excitation

MC	Motion Compensation
MCER	Motion Compensated Error Residual
MELP	Mixed Excitation Linear Prediction
MOS	Mean Opinion Score
MPEG	Motion Picture Expert Group, also a video coding standard designed by this group that is widely used
MSB	Most Significant Bit
MV	Motion Vector, a vector to estimate the motion in a frame
NLF	Non-Linear Filtering
NTT	Nippon Telegraph and Telephone Company
OFDM	Orthogonal Frequency Division Multiplexing
P-frames	Predicted-frames
PCM	Pulse Code Modulation
PCN	Personal Communications Network
PDC	Personal Digital Cellular
PHP	Personal Handy Phone
PLMR	Public Land Mobile Radio
PRMA	Packet Reservation Multiple Access
PS	Portable Station
PSAM	Pilot Symbol Assisted Modulation, a technique where known symbols (pilots) are transmitted regularly. The effect of channel fading on all symbols can then be estimated by interpolating between the pilots
PSD	Power Spectral Density
PSI	Pitch Synchronous Innovation
PWI	Prototype Waveform Interpolation
Q-component	Quadrature-component
QAM	Quadrature Amplitude Modulation
QCIF	Quarter Common Intermediate Format Frames containing 176 pixels vertically and 144 pixels horizontally
QT	Quad Tree
RACE	Research in Advanced Communications Equipment

RC filtering	Raised Cosine filtering
RF	Radio Frequency
RPE	Regular Pulse Excitation
SBC	Sub Band Coding
SEGSNR	Segmental Signal-to-Noise Ratio
SEGSNR-DEG	Segmental Signal-to-Noise Ratio Degradation
SNR	Signal to Noise Ratio, noise energy compared to the signal energy
TBPE	Transform Binary Pulse Excitation
TC	Transform Coding
TCM	Trellis Coded Modulation
TDMA	Time Division Multiple Access
TTIB	Transparent Tone in Band
UMTS	Universal Mobile Telecommunications System
V.29-V.34	ITU Data Transmission Modems
VAD	Voice Activity Detection
VQ	Vector Quantisation
VSELP	Vector Sum Excited Linear Prediction
WLAN	Wireless Local Area Network

Chapter 10

Third-Generation Wireless Systems

K. Yen and **L. Hanzo**[1]

10.1 Introduction

The evolution of third-generation (3G) systems began in the late 1980s, when the International Telecommunication Union's - Radiocommunication Sector (ITU-R) Task Group (TG) 8/1 defined the requirements for the 3G mobile radio systems. This initiative was then known as Future Public Land Mobile Telecommunication System (FPLMTS) [1,2]. This led to the identification of the frequency spectrum for FPLMTS on a world-wide basis during the World Administrative Radio Conference (WARC) in 1992 [2], as the bands 1885-2025 MHz and 2110-2200 MHz - an issue to be detailed in the context of Figure 10.1 during our further discourse.

The tongue-twisting acronym of FPLMTS was also aptly changed to IMT-2000, which refers to the International Mobile Telecommunications system in the year 2000. Besides possessing the ability to support services from rates of a few kbps to as high as 2 Mbps in a spectrally efficient way, IMT-2000 aimed to provide a seamless global radio coverage for global roaming. This implied the ambitious goal of aiming to connect virtually any two mobile terminals world-wide. The IMT-2000 system is aiming to be flexible in order to operate in any propagation environment, such as indoor, outdoor to indoor and vehicular scenarios. It is also aiming to be sufficiently flexible to handle so-called circuit as well as packet mode

[1]University of Southampton and Multiple Access Communications Ltd

services and to handle services of variable data rates. In addition, these requirements must be fulfilled with a quality of service (QoS) comparable to that of the current wired network at an affordable cost.

Several regional standard organizations - led by the European Telecommunications Standards Institute (ETSI) in Europe, by the Association of Radio Industries and Businesses (ARIB) in Japan and by the Telecommunications Industry Association (TIA) in the United States - have been dedicating their efforts to specifying the standards for IMT-2000. A total of 15 Radio Transmission Technology (RTT) IMT-2000 proposals were submitted to ITU-R in June 1998, five of which are satellite based solutions, while the rest are terrestrial solutions. Table 10.1 shows a list of the terrestrial-based proposals submitted by the various organizations and their chosen radio access technology. Although Table 10.1 is very informative, reflecting a variety of views across the wireless research community, which span the range of cordless telephony-based solutions, such as the Digital European Cordless Telecommunications (DECT) system of Table 10.1, or the second-generation (2G) IS-136 system, here we will concentrate on the CDMA-based solutions. A rudimentary discussion on CDMA was provided in Chapter 1 in the context of the Pan-American IS-95 system and in this chapter a basic familiarity with CDMA principles is assumed.

It transpires from Table 10.1 that most standardization bodies have based their terrestrial oriented solutions on Wideband-CDMA (W-CDMA), due to its previously mentioned advantageous properties, which satisfy most of the requirements for 3G mobile radio systems. W-CDMA is aiming to provide improved coverage in most propagation environments in addition to an increased user capacity. Furthermore, it simplifies frequency planning due to its unity frequency reuse. As argued in Chapter 1, CDMA has the ability to combat - or in fact to benefit from - multipath fading through RAKE multipath diversity combining [3–5]. Hence, in this chapter we will concentrate on the proposed terrestrial transmission technologies advocated by the three major regional standardization bodies, namely ETSI, ARIB and TIA, whereby the access technology is based on W-CDMA. The corresponding systems have been termed UMTS Terrestrial Radio Access (UTRA), Wideband-CDMA (W-CDMA) and cdma2000, respectively. In order to avoid confusion between the Japanese W-CDMA proposal itself and the W-CDMA access technology in general, we shall refer to the ARIB's RTT as IMT-2000.

Since ETSI and ARIB have been harmonizing their standardization efforts, aiming for the same W-CDMA technology, their proposals became indeed very similar and hence we shall discuss these two RTT proposals collectively in Section 10.2. The RTT of cdma2000 will be highlighted separately in Section 10.3. At the time of writing, ITU are still deliberating on their decisions concerning a single global standard. Although the proposals have been submitted, active research is still in progress in order to improve and optimize the systems. Hence, the parameters and technolo-

Proposal	Description	Access technology	Source
DECT	Digital Enhanced Cordless Telecommunications	Multicarrier TDMA (TDD)	ETSI Project (EP) DECT
UWC-136	Universal Wireless Communications	TDMA (FDD and TDD)	USA TIA TR45.3
WIMS W-CDMA	Wireless Multimedia and Messaging Services Wideband CDMA	Wideband CDMA (FDD)	USA TIA TR46.1
TD-CDMA	Time-Division Synchronous CDMA	Hybrid with TDMA/CDMA/SDMA (TDD)	Chinese Academy of Telecommunication Technology (CATT)
W-CDMA	Wideband CDMA	Wideband DS-CDMA (FDD and TDD)	Japan ARIB
CDMA II	Asynchronous DS-CDMA	DS-CDMA (FDD)	South Korean TTA
UTRA	UMTS Terrestrial Radio Access	Wideband DS-CDMA (FDD and TDD)	ETSI SMG2
NA: W-CDMA	North America Wideband CDMA	Wideband DS-CDMA (FDD and TDD)	USA T1P1-ATIS
cdma2000	Wideband CDMA (IS-95)	DS-CDMA (FDD and TDD)	USA TIA TR45.5
CDMA I	Multiband synchronous DS-CDMA	Multiband DS-CDMA	South Korean TTA

Table 10.1: Proposals for the radio transmission technology of terrestrial IMT-2000 (obtained from ITU's web site : http://www.itu.int/imt).

gies presented in this chapter may evolve further. It should also be noted that this chapter serves as an overview of the three main proposed systems. Readers may want to refer to a recent book by Ojanperä and Prasad [6], which addresses W-CDMA 3G mobile radio systems in more depth. Again, here we assume that the reader is familiar with the basic CDMA principles.

10.2 UMTS/IMT-2000 Terrestrial Radio Access [7]- [14]

Universal Mobile Telecommunications System (UMTS) is the term introduced by the ETSI/Special Group Mobile (SMG) for the 3G wireless mobile communication system in Europe [1, 8, 9, 15–18]. Research activities for UMTS within ETSI have been spearheaded by the European Union's (EU) sponsored programmes, such as the Research in Advanced Communication Equipment (RACE) [19, 20] and the Advanced Communications Technologies and Services (ACTS) [8, 16, 20] initiative. The RACE programme, which comprised of two phases, was started in 1988 and ended in 1995. The objective of this programme was to investigate and develop testbeds for the air interface technology candidates. The ACTS programme succeeded the RACE programme in 1995. Within the ACTS Future Radio Wideband Multiple Access System (FRAMES) project two multiple access modes have been chosen for intensive study, as the candidates for UMTS terrestrial radio access (UTRA). They are based on Time Division Multiple Access (TDMA) with and without spreading, and on W-CDMA [7, 21, 22].

As early as January 1997, ARIB decided to adopt W-CDMA as the terrestrial radio access technology for their IMT-2000 proposal and proceeded to focus their activities towards the detailed specifications of this technology [18]. Driven by a strong support behind W-CDMA worldwide and this early decision from ARIB, a consensus agreement was reached by ETSI in January 1998 to adopt W-CDMA as the terrestrial radio access technology for UMTS. Since then, ARIB and ETSI have harmonized their standards in order to aim for the same W-CDMA technology. In this section we will highlight the key features of the terrestrial RTT behind the ETSI and ARIB proposals. The descriptions that follow are applicable to both UTRA and IMT-2000, unless it is stated otherwise. Most of the material in this section is based on an amalgam of References [8]- [9].

10.2.1 Characteristics of UTRA/IMT-2000

The proposed spectrum allocations for UTRA and IMT-2000 are shown in Figures 10.1 and 10.2, respectively. As can be seen, UTRA and IMT-2000 are unable to utilize the full allocated frequency spectrum for 3G mobile radio systems, since those frequency bands have also been partially allocated to the DECT and Personal Handyphone System (PHS) , respectively, which were characterized in Table 1.1 of Chapter 1. The radio access supports both Frequency Division Duplex (FDD) and Time Division Duplex (TDD) operations. The operating principles of these two schemes were detailed in Chapter 1, which are augmented here in the context of Figure 10.3.

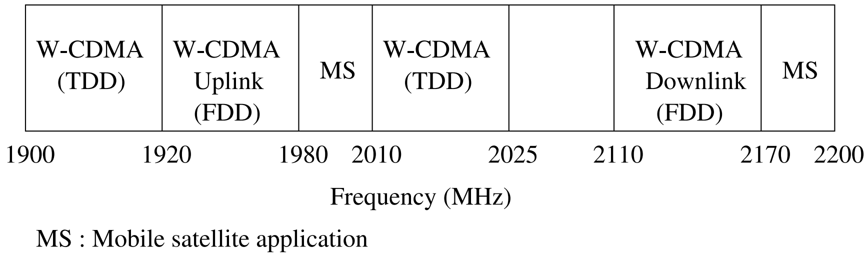

Figure 10.1: The proposed spectrum allocation in UTRA.

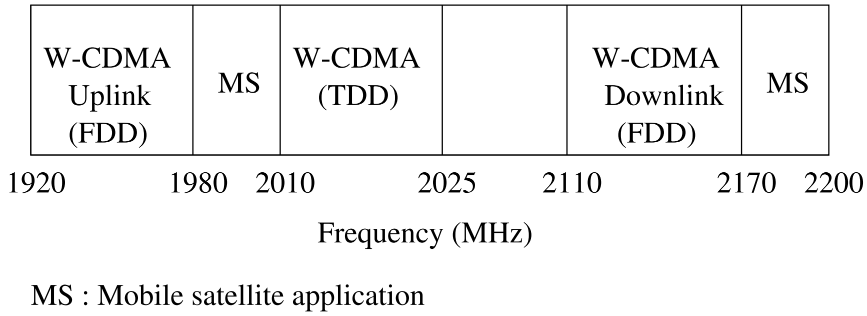

Figure 10.2: The proposed spectrum allocation in IMT-2000.

Specifically, the uplink and downlink signals are transmitted using different carrier frequencies f_1 and f_2, respectively, separated by a frequency guard band in FDD mode. On the other hand, the uplink and downlink messages in the TDD mode are transmitted using the same carrier frequency f_c, but in different time-slots, separated by a guard time. As seen from the spectrum allocation in Figures 10.1 and 10.2, the paired bands of 1920-1980 MHz and 2110-2170 MHz are allocated for FDD operation in the uplink and downlink, respectively, whereas the TDD mode is operated in the remaining unpaired bands [8]. However, in case of asymmetric services, such as for example computer file downloading or video on demand (VoD), only one of the FDD bands is required and hence the more flexible TDD link could potentially double the link's capacity by allocating all time-slots in one direction. The parameters designed for FDD and TDD operations are such that they are mutually compatible so as to ease the implementation of a dual-mode terminal capable of accessing the services offered by both FDD and TDD operators. We note furthermore that recent research advocates

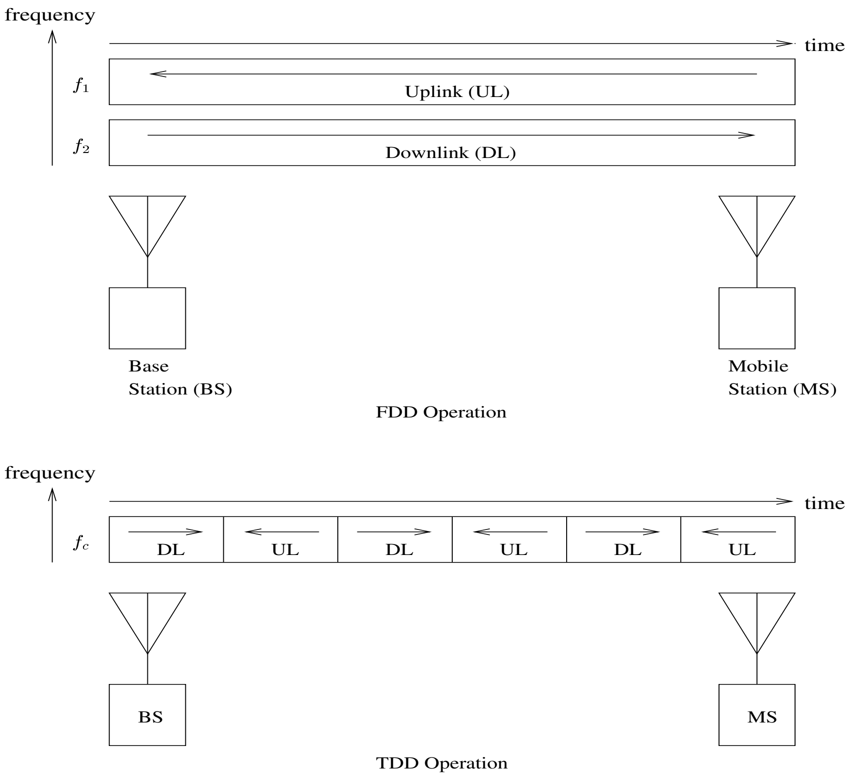

Figure 10.3: Principle of FDD and TDD operation.

the TDD mode quite strongly in the context of burst-by-burst adaptive CDMA modems [23, 24], since the uplink-downlink reciprocity can be advantageously exploited in order to adjust the modem parameters, such as the spreading factor or the number of bits per symbol on a burst-by-burst basis. This allows the system to more efficiently exploit the time variant wireless channel capacity, hence maintaining a higher bits/s/Hz bandwidth efficiency.

Table 10.2 shows the basic parameters of the UTRA/IMT-2000 proposals. Some of these parameters are discussed during our further discourse, but significantly more information can be gleaned concerning these systems by carefully studying the table. It is also informative to compare these parameters to the IS-95 CDMA system parameters of Table 1.1. Both systems are operated at a basic chip rate of 4.096 Mcps, giving a nominal bandwidth of 5 MHz, when using root-raised cosine Nyquist pulse shaping filters (see Chapter 9) with a roll-off factor of 0.22. IMT-2000 has an additional lower chip rate of 1.024 Mcps, corresponding to a bandwidth of 1.25 MHz. Increased chip rates of 8.192 Mcps and 16.384 Mcps are also specified in

Radio access technology	FDD : DS-CDMA TDD : TDMA/CDMA
Operating environments	Indoor/Outdoor to indoor/Vehicular
Chip rate (Mcps)	UTRA : 4.096/8.192/16.384 IMT-2000 : 1.024/4.096/8.192/16.384
Channel bandwidth (MHz)	UTRA : 5/10/20 IMT-2000 : 1.25/5/10/20
Nyquist roll-off factor	0.22
Duplex modes	FDD and TDD
Channel bit-rates (kbps)	FDD (UL) : 16/32/64/128/256/512/1024 FDD (DL) : 32/64/128/256/512/1024/2048 TDD (UL/DL) : 512/1024/2048/4096
Frame length	10 ms
Spreading factor	FDD : variable, 4 to 256 TDD : variable, 2 to 16
Detection scheme	Coherent with time-multiplexed pilot symbols
Inter-cell operation	FDD : Asynchronous TDD : Synchronous
Power control	Open and closed-loop
Transmit power dynamic range	80 dB (UL), 30 dB (DL)
Handover	Soft handover Inter-frequency handover

Table 10.2: UTRA/IMT-2000 basic parameters.

order to cater for much higher user bit-rates (> 2 Mbps).

UTRA/IMT-2000 fulfilled the requirements of 3G mobile radio systems by offering a range of user bit-rates up to 2 Mbps. Various services having different bit-rates and quality of service (QoS) can be readily supported using so-called Orthogonal Variable Spreading Factor (OVSF) codes, which will be highlighted in Section 10.2.6.1, and service multiplexing which will be discussed in Figure 10.12. As opposed to the common pilot channel of the second-generation IS-95 system, which was portrayed in Chapter 1, the third-generation UTRA / IMT-2000 systems invoked dedicated pilot symbols embedded in the users' data-stream. These can be invoked in order to support the operation of adaptive antennae at the base station, which was not facilitated by the common pilot channel of the IS-95 system.

Irrespective of whether a common pilot channel is used or dedicated pilots are embedded in the data, they facilitate the employment of coherent detection. Coherent detection is known to provide better performance, than non-coherent detection [26], a fact also argued in Chapter 9. Furthermore, the inclusion of short spreading codes enables the implementation of various performance enhancement techniques, such as interference cancellers and joint-detection algorithms. In order to support flexible system deployment in indoor and outdoor environments, **inter-cell-asynchronous operation** is used in the FDD mode. This implies that no external timing source, such as a beacon or Global Positioning System (GPS) is required. However, in the TDD mode inter-cell synchronization is required in order to be able to seamlessly access the time-slots offered by adjacent Base Stations (BS) during handovers. This is achieved by maintaining synchronization between the base stations.

Radio access is concerned mainly with the physical layer of the International Standardization Organization/Open Systems Interconnection (ISO/OSI) Reference Model. Hence, in the following sections we will mainly concentrate on the physical layer of the UTRA/IMT-2000 proposals. We note here, furthermore, that there have been proposals in the literature for allowing TDD operation also in certain segments of the FDD spectrum, since FDD is incapable of surrendering the uplink or downlink frequency band of the duplex link, when the traffic demand is basically simplex. In fact, segmenting the spectrum in FDD/TDD bands inevitably results in some inefficiency in bandwidth utilization terms, especially in the case of asymmetric or simplex traffic. Hence in reference [27] the idea of eliminating the dedicated TDD band was investigated, where TDD was invoked within the FDD band by simply allowing TDD transmissions in either the uplink or downlink frequency band, depending on which one was less interfered with. This flexibility is unique to CDMA, since as long as the amount of interference is not excessive, FDD and TDD can share the same bandwidth. This would be particularly feasible in the indoor scenario of [27], where the surrounding outdoor cell could be using FDD, while the indoor cell would reuse the same frequency band in TDD mode. The buildings' walls and partitions could mitigate the interference between the FDD/TDD schemes.

10.2.2 Transport Channels

Transport channels are offered by the physical layer to the higher OSI layers and they can be classified into two main groups, as shown in Table 10.3 [7,8]. The Dedicated transport CHannel (DCH) is related to a specific mobile station-base station link and it is used to carry user and control information between the network and a mobile station. Hence the DCHs are bidirectional channels. There are four transport channels within the common transport channel group, as shown in Table 10.3. The Broadcast Control Channel (BCCH) is used to carry system- and cell-specific information on the downlink (DL) to all mobiles over the entire cell. This channel conveys information, such as the downlink transmit power of the base station and the uplink (UL) interference power measured at the base station, which are vital for the mobile station in adjusting its transmit power required for the target Signal-to-Interference plus Noise Ratio (SINR) of the base station, as we shall see in Section 10.2.8. The Forward Access Channel (FACH) of Table 10.3 is a downlink common channel used for carrying control information and short user data packets to mobile stations, if the system knows the serving base station of the mobile station. On the other hand, the Paging Channel (PCH) of Table 10.3 is used to carry control information

Dedicated transport channel	Common transport channel
Dedicated Channel (DCH) (UL/DL)	Broadcast Control Channel (BCCH) (DL)[†] Forward Access Channel (FACH) (DL) Paging Channel (PCH) (DL) Random Access Channel (RACH) (UL)

[†]In IMT-2000, this is known as Broadcast Channel (BCH)

Table 10.3: UTRA/IMT-2000 transport channels.

to a mobile station, when the serving base station of the mobile station is unknown in order to page the mobile station, when there is a call for the mobile station. The Random Access Channel (RACH) of Table 10.3 is an uplink channel used by the mobile station to carry control information and short user data packets to the base station in order to support the mobile station's access to the system, when it wishes to set up a call.

The philosophy of these channels is fairly plausible and it is informative and enlightening to explore the differences between the somewhat less flexible control regime of the 2nd-generation GSM system of Chapter 8 and the more advanced 3rd-generation proposals, which we leave for the motivated reader due to lack of space. Suffice to say here that unfortunately it is unfeasible to design the control regime of a sophisticated mobile radio system by 'direct synthesis' and hence some of the solutions reviewed throughout this section in the context of the 3G proposals may appear somewhat heuristic and quite ingenious. These solutions constitute an amalgam of the wireless research community's experience in the design of the existing second-generation systems and of the lessons learned from their operation. Further contributing factors in the design of the 3G systems were based on solving the signalling problems specific to the favoured physical layer traffic channel solutions, namely CDMA. In order to mention only one of them, the TDMA-based GSM system of Chapter 8 was quite robust against power control inaccuracies, while the Pan-American IS-95 CDMA system required an accurate power control. As we will see in Section 10.2.8 during our forthcoming discourse, the power control problem was solved quite elegantly in the 3G proposals. We will also see that statistical multiplexing schemes, such as ALOHA - the original root of the recently more familiar Packet Reservation Multiple Access (PRMA) procedure highlighted for example in Chapter 9 - found their way into public mobile radio systems. A variety of further interesting solutions have also found applications in these 3G proposals, which are the results of the past decade of wireless system research. Let us now review the range of physical channels in the next section.

10.2.3 Physical Channels

The transport channels are transmitted using the physical channels. The physical channels are organized in terms of superframes, radio frames and timeslots, as shown in Figure 10.4. The philosophy of this hierarchical

Dedicated Physical Channels	Transport Channels
Dedicated Physical Data Channel (DPDCH) (UL/DL)	DCH
Dedicated Physical Control Channel (DPCCH) (UL/DL)	

Common Physical Channels	Transport Channels
Physical Random Access Channel (PRACH) (UL)	RACH
Primary Common Control Physical Channel (PCCPCH) (DL)	BCCH
Secondary Common Control Physical Channel (SCCPCH) (DL)	FACH
Synchronization Channel (SCH) (DL)	PCH

Table 10.4: Mapping the transport channels of Table 10.3 to the UTRA physical channels. The equivalent mapping of IMT-2000 is seen in Table 10.5.

frame structure is also reminiscent to a certain degree of the GSM TDMA frame hierarchy of Chapter 8. However, while in GSM each TDMA user had an exclusive slot-allocation, in W-CDMA the number of simultaneous users supported is dependent on the users' required bit-rate and their associated spreading factors. The mobile stations can transmit continuously in all slots or discontinuously, for example when invoking a voice activity detector (VAD). Some of these issues will be addressed in Section 10.2.4.

As seen in Figure 10.4, the UTRA/IMT-2000 superframe consists of 72 radio frames, with 16 timeslots within each radio frame. The duration of each timeslot is 0.625 ms, which gives a duration of 10 ms and 720 ms for the radio frame and superframe, respectively. The 10 ms frame-duration also conveniently coincides for example with the frame-length of the ITU's G729 speech codec for speech communications, while it is a 'sub-multiple' of the GSM system's various full- and half-rate speech codec's frame durations, which were detailed in Chapter 8. We also note that a convenient mapping of the video-stream of the H.263 videophone codec of Chapter 9 can be arranged on the 10 ms-duration radio frames for supporting interactive video services, while on the move. In the FDD mode, a downlink physical channel is defined by its spreading code and frequency. Furthermore, in the uplink, the modem's orthogonal in-phase and quadrature-phase channels are used to deliver the data and control information simultaneously in parallel on the modem's I and Q branches - as it will be augmented in Figure 10.18 - and hence the knowledge of the relative carrier phase, namely whether the I or Q branch is involved, constitutes part of the physical channel's identifier. On the other hand, in the TDD mode, a physical channel is defined by its spreading code, frequency and timeslot. The format of the physical channels is different for UTRA and IMT-2000. Hence, we will highlight them individually, commencing with the UTRA structure.

10.2.3.1 UTRA Physical Channels

Similarly to the transport channels of Table 10.3, the physical channels in UTRA can also be classified, as dedicated and common channels. Table 10.4 shows the type of physical channels and the corresponding mapping of transport channels on the physical channels in UTRA.

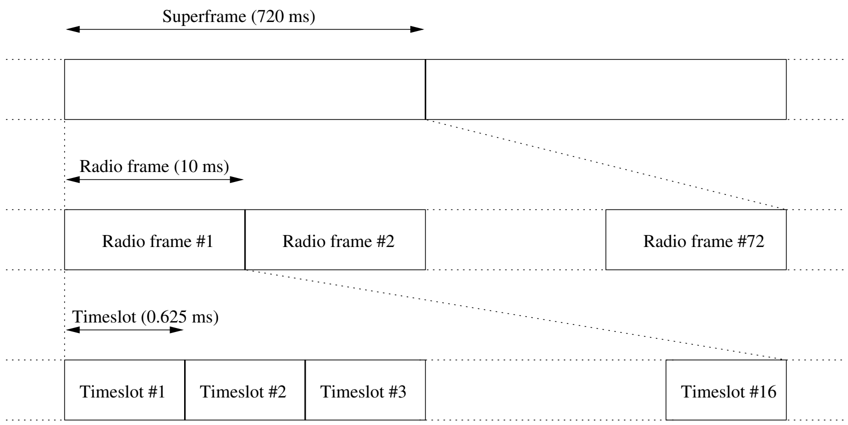

Figure 10.4: UTRA/IMT-2000 physical channel structure. On the UTRA downlink DPDCH and DPCCH are interspersed by time-multiplexing. On the uplink they are mapped to the I and Q modem branches, as it will be augmented in the context of Figure 10.18.

The configuration of the information in the timeslots of the physical channels differs from one another in the uplink and downlink, as well as in the FDD and TDD modes. Figures 10.5 and 10.6 show the structure of one timeslot for each physical channel on the downlink (DL) and uplink (UL), respectively, in the FDD mode. The timeslot structures of the TDD mode will be highlighted subsequently during our further discourse in this section. The structure of the Synchronisation Channel (SCH) will be explained in more detail in Section 10.2.9.

The dedicated physical channel of Figure 10.5 can be divided into a dedicated physical data channel (DPDCH) and a dedicated physical control channel (DPCCH), both of which are bi-directional. The DPDCH is used to transmit the DCH information between the base station and mobile station. The DPCCH is used to transmit the pilot symbols, transmit power control (TPC) commands and an optional so-called transport-format indicator (TFI). At the time of writing, the number of pilot symbols and the length of the TPC as well as TFI segments, which constitute the total overhead of the data channels, is undecided. Given that the TPC and TFI segments render the transmission packets 'self-descriptive', the system becomes very flexible, supporting burst-by-burst adaptivity, which sub-

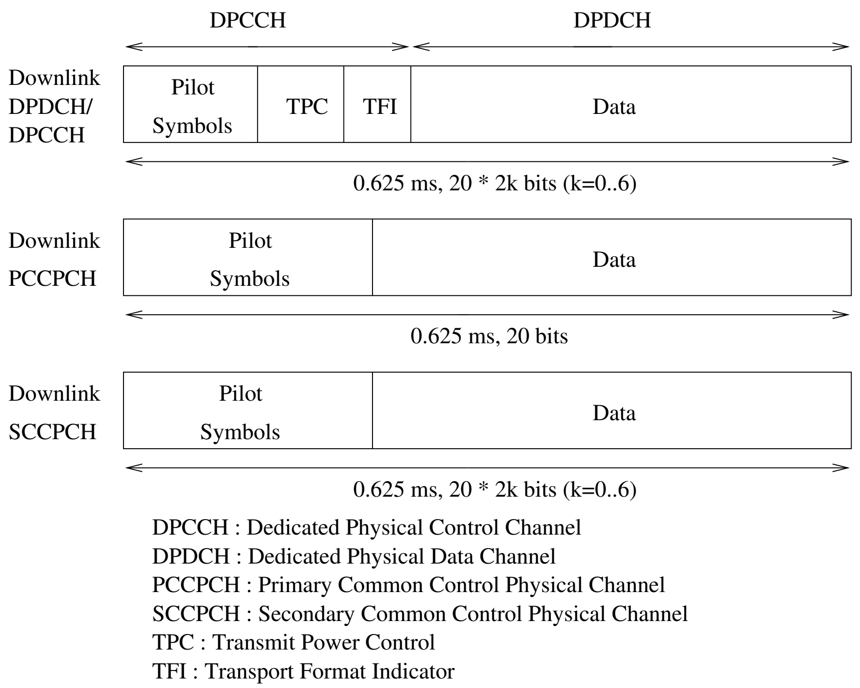

Figure 10.5: UTRA downlink FDD physical channel timeslot configuration, which are mapped to the time slots of Figure 10.4. On the UTRA downlink DPDCH and DPCCH are interspersed by time-multiplexing. On the uplink they are mapped to the I and Q modem branches, as it will be augmented in the context of Figure 10.18. The equivalent IMT-2000 structure is seen in Figure 10.7.

stantially improves the system's performance [23, 24], although this side-information is vulnerable to transmission errors. The pilot symbols are used to facilitate coherent detection on both the uplink and downlink - as it was discussed in Chapter 9 in the context of QAM, - and also to enable the implementation of performance enhancement techniques, such as adaptive antennas and interference cancellation. The TPC commands provide a fast and efficient power control scheme, which is essential in DS-CDMA using the techniques to be highlighted in Section 10.2.8. The TFI carries information concerning the instantaneous parameters of each transport channel multiplexed on the physical channel.

On the UTRA FDD uplink of Figure 10.6, the DPDCH and DPCCH messages of Table 10.4 are transmitted in parallel on the in-phase (I) and quadrature-phase (Q) branches of the modem, as it will become more explicit during our further discourse in the context of Figure 10.18 [7]. By contrast, at the top of the downlink structure of Figure 10.5, the DPDCH

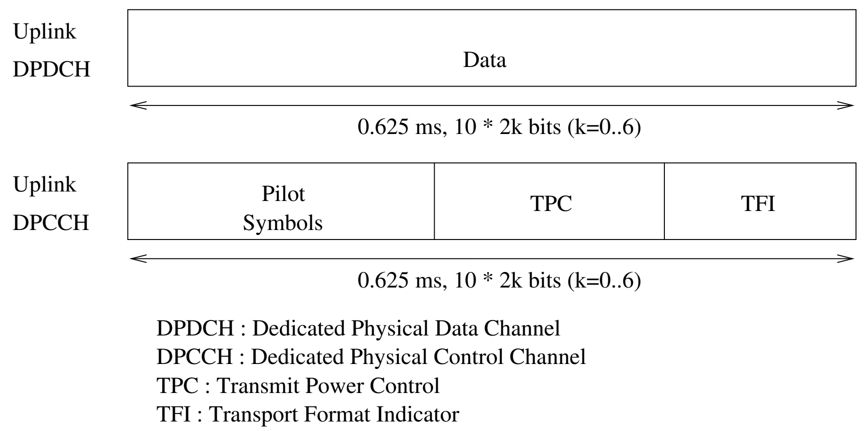

Figure 10.6: UTRA uplink FDD physical channel timeslot configuration, which is mapped to the time slots of Figure 10.4. The DPDCH and DPCCH messages are transmitted in parallel on the I and Q branches of the modem of Figure 10.18. The equivalent IMT-2000 uplink FDD time-slot configuration is seen in Figure 10.8. These DPDCH and DPCCH bursts are time-multiplexed at the top of Figure 10.5, yielding 20×2^k bits per 0.625 ms.

and DPCCH are time-multiplexed into one physical channel time-slot of Figure 10.4. The reason for the parallel transmission on the uplink is to avoid Electromagnetic Compatibility (EMC) problems due to discontinuous transmission of the DPDCH of Table 10.4 [18]. Discontinuous transmission occurs, when temporarily there are no data to transmit, but the link is still maintained by the DPCCH. If the uplink DPCCH were time-multiplexed with the DPDCH, as in the downlink of Figure 10.6, this could create short, sharp energy spikes. Since the mobile station may be located near sensitive electrical equipment, these spikes could affect these equipment.

The Primary Common Control Physical Channel (PCCPCH) of Table 10.4 and Figure 10.5 is used by the base station in order to continuously broadcast the BCCH information at a fixed rate of 20 bits/0.625 ms = 32 kbps to all mobiles in the cell. The Secondary Common Control Physical Channel (SCCPCH) of Table 10.4 and Figure 10.5 carries the FACH and PCH information on the downlink and they are transmitted only, when data are available for transmission. Knowledge of the SCCPCH bit-rate can be acquired from the BCCH information transmitted on the PCCPCH.

The parameter k in Figures 10.5 and 10.6 determines the spreading factor (SF) of the physical channel. The highest SF is 256 for $k = 0$, which corresponds to the lowest channel bit-rate and the highest spreading gain, while the highest channel bit-rate has a SF of 4, when $k = 6$. Hence the bit-rates available for the uplink DPDCH are 16/32/64/128/256/512/1024 kbps, due to the associated 'payload' of 10×2^k bits per 0.625 ms bursts in Figure 10.6, where $k = 0 \ldots 6$. Recall that the uplink structure of Figure 10.6 invoked I/Q multiplexing, as it will be demonstrated in Figure 10.18. By contrast, the downlink structure of Figure 10.5 refrains from I/Q-multiplexing and the timeslot payload is 20×2^k bits per 0.625 ms, but the exact data rate is unspecified.

This hierarchically structured set of legitimate rates provides a high flexibility in terms of the services supported. Notice that the channel bit-rates of the downlink dedicated physical channels are twice as high as those of the uplink dedicated physical channels. This is due to the time-multiplexed DPCCH and DPDCH on the downlink of Figure 10.5, while the DPCCH and DPDCH are transmitted in parallel on the modem's I and Q branches in the uplink of Figures 10.6 and 10.18. If higher bit-rates are required, then several DPDCHs with only one DPCCH can be transmitted in parallel, using a technique known as multicode transmission [25], which will be explained in more detail in the context of Figure 10.16 in Section 10.2.5. The SCCPCH also has a variable bit-rate, similarly to that of the downlink dedicated physical channel portrayed at the bottom of Figure 10.5. On the other hand, again, the PCCPCH has a constant bit-rate of 20 bits/0.625 ms = 32 kbps. Since the chip rate is 4.096 Mcps and each time slot has a duration of 0.625 ms, there will be 4.096 Mcps $\times$ 0.625 ms = 2560 chips per time slot.

At this stage it is worth mentioning that the available control channel rates are significantly higher in the 3G systems, than in their 2G counterparts of Table 1.1 in Chapter 1. For example, the maximum BCCH signalling rate in GSM is about an order of magnitude lower than the above mentioned 32 kbps UTRA BCCH rate. In general, this increased control channel rate will support a significantly more flexible system control than the 2G systems. For comparison, we refer to the 'Control Channel Rate' row of Table 1.1. Having highlighted the UTRA physical channels, let us now consider the corresponding IMT-2000 solutions.

10.2.3.2 IMT-2000 Physical Channels

The type of physical channels and their mapping to/from the transport channels in IMT-2000 are shown in Table 10.5. The dedicated channels of IMT-2000 are basically similar to those of Table 10.4 in UTRA. The differences are in the common physical channels. The so-called 'perch' channel has a similar function to that of the SCH in UTRA. However, as seen from the mapping in Table 10.5, the Broadcast Channel (BCH) information is also carried by the perch channel, whereas in UTRA an additional physical channel, namely the PCCPCH of Figure 10.5 is used to carry the BCCH information.

These physical channels are also arranged in terms of superframes, radio frames and timeslots, with parameters similar to those in UTRA, as it was shown in Figure 10.4. However, the configuration of the timeslots is slightly

Dedicated Physical Channels	Transport Channels
Dedicated Physical Data Channel (DPDCH) (UL/DL)	DCH
Dedicated Physical Control Channel (DPCCH) (UL/DL)	

Common Physical Channels	Transport Channels
Physical Random Access Channel (PRACH) (UL)	RACH
Perch Channel (DL)	BCH*
Common Physical Channel (CPCH) (DL)	FACH
	PCH

* BCH in IMT-2000 corresponds to BCCH in UTRA

Table 10.5: Mapping the transport channels of IMT-2000 to physical channels. The equivalent mapping of UTRA is seen in Table 10.4.

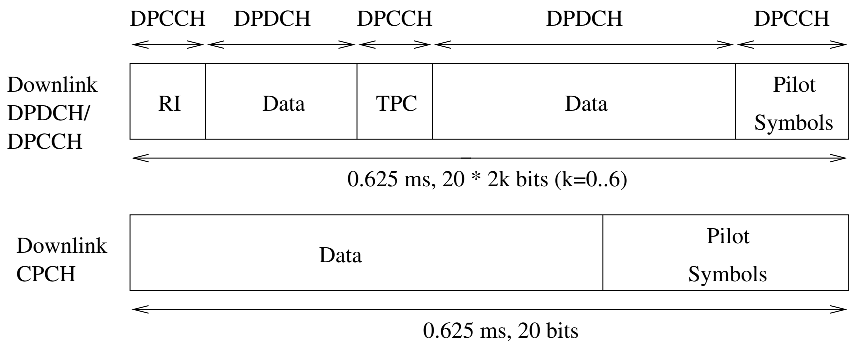

DPDCH : Dedicated Physical Data Channel
DPCCH : Dedicated Physical Control Channel
CPCH : Common Control Channel
TPC : Transmit Power Control
RI : Rate Information

Figure 10.7: IMT-2000 FDD downlink physical channel timeslot configuration, which is mapped to the time slots of Figure 10.4. On the uplink DPDCH and DPCCH are mapped to the I and Q modem branches, as it will be augmented in the context of Figure 10.18. The equivalent UTRA structure is seen in Figure 10.5.

different from those in UTRA, which is demonstrated by Figures 10.7 and 10.8 for the FDD downlink and uplink, respectively. The Rate Information (RI) at the top of Figure 10.7 has the same function as the TFI of Figure 10.5 in UTRA, rendering the transmission bursts 'self-descriptive' and hence IMT-2000 is also capable of supporting burst-by-burst adaptivity [23, 24].

In contrast to the previous FDD structures of Figures 10.5-10.8, in TDD operation, the burst structure of Figure 10.9 is used, where each time-slot's

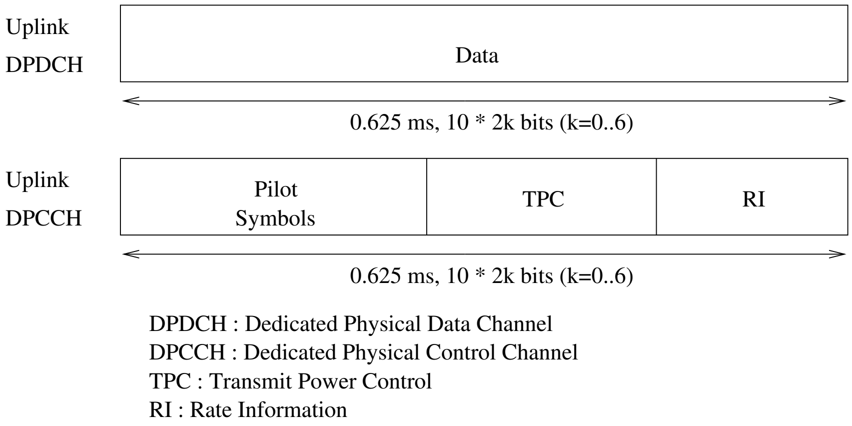

Figure 10.8: IMT-2000 FDD uplink physical channel timeslot configuration, which is mapped to the time slots of Figure 10.4. On the IMT-2000 downlink DPDCH and DPCCH are interspersed by time-multiplexing. On the uplink they are mapped to the I and Q modem branches, as it will be augmented in the context of Figure 10.18. The equivalent UTRA structure is seen in Figure 10.6.

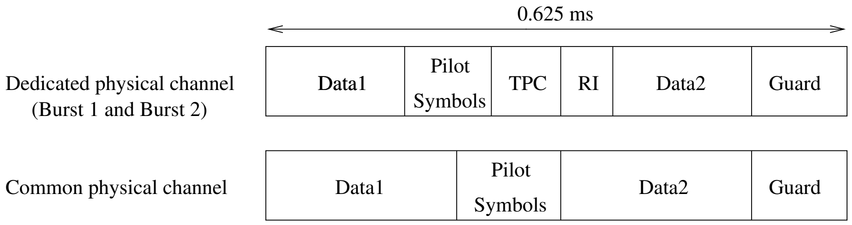

Figure 10.9: Burst configuration in the IMT-2000/UTRA TDD mode, which is augmented in Figure 10.11 for the dedicated physical channel.

transmitted information can be arbitrarily allocated to the downlink or uplink, with the exception of the first burst in the TDD frame of Figure 10.10, which is always assigned to the downlink. Hence, this flexible allocation of the uplink and downlink burst in the TDD mode enables the use of an adaptive modem [23, 24] whereby the modem parameters, such as the spreading factor or the number of bits per symbol can be adjusted on a burst-by-burst basis to optimize the link quality. This first slot, known as the 'beacon slot' only contains the downlink physical control information, such as the BCCH, PCH, SCH or FACH information of Tables 10.4 and 10.5 for UTRA and IMT-2000, respectively. Three examples of possible TDD uplink/downlink allocations are shown in Figure 10.10. A symmetric uplink/downlink allocation refers to a scenario, where an equal number of downlink and uplink bursts are allocated within a frame, while in asymmetric uplink/downlink

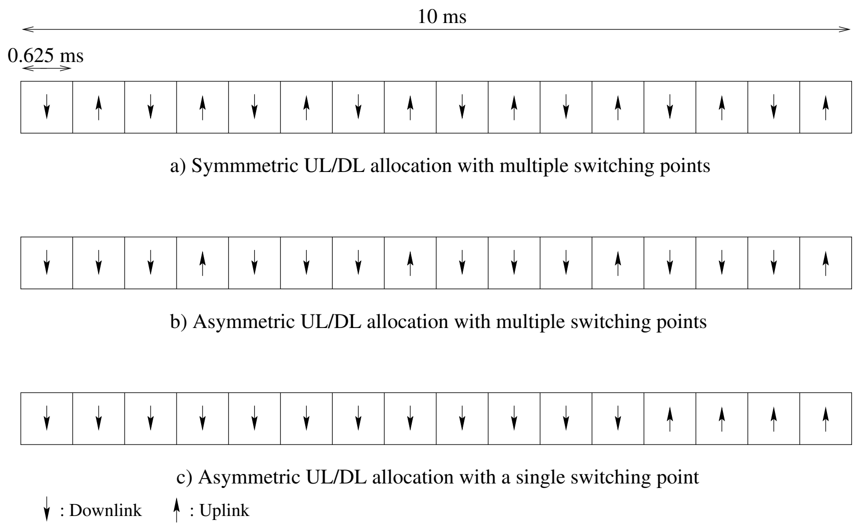

Figure 10.10: Uplink/downlink allocation examples for the 16 slots in IMT-2000 and UTRA TDD operation using the timeslot configurations of Figure 10.9. The first slot is always a downlink slot, providing physical control information for the mobile station, such as the BCCH, PCH, SCH or FACH information.

allocation, there is an unequal number of uplink and downlink bursts, such as for example in 'near-simplex' file download or video-on-demand. In the TDD mode, the configuration of the information in the burst differs from that in FDD mode due to the presence of a guard time. Figure 10.9 shows an example of the TDD burst configuration for the common and dedicated physical channels. In UTRA, two different traffic burst structures, known as Burst 1 and Burst 2, are defined, as shown in Figure 10.11. The parameter k, where $k = 0, 1, 2, 3$ in Figure 10.11 determines the spreading factor of the burst. Hence, the spreading factor of a TDD burst can be variable, ranging from $976/(61 \times 2^3) = 2$ to $976/(61 \times 2^0) = 16$, as derived from Burst 1. Following the same approach, it can be easily shown that the spreading factor of Burst 2 is also in the range of 2 to 16, which was stipulated earlier in Table 10.2. With these spreading factors, the channel bit-rate of a single QPSK modulated TDD burst can be 512/1024/2048/4096 kbps, as given in Table 10.2. Having highlighted the basic features of the various UTRA/IMT-2000 channels, let us now consider, how the various services are error protected, interleaved and multiplexed on the DPDCH, an issue discussed with reference to Figure 10.12 in the context of UTRA/IMT-2000.

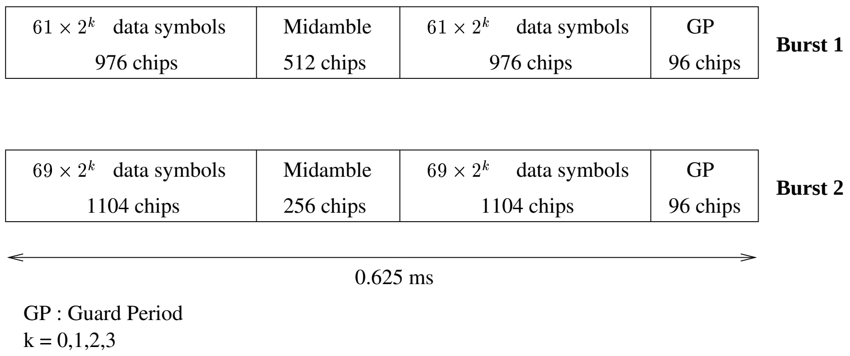

Figure 10.11: Configuration of two different types of traffic bursts, as defined in UTRA, namely Burst 1 and Burst 2. The midamble contains the control symbols such as the pilot symbols, the TPC and RI, as portrayed in Figure 10.9. At the time of writing, the number of symbols in the respective fields in a TDD burst is still undecided in IMT-2000.

10.2.4 Service Multiplexing and Channel Coding in UTRA/IMT-2000

Service multiplexing is employed, when multiple services of identical and/or different bit-rates requiring different quality of service (QoS) belonging to the same user's connection are transmitted. An example would be the simultaneous transmission of voice, video, data and handwriting transmission service for a multimedia application. These issues were also addressed in Chapter 9, where PRMA was used for multiplexing the various services. Accordingly, each service is represented by its corresponding transport channels, as described in Section 10.2.2. A possible method of transmitting multiple services is by using code multiplexing with the aid of orthogonal codes. Every service could have its own DPDCH and DPCCH, each assigned to a different orthogonal code. This method is not very efficient, however, since a number of orthogonal codes would be reserved by a single user, while on the uplink it would also inflict self-interference. Alternatively, these services can be time-multiplexed into one or several DPDCHs, as shown in Figure 10.12 for UTRA/IMT-2000.

Transport channels belonging to different services with different QoS requirements are first channel coded individually, using various coding techniques. Several forward error correction (FEC) techniques are proposed for channel coding. The FEC technique used is dependent on the QoS requirement of that specific service. The potential FEC techniques are listed in Table 10.6, together with their corresponding parameters. Convolutional coding is used for services with a BER requirement on the order of 10^{-3}, for example, for voice services. For services requiring a lower BER, namely

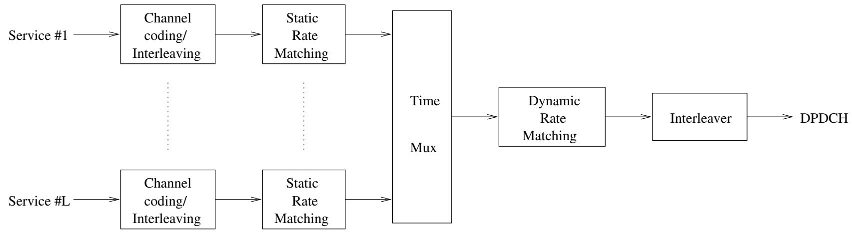

Figure 10.12: Service multiplexing in UTRA/IMT-2000.

	Convolutional	Reed-Solomon	Turbo†
BER requirement	10^{-3}	10^{-6}	10^{-6}
Rate	1/4 to 1	TBD‡	1/3 or 1/2
Constraint length	9	N/A	3

†Turbo coding is still under investigation in ETSI, optional in IMT-2000
‡TBD : To be decided

Table 10.6: UTRA and IMT-2000 channel coding parameters.

on the order of 10^{-6}, additional outer Reed-Solomon (RS) coding and outer interleaving concatenated with the inner convolutional coding is applied. These techniques were discussed in depth in Chapter 4. Instead of RS coding, turbo coding is proposed in IMT-2000 as an optional coding scheme. Turbo coding is known to guarantee a high performance [28] over AWGN channels at the cost of increased interleaving-induced latency or delay and at a high implementational complexity. At the time of writing, turbo coding is still under investigation within the ETSI. Each coded transport channel is then interleaved by the 'Channel coding/Interleaving' block, as shown in Figure 10.12. The depth of this so-called inner interleaving can range from one radio frame (10 ms) to as high as 80 ms, depending on the type of service being interleaved. For example, for a speech service, which belongs to the so-called real-time or interactive services, but can tolerate a BER of $10^{-3} to 10^{-2}$, decoding time is critical and hence a short interleaver depth is more feasible. On the other hand, for non-real-time services, such as data services, more emphasis is placed on achieving a low BER, than on fast decoding time, and hence a higher interleaver depth is more beneficial. The effect of the interleaver depth was also studied in Chapter 4.

The output of each coded transport channel of Figure 10.12 will have a different bit-rate. Hence, before time-multiplexing them on a physical channel, a so-called **static rate matching** procedure is required, as seen in Figure 10.12. Static rate matching is coordinated amongst the different coded transport channels, such that the bit-rate of each channel is adjusted to a level that fulfils its minimum QoS requirements [8]. On the downlink, the bit-rate is also adjusted so that the total instantanenous transport channel bit-rate approximately matches the defined bit-rate of the physical channel, as listed in Table 10.2. Static rate matching is based on code puncturing, which was treated in Chapter 4, and repetition.

After static rate matching, the coded transport channels are time-multiplexed, as portrayed in Figure 10.12 in order to produce the DPDCH 'payload'. The total instantaneous bit-rate of the DPDCH 'payload' may not be equal to the defined DPDCH bit-rate. Hence, a process referred to as **dynamic rate matching** is used to match the instantaneous bit-rate to one of the defined DPDCH bit-rates highlighted in Section 10.2.3. If the instantaneous bit-rate exceeds the maximum defined DPDCH bit-rate of 1.024 Mbps, then multicode transmission is invoked, which is highlighted in Section 10.2.5, whereby several DPDCHs are transmitted in parallel. After the bit-rate of the multiplexed channels is matched to that of the DPDCH, the data are interleaved, as seen in Figure 10.12.

Having highlighted the various channel coding techniques and having seen the structures of the physical channels in FDD mode and TDD mode, as illustrated by Figures 10.5-10.8 and Figure 10.11, respectively, let us now consider, how services of different bit-rates are mapped on the dedicated physical data channels (DPDCH) of Figures 10.5-10.8 and Figure 10.11 with the aid of two examples. Specifically, we consider the mapping of several speech services on the DPDCH in FDD mode and an example of the mapping of a 2.048 Mbps data service on the DPDCH in TDD mode.

10.2.4.1 Mapping Several Speech Services to the Physical Channels in FDD Mode [11]

In this example we shall assume that an 8 kbps G.729 speech codec was used to compress the speech signal, generating 80 bits/10 ms. As illustrated in Figure 10.12, each service is first channel coded, before it is time-multiplexed with other services in order to produce a single bit stream. Figure 10.13 shows the channel coding procedure of an 8 kbps speech service. Speech services usually have a moderate BER requirement, in the region of 10^{-3}. Hence, according to Table 10.6, convolutional coding will be employed. Since the duration of a radio frame in UTRA/IMT-2000 is 10 ms, the incoming 8 kbps bit stream is first split into segments of 10 ms, with each segment containing a total of 8 kbps $\times$ 10 ms = 80 bits, as demonstrated in Figure 10.13. A 16-bit CRC checksum is then attached to each 80-bit segment for the purpose of error detection. As a result, the number of bits in a segment is increased to 16 + 80 = 96 bits, as illustrated in Figure 10.13. Next, a block of 8 tail bits is concatenated to the 96-bit segment in order to flush the shift registers of the convolutional encoder, as discussed also in the GSM system of Chapter 8. Thus a total of 96 + 8 = 104 bits are conveyed to the convolutional encoder, as shown in Figure 10.13. A coding rate of $R = 1/3$ and a constraint length of $K = 9$ is used for the convolutional encoding, as listed in Table 10.6. The output of the convolutional encoder will have a total of 104 bits $\times$

3 = 312 bits per 10 ms segment. Interleaving, which is optional, can be performed across the frame after the convolutional encoding. The output of the channel coding/interleaving block in Figure 10.12 constitutes a so-called 'dedicated channel (DCH) radio unit', which is a 312-bit segment in this case, as shown in Figure 10.13. Hence, the channel coding process has increased the bit-rate of an 8 kbps speech service to 31.2 kbps.

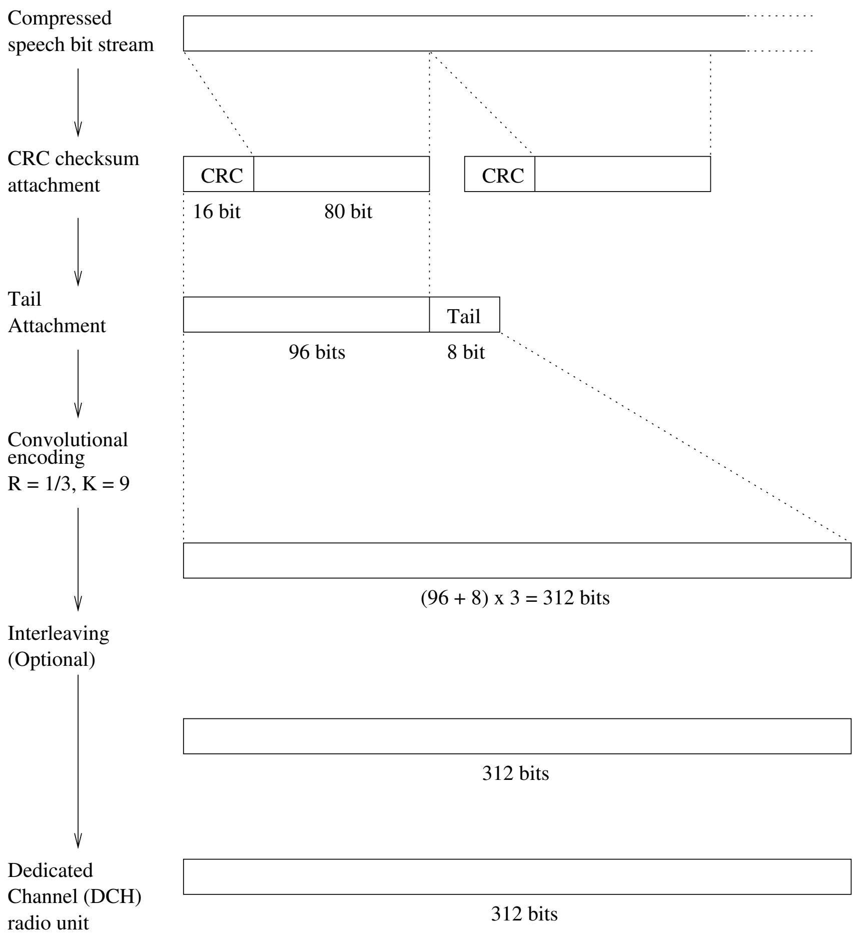

Figure 10.13: Convolutional coding of an 8 kbps speech service.

In order to illustrate the concept of service multiplexing and how these multiplexed services are eventually mapped on the DPDCH, let us assume that there are Q number of simultaneous speech services to be transmitted in the same connection in the FDD mode. These speech services are individually channel coded, as shown in Figure 10.12 and the channel coding procedure is illustrated in Figure 10.13. Hence, there will be Q separate DCH radio units at the input of the time-multiplexer of Figure 10.12, as shown in Figure 10.14. These DCHs are time-multiplexed in order to produce a single bit stream. We mentioned in Section 10.2.3, and also emphasized in Table 10.2 and in Figures 10.5-10.8 that a single dedicated physical data channel (DPDCH) can assume one of the available channel bit-rates, namely 16/32/64/128/256/512/1024 kbps. Since the bit-rate of the time-multiplexed DCHs may not be equal to any one of these bit rates, rate matching has to be employed in order to adapt the time-multiplexed bit-rate to one of the available DPDCH bit-rates within one radio frame, as shown in Figure 10.12. As mentioned previously, rate matching can be performed by bit puncturing or repetition. Hence for example, if only one DCH is present, which has a bit-rate of 31.2 kbps, then rate matching will increase this bit-rate to the nearest available DPDCH bit-rate, which is 32 kbps or 320 bits per radio frame. In the event, when the bit-rate of the time-multiplexed DCH bit stream exceeds the maximum available bit-rate, then multicode transmission is used, which will be highlighted in Section 10.2.5. In this case, the bit-rate will be matched to any of the available channel bit-rates within one radio frame, namely to $L\times$ 16/32/64/128/256/512/1024 kbps, where L denotes the number of radio frames of equal rate required to convey the information, as illustrated in Figure 10.14. After the bit-rate is matched, interleaving is performed across each of the L radio frames in order to produce the L DPDCHs. Let us now consider the channel coding and mapping procedures of a 2.048 Mbps data service.

10.2.4.2 Mapping a 2.048 Mbps Data Service to the Physical Channels in TDD Mode [10]

In contrast to 2G mobile systems, 3G mobile systems must be capable of supporting data services with rates as high as 2 Mbps. Hence in this example we will illustrate the mapping of a 2 Mbps data service to the dedicated physical data channels (DPDCH) in TDD mode using the TDD bursts shown in Figure 10.11. Unlike speech services, which have a moderate BER requirement, a low BER on the order of 10^{-6} is often required for the transmission of data services. Hence, more powerful FEC methods, such as turbo coding and concatenated inner convolutional/outer Reed-Solomon (RS) coding are needed for channel coding, as shown in Table 10.6. In this example, concatenated convolutional/RS coding will be invoked as the channel coding technique. Similarly to the channel coding of a speech service, as given in Figure 10.13, the incoming data bit stream of the 2 Mbps data service is broken down into 10 ms segments, each containing 2 Mbps $\times$ 10 ms = 20480 bits, as it can be seen in Figure 10.15. Each segment is first coded using the outer Reed-Solomon coding scheme. Since the RS coding rate is undecided at the time of writing, we will use the coding rate of 200/210 in this example, as it was given in reference [10] noting that a number of different-rate RS-coded user scenarios were also exemplified

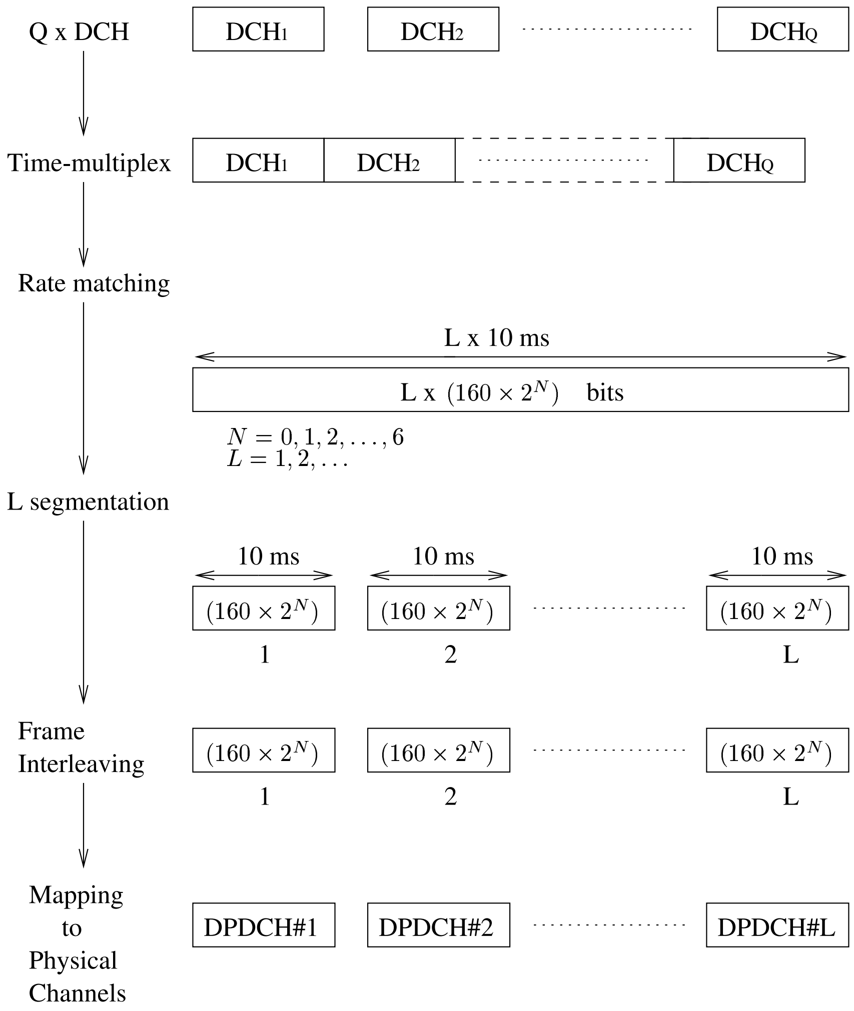

Figure 10.14: Mapping of the channel coded speech service portrayed in Figure 10.13 to the dedicated physical data channels of Figures 10.5-10.8 in FDD mode. The value L denotes the number of radio frames required to convey the information. When $L > 1$, multicode transmission, as highlighted in Section 10.2.5, is employed. When $L = 1$, single code transmission is used. The corresponding schematic is seen in Figure 10.12.

in the standard. Hence, the number of bits in a segment is increased to $20480 \times 210/200 = 21504$ bits at the output of the outer RS encoder, as displayed in Figure 10.15. After the outer interleaving, X number of signalling bits from Layer 2 of the OSI seven-layer structure and 16 blocks of 8 tail bits are then added to the 21504-bit segment, before the inner convolutional coding is applied. Following the example in reference [10], a convolutional coding rate of 2/3 is used. Hence after channel coding, the segment would contain $[21504 + X + (16 \times 8)] \times 3/2 = 32256 + 3X/2 + 192$ coded bits. These coded bits have to be mapped to the TDD physical channels of Figure 10.11, where two configurations are defined, namely Burst 1 and Burst 2. Assuming a spreading factor of 16, Burst 1 can accommodate a total of 2×976 chips/16=122 symbols, which constitute 244 bits, when QPSK modulation is used. On the other hand, Burst 2 can accommodate 2×1104 chips/16=138 symbols or 276 bits. In TDD mode, two methods can be used to transmit a block of data, either allocating several time-slots or allocating several orthogonal codes per time-slot, as in multicode transmission. Each burst must contain either 244 bits or 276 bits, again, assuming that the spreading factor is 16. Hence, either bit puncturing or repetition has to be used in order to adapt the coded bit stream such that the total number of bits in the segment becomes an integer factor of either 244 bits, as in Burst 1, or 276 bits, as in Burst 2. At the left of Figure 10.15, we see that puncturing is used in order to reduce the total number of bits to $117 \times 244 = 28548$ bits, such that 117 bursts of 'Burst 1' are used for transmission. Alternatively, the coded bit stream can be punctured in order to reduce the total number of bits in a segment to $104 \times 276 = 28704$ bits, as illustrated at the right of Figure 10.15 for transmission, using 104 'Burst 2' type packets. These bits are then QPSK modulated and mapped to the dedicated physical channels seen in Figure 10.11.

Following the above brief discussions on service multiplexing, channel coding and interleaving, let us now concentrate on the aspects of variable-rate and multicode transmission in UTRA/IMT-2000.

10.2.5 Variable Rate and Multicode Transmission in UTRA/IMT-2000

Three different techniques have been proposed for supporting variable rate transmission, namely multicode-, modulation-division multiplexing-(MDM) and multiple processing gain (MPG) based techniques [29]. UTRA and IMT-2000 employ a number of different processing gains, or variable spreading factors in order to transmit at different channel bit-rates, as highlighted previously in Section 10.2.3. We argued in Chapter 1 that the spreading factor has a direct effect on the performance and capacity of a DS-CDMA system. Since the chip rate is constant, the spreading factor - which is defined as the ratio of the spread bandwidth to the original information bandwidth - becomes lower, as the bit-rate increases. Hence, there is a limit to the value of the spreading factor used, which is 4 in FDD mode in the proposed 3G standards. Multicode transmission [25, 29, 30] is used, if the total bit rate to be transmitted exceeds the maximum bit-rate supported by a single DPDCH, which was stipulated as 1.024 Mbps. When

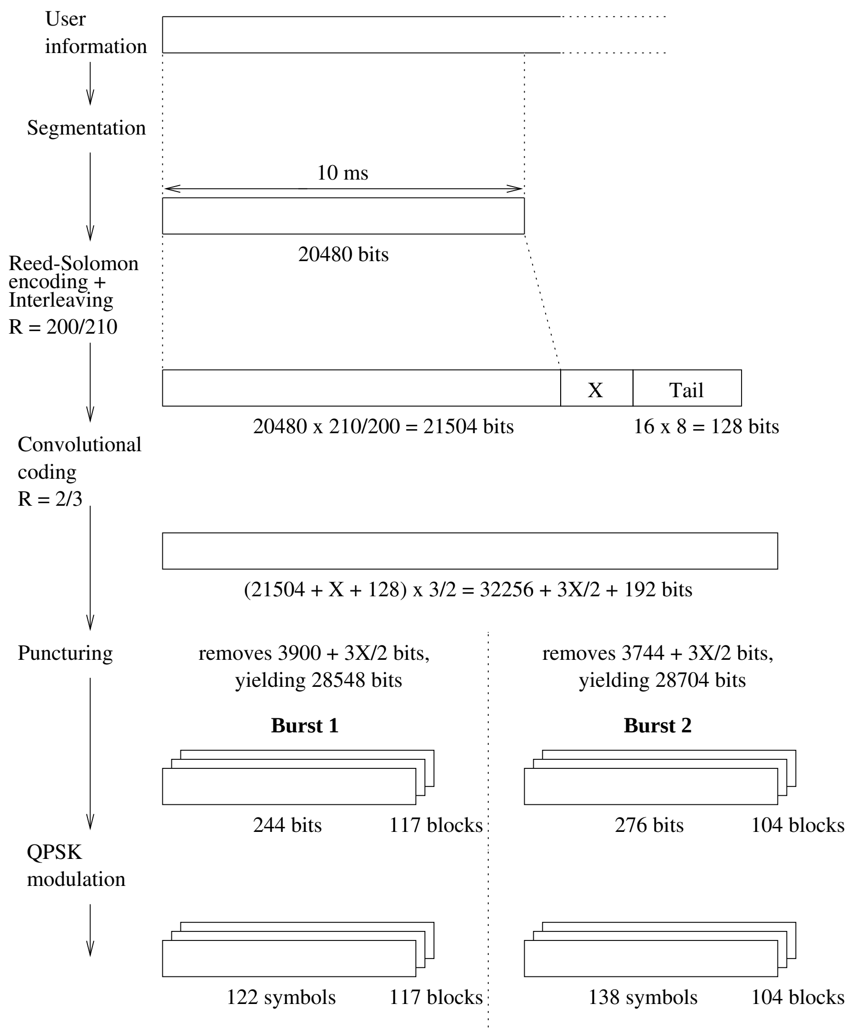

Figure 10.15: Channel coding of a 2 Mbps data service using concatenated convolutional/Reed-Solomon coding and mapping to the TDD dedicated physical channels, namely Burst 1 and Burst 2, as shown in Figure 10.11 for a spreading factor of 16. The corresponding schematic is seen in Figure 10.12.

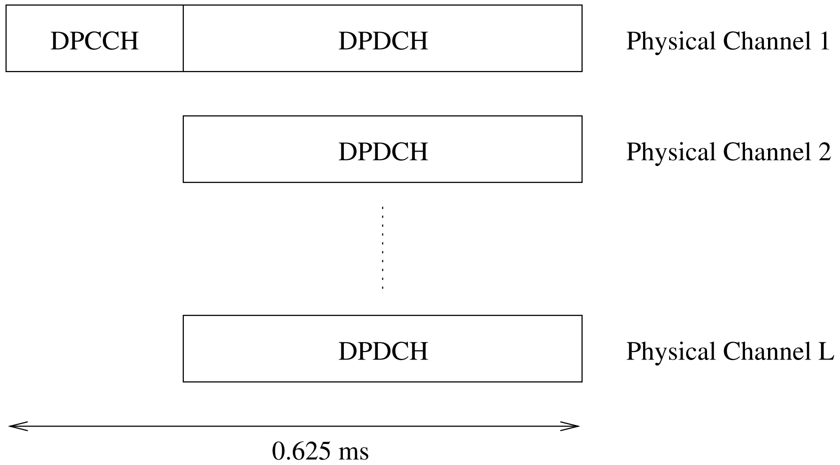

Figure 10.16: Downlink FDD slot format for multicode transmission in IMT-2000/UTRA, based on Figure 10.5, but dispensing with transmitting DPCCH over all multicode physical channels.

this happens, the bit-rate is split amongst a number of spreading codes and the information is transmitted using two or more codes. However, only one DPCCH is transmitted during this time. Hence, on the uplink, one DPCCH and several DPDCH are code-multiplexed and transmitted in parallel, as it will be augmented in the context of Figure 10.18. On the downlink, the DPDCH and DPCCH are time-multiplexed on the first physical channel associated with the first spreading code. If more physical channels are required, the DPCCH part in the slot will be left blank, as shown in Figure 10.16.

10.2.6 Spreading and Modulation

As we argued in Chapter 1, the performance of DS-CDMA is interference limited [31]. The majority of the interference originates from the transmitted signals of other users within the same cell, as well as from neighbouring cells. This interference is commonly known as multiple access interference (MAI). Another source of interference, albeit less dramatic, is a result of the wideband nature of CDMA, which causes several replicas of the transmitted signal to reach the receiver at different time instants, hence inflicting what is known as inter-path interference. However, the advantages gained from wideband transmissions, such as multipath diversity and the noise-like properties of interference, outweigh the drawbacks.

In order to reduce the MAI and hence to improve the systems's performance and capacity, **the IMT-2000/UTRA physical channels are spread using two different codes, namely the so-called channel-**

ization code[2] **and a typically longer so-called scrambling code.** By contrast, recall that in the IS-95 CDMA system of Chapter 1, for example in the downlink schematic of Figure 1.42, there were three different orthogonal codes. Namely the 64-chip Walsh-codes of Figure 1.41, the inphase and quadrature-phase pseudo-noise sequences, PNI and PNQ, which are the so-called 'short-codes' of 32768 chip-duration and the $2^{42}-1$ chip-duration long codes. The IS-95 short codes are the same cell-specific codes in both the uplink and downlink, while the long codes are user-specific and they are also identical in the uplink and downlink. The cdma2000 system of Section 10.3 follows the IS-95 philosophy.

10.2.6.1 Orthogonal Variable Spreading Factor Codes in UTRA/IMT-2000

The UTRA/IMT-2000 channelization codes are derived from a set of orthogonal codes known as Orthogonal Variable Spreading Factor (OVSF) codes [32]. OVSF codes are generated from a tree-structured set of orthogonal codes, such as the Walsh-Hadamard codes of Chapter 1, using the procedure shown in Figure 10.17. Each channelization code is denoted by $c_{N,n}$, where $n = 1, 2, \ldots, N$ and $N = 2^x, x = 2, 3, \ldots 8$. Each code $c_{N,n}$ is derived from the previous code $c_{(N/2),n}$ as follows [32] :

$$\begin{bmatrix} c_{N,1} \\ c_{N,2} \\ c_{N,3} \\ \vdots \\ c_{N,N} \end{bmatrix} = \begin{bmatrix} c_{(N/2),1} | c_{(N/2),1} \\ c_{(N/2),1} | \bar{c}_{(N/2),1} \\ c_{(N/2),2} | c_{(N/2),2} \\ \vdots \\ c_{(N/2),(N/2)} | \bar{c}_{(N/2),(N/2)} \end{bmatrix}, \tag{10.1}$$

where [|] denotes an augmented matrix and $\bar{c}_{(N/2),n}$ is the binary complement of $c_{(N/2),n}$. Hence, for example, according to Equation (10.1) and Figure 10.17 $c_{N,1} = c_{8,1}$ is created by simply concatenating $c_{(N/2),1}$ and $c_{(N/2),1}$, which simply doubles the number of chips. By contrast, $c_{N,2} = c_{8,2}$ is generated by attaching $\bar{c}_{(N/2),1}$ to $c_{(N/2),1}$. From Equation (10.1) we see that, for example, $c_{N,1}$ and $c_{N,2}$ at the left-hand side of Equation (10.1) are not orthogonal to $c_{(N/2),1}$, since the first half of both was derived from $c_{(N/2),1}$ in Figure 10.17, but they are orthogonal to $c_{(N/2),n}, n = 2, 3, \ldots, (N/2)$. The code $c_{(N/2),1}$ in Figure 10.17 is known as the mother code of the codes $c_{N,1}$ and $c_{N,2}$, since these two codes are derived from $c_{(N/2),1}$. The codes on the 'highest'-order branches ($k = 6$) of the tree at the left of Figure 10.17 have a spreading factor of 4 and they are used for transmission at the highest possible bit-rate for a single channel, which is 1024 kbps. On the other hand, the codes on the 'lowest'-order branches ($k = 0$) of the tree at the right of Figure 10.17 have a spreading factor of 256 and these are used for transmission at the lowest bit-rate,

[2] In IMT-2000, the channelization codes are known as spreading codes.

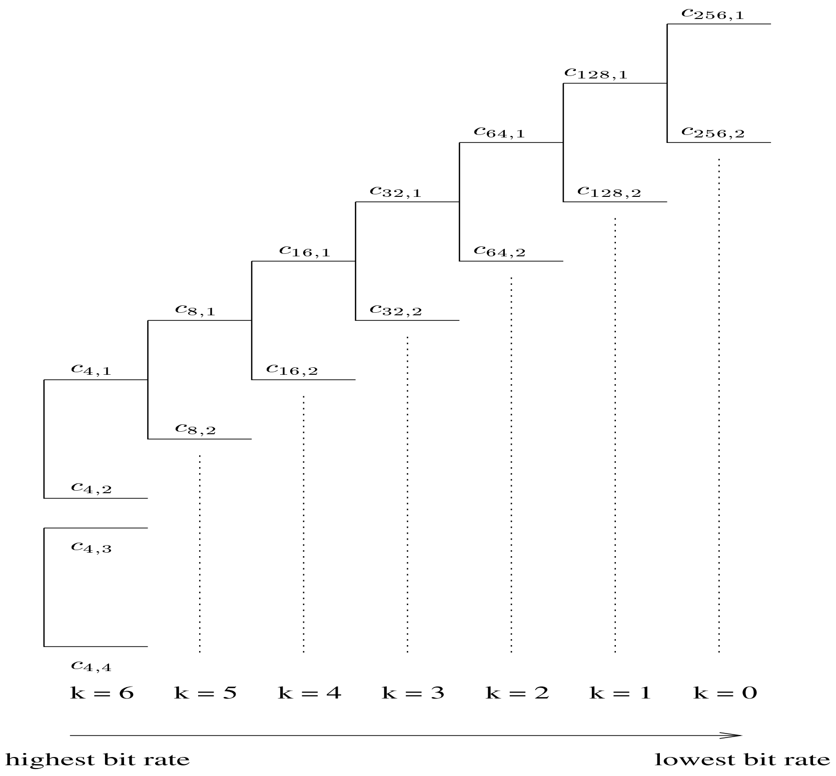

Figure 10.17: Orthogonal variable-spreading factor code tree in UTRA/IMT-2000 according to Equation 10.1. The parameter k in the figure is directly related to that found in Figures 10.5-10.8.

which is 16 kbps. Orthogonality between parallel transmitted channels of the same bit rate is preserved by assigning each channel a different orthogonal code accordingly. For channels with different bit-rates transmitting in parallel, orthogonal codes are assigned, ensuring that no code is the mother-code of the other. Hence, OVSF channelization codes provide total isolation between different users' physical channels on the downlink which transmits all codes synchronously and hence eliminates multiple access interference. OVSF channelization codes also provide orthogonality between the different DPDCHs seen in Figure 10.16 during multicode transmission.

However, since there is only a limited set of OVSF codes, which is likely to be insuffcient to support a large user-population, while also allowing identification of the base stations by the mobile stations on the downlink, **each cell will reuse the same set of OVSF codes**. However, orthogonal codes, such as the orthogonal OVSF codes, in general exhibit poor asynchronous cross-correlation properties [33] and hence the cross-correlations of the OVSFs of adjacent asynchronous base stations will become unacceptably high, degrading the correlation receiver's performance at the mobile station. On the other hand, certain long codes such as Gold codes, exhibit low asynchronous cross-correlation, which is advantageous in CDMA applications [3]. Hence in UTRA/IMT-2000, cell-specific long codes are used in order to reduce the inter-cell interference on the downlink. On the uplink, MAI is reduced by assigning different scrambling codes to different users. Table 10.7 shows the parameters and techniques used for spreading and modulation in UTRA and IMT-2000, which will be discussed in depth in the next section.

	Channelization codes	Scrambling codes
Type of codes	OVSF (Section 10.2.6.1)	DL : Gold codes (UTRA/IMT-2000), Extended very large (VL) Kasami codes (UTRA) UL : Gold codes
Code length	Variable	DL : 10 ms of $(2^{18}-1)$-chip Gold code UL : 10 ms of $(2^{41}-1)$-chip Gold code, 256-chip Kasami code (UTRA), 737.28 s of $(2^{41}-1)$-chip Gold code (IMT-2000)
Type of spreading	DL : BPSK UL : BPSK	DL : BPSK (UTRA), QPSK (IMT-2000) UL : QPSK
Data Modulation	DL : QPSK (FDD and TDD) UL : BPSK (FDD), QPSK (TDD)	

Table 10.7: UL/DL and FDD/TDD spreading and modulation parameters in UTRA/IMT-2000.

10.2.6.2 Uplink Spreading and Modulation

Let us commence our discourse with a brief note concerning the choice of spreading codes in general [34,35]. Suffice to say that the traditional measures used in comparing different codes are their cross-correlations (CCL) and auto-correlation (ACL). If the CCL of the channelization codes of different users is non-zero, this will increase their interference, as perceived by the receiver. Hence a low CCL reduces the MAI. The so-called out-of-phase ACL of the codes, on the other hand, plays an important role during the initial synchronization between the base station and mobile station, which has to be sufficiently low in order to minimize the probability of synchronizing to the wrong ACL peak. Let us now continue our discourse with the uplink spreading issues with reference to Table 10.7. A model of the uplink transmitter for a single DPDCH is shown in Figure 10.18 [7]. We have seen in Figure 10.6 that the DPDCH and DPCCH are transmitted in parallel on the I and Q branches of the uplink, respectively. Hence, to avoid I/Q channel interference, different orthogonal spreading codes are assigned to the DPDCH and DPCCH on the I and Q branches, respectively. The technique is referred to **as dual-channel spreading**. These two channelization codes for DPDCH and DPCCH, denoted by c_D and c_C in Figure 10.18, respectively, are allocated in a pre-defined order. Hence, the base station and mobile station only need to know the spreading factor of the channelization codes, but not the code itself. After spreading, the

BPSK modulated I and Q branch signals are summed in order to produce a complex signal, where G in Figure 10.18 is a power gain adjustment for the DPCCH. In the event of multi-code transmission, different orthogonal spreading codes are assigned to each DPDCH for the sake of maintaining orthogonality and they can be transmitted on either the I or Q branch. In this case, the base station and mobile station have to agree on the number of channelization codes to be used.

The complex signal is then scrambled by a user-specific complex scrambling code, denoted by c_{scramb} in Figure 10.18 [7]. This scrambling code is a complex Gold code constructed from two m-sequences using the polynomials of $1+X^3+X^{41}$ and $1+X^{20}+X^{41}$, following the procedure highlighted by Proakis in reference [26]. This code is also shown in Table 10.7. The Q-branch Gold code is a shifted version of the I-branch Gold code, where a shift of 1024 chips was recommended. Each Gold code is rendered different from one another by assigning a unique initial state to one of the shift registers of the m-sequence. The initial state of the other shift register is a continuous sequence of logical '1'. The base station will inform the mobile station about the specific initial sequence used via the access grant message. Complex-valued scrambling balances the power on the I and Q branches. This can be shown by letting c_s^I and c_s^Q be the I and Q branch scrambling codes, respectively. The spread data of Figure 10.18 [7] can be written as:

$$d(t) = c_D \cdot b_{\mathrm{DPDCH}} + jG \cdot c_C \cdot b_{\mathrm{DPCCH}}, \tag{10.2}$$

where b_{DPDCH} and b_{DPCCH} represent the DPDCH message and the DPCCH message, respectively. Assuming that the power level in the I and Q branches of Figure 10.18 is unbalanced due to their different bit-rates or different QoS requirements on DPDCH and DPCCH and if only real-valued scrambling is used, then the output becomes:

$$s(t) = c_s^I \left(c_D \cdot b_{\mathrm{DPDCH}} + jG \cdot c_C \cdot b_{\mathrm{DPCCH}}\right), \tag{10.3}$$

which is also associated with an unbalanced power level on the I and Q branches. By contrast, if complex-valued scrambling is used, then the output of Figure 10.18 [7] becomes:

$$\begin{aligned} s(t) &= \left(c_D \cdot b_{\mathrm{DPDCH}} + jG \cdot c_C \cdot b_{\mathrm{DPCCH}}\right) \cdot \left(c_s^I + jc_s^Q\right) && (10.4)\\ &= c_s^I \cdot c_D \cdot b_{\mathrm{DPDCH}} - G \cdot c_s^Q \cdot c_C \cdot b_{\mathrm{DPCCH}} && (10.5)\\ &\quad +j\left(c_s^Q \cdot c_D \cdot b_{\mathrm{DPDCH}} + G \cdot c_s^I \cdot c_C \cdot b_{\mathrm{DPCCH}}\right). && (10.6) \end{aligned}$$

As it can be seen, the power on the I and Q branches is the same, regardless of the power level of the DPDCH and DPCCH. Hence complex scrambling improves the power efficiency by reducing the peak-to-average power fluctuation. This also relaxes the linearity requirements of the up-link power amplifier used. The whole process of spreading using orthogonal codes and complex-valued scrambling codes is known in this context as Orthogonal

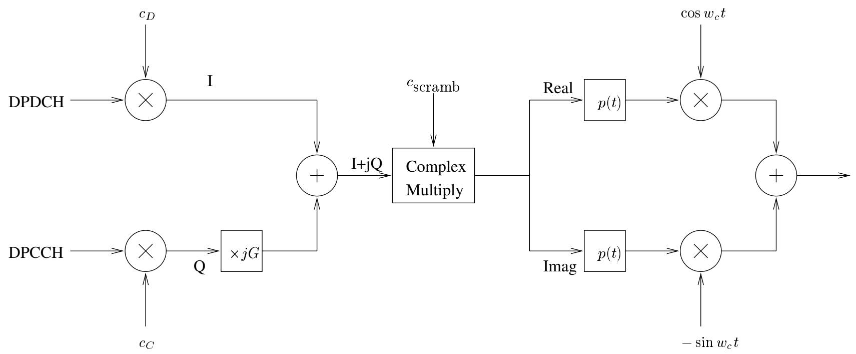

Figure 10.18: FDD uplink transmitter in UTRA/IMT-2000.

Complex QPSK (OCQPSK) modulation[3]. The pulse shaping filters, $p(t)$, are root-raised cosine Nyquist filters with a roll-off factor of 0.22, which were introduced in Chapter 9.

Because of the asynchronous nature of the mobile stations' uplink transmissions, every user can employ the same set of channelization codes. In UTRA, instead of the long Gold scrambling code of $(2^{41}-1)$ chip duration, short scrambling codes such as extended very large (VL)-Kasami codes of length 256 chips can be used. This code was introduced in order to ease the implementation of multiuser detection at the base station [18]. Explicitly, the multiuser detector has to invert the so-called system matrix [36], the dimension of which is proportional to the sum of the channel impulse response duration and the spreading code duration. Hence using a relatively short spreading code is an important practical consideration. Let us now consider the downlink modulation and spreading.

10.2.6.3 Downlink Spreading and Modulation

The time-multiplexed DPDCH and DPCCH burst at the top of Figure 10.5 are first QPSK modulated in order to form the I and Q channels, before spreading to the chip rate using the OVSF channelization code c_{ch} of Section 10.2.6.1. Different users are assigned different channelization codes for maintaining their orthogonality. The base station will inform the users about their corresponding channelization codes via the Access Grant Message.

The resulting signal in Figure 10.19 is then scrambled by a cell-specific scrambling code c_{scramb}. As seen in Table 10.7, this scrambling code is in a complex, i.e. QPSK form in IMT-2000, while in UTRA, it is in a real or BPSK form. The scrambling code is selected from one of 32 groups of scrambling codes, each group containing 16 different scrambling codes, giving a total of 512 available scrambling codes [12]. The reason for catego-

[3]OCQPSK is also known as Hybrid PSK (HPSK)

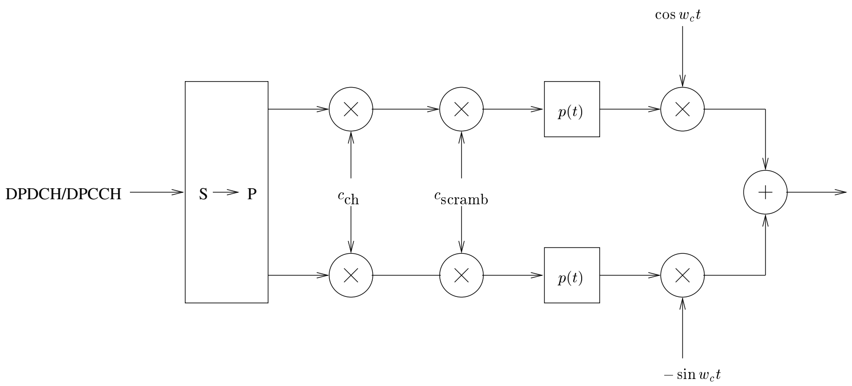

Figure 10.19: FDD/TDD downlink transmitter in UTRA/IMT-2000.

rizing the scrambling codes into groups is to facilitate fast cell identification, which will be augmented in Section 10.2.9. Similarly to the downlink, the pulse shaping filters are root-raised cosine Nyquist filters with a roll-off factor of 0.22, which were discussed in Chapter 9. Figure 10.19 shows the model of a UTRA/IMT-2000 downlink transmitter for one user.

10.2.7 Random Access

If data transmission is initiated by a mobile station, it is required to send a random access request to the base station. Since such requests can occur at any time, collisions may result, when two or more mobile stations attempt to access the network simultaneously. Hence in order to reduce the probability of a collision, the random access procedure in UTRA is based on the slotted ALOHA technique [8], which is a statistical multiplexing procedure similar to the PRMA technique discussed in Chapter 9.

Random access requests are transmitted to the base station via the Random Access Channel (RACH). UTRA and IMT-2000 have different RACH burst structures. The burst structure of the RACH in UTRA is shown in Figure 10.20 which is transmitted according to the regime of Figure 10.22, as it will be described during our forthcoming discourse. The duration of one random access burst is 11.25 ms. It consists of a preamble and a message part, while between the preamble and message portion of the burst there is an idle period of 0.25 ms duration. The purpose of the idle period is to allow the base station to detect the preamble and then to prepare subsequently for receiving the message itself [8]. The preamble carries a signature, which is a complex orthogonal Gold code of length 16, spread by a cell-specific 256-chip orthogonal Gold code. The structure of the message part is shown in Figure 10.21, whereby the data and control information are transmitted in parallel, again, by mapping them on the I and Q modem branches, as seen in Figure 10.18. The control part seen at the bottom of

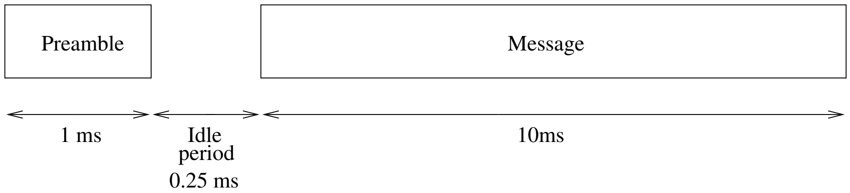

Figure 10.20: Structure of the UTRA random access burst, which is detailed in Figure 10.21.

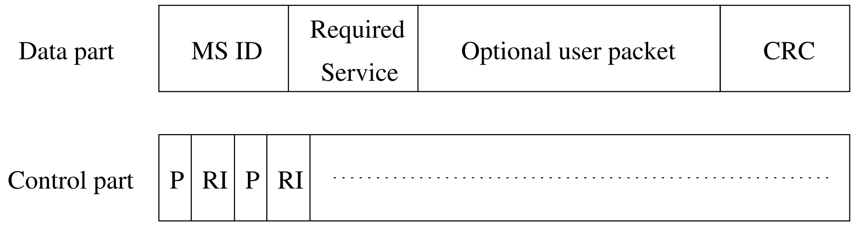

Figure 10.21: Structure of the 10 ms-duration UTRA random access burst message part seen in Figure 10.20. The data and control parts are mapped on the I and Q modem branches in Figure 10.18. RI is the spreading-factor-related rate information, while P represents the pilots.

Figure 10.21 simply contains the pilot symbols (P) and rate information (RI), which contains information about the spreading factor used by the data part. Hence this control part must be detected first in order to infer the spreading factor of the data part at the top of Figure 10.21. The control part has a fixed bit-rate with a spreading factor of 256. On the other hand, the data part of Figure 10.21 can have a spreading factor ranging from 32 to 256, which is communicated to the base station with the aid of the RI in the control part, as mentioned previously. The data part consists of a random mobile station identification (MS ID), a ‘Required Service’ field and Cyclic Redundancy Checking (CRC) for error detection. The required service indicates the function of the random access burst. If the actual information packets to be transmitted from the mobile station are short and infrequent, then these packets can be transmitted in the 1‘Optional user packet’ field of Figure 10.21. However, if the packets to be transmitted are long and frequent, then the mobile station will request a dedicated physical channel to be set up in order to transmit those packets. Whether a short packet is transmitted or a request is made for allocating a dedicated physical channel, is indicated in the required service field.

Before any random access burst can be transmitted, the mobile station has to obtain certain information via the downlink BCCH transmitted on the Primary CCPCH according to the format of Figure 10.5. The informa-

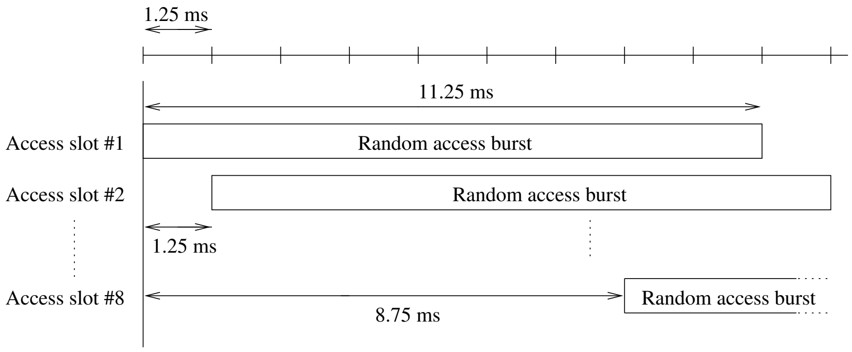

Figure 10.22: ALOHA-based physical uplink random access bursts in UTRA, which are transmitted using the RACH burst format of Figures 10.21 and 10.21.

tion includes the cell-specific spreading codes for the preamble and the message of Figures 10.20 and 10.21 itself, the available signatures, the uplink access slots of Figure 10.22, which can be contended for in ALOHA mode and the spreading factors for the message, the interference level measured at the base station, and the Primary CCPCH transmit power level. All this information can be readily available, once synchronization is achieved, as it will be discussed in Section 10.2.9.

The random access slot starting instants are spaced 1.25 ms apart in Figure 10.22. The random access burst can only be transmitted in one of these access slots. Hence, the physical random access channel scheduling takes place, as shown in Figure 10.22, with 8 available access slots in a 10 ms frame duration. After acquiring all the necessary information via the BCCH which is mapped on the PCCPCH according to the format of Figure 10.5, the mobile station will randomly select a signature from the available signatures and will commence transmitting its uplink RACH bursts according to the formats of Figures 10.20 and 10.21 on a randomly selected access slot chosen from the set of available access slots as seen in Figure 10.22. The transmit power is adjusted via an open-loop power control scheme, which will be highlighted in Section 10.2.8.2 since at this stage of the mobile station's access no closed-loop power-control is possible.

After the RACH burst is transmitted, the mobile station will listen for the acknowledgement of reception transmitted from the base station on the FACH of Table 10.4. If the mobile station fails to receive any acknowledgement after some pre-defined time, it will retransmit the RACH burst in another randomly selected slot of Figure 10.22 and the procedure is repeated.

In IMT-2000 a different random access burst structure is used, which is shown in Figure 10.23. The data are carried on the I branch, while the signature is repeatedly transmitted on the Q branch of the modem, as seen

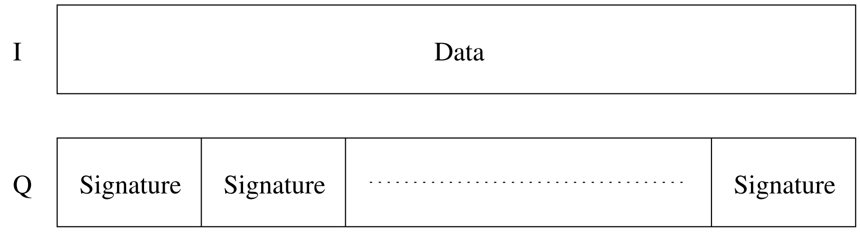

Figure 10.23: Structure of the 10 ms-duration IMT-2000 uplink random access burst. The corresponding UTRA-burst was shown in Figure 10.21, while the ALOHA procedure obeys Figure 10.22. The data and the signature are mapped to the I and Q branches of Figure 10.18.

in Figure 10.18. The procedure of access request is the same as in UTRA. Let us now consider the issues of power control in the next section.

10.2.8 Power Control

Accurate power control is essential in CDMA in order to mitigate the so-called near-far problem [37, 39], as we argued in Chapter 1. Furthermore, power control has a dramatic effect on the coverage and capacity of the system.

10.2.8.1 Closed-Loop Power Control in UTRA/IMT-2000

Closed-loop power control is employed on both the uplink and downlink. Since the power control procedure is the same on both links, we will only elaborate on the uplink procedure, noting that the TPC commands are conveyed in the downlink and uplink directions according to the format of Figures 10.5 and 10.6, respectively.

The base station measures the received power of the desired uplink DPCCH transmitted using the schematic of Figure 10.18 after RAKE combining and also estimates the total received interference power in order to obtain the estimated Signal-to-Interference Ratio (SIR). This SIR estimation process is performed every 0.625 ms, or a timeslot duration, in which the SIR estimate is compared to a target SIR. The value of the target SIR depends on the required quality of the connection. According to the values of the measured and required SIRs, the base station will generate a transmit power control (TPC) command, which is conveyed to the mobile station using the burst at the top of Figure 10.5. If the estimated SIR is higher than the target SIR, the TPC command will instruct the mobile station to lower the transmit power of the DPDCH and DPCCH by a step size of Δ_{TPC} dB. Otherwise, the TPC command will instruct the mobile station to increase the transmit power by the same step size. The step size may differ from cell to cell and it is typically 0.25-1.5 dB[4]. Explicitly, transmitting at an unnecessarily high power reduces the battery life, while degrading other users' reception quality, who - as a consequence - may request a power increment, ultimately resulting in an unstable overall system operation.

On the downlink, so-called base station-diversity combining may take place, whereby two or more base stations transmit the same information to the mobile station in order to enhance its reception. These base stations are known as the active base station set of the mobile station. Power control is performed by all the base stations independently. Hence, the mobile station may receive different TPC commands from its active set of base stations. In this case, the mobile station will adjust its transmit power according to a simple algorithm, increasing the transmit power only, if the TPC commands from all the base stations indicate an 'increase power' instruction. If one of the base stations issued a 'decrease power' TPC command, then the mobile station will decrease its transmit power according to the required step size. If the mobile station received more than one 'decrease power' TPC command, then it will decrease its transmit power according to the largest step size indicated. In this way, the multiuser interference will be kept to a minimum without significant deterioration of the performance, since at least one base station has a good reception. Again, the uplink and downlink procedures are identical, obeying the TPC transmission formats of Figures 10.5 and 10.6, respectively.

10.2.8.2 Open-Loop Power Control During the Mobile Station's Access

As mentioned in Section 10.2.7, open-loop power control is used to adjust the transmit power for the random access burst of Figures 10.20-10.23, since no closed-loop operation is feasible at this stage of the mobile station's access request. Prior to any data burst transmission, the mobile station would have acquired information about the interference level measured at the base station and also about the base station's Primary CCPCH transmitted signal level, which are conveyed to the mobile station via the BCCH according to the format of Figure 10.5. At the same time, the mobile station would also measure the power of the received Primary CCPCH. Hence, with the knowledge of the transmitted and received power of the Primary CCPCH, the downlink path loss can be found. The random access burst of Figures 10.20-10.23 should be received by the base station under all practical conditions. Since the interference level and the path loss are now known, the required transmitted power of the random access burst can be readily calculated.

[4] In IMT-2000, the step size is fixed at 1dB

10.2.9 Cell Identification

System- and cell-specific information are conveyed via the BCCH transmitted by the Primary CCPCH of Table 10.4 and Figure 10.5 in UTRA or over the so-called Perch Channel of Table 10.5 in IMT-2000, which is transmitted according to the format of Figure 10.24 from the corresponding base station to the mobile station, as mentioned in Section 10.2.3. Figure 10.24 will be detailed in our forthcoming discourse. Before a mobile station can access the network, a variety of system- and cell-specific information has to be obtained. The Primary CCPCH of Figure 10.5 is also spread by a cell-specific scrambling code, identical to the scrambling code c_{scramb} shown in Figure 10.19, which minimises the inter-cell interference and assists in identifying the cells. Hence, the first step for the mobile station is to recognize this scrambling code and to synchronize with the corresponding base station.

As specified in Section 10.2.6.3, there are a total of 32×16=512 downlink scrambling codes available in the network. Theoretically it is possible to achieve scrambling code identification by cross-correlating the Primary CCPCH broadcast signal with all the possible 512 scrambling codes. However, this would be an extremely tedious and slow process, unduly delaying the mobile station's access to the network. Furthermore, synchronization between the base station and the mobile station has to be established. In order to achieve a fast cell identification by the mobile station, UTRA and IMT-2000 adopted a 3-step approach [38], which invoked the synchronization channel (SCH) and the perch channel broadcast from all the base stations in the network, respectively. The perch channel of IMT-2000 basically carries out the functions of the SCH in UTRA. The SCH is transmitted during frame synchronization along with all the downlink physical channels, as it will be highlighted in the context of Figure 10.24. The concept behind this 3-step approach is to divide the total number of possible scrambling codes into groups, in this case into 32 groups, each containing a smaller set of scrambling codes, namely 16 codes, yielding a total of 512 codes. Once the knowledge of which group the scrambling code belongs to is acquired, the mobile station can proceed to search for the correct scrambling code from a smaller subset of the possible codes.

The frame structure of the downlink synchronization channel is shown in Figure 10.24, where the slots correspond to those shown in Figure 10.4. It consists of two sub-channels, the so-called Primary SCH and Secondary SCH, transmitted in parallel using orthogonal code multiplexing. As seen in Figure 10.24, in the Primary SCH an unmodulated orthogonal Gold code, known as the Primary Synchronization Code (PSC), of length 256 chips is transmitted periodically at the beginning of each slot, which is denoted by c_p in Figure 10.24. The same PSC is used by all the base stations in the network. This allows the mobile station to establish slot-synchronization and to proceed to the frame-synchronization phase with the aid of the secondary SCH. On the Secondary SCH, a sequence of 16 different consecutive unmodulated orthogonal Gold codes, each of length 256 chips, are transmitted with a period of one radio frame duration, ie 10 ms, as seen at the bottom of Figure 10.24. An example of this sequence would be

$$c_1\ c_1\ c_2\ c_{11}\ c_6\ c_3\ c_{15}\ c_7\ c_8\ c_8\ c_7\ c_{15}\ c_3\ c_6\ c_{11}\ c_2, \tag{10.7}$$

where each of these 16 orthogonal Gold codes are selected from a set of 17 different orthogonal Gold codes, known as Secondary Synchronization Codes (SSC). These 17 SSCs are also orthogonal to the PSC. The specific sequence of 16 SSCs, denoted by $c_i^1, \ldots, c_i^{16}$ where $i = 1, \ldots, 17$ in Figure 10.24 is used as a code in order to identify and signal to the mobile station, which of the 32 scrambling code groups the scrambling code - which is used by the particular base station concerned - belongs to. Specifically, when each of the 17 legitimate 256-chip sequences can be picked for any of the 16 positions in Figure 10.24 and with no other further constraints, one could construct

$$\begin{aligned} c_{i,j}^{\text{repeated}} &= \begin{pmatrix} i+j-1 \\ j \end{pmatrix} \\ &= \frac{(i+j-1)!}{j!(i-1)!} \\ &= \frac{32!}{16! \cdot 16!} \\ &= 601,080,390 \end{aligned} \tag{10.8}$$

different such sequences, where $i = 17$ and $j = 16$. However, the 16 different 256-chip sequences seen at the bottom of Figure 10.24 must be constructed such that their cyclic shifts are also unique. In other words, none of the cyclic shifts of the 32 required $16 \times 256 = 4096$-chip sequences can be identical to any of the other sequences' cyclic shifts. Provided that these conditions are satisfied, the 16 specific 256-chip secondary SCH sequences can be recognized within one 10 ms-radio frame-duration of 16 slots and hence both slot and frame synchronization can be established within the particular frame received. The BCH data of Table 10.5 in IMT-2000 and the pilot symbols following the PSC only appeared in the perch channel, as illustrated by the dotted slot in Figure 10.24. By contrast, these two types of information are transmitted in the PCCPCH in UTRA, as shown in Figure 10.5. Using this technique, initial cell identification and synchronization can be carried out in three basic steps. **Step one:** The mobile station uses the 256-chip PSC of Figure 10.24 to perform cross-correlation with all the received Primary SCHs of the base stations in its vicinity. The base station with the highest correlator output is then chosen, which constitutes the best cell site with the lowest path loss. Several periodic correlator output peaks have to be identified in order to achieve a high detection re-

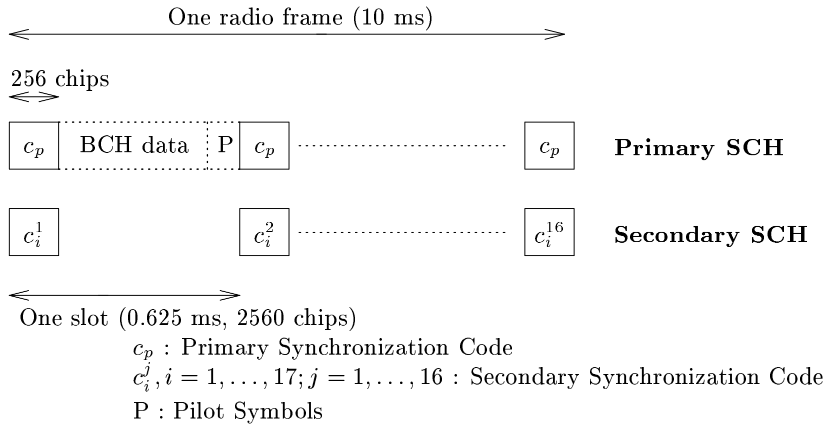

Figure 10.24: Frame structure of the UTRA/IMT-2000 downlink synchronization channel, which is mapped on the slots of Figure 10.4. The primary and secondary SCH are transmitted in parallel using orthogonal codes. In IMT-2000, the BCH data are correlated with the possible scrambling codes [8].

liability. Slot synchronization is also achieved in this step by recognizing the 16 consecutive c_p sequences, providing 16 periodic correlation peaks.

Step two: Once the best cell site is identified, the scrambling code group of that cell site is found by cross-correlating the Secondary SCH with the 17 possible SSCs in each of the 16 timeslots of Figure 10.24. This can be easily implemented using 17 correlators, since the timing of the SSCs is known from Step 1. Hence, there are a total of $16 \times 17 = 272$ correlator outputs. From these outputs, a total of $32 \times 16 = 512$ decision variables corresponding to the 32 possible sequences and 16 cyclic shifts of each $16 \times 256 = 4096$-chip sequence are obtained. The highest decision variable determines the scrambling code group. Consequently, frame synchronization is also achieved.

Step three: With the scrambling code group identified and frame synchronization achieved, the scrambling code is acquired in UTRA by cross-correlating the received Primary CCPCH signal symbol-by-symbol with the 16 possible scrambling codes belonging to the identified group. In IMT-2000, the cross-correlation is performed on the BCH data symbol-by-symbol. Once the exact scrambling code is identified, the BCCH information of Table 10.4, which is conveyed by the PCCPCH of Figure 10.5, can be detected. Let us now consider some of the associated handover issues.

10.2.10 Handover

Theoretically, DS-CDMA has a frequency reuse factor of one [40]. This implies that neighbouring cells can use the same carrier frequency without interfering with each other, unlike in TDMA or FDMA. Hence, seamless uninterrupted handover can be achieved, when mobile users move between cells, since no switching of carrier frequency and synthesizer re-tuning is required. However, in hierarchical cell structures (HCS)[5], using a different carrier frequency is necessary in order to reduce the inter-cell interference. In this case, interfrequency handover is required. Furthermore, since the various operational GSM systems used different carrier frequencies, handover from UTRA systems to GSM systems will have to be supported during the transitory migration phase, while these systems will co-exist. Hence, handovers in terrestrial UMTSs can be classified into inter-frequency and intra-frequency handovers.

10.2.10.1 Intra-frequency Handover or Soft Handover

Soft handover [41, 42] involves no frequency switching, since the new and old cells use the same carrier frequency. The mobile station will continuously monitor the received signal levels from the neighbouring cells and compares them against a set of thresholds. This information is fed back to the network. Based on this information, if a weak or strong cell is detected, the network will instruct the mobile station to drop or add the cell from/to its active base station set. In order to ensure a seamless handover, a new link will be established before relinquishing the old link, using the so-called 'make before break' approach.

10.2.10.2 Inter-frequency Handover or Hard Handover

In order to achieve handovers between different carrier frequencies without affecting the data flow, a technique known as slotted mode[6] can be used [43]. According to this technique, the downlink data, which normally occupy the entire 10 ms frame of Figure 10.25 are 'time-compressed', such that they only occupy a portion of the frame, while no data are transmitted during the remaining portion, as shown in Figure 10.25. The latter portion is known as the idle period and it has a variable duration. The idle period can occur at the beginning, at the centre, or at the end of the frame. The compression of data can be achieved by channel-code puncturing, a procedure, which obliterates some of the coded parity bits, thereby slightly reducing the code's error correcting power (see Chapter 4), or by adjusting the coding rate. In order to maintain the quality of the link, the instantaneous power is also increased during the slotted mode operation. After receiving the data, the mobile station can use this idle period in the frame in order to switch

[5] Microcells overlaid by a macrocell.
[6] Slotted mode is also known as Compressed Mode

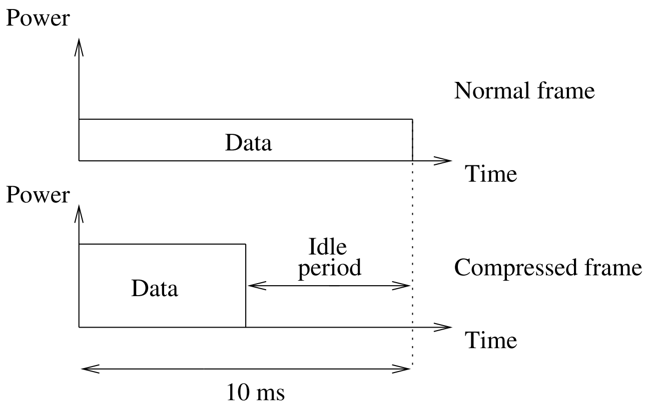

Figure 10.25: Downlink frame structure during slotted mode of operation during UMTS/IMT-2000 handovers.

to other carrier frequencies of other cells and to perform the necessary link-quality measurements for handover.

Alternatively, a dual receiver can be used in order to perform inter-frequency handovers. One receiver can be tuned to the desired carrier frequency for reception, while the other receiver can be used to perform handover link-quality measurements at other carrier frequencies. This method results in a higher hardware complexity at the mobile station.

The 10 ms frame length of UTRA/IMT-2000 was chosen such that it is compatible with the multiframe length of 120 ms in GSM, as seen in Chapter 8. Hence, the mobile station is capable of receiving the Frequency Correction Channel (FCCH) and Synchronization Channel (SCH) in the GSM frame using slotted mode transmission and to perform the necessary handover link-quality measurements [6].

10.2.11 Inter-cell Time Synchronization in the UTRA/ IMT-2000 TDD mode

Time-synchronization between base stations is required, when operating in TDD mode in order to support seamless handovers. A simple method of maintaining inter-cell synchronization is by periodically broadcasting a so-called beacon code from a source to all the base stations. The propagation delay can be easily calculated from the fixed distance between the source and the receiving base stations. There are three possible ways of transmitting this beacon code: via the terrestrial radio link, via the physical wired network, or via the Global Positioning System (GPS).

Global time-synchronization in 3G mobile radio systems is achieved by dividing the synchronous coverage region into three areas, namely the so-called sub-area, main-area and coverage area, as shown in Figure 10.26.

Inter-cell synchronization within a sub-area is provided by a sub-area bea-

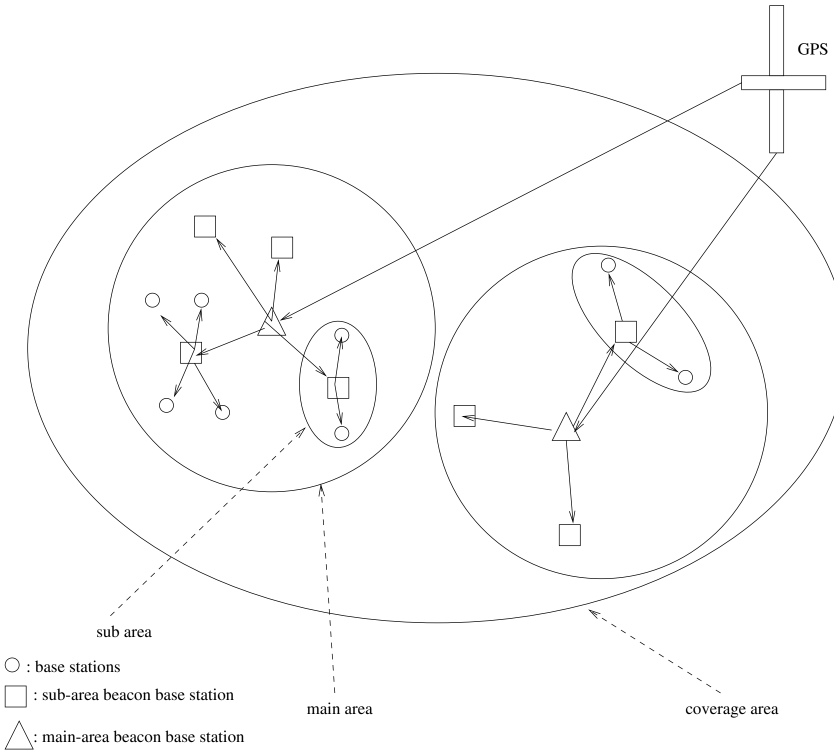

Figure 10.26: Inter-cell time-synchronization in UTRA/IMT-2000 TDD mode.

con base station. Since the sub-area of Figure 10.26 is smaller than the main-area, transmitting the beacon code via the terrestrial radio link or the physical wired network is more feasible. All the sub-area beacon base stations in a main-area are in turn synchronized by a main-area beacon base station. Similarly, the beacon code can be transmitted via the terrestrial radio link or the physical wired network. Finally, all the main-area beacon base stations are synchronised using the GPS system. The main advantage of dividing the coverage regions into smaller areas is that each lower hierarchical area can still operate on its own, even if the synchronization link with the higher hierarchical areas is lost. Having reviewed the basic features of UTRA/IMT-2000, let us now consider the Pan-American cdma2000 system.

Radio Access Technology	DS-CDMA, Multicarrier CDMA
Operating environments	Indoor/Outdoor to indoor/Vehicular
Chip rate (Mcps)	1.2288/3.6864/7.3728/11.0592/14.7456
Channel bandwidth (MHz)	1.25/3.75/7.5/11.25/15
Duplex modes	FDD and TDD
Frame length	5 and 20 ms
Spreading factor	variable, 4 to 256
Detection scheme	Coherent with common pilot channel
Inter-cell operation	FDD : Synchronous TDD : Synchronous
Power control	Open- and closed-loop
Handover	Soft-handover Inter-frequency handover

Table 10.8: The cdma2000 basic parameters.

10.3 The cdma2000 Terrestrial Radio Access [44]- [46]

The current 2G mobile radio systems standardised by TIA in the United States are IS-95-A and IS-95-B [44]. The radio access technology of both systems is based on narrowband DS-CDMA with a chip rate of 1.2288 Mcps, which gives a bandwidth of 1.25 MHz. The basic features of this system were summarized in Table 1.1 of Chapter 1. IS-95-A was commercially launched in 1995, supporting circuit and packet mode transmissions at a maximum bit-rate of only 14.4 kbps [44]. An enhancement to the IS-95-A standards, known as IS-95-B, was developed and introduced in 1998 in order to provide higher data rates, on the order of 115.2 kbps [18]. This was feasible without changing the physical layer of IS-95-A. However, this still falls short of the 3G mobile radio system requirements. Hence the technical committee TR45.5 within TIA has proposed cdma2000, a 3G mobile radio system that is able to meet all the requirements laid down by ITU. One of the problems faced by TIA is that the frequency bands allocated for the 3G mobile radio system, identified during WARC'92 to be 1885-2025 MHz and 2110-2200 MHz, has already been allocated for Personal Communications Services (PCS) in the United States from 1.8 GHz to 2.2 GHz. In particular, the CDMA PCS based on the IS-95 standards has been allocated the frequency bands of 1850-1910 MHz and 1930-1990 GHz. Hence, the 3G mobile radio systems have to fit into the allocated bandwidth without imposing significant interference on the existing applications. Thus, the framework for cdma2000 was designed such that it can be overlaid on IS-95 and it is backwards compatible with IS-95. Most of this section is based on references [44]- [46].

10.3.1 Characteristics of cdma2000

The basic parameters of cdma2000 are shown in Table 10.8. The cdma2000

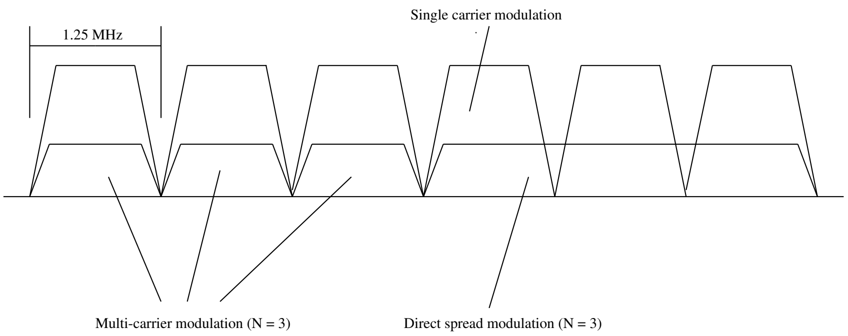

Figure 10.27: Example of an overlay deployment in cdma2000. The multi-carrier mode is only used in the downlink.

system has a basic chip rate of 3.6864 Mcps, which is accommodated in a bandwidth of 3.75 MHz. This chip rate is in fact three times the chip rate used in the IS-95 standards, which is 1.2288 Mcps. Accordingly, the bandwidth was also trebled. Hence, the existing IS-95 networks can also be used to support the operation of cdma2000. Higher chip rates on the order of $N \times 1.2288$ Mcps, $N = 6, 9, 12$ are also supported. These are used to enable higher bit-rate transmission. The value of N is an important parameter in determining the channel coding rate and the channel bit-rate. In order to transmit the high chip-rate signals ($N > 1$), two modulation techniques are employed. In the **direct-spread modulation mode**, the symbols are spread according to the chip-rate and transmitted using a single carrier, giving a bandwidth of $N \times 1.25$ MHz. This method is used on both the uplink and downlink. In **multicarrier (MC) modulation**, the symbols to be transmitted are de-multiplexed into separate signals, each of which is then spread at a chip rate of 1.2288 Mcps. N different carrier frequencies are used to transmit these spread signals, each of which has a bandwidth of 1.25 MHz. This method is used for the downlink only, since in this case, transmit diversity can be achieved by transmitting the different carrier frequencies over spatially separated antennas.

By using multiple carriers, cdma2000 is capable of overlaying its signals on the existing IS-95 1.25 MHz channels and its own channels, while maintaining orthogonality. An example of an overlay scenario is shown in Figure 10.27. Higher chip rates are transmitted at a lower power, than lower chip rates. Hence, the interferences are kept to a minimum.

Similarly to UTRA and IMT-2000, cdma2000 also supports TDD operation in unpaired frequency bands. In order to ease the implementation of a dual-mode FDD/TDD terminal, most of the techniques used for FDD operation can also be applied in TDD operation. The difference between these two modes is in the frame structure, whereby an additional guard time has to be included for TDD operation.

Dedicated Physical Channels (DPHCH)	Common Physical Channels (CPHCH)
Fundamental Channel (FCH) (UL/DL) Supplemental Channel (SCH) (UL/DL) Dedicated Control Channel (DCCH) (UL/DL) Dedicated Auxiliary Pilot Channel (DAPICH) (DL) Pilot Channel (PICH) (UL)	Pilot Channel (PICH) (DL) Common Auxiliary Pilot Channel (CAPICH) (DL) Forward Paging Channel (PCH) (DL) Sync Channel (SYNC) (DL) Access Channel (ACH) (UL) Common Control Channel (CCCH) (UL/DL)

Table 10.9: The cdma2000 physical channels.

In contrast to UTRA and IMT-2000, where the pilot symbols of Figures 10.5 and 10.7 are time-multiplexed with the dedicated data channel on the downlink, cdma2000 employs a common code multiplexed continuous pilot channel on the downlink, as in the IS-95 system of Chapter 1. The advantage of a common downlink pilot channel is that no additional overhead is incurred for each user. However, if adaptive antennas are used, then additional pilot channels have to be transmitted from each antenna.

Another difference with respect to UTRA and IMT-2000 is that the base stations are operated in synchronous mode in cdma2000. As a result of this, the same PN code but with different phase offsets can be used to distinguish the base stations. Using one common PN sequence can expedite cell acquisition as compared to a set of PN sequences, as we have seen in Section 10.2.9 for IMT-2000/UTRA. Let us now consider the cdma2000 physical channels.

10.3.2 Physical Channels in cdma2000

The physical channels (PHCH) in cdma2000 can be classified into two groups: Dedicated Physical Channels (DPHCH) and Common Physical Channels (CPHCH). DPHCHs carry information between the base station and a single mobile station, while CPHCHs carry information between the base station and several mobile stations. Table 10.9 shows the collection of physical channels in each group. These channels will be elaborated on during our further discourse. Typically, all physical channels are transmitted using a frame length of 20 ms. However, the control information on the so-called Fundamental Channel (FCH) and Dedicated Control Channel (DCCH) can also be transmitted in 5 ms frames.

Each base station transmits its own downlink Pilot Channel (PICH), which is shared by all the mobile stations within the coverage area of the base station. Mobile stations can use this common downlink PICH in order to perform channel estimation for coherent detection, soft handover and for fast acquisition of strong multipath rays for RAKE combining. The PICH is transmitted orthogonally along with all the other downlink physical channels from the base station by using a unique orthogonal code (Walsh code 0) as in the IS-95 system of Table 1.1 in Chapter 1. The optional Common Auxiliary Pilot Channels (CAPICH) and Dedicated Auxiliary Pilot Channels (DAPICH) are used to support the implementation of antenna arrays. CAPICHs provide spot coverage shared amongst a group of mobile

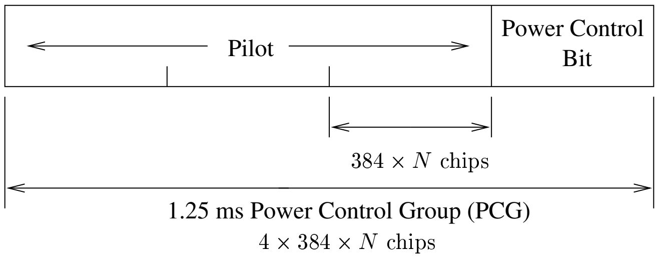

Figure 10.28: Uplink pilot channel structure in cdma2000 for a 1.25 ms duration PCG, where $N = 1, 3, 6, 9, 12$ is the rate-control parameter.

stations, while a DAPICH is directed towards a particular mobile station. Every mobile station also transmits an orthogonal code-multiplexed uplink pilot channel (PICH), which enables the base station to perform coherent detection in the uplink as well as to detect strong multipaths and to invoke power control measurements. This differs from IS-95, which supports only non-coherent detection in the uplink due to the absence of a coherent uplink reference. In addition to the pilot symbols, the uplink PICH also contains time-multiplexed power control bits assisting in downlink power control. A power control bit is multiplexed onto the 20 ms frame every 1.25 ms, giving a total of 16 power control bits per 20 ms frame or 800 power updates per second, implying a very agile, fast response power control regime. Each 1.25 ms duration is referred to as a Power Control Group, as shown in Figure 10.28.

The use of two dedicated data physical channels, namely the so-called Fundamental (FCH) and Supplemental (SCH) channels, optimizes the system during multiple simultaneous service transmissions. Each channel carries a different type of service and is coded and interleaved independently. However, in any connection, there can be only one FCH, but several SCHs can be supported. For a FCH transmitted in a 20 ms frame, two sets of uncoded data rates, denoted as Rate Set 1 (RS1) and Rate Set 2 (RS2), are supported. The data rates in RS1 and RS2 are 9.6/4.8/2.7/1.5 kbps and 14.4/7.2/3.6/1.8 kbps, respectively. Regardless of the uncoded data rates, the coded data rate is 19.2 kbps and 38.4 kbps for RS1 and RS2, respectively, when the rate-control parameter is $N = 1$. The 5 ms frame only supports one data rate, which is 9.6 kbps. The SCH is capable of transmitting higher data rates, than the FCH. The SCH supports variable data rates ranging from 1.5 kbps for N=1 to as high as 2073.6 kbps, when N=12. Blind rate detection [47] is used for SCHs not exceeding 14.4 kbps, while rate information is explicitly provided for higher data rates. The dedicated control physical channel has a fixed uncoded data rate of 9.6 kbps on both 5ms and 20 ms frames. This control channel rate is more than an order of magnitude higher than that of the IS-95 system in Table 1.1, and hence supports a substantially enhanced system control.

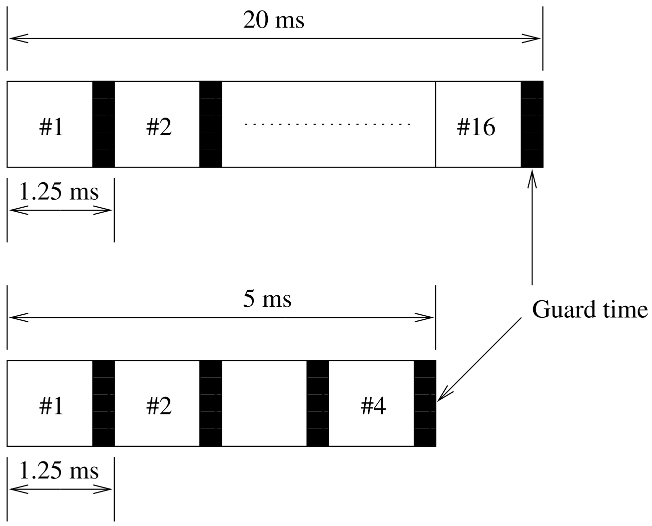

Figure 10.29: The cdma2000 TDD frame structure.

The Sync Channel (SYCH) - note the different acronym in comparison to the SCH abbreviation in UTRA/IMT-2000 - is used to aid the initial synchronization of a mobile station to the base station and to provide the mobile station with system-related information, including the Pseudo Noise (PN) sequence offset, which is used to identify the base stations and the long code mask, which will be defined explicitly in Section 10.3.4. The SYCH has an uncoded data rate of 1.2 kbps and a coded data rate of 4.8 kbps.

Paging functions and packet data transmission are handled by the downlink Paging Channel (PCH) and the downlink Common Control Channel (CCCH). The uncoded data rate of the PCH can be either 4.8 kbps or 9.6 kbps. The CCCH is an improved version of the PCH, which can support additional higher data rates, such as 19.2 and 38.4 kbps. In this case, a 5 ms or 10 ms frame length will be used. The PCH is included in cdma2000 in order to provide IS-95-B functionality.

In TDD mode, the 20 ms and 5 ms frames are divided into 16 and 4 timeslots, respectively. This gives a duration of 1.25 ms per timeslot, as shown in Figure 10.29. A guard time of 52.08 μs and 67.44 μs is used for the downlink in multicarrier modulation and for direct spread modulation, respectively. In the uplink, the guard time is 52.08 μs. Having described the cdma2000 physical channels of Table 10.9, let us now consider the service multiplexing and channel coding aspects.

10.3.3 Service Multiplexing and Channel Coding

Services of different data rates and different QoS requirements are carried by different physical channels, namely by the FCH and SCH of Table 10.9. This differs from UTRA and IMT-2000, whereby different services were time multiplexed onto one or more physical channels, as seen in Figure 10.12. These channels in cdma2000 are code-multiplexed using Walsh codes. Two types of coding schemes are used in cdma2000, as shown in Table 10.10. Basically, all channels use convolutional codes for forward error correction which were discussed in Chapter 4. However, for SCHs at rates higher than 14.4 kbps, turbo coding [28] is preferable. The rate of the input data stream is matched to the given channel rate by either adjusting the coding rate, or using symbol repetition with and without symbol puncturing, or alternatively, by sequence repetition. Tables 10.11 and 10.12 show the coding rate and the associated rate matching procedures for the various downlink and uplink physical channels, respectively, when $N = 1$. Following the above brief notes on the cdma2000 channel coding and service multiplexing issues, let us now focus our attention on the spreading and modulation processes.

	Convolutional	Turbo
Rate	1/2 or 1/3 or 1/4	1/2 or 1/3 or 1/4
Constraint length	9	4

Table 10.10: The cdma2000 channel coding parameters.

10.3.4 Spreading and Modulation

There are generally three layers of spreading in cdma2000, as shown in Table 10.13. Each user's uplink signal is identified by different offsets of a long code, a procedure which is similar to that of the IS-95 system portrayed in Chapter 1. As seen in Table 10.13, this long code is an m-sequence with a period of $2^{42} - 1$ chips. The construction of m-sequences was highlighted by Proakis in reference [26]. Different user offsets are obtained using a long code mask. Orthogonality between the different physical channels of the same user belonging to the same connection in the uplink is maintained by spreading using Walsh codes, which were introduced in Chapter 1.

In contrast to the IS-95 downlink of Figure 1.42, whereby Walsh code spreading is performed prior to QPSK modulation, the data in cdma2000 are first QPSK modulated, before spreading the resultant I and Q branches with the same Walsh code. In this way, the number of Walsh codes available is increased twofold due to the orthogonality of the I and Q carriers. The length of the uplink/downlink (UL/DL) channelization Walsh codes of Table 10.13 varies according to the data rates. All the base stations in the system are distinguished by different offsets of the same complex downlink m-sequence, as indicated by Table 10.13. This downlink m-sequence code

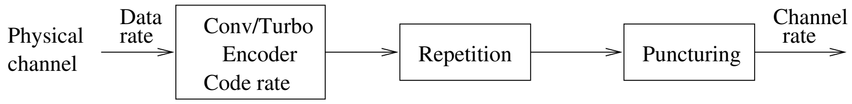

Physical Channel	Data Rate	Code Rate	Repetition	Puncturing	Channel rate
SYCH	1.2 kbps	1/2	$\times 2$	0	4.8 ksps
PCH	4.8 kbps	1/2	$\times 2$	0	19.2 ksps
	9.6 kbps	1/2	$\times 1$	0	19.2 ksps
CCCH	9.6 kbps	1/2	$\times 1$	0	19.2 ksps
	19.2 kbps	1/2	$\times 1$	0	38.4 ksps
	38.4 kbps	1/2	$\times 1$	0	76.8 ksps
FCH	1.5 kbps	1/2	$\times 8$	1 of 5	19.2 ksps
	2.7 kbps	1/2	$\times 4$	1 of 9	19.2 ksps
	4.8 kbps	1/2	$\times 2$	0	19.2 ksps
	9.6 kbps	1/2	$\times 1$	0	19.2 ksps
	1.8 kbps	1/3	$\times 8$	1 of 9	38.4 ksps
	3.6 kbps	1/3	$\times 4$	1 of 9	38.4 ksps
	7.2 kbps	1/3	$\times 2$	1 of 9	38.4 ksps
	14.4 kbps	1/3	$\times 1$	1 of 9	38.4 ksps
SCH	9.6 kbps	1/2	$\times 1$	0	19.2 ksps
	19.2 kbps	1/2	$\times 1$	0	38.4 ksps
	38.4 kbps	1/2	$\times 1$	0	76.8 ksps
	76.8 kbps	1/2	$\times 1$	0	153.6 ksps
	153.6 kbps	1/2	$\times 1$	0	307.2 ksps
	307.2 kbps	1/2	$\times 1$	0	614.4 ksps
	14.4 kbps	1/3	$\times 1$	1 of 9	38.4 ksps
	28.8 kbps	1/3	$\times 1$	1 of 9	76.8 ksps
	57.6 kbps	1/3	$\times 1$	1 of 9	153.6 ksps
	115.2 kbps	1/3	$\times 1$	1 of 9	307.2 ksps
	230.4 kbps	1/3	$\times 1$	1 of 9	614.4 ksps
DCCH	9.6 kbps	1/2	$\times 1$	0	19.2 ksps

Table 10.11: The cdma2000 downlink physical channel (see Table 10.9) coding parameters for $N = 1$, where Repetition $\times 2$ implies transmitting a total of two copies.

is the same as that used in IS-95, which has a period of $2^{15} = 32768$ and it is derived from m-sequences. The feedback polynomials of the shift registers for the I and Q sequences are $X^{15} + X^{13} + X^9 + X^8 + X^7 + X^5 + 1$ and $X^{15} + X^{12} + X^{11} + X^{10} + X^6 + X^5 + X^4 + X^3 + 1$, respectively. The offset of these codes must satisfy a minimum value, which is equal to $N \times 64 \times$Pilot_Inc, where Pilot_Inc is a so-called code reuse parameter, which depends on the topology of the system, analogously to the frequency reuse factor in FDMA. Let us now focus our attention on downlink spreading issues more closely.

10.3.4.1 Downlink Spreading and Modulation

Figure 10.30 shows the structure of a downlink transmitter for a physical channel. In contrast to the IS-95 downlink transmitter shown in Figure 1.42 of Chapter 1, the data in the cdma2000 downlink transmitter shown in Figure 10.30 are first QPSK modulated before spreading using Walsh codes. As a result, the number of Walsh codes available is increased twofold due to the orthogonality of the I and Q carriers, as mentioned previously. The

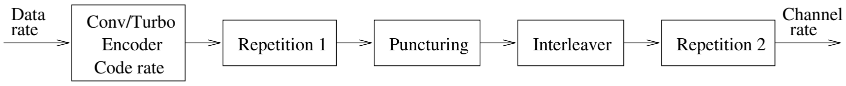

Physical channel	Data rate	Code rate	Repetition 1	Puncturing	Repetition 2	Channel rate
CCCH	19.2 kbps	1/4	×1	0	×4	307.2 ksps
	38.4 kbps	1/4	×1	0	×2	307.2 ksps
FCH	1.5 kbps	1/4	×8	1 of 5	×8	307.2 ksps
	2.7 kbps	1/4	×4	1 of 9	×8	307.2 ksps
	4.8 kbps	1/4	×2	0	×8	307.2 ksps
	9.6 kbps	1/4	×1	0	×8	307.2 ksps
	1.8 kbps	1/4	×16	1 of 3	×4	307.2 ksps
	3.6 kbps	1/4	×8	1 of 3	×4	307.2 ksps
	7.2 kbps	1/4	×4	1 of 3	×4	307.2 ksps
	14.4 kbps	1/4	×2	1 of 3	×4	307.2 ksps
SCH	9.6 kbps	1/4	×1	0	×16	614.4 ksps
	19.2 kbps	1/4	×1	0	×8	614.4 ksps
	38.4 kbps	1/4	×1	0	×4	614.4 ksps
	76.8 kbps	1/4	×1	0	×2	614.4 ksps
	153.6 kbps	1/4	×1	0	×1	614.4 ksps
	307.2 kbps	1/2	×1	0	×1	614.4 ksps
ACH	4.8 kbps	1/4	×1	0	×8	307.2 ksps
	9.6 kbps	1/4	×1	0	×4	307.2 ksps
DCCH	9.6 kbps	1/4	×1	0	×4	307.2 ksps

Table 10.12: The cdma2000 uplink physical channel (see Table 10.9) coding parameters for $N = 1$, where Repetition $\times 2$ implies transmitting a total of two copies.

	Channelization Codes (UL/DL)	User-specific scrambling-codes (UL)	Cell-specific scrambling codes (DL)
Type of codes	Walsh codes	Different offsets of a real m-sequence	Different offsets of a complex m-sequence
Code length	Variable	$2^{42} - 1$ chips	2^{15} chips
Type of Spreading	BPSK	BPSK	QPSK
Data Modulation	DL : QPSK UL : BPSK		

Table 10.13: Spreading parameters in cdma2000.

user data are first scrambled by the long scrambling code by assigning a different offset to different users for the purpose of improving user privacy, which is then mapped to the I and Q channels. This long scrambling code is identical to the uplink user-specific scrambling code given in Table 10.13. The downlink pilot channels of Table 10.9 (PICH, CAPICH, DAPICH) and the SYNC channel are not scrambled with a long code since there is no need for user-specificity. The uplink power control symbols are inserted into the FCH at a rate of 800 Hz, as it was shown in Figure 10.30. The I and Q channels are then spread using a Walsh code and complex multiplied with the cell-specific complex PN sequence of Table 10.13, as portrayed in Figure 10.30. Each base station's downlink channel is assigned a different Walsh code in order to eliminate any intra-cell interference since all Walsh codes transmitted by the serving base station are received synchronously.

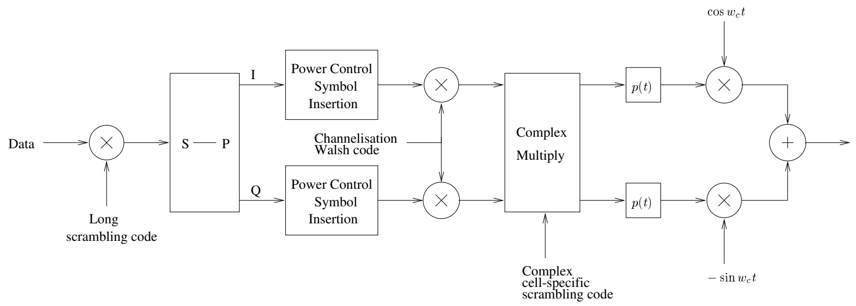

Figure 10.30: The cdma2000 downlink transmitter. The long scrambling code is used for the purpose of improving user privacy. Hence, only the paging channels and the traffic channels are scrambled with the long code. The common pilot channel and the SYNC channel are not scrambled by this long code (the terminology of Table 10.13 is used).

The length of the downlink channelization Walsh code of Table 10.13 is determined by the type of physical channel and its data rate. Typically for $N = 1$, downlink FCHs with data rates belonging to RS1, i.e. those transmitting at 9.6/4.8/2.7/1.5 kbps, use a 128-chip Walsh code and those in RS2, transmitting at 14.4/7.2/3.6/1.8 kbps use a 64-chip Walsh code. Walsh codes for downlink SCHs can range from 4-chip to 128-chip Walsh codes. The downlink PICH is an unmodulated sequence (all 0s) spread by Walsh code 0. Finally, the complex spread data in Figure 10.30 is baseband filtered using the Nyquist filter impulse responses $p(t)$ in Figure 10.30 and modulated on a carrier frequency.

For the case of multi-carrier modulation, the data are split into N branches immediately after the long code scrambling of Figure 10.30 which was omitted in the figure for the sake of simplicitly. Each of the N branches is then treated as a separate transmitter and modulated using different carrier frequencies.

10.3.4.2 Uplink Spreading and Modulation

The uplink cdma2000 transmitter is shown in Figure 10.31. The uplink PICH and DCCH of Table 10.9 are mapped to the I data channel, while the uplink FCH and SCH of Table 10.9 are mapped to the Q channel in Figure 10.31. Each of these uplink physical channels belonging to the same user is assigned different Walsh channelization codes in order to maintain orthogonality, with higher rate channels using shorter Walsh codes. The I and Q data channels are then spread by complex multiplication with the user-specifically offset real m-sequence based scrambling code of Table 10.13 and a complex scrambling code, which is the same for all the mobile stations in the system, as seen at the top of Figure 10.31. However,

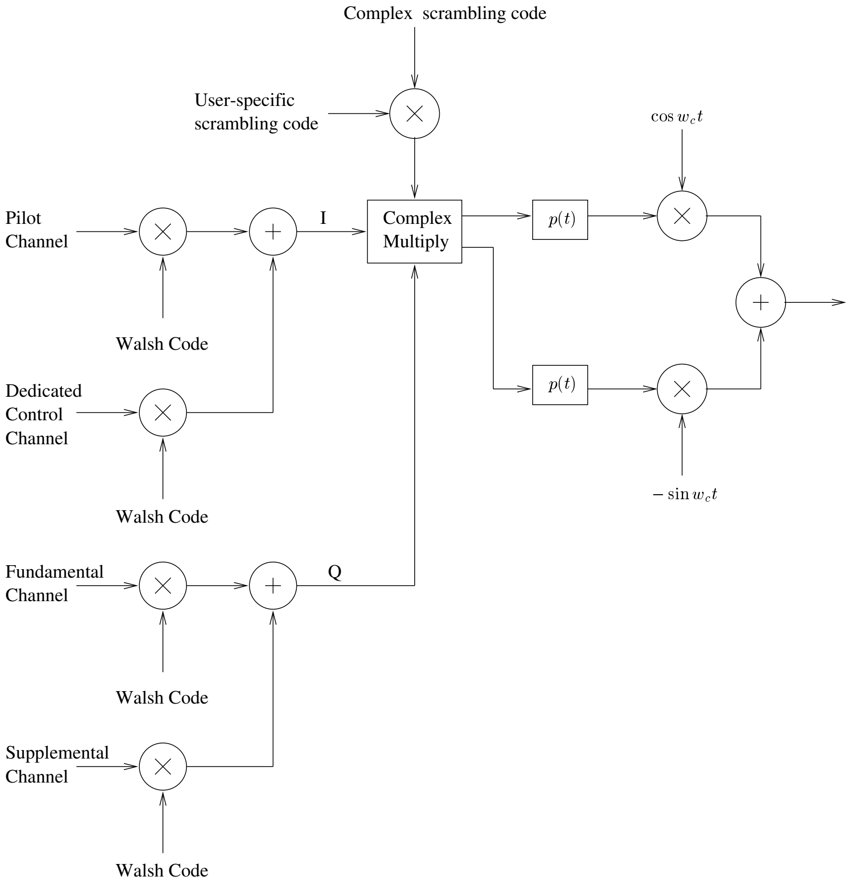

Figure 10.31: The cdma2000 uplink transmitter. The complex scrambling code is identical to the downlink cell-specific complex scrambling code of Table 10.13 used by all the base stations in the system (the terminology of Table 10.13 is used).

this latter complex scrambling code is not explicity shown in Table 10.13, since it is identical to the downlink cell-specific scrambling code. This complex scrambling code is only used for the purpose of quadrature spreading. Hence, in order to reduce the complexity of the base station receiver, this complex scrambling code is identical to the cell-specific scrambling code of Table 10.13 used on the downlink by all the base stations. Let us now consider the cdma2000 random access process.

10.3.5 Random Access

The mobile station initiates an access request to the network by repeatedly transmitting a so-called 'access probe', until a request acknowledgement is received. This entire process of sending a request is known as an 'access attempt'. Within a single access attempt, the request may be sent to several base stations. An access attempt addressed to a specific base station is known as a 'sub-attempt'. Within a sub-attempt, several access probes with increasing power can be sent. Figure 10.32 shows an example of an access attempt. The access probe transmission follows the slotted ALOHA

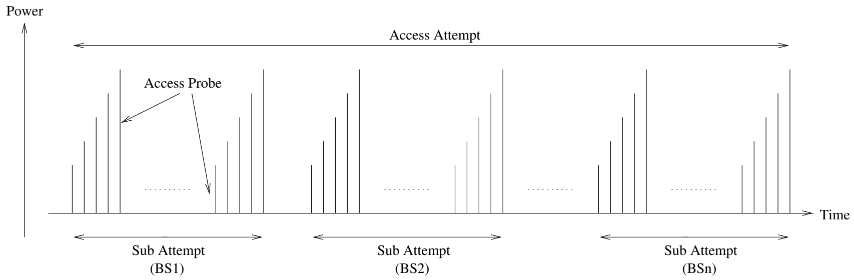

Figure 10.32: An access attempt by a mobile station in cdma2000 using the access probe of Figure 10.33.

algorithm, which is a relative of PRMA portrayed in Chapter 9. An access probe can be divided into two parts, as shown in Figure 10.33 The access

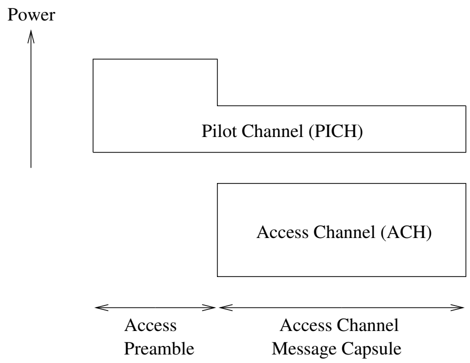

Figure 10.33: A cdma2000 access probe transmitted using the regime of Figure 10.32.

preamble carries a non-data bearing pilot channel, at an increased power level. The so-called 'access channel message capsule' carries the data bearing Access Channel (ACH) or uplink Common Control Channel (CCCH) messages of Table 10.9 and the associated non-data bearing pilot channel. The structure of the pilot channel is similar to that of the uplink pilot channel (PICH) of Figure 10.28 except that in this case, there are no time-multiplexed power control bits. The preamble length in Figure 10.33 is an integer multiple of the 1.25 ms slot intervals. The specific access preamble length is indicated by the base station, which depends on how fast the base station can search the PN code space in order to recognize an access attempt. The ACH is transmitted at a fixed rate of either 9.6 or 4.8 kbps, as seen in Table 10.12. This rate is constant for the duration of the access probe of Figure 10.32. The ACH or CCCH and their associated pilot channel are spread by the spreading codes of Table 10.13, as shown in Figure 10.34. Different ACHs or CCCHs and their associated pilot channels are spread by different long codes.

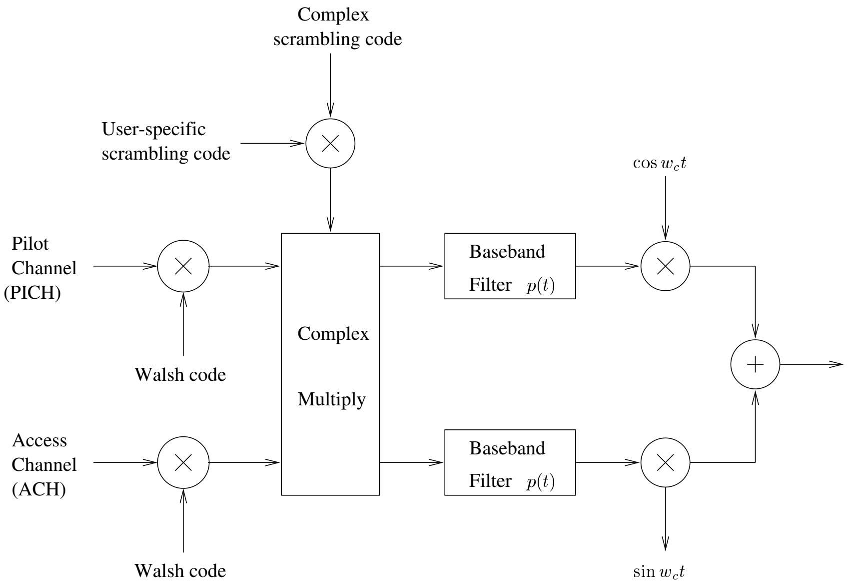

Figure 10.34: The cdma2000 access channel modulation and spreading. The complex scrambling code is identical to the downlink cell-specific complex scrambling code of Table 10.13 used by all the base stations in the system (the terminology of Table 10.13 is used).

The access probes of Figure 10.33 are transmitted in pre-defined slots, where the slot length is indicated by the base station. Each slot is sufficiently long in order to accommodate the preamble and the longest message of Figure 10.33. The transmission must begin at the start of each 1.25 ms slot. If an acknowledgement of the most recently transmitted probe is not received by the mobile station after a time-out period, another probe is transmitted in another randomly chosen slot, obeying the regime of Figure 10.32.

Within a sub-attempt of Figure 10.32, a sequence of access probes is transmitted, until an acknowledgement is received from the base station.

Each successive access probe is transmitted at a higher power compared to the previous access probe, as shown in Figure 10.35. The initial power (IP) of the first probe is determined by the open-loop power control plus a nominal offset power that corrects for the open-loop power control imbalance between uplink and downlink. Subsequent probes are transmitted at a power level higher than the previous probe. This increased level is indicated by the Power Increment (PI). Following the above discussions on the mobile station's random access procedures, let us now highlight some of the cdma2000 handover issues.

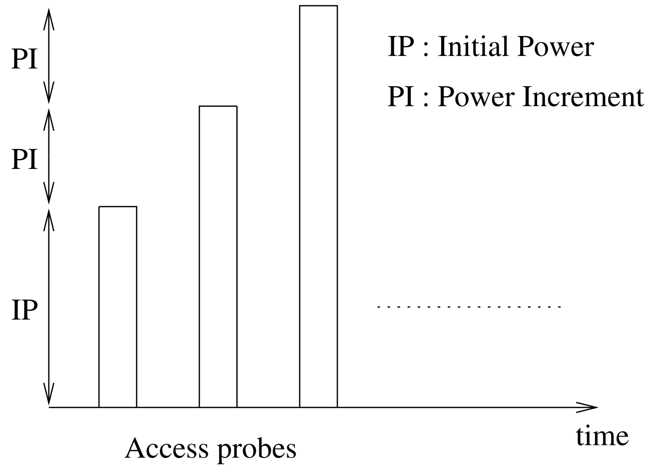

Figure 10.35: Access probes within a sub-attempt of Figure 10.32.

10.3.6 Handover

Intra-frequency or soft-handover is initiated by the mobile station. While communicating, the mobile station may receive the same signal from several base stations. These base stations constitute the so-called 'Active Set' of the mobile station. The mobile station will continuously monitor the power level of the received pilot channels (PICH) transmitted from neighbouring base stations, including those from the mobile station's active set. The power levels of these base stations are then compared against a set of thresholds according to an algorithm, which will be highlighted during our further discourse. The set of thresholds consists of the so-called static thresholds, which are maintained at a fixed level, and the so-called dynamic thresholds, which are dynamically adjusted based on the total received power. Subsequently, the mobile station will inform the network, when any of the monitored power levels exceeds the thresholds.

Whenever the mobile station detects a PICH, whose power level exceeds a given static threshold, denoted as T_1, this PICH will be moved to a so-called candidate set and will be searched and compared more frequently against a dynamically adjusted threshold denoted as T_2. This value of T_2 is a function of the received power levels of the PICHs of the base stations in the active set. This process will determine, whether the candidate base station is worth adding to the active set. If the overall power level in the active set is weak, then adding a base station of higher power would improve the reception. By contrast, if the overall power level in the active set is relatively high, then adding another high-powered base station may not only be unnecessary, it will in fact utilize more network resources.

For the base stations that are already in the active set, the power level of their corresponding PICH is compared against a dynamically adjusted threshold, denoted as T_3, which is also a function of the total power of the PICH in the active set, similar to T_2. This is to ensure that each base station in the active set is contributing sufficiently to the overall power level. If any of the PICH's power level dropped below T_3, after a specified period of time allowed in order to eliminate any uncertainties due to fading which may have caused fluctuations in the power level, the base station will be, again, moved to the candidate set where it will be compared with a static threshold T_4. At the same time, the mobile station will report to the network the identity of the low-powered base station in order to allow the corresponding base station to increase its transmit power. If the power level decreases further below a static threshold, denoted as T_4, then the mobile station will again report this to the network and the base station is subsequently dropped from the candidate set.

Inter-frequency or hard-handovers can be supported between cells having different carrier frequencies. Here we conclude our discussions on the cdma2000 features and provide some rudimentary notes on a number of advanced techniques, which can be invoked in order to improve the performance of the 3G W-CDMA systems.

10.4 Performance Enhancement Features

The treatment of adaptive antennas, multiuser detection, interference cancellation or the portrayal of transmit diversity techniques is beyond the scope of this chapter. Here we simply provide a few pointers to the associated literature.

10.4.1 Adaptive Antennas

The transmission of time-multiplexed pilot symbols on both the uplink and downlink as seen for UTRA and IMT-2000 in Figures 10.5-10.8 facilitates the use of adaptive antennas. Adaptive antennas are known to enhance the capacity and coverage of the system [48,49].

10.4.2 Multiuser Detection/Interference Cancellation

Following Verdu's seminal paper [50], extensive research has shown that Multiuser Detection (MUD) [36,51–57] and Interference Cancellation techniques [58–69] can substantially improve the performance of the CDMA link in comparison to conventional RAKE receivers. However, using long scrambling codes increases the complexity of the MUD [18]. As a result, UTRA introduced an optional short scrambling code namely the extended Kasami code of Table 10.7, as mentioned in Section 10.2.6.2 in order to reduce the complexity of MUD [8]. Another powerful technique is invoking burst-by-burst adaptive CDMA [23, 24] in conjunction with MUD.

On the other hand, interference cancellation schemes require accurate channel estimation in order to reproduce and deduct or cancel the interference. Several stages of cancellation are required in order to achieve a good performance, which in turn increases the canceller's complexity. It was shown that recursive channel estimation in a multistage interference canceller improved the accuracy of the channel estimation and hence gave better BER performance [70].

Due to the complexity of the multiuser or interference canceller detectors, it is not feasible to implement them in the mobile station. Hence, MUD or interference cancellation are optionally proposed for the uplink in the base station at the time of writing.

10.4.3 Transmit Diversity

10.4.3.1 Time Division Transmit Diversity

In Time Division Transmit Diversity (TDTD), the dedicated downlink transmit signal is switched between base stations. The transmitting base station can be selected according to either a fixed pattern or based on the quality of the signal received by the mobile station. The latter technique is known as Selection Transmit Diversity (STD) [71], while the former is known as Time Switched Transmission Diversity (TSTD) [72].

In TSTD, suppose there are several separate antennas involved in the transmission. Each antenna transmits one timeslot of the downlink dedicated channel frame in turn, in a fixed pattern. Signals for other users may have a different pattern. In STD, the transmitting antenna is dynamically selected based on a control signal transmitted from the mobile station periodically, indicating the mobile station's perceived preference. Each antenna involved in the diversity will transmit a Primary CCPCH. The control signal transmitted by the mobile station carries information about the quality of the received Primary CCPCH signal at the mobile station. The best received Primary CCPCH from the corresponding antenna will then be invoked in order to transmit the user's signal.

10.4.3.2 Orthogonal Transmit Diversity [6]

In Orthogonal Transmit Diversity (OTD), the signal is transmitted using two separate antennas. These signals are spread using different orthogonal channelization codes, so that self-interference is eliminated in flat fading.

$*$ $*$

We have presented an overview of the terrestrial radio transmission technology of 3G mobile radio systems proposed by ETSI, ARIB and TIA. All three proposed systems are based on Wideband-CDMA. Despite the call for a common global standard, there are some differences in the proposed technologies, notably the chip rates and inter-cell operation. These differences are partly due to the existing 2G infrastructure already in use all over the world, specifically due to the heritage of the GSM and the IS-95 systems. Huge capital has been invested in these current 2G mobile radio systems. Hence, the respective regional standard bodies have endeavoured to ensure that the 3G systems are compatible with the 2G systems. Due to the diversified nature of these 2G mobile radio systems, it is not an easy task to reach a common 3G standard that can maintain perfect backwards compatibility.

Bibliography

[1] **J. Rapeli**, "UMTS:Targets, System Concept, and Standardization in a Global Framework," *IEEE Personal Communications*, vol. 2, no. 1, pp. 20–28, February 1995.

[2] **M.H. Callendar,** "Future Public Land Mobile Telecommunication Systems," *IEEE Personal Communications*, vol. 12, no. 4, pp. 18–22, 1994.

[3] **A.J. Viterbi,** *CDMA-Principles of Spread Spectrum Communication*, Addison Wesley, 1995.

[4] **S.G. Glisic** and **B. Vucetic,** *Spread Spectrum CDMA Systems for Wireless Communications*, Artech House Publishers, 1997.

[5] **R. Prasad,** *CDMA for Wireless Personal Communications*, Artech House, 1996.

[6] **T. Ojanperä** and **R. Prasad,** *Wideband CDMA for Third Generation Mobile Communications*, Artech House, 1998.

[7] **A. Toskala**, **J.P. Castro**, **E. Dahlman**, **Matti Latva-aho**, and **Tero Ojanperä,** "FRAMES FMA2 Wideband-CDMA for UMTS," *European Transactions on Telecommunications*, vol. 9, no. 4, pp. 325–336, July-August 1998.

[8] **E. Dahlman**, **B. Gudmundson**, **M. Nilsson**, and **Johan Sköld,** "UMTS/IMT-2000 Based on Wideband CDMA," *IEEE Communications Magazine*, vol. 36, no. 9, pp. 70–80, September 1998.

[9] **T. Ojanperä,** "Overview of Research Activities for Third Generation Mobile Communication," in *Wireless Communications TDMA versus CDMA*, Savo G. Glisic and Pentti A. Leppänen, Eds., pp. 415–446. Kluwer Academic Publishers, 1997.

[10] **ETSI/SMG/SMG2,** "The ETSI UMTS Terrestrial Radio Access (UTRA) ITU-R RTT Candidate Submission," Tech. Rep., European Telecommunications Standards Institute, June 1998.

[11] **ARIB,** "Japan's Proposal for Candidate Radio Transmission Technology on IMT-2000 : W-CDMA," Tech. Rep., Association of Radio Industries and Businesses, June 1998.

[12] **F. Adachi**, **M. Sawahashi**, and **H. Suda,** "Wideband DS-CDMA for Next-generation Mobile Communications Systems," *IEEE Communications Magazine*, vol. 36, no. 9, pp. 56–69, September 1998.

[13] **F. Adachi** and **M. Sawahashi,** "Wideband Wireless Access Based on DS-CDMA," *IEICE Transactions on Communications*, vol. E81-B, no. 7, pp. 1305–1316, July 1998.

[14] **A. Sasaki,** "Current Situation of IMT-2000 Radio Transmission Technology Study in Japan," *IEICE Transactions on Communications*, vol. E81-B, no. 7, pp. 1299–1304, July 1998.

[15] **P.-G. Andermo** and **L.-M. Ewerbring,** "A CDMA-Based Radio Access Design for UMTS," *IEEE Personal Communications*, vol. 2, no. 1, pp. 48–53, February 1995.

[16] **P.W. Baier**, **P. Jung**, and **A. Klein,** "Taking the Challenge of Multiple Access for Third-Generation Cellular Mobile Radio Systems - A European View," *IEEE Communications Magazine*, vol. 34, no. 2, pp. 82–89, February 1996.

[17] **E. Berruto**, **M. Gudmundson**, **R. Menolascino**, **W. Mohr**, and **M. Pizarroso,** "Research Activities on UMTS Radio Interface, Network Architectures, and Planning," *IEEE Communications Magazine*, vol. 36, no. 2, pp. 82–95, February 1998.

[18] **T. Ojanperä** and **R. Prasad,** "An Overview of Air Interface Multiple Access for IMT-2000/UMTS," *IEEE Communications Magazine*, vol. 36, no. 9, pp. 82–95, September 1998.

[19] **A. Baier**, **U.-C. Fiebig**, **W. Granzow**, **Wolfgang Koch**, **Paul Teder**, and **Jörn Thielecke,** "Design Study for a CDMA-Based Third-Generation Mobile System," *IEEE Journal on Selected Areas in Communications*, vol. 12, no. 4, pp. 733–743, May 1994.

[20] **J. Schwarz da Silva**, **Bernard Barani**, and **Bartolomé Arroyo-Fernández,** "European Mobile Communications on the Move," *IEEE Communications Magazine*, vol. 34, no. 2, pp. 60–69, February 1996.

[21] **E. Nikula**, **A. Toskala**, **E. Dahlman**, **Laurent Girard**, and **Anja Klein,** "FRAMES Multiple Access for UMTS and IMT-2000," *IEEE Personal Communications*, vol. 5, no. 2, pp. 16–24, April 1998.

[22] **F. Ovesjö**, **E. Dahlman**, **T. Ojanperä**, **Antti Toskala**, and **Anja Klein,** "FRAMES Multiple Access Mode 2 - Wideband CDMA," in *IEEE International Conference on Personal, Indoor and Mobile Radio Communication*, Helsinki, Finland, pp. 42–46, September 1997, PIMRC'97.

[23] **E. L. Kuan**, **C. H. Wong** and **L. Hanzo,** "Burst-by-burst Adaptive Joint Detection CDMA," *to appear in Proc. of VTC'99*, Houston, USA, May, 1999.

[24] **E. L. Kuan**, **C. H. Wong** and **L. Hanzo,** "Upper-bound Performance of Burst-by-burst Adaptive Joint Detection CDMA," *submitted to IEEE Communications Letters*, 1998.

[25] **F. Adachi**, **K. Ohno**, **A. Higashi**, **Tomohiro Dohi**, and **Yukihiko Okumura,** "Coherent multicode DS-CDMA mobile Radio Access," *IEICE Transactions on Communications*, vol. E79-B, no. 9, pp. 1316–1324, September 1996.

[26] **J.G. Proakis,** *Digital Communications*, McGraw-Hill, 1995.

[27] **M. O. Sunay**, **Z. -C. Honkasalo**, **A. Hottinen**, **H. Honkasalo** and **L. Ma,** "A Dynamic Channel Allocation Based TDD DS CDMA Residential Indoor System," *IEEE 6th International Conference on Universal Personal Communications, ICUPC'97*, San Diego, pp. 228–234, October 1997.

[28] **A. Fujiwara**, **H. Suda**, and **F. Adachi,** "Turbo Codes Application to DS-CDMA Mobile Radio," *IEICE Transactions on Communications*, vol. E81A, no. 11, pp. 2269–2273, November 1998.

[29] **M. J. Juntti,** "System Concept Comparison for Multirate CDMA with Multiuser Detection," in *Proceedings of the IEEE Vehicular Technology Conference*, Ottawa, Canada, May 1998, pp. 18–21.

[30] **S. Ramakrishna** and **J. M. Holtzman,** "A Comparison between Single Code and Mulitple Code Transmission Schemes in a CDMA System," in *Proceedings of the IEEE Vehicular Technology Conference*, Ottawa, Canada, May 1998, pp. 791–795.

[31] **M. B. Pursley,** "Performance Evaluation for Phase-Coded Spread-Spectrum Multiple-Access Communication-Part I: System Analysis," *IEEE Transactions on Communications*, vol. COM-25, no. 8, pp. 795–799, August 1977.

[32] **F. Adachi**, **M. Sawahashi**, and **K. Okawa,** "Tree-structured Generation of Orthogonal Spreading Codes with Different Lengths for Forward Link of DS-CDMA Mobile Radio," *Electronic Letters*, vol. 33, no. 1, pp. 27–28, January 1997.

[33] **R. F. Ormondroyd** and **J. J. Maxey,** "Performance of Low Rate Orthogonal Convolutional Codes in DS-CDMA," *IEEE Transactions on Vehicular Technology*, vol. 46, no. 2, pp. 320–328, May 1997.

[34] **M. K. Simon**, **J. K. Omura**, **R. A. Scholtz** and **B. K. Levitt,** "Spread Spectrum Communications Handbook," McGraw-Hill, 1994.

[35] **T. Kasami,** "Combinational Mathematics and its Applications," University of North Carolina Press, 1969.

[36] **E. L. Kuan** and **L. Hanzo,** "Joint Detection CDMA Techniques for Third-generation Transceivers," *Proceedings of ACTS'98*, Rhodos, Greece, June 1998, pp 727-732.

[37] **A. Chockalingam**, **Paul Dietrich**, **Laurence B. Milstein**, and **Ramesh R. Rao,** "Performance of Closed-Loop Power Control in DS-CDMA Cellular Systems," *IEEE Transactions on Vehicular Technology*, vol. 47, no. 3, pp. 774–789, August 1998.

[38] **K Higuchi**, **M Sawahashi**, and **F Adachi,** "Fast Cell Search Algorithm in DS-CDMA Mobile Radio using Long Spreading Codes," in *Proceedings of the IEEE Vehicular Technology Conference*, Phoenix, U.S.A., May 1997, vol. 3, pp. 1430–1434.

[39] **R. R. Gejji,** "Forward-Link-Power Control in CDMA Cellular-Systems," *IEEE Transactions on Vehicular Technology*, vol. 41, no. 4, pp. 532–536, November 1992.

[40] **W.C.Y. Lee,** "Overview of Cellular CDMA," *IEEE Transactions on Vehicular Technology*, vol. 40, no. 2, pp. 291–302, May 1991.

[41] **D. Wong** and **T. J. Lim,** "Soft Handoffs in CDMA Mobile Systems," *IEEE Personal Communications*, vol. 4, no. 6, pp. 6–17, December 1997.

[42] **C. C. Lee** and **R. Steele,** "Effects of Soft and Softer Handoffs on CDMA System Capacity," *IEEE Transactions on Vehicular Technology*, vol. 47, no. 3, pp. 830–841, August 1998.

[43] **M Gustafsson**, **K Jamal**, and **E Dahlman,** "Compressed Mode Techniques for Inter-frequency measurements in a wide-band DS-CDMA system," in *IEEE International Conference on Personal, Indoor and Mobile Radio Communication*, Helsinki, Finland, September 1997, PIMRC'97, pp. 231–235.

[44] **D.N. Knisely**, **S. Kumar**, **S. Laha**, and **S. Nanda,** "Evolution of Wireless Data Services : IS-95 to cdma2000," *IEEE Communications Magazine*, vol. 36, no. 10, pp. 140–149, October 1998.

[45] **TIA,** "The cdma2000 ITU-R RTT Candidate Submission," Tech. Rep., Telecommunications Industry Association, 1998.

[46] **D. N. Knisely**, **Q. Li**, and **N. S. Rames,** "cdma2000 : A Third Generation Radio Transmission Technology," *Bell Labs Technical Journal*, vol. 3, no. 3, pp. 63–78, July-September 1998.

[47] **Y. Okumura** and **F. Adachi,** "Variable-Rate Data Transmission with Blind Rate Detection for Coherent DS-CDMA Mobile Radio," *IEICE Transactions on Communications*, vol. E81B, no. 7, pp. 1365–1373, July 1998.

[48] **J. C. Liberti**, **Jr. and T. S. Rappaport,** "Analytical Results for Capacity Improvements in CDMA," *IEEE Transactions on Vehicular Technology*, vol. 43, no. 3, pp. 680–690, August 1994.

[49] **J. H. Winters,** "Smart Antennas for Wireless Systems," *IEEE Personal Communications*, vol. 5, no. 1, pp. 23–27, February 1998.

[50] **S. Verdu,** "Minimum Probability of Error for Asynchronous Gaussian Multiple-Access Channel," *IEEE Transactions on Communications*, vol. 32, no. 1, pp. 85–96, January 1986.

[51] **S. Moshavi,** "Multi-User Detection for DS-CDMA Communications," *IEEE Communications Magazine*, vol. 34, no. 10, pp. 124–136, October 1996.

[52] **T. J. Lim** and **L. K. Rasmussen,** "Adaptive Symbol and Parameter Estimation in Asynchronous Multiuser CDMA Detectors," *IEEE Transactions on Communications*, vol. 45, no. 2, pp. 213–220, February 1997.

[53] **T. J. Lim** and **S. Roy,** "Adaptive Filters in Multiuser (MU) CDMA Detection," *Wireless Networks*, vol. 4, no. 4, pp. 307–318, June 1998.

[54] **L. Wei**, **L. K. Rasmussen** and **R. Wyrwas,** "Near Optimum Tree-search Detection Schemes for Bit-synchronous Multiuser CDMA Systems over Gaussian and Two-path Rayleigh Fading Channels," *IEEE Transactions on Communications*, vol. 45, no. 6, pp. 691–700, June 1997.

[55] **T. J. Lim** and **M. H. Ho,** "LMS-Based Simplifications to the Kalman Filter Multiuser CDMA Detector," *Proceedings of IEEE Asia-Pacific Conference on Communications/International Conference on Communication Systems*, Singapore, November, 1998.

[56] **D. You** and **T. J. Lim,** "A Modified Blind Adaptive Multiuser CDMA Detector," *Proceedings of IEEE International Symposium on Spread Spectrum Techniques and Application*, Sun City, South Africa, pp. 878–882, September 1998.

[57] **S. M. Sun**, **L. K. Rasmussen**, **T. J. Lim** and **H. Sugimoto,** "Impact of Estimation Errors on Multiuser Detection in CDMA," *Proceedings of IEEE Vehicular Technology Conference*, Ottawa, Canada, pp. 1844–1848, May 1998.

[58] **Y. Sanada** and **Q. Wang,** "A Co-Channel Interference Cancellation Technique Using Orthogonal Convolutional Codes on Multipath Rayleigh Fading Channel," *IEEE Transactions on Vehicular Technology*, vol. 46, no. 1, pp. 114–128, February 1997.

[59] **M.K. Varanasi** and **B. Aazhang,** "Multistage Detection in Asynchronous Code-Division Multiple-Access Communications," *IEEE Transactions on Communications*, vol. 38, no. 4, pp. 509–519, April 1990.

[60] **P. Patel** and **J. Holtzman,** "Analysis of a Simple Successive Interference Cancellation Scheme in a DS/CDMA System," *IEEE Journal on Selected Areas in Communications*, vol. 12, no. 5, pp. 796–807, June 1994.

[61] **P. H. Tan** and **L. K. Rasmussen,** "Subtractive Interference Cancellation for DS-CDMA Systems," *Proceedings of IEEE Asia-Pacific Conference on Communications/International Conference on Communication Systems*, Singapore, November, 1998.

[62] **K. L. Cheah**, **H. Sugimoto**, **T. J. Lim**, **L. K. Rasmussen** and **S. M. Sun,** "Performance of Hybrid Interference Canceller with Zero-Delay Channel Estimation for CDMA," *Proceedings of IEEE Global Communications Conference '98*, Australia, pp. 265–270, November 1998.

[63] **S. M. Sun**, **L. K. Rasmussen** and **T.J. Lim,** "A Matrix-Algebraic Approach to Hybrid Interference Cancellation in CDMA," *Proceedings of IEEE International Conference on Universal Personal Communications '98*, Florence, Italy, pp. 1319–1323, October 1998.

[64] **A. L. Johansson** and **L. K. Rasmussen,** "Linear Group-wise Successive Interference Cancellation in CDMA," *Proceedings of IEEE International Symposium on Spread Spectrum Techniques and Application*, Sun City, South Africa, pp. 121–126, September 1998.

[65] **S. M. Sun**, **L. K. Rasmussen**, **H. Sugimoto** and **T. J. Lim,** "A Hybrid Interference Canceller in CDMA," *Proceedings of IEEE International Symposium on Spread Spectrum Techniques and Application*, Sun City, South Africa, pp. 150–154, September 1998.

[66] **D. Guo**, **L. K. Rasmussen**, **S. M. Sun**, **T. J. Lim** and **C. Cheah,** "MMSE-Based Linear Parallel Interference Cancellation in CDMA," *Proceedings of IEEE International Symposium on Spread Spectrum Techniques and Application*, Sun City, South Africa, pp. 917–921, September 1998.

[67] **L. K. Rasmussen**, **D. Guo**, **Y. Ma** and **T. J. Lim,** "Aspects on Linear Parallel Interference Cancellation in CDMA," *Proceedings of IEEE International Symposium on Information Theory '98*, Cambridge, US, pp. 37, August 1998.

[68] **L. K. Rasmussen**, **T. J. Lim**, **H. Sugimoto** and **T. Oyama,** "Mapping Functions for Successive Interference Cancellation in CDMA," *Proceedings*

of IEEE Vehicular Technology Conference, Ottawa, Canada, pp. 2301–2305, May 1998.

[69] **S. M. Sun**, **T. J. Lim**, **L. K. Rasmussen**, **T. Oyama**, **H. Sugimoto** and **Y. Matsumoto,** "Performance Comparison of Multi-stage SIC and Limited Tree-Search Detection in CDMA," *Proceedings of IEEE Vehicular Technology Conference*, Ottawa, Canada, pp. 1854–1858, May 1998.

[70] **Mamoru Sawahashi**, **Yoshinori Miki**, **Hidehiro Andoh**, and **Kenichi Higuchi,** "Pilot Symbol-Assisted Coherent Multistage Interference Canceller Using Recursive Channel Estimation for DS-CDMA Mobile Radio," *IEICE Transactions on Communications*, vol. E79-B, no. 9, pp. 1262–1269, September 1996.

[71] **A. Wittneben** and **T. Kaltenschnee,** "TX Selection Diversity with Prediction: Systematic Nonadaptive Predictor Design," *IEEE 44th Vehicular Technology Conference, 1994*, pp. 1246–1250, June 1994.

[72] **A. Hottinen** and **R. Wichman,** "Transmit Diversity by Antenna Selection in CDMA Downlink," in *Proceedings of ISSSTA '98*, Sun City, South Africa, September 1998.

Glossary

2G	Second Generation
3G	Third Generation
ACL	Auto Correlation
ACTS	Advanced Communications Technology and Services
ARIB	Association of Radio Industries and Businesses
AWGN	Additive White Gaussian Noise
BCCH	Broadcast Control Channel
BER	Bit Error Rate
BPSK	Binary Phase Shift Keying
BS	Base Station
CAPICH	Common Auxiliary Pilot Channel
CCCH	Common Control Channel
CCL	Cross Correlation
CDMA	Code Division Multiple Access
CPHCH	Common Physical Channel
CRC	Cyclic Redundancy Check
DAPICH	Dedicated Auxiliary Pilot Channel
DCCH	Dedicated Control Channel
DCH	Dedicated Channel
DECT	Digital Enhanced Cordless Telecommunications
DL	Downlink
DPCCH	Dedicated Physical Control Channel
DPDCH	Dedicated Physical Data Channel
DPHCH	Dedicated Physical Channel
DS-CDMA	Direct Sequence Code Division Multiple Access
EMC	Electromagnetic Compatibility

ETSI	European Telecommunications Standards Institute
EU	European Union
FACH	Forward Access Channel
FCCH	Frequency Correction Channel
FCH	Fundamental Channel
FDD	Frequency Division Duplex
FDMA	Frequency Division Multiple Access
FEC	Forward Error Correction
FPLMTS	Future Public Land Mobile Telecommunication System
FRAMES	Future Radio Wideband Multiple Access System
GPS	Global Positioning System
HCS	Hierarchical Cell Structure
IMT-2000	International Mobile Telecommunications 2000
ISO/OSI	International Standardization Organization/Open Systems Interconnection
ITU	International Telecommunication Union
ITU-R	International Telecommunication Union - Radiocommunication Sector
MAI	Multiple Access Interference
MC	Multicarrier
MDM	Modulation Division Multiplexing
MPG	Multiple Processing Gain
MS	Mobile Station
OCQPSK	Orthogonal Complex Quadrature Phase Shift Keying
OVSF	Orthogonal Variable Spreading Factor
PCCPCH	Primary Common Control Physical Channel
PCH	Paging Channel
PCS	Personal Communications Services
PHCH	Physical Channel
PHS	Personal Handyphone System
PICH	Pilot Channel
PN	Pseudo Noise
PRMA	Packet Reservation Multiple Access
PSC	Primary Synchronization Code
QoS	Quality of Service
QPSK	Quadrature Phase Shift Keying

RACE	Research in Advanced Communication Equipment
RACH	Random Access Channel
RI	Rate Information
RS	Reed-Solomon
RTT	Radio Transmission Technology
SCCPCH	Secondary Common Control Physical Channel
SCH	Synchronisation Channel
SF	Spreading Factor
SIR	Signal-to-Interference Ratio
SSC	Secondary Synchronization Code
SYCH	Sync Channel
TDD	Time Division Duplex
TDMA	Time Division Multiple Access
TFI	Transport Format Indicator
TIA	Telecommunications Industry Association
TPC	Transmit Power Control
UL	Uplink
UMTS	Universal Mobile Telecommunications System
UTRA	Universal Mobile Telecommunications System Terrestrial Radio Access
VoD	Video on Demand
W-CDMA	Wideband Code Division Multiple Access
WARC	World Administrative Radio Conference

Index

R

S

Z

Author Index

C

Q

R

S

T

U

V

W